

**DEEL 1: NEDERLANDSTALIGE SAMENVATTING**  
**PART 1: DUTCH SUMMARY**



## Inhoudsopgave

### DEEL 1

Inhoudsopgave.....	3
Lijst van symbolen en afkortingen.....	6
Samenvatting .....	10
<b>1 Inleiding.....</b>	<b>12</b>
<b>1.1. De SBI.....</b>	<b>12</b>
<b>1.2. Evaluatie en rapportering van onzekerheid.....</b>	<b>13</b>
<b>1.3. Gevolgde aanpak .....</b>	<b>14</b>
<b>2 Meetprincipe en berekeningsprocedures .....</b>	<b>17</b>
<b>3 Gasanalyse.....</b>	<b>19</b>
<b>4 Massadebiet.....</b>	<b>20</b>
<b>4.1. Introductie.....</b>	<b>20</b>
<b>4.2. Artikel 1.....</b>	<b>20</b>
<b>4.3. Artikel 2.....</b>	<b>22</b>
<b>4.4. Artikel 3.....</b>	<b>24</b>
<b>4.5. Artikel 4.....</b>	<b>25</b>
<b>5 Dynamisch gedrag .....</b>	<b>26</b>
<b>5.1. Bandbreedte .....</b>	<b>26</b>
<b>5.2. Filters.....</b>	<b>27</b>
<b>5.3. Voorgestelde wijzigingen .....</b>	<b>31</b>
<b>6 Onzekerheid.....</b>	<b>35</b>
<b>7 Evaluatie en resultaten van het Analytisch Model.....</b>	<b>40</b>
<b>7.1. Inleiding.....</b>	<b>40</b>
<b>7.2. Evaluatie van het Model .....</b>	<b>40</b>
<b>7.3. Gebruik van het model ter verbetering van de testmethode .....</b>	<b>42</b>
<b>8 Besluiten .....</b>	<b>48</b>

**Referenties..... 54**

## **DEEL 2**

Engelstalig kerndocument.

Dankbaar voor de schoonheid van het Leven  
dank ik  
mijn vrouw en kinderen,  
evenals mijn ouders en schoonouders,  
mijn manager Prof. Paul Vandavelde en promotor Prof. Erik Dick.

Ik richt ook een woord van dank tot  
Prof. Jean-Pierre Martens en Prof. Robin De Keyser van de UGent  
en Prof. Jeroen van Beeck van het Von Karman Instituut, Sint-Genesius-Rode  
voor geboden inzichten.

Ir. Rudolf Van Mierlo van het TNO, Delft  
en Prof. Bart Merci en Dr. Erwin Theuns van de UGent  
wil ik danken voor samenwerking rond enkele artikels.

Verder wens ik allen te danken die mij op een of andere manier gesteund  
en/of geholpen hebben bij het verwezenlijken van dit proefschrift en in het bijzonder dank ik  
Mevr. Marthe Vandavelde en Mevr. Els Van Gysel,  
Prof. Gilbert De Mey, Dr. Saïd Dhimdi, Ir. Pjotr Kawka, Ir. Mihaela Sbarciog, Ir. Wim Meeus,  
Dhr. Patrick Ysebie, Dhr. Martin Cambier, Mevr. Leen De Clippel, Dhr. Patrick Depue,  
Dhr. Pascal De Jonge en Dhr. Jurgen Delamper.

## Lijst van symbolen en afkortingen

A	sectie van de rookgasbuis	[m <sup>2</sup> ]
c	$\sqrt{2T_{298}/\rho_{298}} \cong 22.4$	[K.m <sup>3</sup> /kg] <sup>1/2</sup>
$c_x^y$	gevoelheidscoëfficiënt van x t.o.v. y	
$c_p$	warmtecapaciteit	[J/kg.K]
D	diameter	[m]
e	fout	
E	verbrandingswaarde per eenheidsvolume verbruikte zuurstof (bij 298 K)	[MJ/Nm <sup>3</sup> O <sub>2</sub> ]
E'	verbrandingswaarde per eenheidsmassa verbruikte zuurstof	[MJ/kg O <sub>2</sub> ]
$f_s$	bemonsteringsfrequentie	[Hz]
F	zichtbaarheidfactor	[-]
G( $\omega$ )	versterking in het frequentiedomein	[-]
h	convectiecoëfficiënt	[W/m <sup>2</sup> .K]
$\Delta h_c$	verbrandingswaarde	[kJ/kg]
H	enthalpie	[kJ/kg]
Im{x}	imaginair deel van x	
j	operator imaginaire getallen ( $j^2 = -1$ )	
k	dekkingsgraad	[-]
k	thermische conductiviteit	[W/m.K]
$k_t$	correctiefactor snelheidsprofiel	[-]
$k_p$	ijkfactor verschildruksonde	[-]
L	lengte	[m]
£	Laplace operator	
m	gemiddelde waarde	
$\dot{m}$	massadebiet	[kg/s]
n or N	aantal monsternamen	
Nu	Nusseltgetal	[-]
O()	grootteorde van	
p	barometrische druk	[Pa]
P(x)	probabiliteitsfunctie	
Pr	Prandtlgetal	[-]
$\dot{Q}$	warmtevrijstellingsvermogen	[kW]
r	herhaalbaarheidslimiet	

$r(x_i, x_j)$	Pearson correlatiecoëfficiënt	[-]
Re	Reynoldsgetal	[-]
$\text{Re}\{x\}$	reëel deel van x	
s	Laplace operator	
s	geschatte standaard afwijking	
$s^2$	geschatte variantie	
$s_r$	geschatte standaardafwijking op de herhaalbaarheid	
$s_R$	geschatte standaardafwijking op de reproduceerbaarheid	
t	tijd	[s]
$t_s$	bemonsteringsinterval	[s]
T	temperatuur	[K]
$u(x)$	standaard onzekerheid op x	
U	geëxpandeerde onzekerheid	
v	snelheid	[m/s]
V	volume	[m <sup>3</sup> ]
$\dot{V}_{D298}$	volumedebiet doorheen de rookgasbuizen (298 K)	[m <sup>3</sup> /s]
$w_i$	wegingsfactor	
$\bar{x}$	geschat gemiddelde	
$X_{O_2}$	concentratie van, in dit geval, zuurstof	[Vol%]
$X_{O_2}^{D^\circ}$	Initiële zuurstofconcentratie in de rookgasbuizen	[Vol%]
$X_{O_2}^{A^\circ}$	Initiële zuurstofconcentratie zoals gemeten door de analyser	[Vol%]
$X_{O_2}^A$	Actuele zuurstofconcentratie zoals gemeten door de analyser	[Vol%]
z	operator Z-transformatie	

### Griekse symbolen

$\alpha$	expansiefactor	
$\delta$	systematische fout	
$\Delta$	differentieoperator	
$\varepsilon$	emissiviteit	[-]
$\mu$	gemiddelde	
$\nu$	kinematische viscositeit	[m <sup>2</sup> /s]
$\rho$	dichtheid	[kg/m <sup>3</sup> ]
$\sigma$	standaardafwijking	
$\sigma^2$	variantie	

$\tau$	tijdsconstante	[s]
$\varphi$	relatieve vochtigheid	[%]
$\phi$	depletiefactor	
$\Phi(\omega)$	faseverschuiving in het frequentiedomein	
$\omega$	circulaire frequentie	[rad/s]

### Onderschriften

$A^\circ$	initiële waarde analyser
atm	atmosfeer
av	gemiddeld
b	systematische fout
c	gecombineerd
$D^\circ$	initiële waarde gemeten in de rookgasbuizen
eff	effectief
f	vorming
ms	meetsectie
rect	rechthoekig
st.dev.	standaard afwijking
trap	trapezoïdaal
trian	triangulair

### Bovenschriften

$^\circ$	initieel
l	lagere
u	hogere

### Afkortingen

ABS	Absoluut
ARHE	Gemiddelde mate van warmte vrijstelling
BW	bandbreedte
CEN	Europees normalisatie-instituut
CPD	Bouwproductenrichtlijn; 89/106/CE
DAQ	Data-acquisitiesysteem



DMM	Digitale Multimeter
EGOLF	Europese groep van organisaties voor brandtesten, inspectie en certificatie
EN	Europese norm
FIGRA	Groeisnelheid van een brand
FS	Volledig bereik
GUM	Gids ter bepaling van de onzekerheid in metingen <sup>[13]</sup>
HRR	Warmtevrijstellingsvermogen
ISO	Internationaal normalisatie-instituut
MARHE	Maximale gemiddelde warmtevrijstelling
MAX	Maximum van
MR	Meetbereik
PLC	Netcyclus
PLC	Industriële processor
ppm	delen per miljoen
REL	Relatief
RC	Room corner test; ISO 9705 <sup>[6]</sup>
RTD	Temperatuursmeting door middel van weerstand
SBI	Single Burning Item test; EN13823 <sup>[2]</sup>
SBI RR1	Eerste ringonderzoek met betrekking tot de SBI; 1997
SBI RR2	Tweede ringonderzoek met betrekking tot de SBI; 2003 - 2004
SPR	Rookproductievermogen
THR600s	Totale warmtevrijstelling in de eerste tien minuten vanaf blootstelling aan de vlammen

## Samenvatting

In 1989 publiceerde de Europese Commissie de Bouwproductenrichtlijn 89/106/CE met als doel een ééngemaakte markt te creëren voor bouwproducten. Deze richtlijn is de rechtstreekse aanleiding tot het invoeren van een nieuw Europees classificatiesysteem EN 13501<sup>[1]</sup> dat zowel reactie bij brand als weerstand tegen brand omhelst. Dit nieuwe systeem, dat ook wel EUROCLASSES genoemd wordt, werd operationeel in 2002 met het publiceren van de betreffende norm. Datzelfde jaar verschenen de eerste bouwproducten met CE-markering op de markt. Dankzij de CE-markering kunnen deze producten vrij verhandeld worden binnen de grenzen van de Europese handelsassociatie.

In het domein van reactie bij brand diende een volledig nieuw classificatiesysteem ontworpen te worden, gebaseerd op zes verschillende brandtesten. Zoveel als mogelijk en/of politiek aanvaardbaar, werden bestaande ISO of nationale test methoden gebruikt. Men beschouwde het echter wel noodzakelijk om een nieuwe middelschalige test te ontwikkelen, namelijk de Single Burning Item test (SBI) EN13823<sup>[2]</sup> – vrij vertaald de “Eén Brandend Object” test, zo genoemd omwille van het brandscenario dat hij verondersteld wordt te simuleren. De SBI is de hoeksteen van het nieuwe Europese classificatiesysteem.

De SBI genereert dynamische gegevens over het brandgedrag van een materiaal zoals warmte vrijstellingsvermogen (HRR) en rookproductievermogen (SPR). Deze gegevens worden elementair geacht bij het beoordelen van een materiaal op zijn brandgedrag.

Overeenkomstig EN ISO 17025<sup>[9]</sup>, *Algemene vereisten omtrent de competenties van test- en kalibratielaboratoria*, en ISO 10012-1<sup>[14]</sup>, *omtrent het verzekeren van de kwaliteit van meetapparatuur*, dienen onzekerheden op de metingen opgenomen te worden in zowel de test- als kalibratierapporten. De algemene principes voor het evalueren en het rapporteren van onzekerheden worden beschreven in de Richtlijn tot het bepalen van onzekerheden op metingen, GUM<sup>[13]</sup>, maar dienen geïnterpreteerd en toegepast te worden op brandtesten.

Verscheidene auteurs hebben getracht de onzekerheden gerelateerd aan de HRR en SPR te kwantificeren<sup>[67][65][48][66]</sup>. Echter, uit een vergelijkende studie van alle belangrijke ringonderzoeken, besloot Janssens<sup>[53]</sup> dat de onzekerheid veel groter is dan de waarden gevonden langs analytische weg. Dit was in het bijzonder het geval voor middelschalige en grootschalige tests.

Deze doctoraalscriptie onderzoekt mogelijke technische verklaringen hiervoor, ze stelt wijzigingen aan de analytische modellen voor en ontwikkelt een tijdsafhankelijk analytisch model.

Bijkomend beschouwt deze doctoraalscriptie enkele in de GUM onbehandelde thema's.

Sinds de ontwikkeling van de SBI werden twee ringonderzoeken georganiseerd in een internationale context. Dit resulteerde in een experimenteel bepaalde onzekerheid op de testmethode. Deze resultaten worden vergeleken met de langs analytische weg bekomen schatting van de onzekerheid.

Een sleutelement in het bepalen van het dynamische brandgedrag van een product is de nauwkeurige bepaling van de volumestroom rookgassen doorheen de rookgaskanalen. Actueel wordt hiervoor een bi-directionele lage-snelheidssonde gebruikt<sup>671</sup>. Deze doctoraalscriptie toont echter aan dat deze sonde een belangrijke bijdrage levert in het verbreden van de onzekerheid op de meting.

Daarom werd een nieuwe verschildruksonde ontwikkeld voor het meten van unidirectionele snelheden in rookgaskanalen waarbij naast enkele andere voordelen, de onzekerheid drastisch kon verminderd worden.

Het dynamische gedrag van het SBI testtoestel werd grondig onderzocht en verscheidene voorstellen om hiermee om te gaan werden geformuleerd.

De aanbevelingen uit deze doctoraalscriptie worden overgemaakt aan CEN TC127 teneinde de norm te wijzigen op enkele cruciale punten. Met deze doctoraalscriptie is het inzicht in de SBI en gelijkaardige testtoestellen substantieel toegenomen. Verder biedt deze doctoraalscriptie aan EGOLF, de *European Group of Organisations for Fire testing, Inspection and Certification*, de mogelijkheid om een antwoord te geven op de problemen die ondervonden worden bij het rapporteren van meetonzekerheden bij brandtesten.

# 1 Inleiding

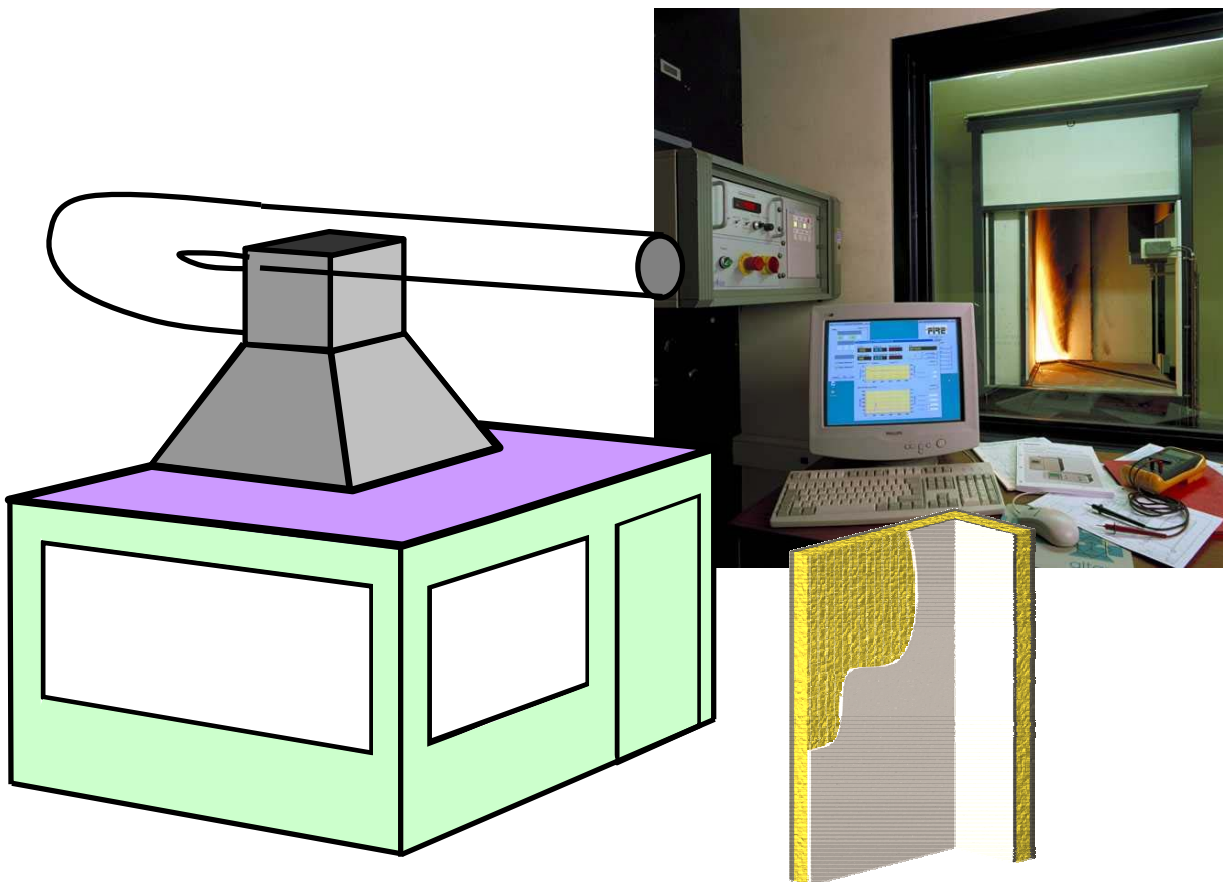
## 1.1. De SBI

De SBI test simuleert een 'single burning item' in de hoek van een kamer, of dus één object zoals een papiermand of zetel die in brand staat. Het toestel wordt voorgesteld in Figuur 1. Het totale blootgestelde proefoppervlak bedraagt 1.5 m bij 1.5 m. Het proefmonster bestaat uit twee delen (met hoogte 1.5 m en breedte 0.5 m en 1 m) die een hoek vormen. Eventuele verbindingstukken dienen toegepast te worden zoals in het eindgebruik.

Een diffuse brander met vermogen van 30 kW wordt in de hoek geplaatst en fungeert als warmte én ontstekingsbron. Het gedrag van het proefmonster wordt gedurende 20 minuten geëvalueerd.

De rookgassen worden verzameld in een afzuigkap en worden geëvacueerd doorheen rookgasbuizen. In deze buizen wordt het massadebiet van de rookgassen bepaald evenals de zuurstof- en koostofdioxideconcentratie. Tevens wordt de opaciteit van de rookgassen gemeten.

Uit deze gegevens wordt dan het warmtevrijstellingsvermogen (HRR) en rookproductievermogen (SPR) berekend in functie van de tijd.



Figuur 1. SBI: test toestel en typisch proefmonster

## 1.2. Evaluatie en rapportering van onzekerheid

De SBI testmethode werd ontwikkeld onder hoge tijdsdruk vermits zij de introductie van de vrije markt voor bouwproducten in Europa ophield. Na goedkeuring van het ontwerp en de prototypen werd een groot ringonderzoek tussen laboratoria gehouden. De resultaten van dit ringonderzoek toonden aan dat de SBI testmethode in staat was de vereiste brandkenmerken op een herhaalbare en reproduceerbare manier te bepalen en dit op een aanvaardbaar niveau. Er werd echter wel geëist dat er gezocht zou worden naar enkele technische verbeteringen.

Daarnaast maakt EN ISO 17025:1999<sup>[9]</sup>, – die de algemene eisen ten aanzien van de bekwaamheid van test- en kalibratielaboratoria voorschrijft – de schatting, de meting en rapportering van onzekerheid op testresultaten verplichtend.

Deze twee factoren, de vraag naar technische verbeteringen en de vereiste om onzekerheid te rapporteren, vormen de directe aanleiding voor deze doctoraalscriptie.

Totnogtoe hebben slechts enkele auteurs over onzekerheid in relatie tot de SBI gepubliceerd, en dit zelfs in een ruimer kader van testtoestellen gebaseerd op de zuurstofdepletie techniek. De zwakke punten in het onderzoek tot dusver zijn dat:

- niet alle relevante fenomenen in rekening genomen werden;
- de schattingen op de onzekerheden van de componenten soms zeer arbitrair gekozen zijn;
- het dynamische gedrag van het toestel niet of onvolledig in rekening gebracht werd;
- covarianties tussen de verschillende meetcomponenten verwaarloosd werden;
- onzekerheden gerelateerd aan de synchronisatie van data verwaarloosd werden.

Voor zover bekend publiceerden enkel Axelsson et al. een studie ter bepaling van de meetonzekerheid op de HRR langs analytische weg voor de middelschalige SBI test. De auteurs onthielden zich om de onzekerheden te bepalen op de classificatieparameters FIGRA en THR600s die afgeleid worden uit HRR.

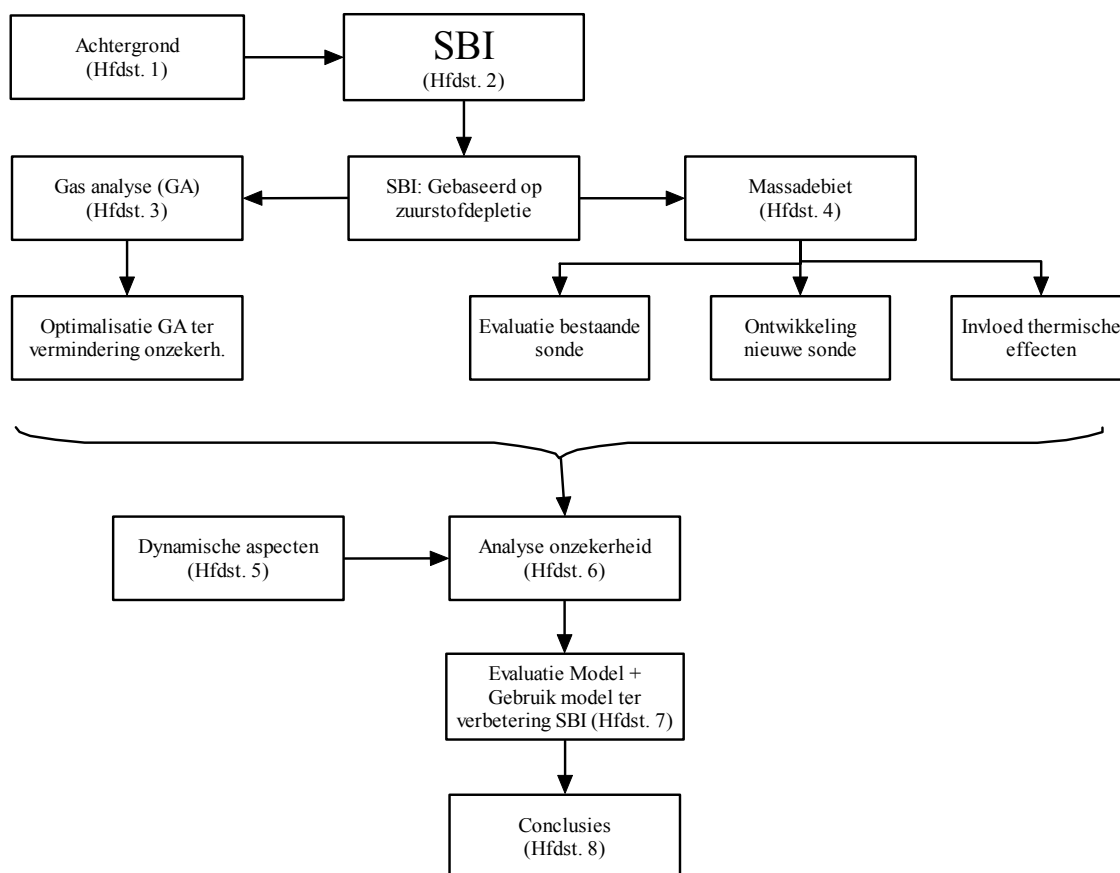
Andere relevante publicaties komen van de hand van Bryant et al. en Enright et al. met de focus op grootschalige respectievelijk kleinschalige proefmethoden.

### 1.3. Gevolgde aanpak

Deze doctoraalscriptie focust op vier onderzoeksdomeinen.

1. De analyse van de rookgasconcentraties.
2. Het massadebiet doorheen de rookgasbuizen.
3. Dynamische aspecten van het SBI toestel.
4. Onzekerheidsanalyse.

De structuur van het werk wordt kort weergegeven in onderstaande flowchart.



Figuur 2. Algemene structuur

Na de algemene schets over het ontstaan en het belang van de SBI in hoofdstuk 1, wordt in hoofdstuk 2 het meetprincipe uitgelegd en worden de belangrijkste berekeningsprocedures voorgesteld.

In hoofdstuk 3 ligt de focus op de gasanalyse. Deze omvat het hele pad van monstername tot analyse. Hoewel de algemene technieken hiervoor gekend zijn, heeft de auteur een geoptimaliseerd systeem samengesteld, gebaseerd op de zuurstofdepletietechniek, specifiek voor brandproeven.

Hoofdstuk 4 behandelt de meting van het massadebiet en bevat een van de belangrijkste bijdragen van dit werk. Na evaluatie van bestaande verschildruksondes (gebruikt ter bepaling van de lokale stromingssnelheid) werd een nieuwe performante sonde ontwikkeld die de tekortkomingen van de bestaande sondes wegwerkt. Bovendien werden voor zowel de nieuwe als de bestaande sondes de ijkfactor bepaald tezamen met de onzekerheid hierop. Dit alles resulteerde in twee artikels die eerder dit jaar aanvaard werden voor publicatie.

Twee bijkomende artikels werden geschreven in samenwerking met twee collega's van hetzelfde departement. In deze artikels ligt het hoofddaccent op de bepaling van de onzekerheid – gerelateerd aan thermische effecten – op de massadebietsmetingen in de SBI en op het verband tussen het veranderend snelheidsprofiel en een nieuw gedefinieerd effectief Reynoldsgetal.

De artikels werden uitgestuurd voor recensie.

Hoofdstuk 5 behandelt de dynamische aspecten van het test toestel en zijn instrumentarium. Verder wordt de *vlakke glijdendgemiddelde filter* – gebruikt om de HRR data te dempen alvorens FIGRA te berekenen – geëvalueerd en wordt een andere (Henderson) filter voorgesteld.

Voorts wordt de vraag gesteld wat de gewenste bandbreedte is voor brandproeven en worden er drie alternatieven voorgesteld voor de huidige meetmethode.

De behandelde aspecten zijn nieuw in het domein van reactie bij brand.

In hoofdstuk 6 worden onzekerheden en gerelateerde aspecten in detail bekeken. De onzekerheid op de HRR en op de hiervan afgeleide classificatieparameters FIGRA en  $THR_{600s}$  wordt bepaald. Het voorgestelde analytische model maakt gebruik van de onzekerheden op de samenstellende individuele componenten. Deze onzekerheden worden in een aansluitende sectie in detail besproken.

Nieuw t.o.v. eerdere studies in dit domein is dat asymmetrische distributies gebruikt worden waar nodig, dat covarianties berekend worden, dat transiënte fenomenen beschouwd worden en dat onzekerheden op de synchronisatie van data in rekening gebracht worden.

In hoofdstuk 7 wordt het model geëvalueerd op basis van de resultaten van een recent ringonderzoek op de SBI. Daarnaast worden de aanbevelingen uit hoofdstukken 5 en 6 geëvalueerd.

In hoofdstuk 8 tenslotte, worden de bevindingen van deze doctoraalscriptie samengevat.

Annex A groepeert de 4 artikels uit hoofdstuk 4. Twee artikels werden aanvaard voor publicatie, de twee andere zijn onder recensie.

Annex B groepeert tussenresultaten en andere belangrijke documenten leidend tot de resultaten vermeld in deze scriptie.



## 2 Meetprincipe en berekeningsprocedures

Het meetprincipe waarop de SBI gebaseerd is, zuurstofdepletie, is gebaseerd op de vaststelling dat, in het algemeen, de verbrandingswaarde per eenheidsmassa verbruikte zuurstof nagenoeg constant is voor het gros van de materialen die typisch in een brand kunnen voorkomen (Huggett<sup>[52]</sup>).

Kent men het massadebiet van de rookgassen evenals de concentratie van zuurstof in deze rookgassen, dan kan men hieruit het zuurstofverbruik gaan berekenen in functie van de tijd en dus het warmtevrijstellingsvermogen (HRR). Enkele correcties kunnen doorgevoerd worden indien ook nog de koolstofdioxide en eventueel de koolstofmonoxide concentraties gemeten worden. Eveneens dient de vochtigheid van de inkomende verbrandingslucht gekend te zijn.

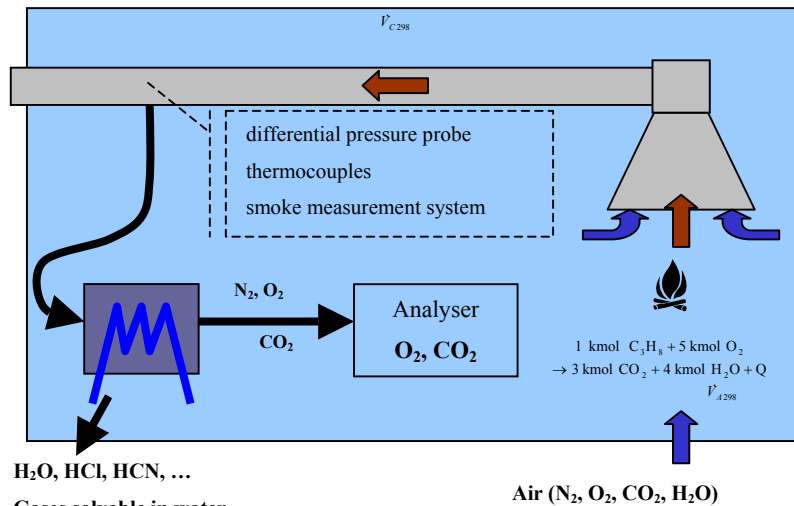
Het te testen proefmonster wordt op een trolley gemonteerd en onder een afzuigkap geplaatst. Hierna wordt de testsequentie gestart die er kort samengevat als volgt uitziet:

- -60 s - 0 s: Registratie van pre-test condities;
- 0 s - 120 s: Registratie van nultoestand-referentie en drift in afwezigheid van verbranding;
- 120 s - 300 s: Registratie van 30kW-referentie en drift met primaire brander ontstoken;
- 300 s - 1560 s: Eigenlijke test met hoofdbrander (30 kW) ontstoken op 300 s; voorbrander wordt uitgeschakeld op 300 s;
- Registratie van eindetest condities voor O<sub>2</sub>, CO<sub>2</sub> en rookmeetsysteem.

De belangrijkste signalen die gemeten worden met een bemonsteringsfrequentie van 1/3 Hz zijn:

- het massadebiet propaan dat naar de brander stroomt [mg/s];
- de zuurstofconcentratie in de verbrandingsgassen [Vol%];
- de koolstofdioxideconcentratie in de verbrandingsgassen [Vol%];
- de koolstofmonoxideconcentratie in de verbrandingsgassen [Vol%] (optioneel);
- het drukverschil over de bi-directionele sonde [Pa];
- de temperatuur ter hoogte van de bi-directionele sonde [K];
- de lichttransmissie doorheen de rookgassen [%].

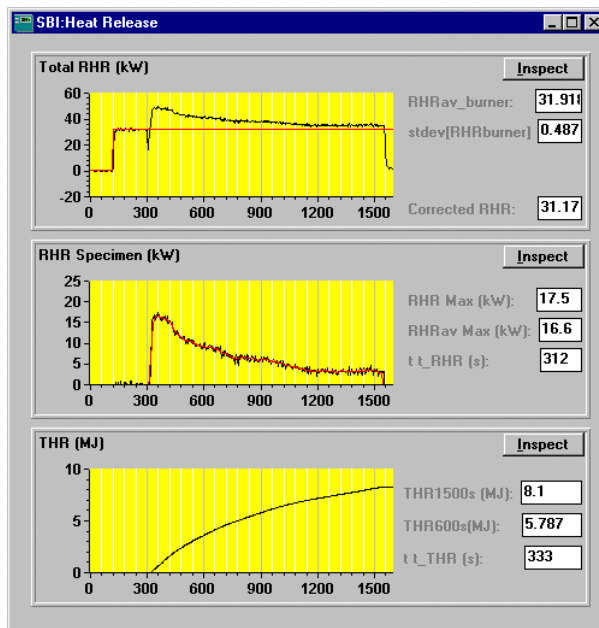
De rookgassen worden afgezogen waarna er een massadebietsmeting gebeurt in de rookgasbuizen en er een staal genomen wordt van de rookgassen. Dit rookgasstaal wordt ontdaan van alle water en van alle componenten oplosbaar in water zoals HCl, HCN, etc. Daarna wordt de zuurstof en koolstofdioxide concentratie bepaald (Figuur 3).



Figuur 3. Schematische voorstelling van het werkingsprincipe van de zuurstofdepletietechniek

Uit deze data wordt dan het HRR berekend in het verloop van de tijd. Eenmaal de test is afgerond, wordt de bijdrage van de brander tot de warmteproductie afgetrokken van de totale warmte vrijstelling. Dit gebeurt op basis van de referentieperiode van 150 s tot 270 s wanneer enkel de primaire brander ontstoken is.

De warmte vrijstelling door het materiaal wordt enerzijds geïntegreerd tot een totale warmteafgifte in de eerste 600 seconden van de test, THR<sub>600s</sub>, anderzijds gedempt met een vlakke glijdend gemiddelde filter alvorens FIGRA te berekenen. FIGRA staat voor Fire Growth Rate en wordt gedefinieerd als het maximum van de curve die ontstaat door de HRR-curve op ieder moment te delen door de verstreken tijd sinds de start van de thermische aanval. Er gelden enkele drempelwaarden waaronder FIGRA gelijk aan nul gesteld wordt.



Figuur 4. Warmte vrijstelling en afgeleiden

### 3 Gasanalyse

Gezien het belang van een correcte meting van het zuurstof en koolstofdioxide gehalte in de rookgassen, werd de gasanalyse – van monsternamen tot analyse – geoptimaliseerd door de auteur in nauwe samenwerking met Siemens België en Siemens Karlsruhe.

Dit heeft uiteindelijk geleid tot een gasanalyse-eenheid die inzetbaar is voor alle testmethoden gebaseerd op het zuurstofdepletie principe. Enkele van de belangrijke verwezenlijkingen zijn:

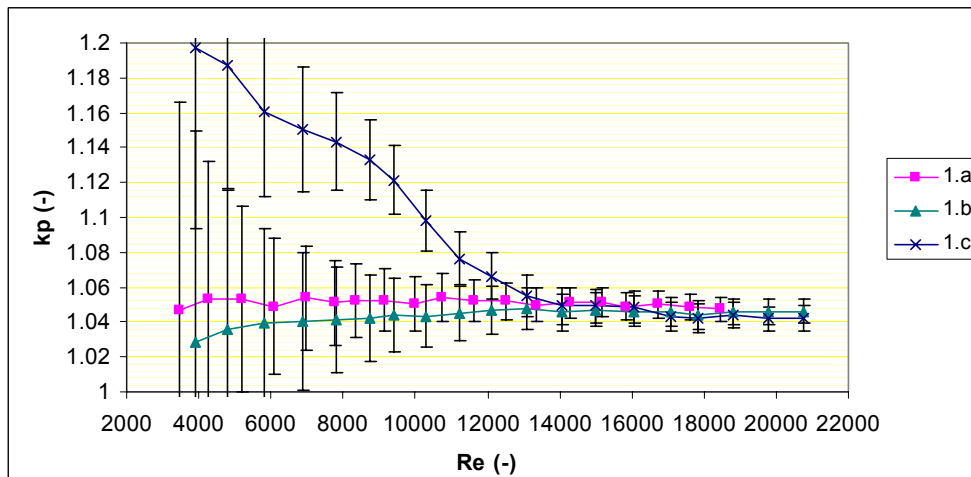
- het beperkt houden van de dode tijd (12 s) en respons tijd (3.5 s);
- het combineren van een paramagnetische zuurstofanalyser en een koolstofdioxide en koolstofmonoxide analyser (IR-principe) in één enkele 19” behuizing;
- het gebruik van omgevingslucht als referentiegas;
- de automatisering van de gasanalysekast zodanig dat deze volledig softwarematig bestuurd kan worden;
- het continu beschikbaar zijn van een diagnose van de analysekast;
- ‘plug & play’ in een compacte behuizing op wielen en met hijsogen voor gemakkelijke inzetbaarheid.



Figuur 5. Vóór en achterzijde (in een cone calorimeter eenheid) van een gasanalysekast

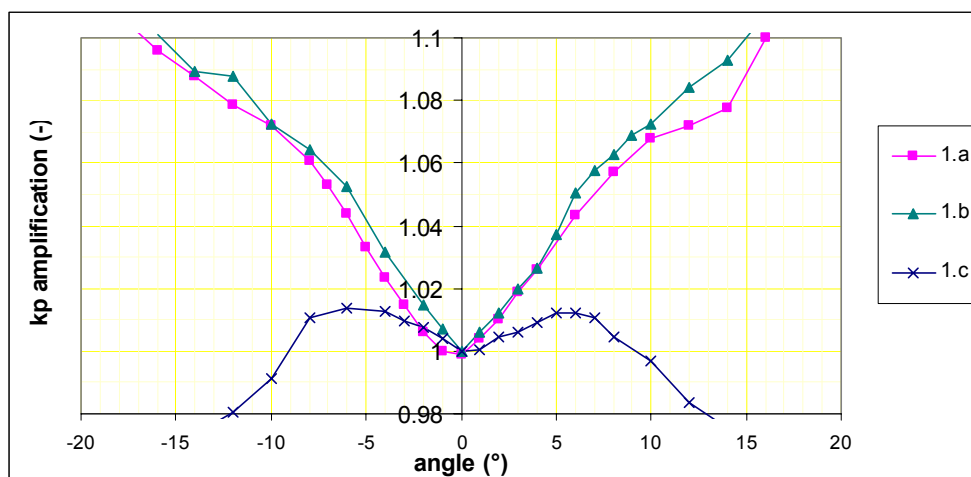


De introductie van deze positioneringstaaf heeft echter enorme gevolgen op het gedrag van de probe. De sonde wordt plots Reynoldsafhankelijk (Figuur 7/1.c) wat dus resulteert in een grote toename van de onzekerheid op de massadebietsmeting indien men de ijkfactor  $k_p$  constant veronderstelt zoals in de SBI norm wordt voorgeschreven.



Figuur 7.  $k_p$  ijkfactor i.f.v.  $Re$  (95% confidentie interval)

Verder wordt het originele ontwerp (Figuur 6.a) geëvalueerd. De originele sonde mag dan wel Reynoldsonafhankelijk zijn in een zeer ruim gebied, haar hoekafhankelijkheid t.o.v. de stroming is niet te verwaarlozen (Figuur 8/1.a).



Figuur 8. Hoekafhankelijkheid ( $Re \approx 10\ 000$ )

Er wordt voorgesteld een nieuwe, verbeterde verschildruksonde te ontwikkelen die Reynoldsonafhankelijkheid combineert met een hoekafhankelijkheid.

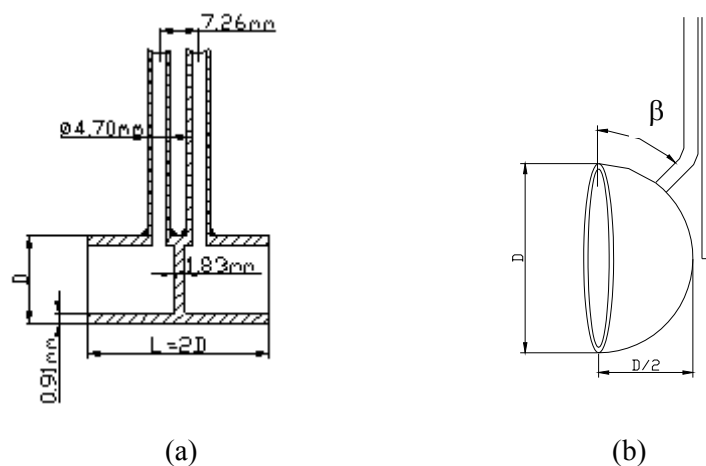
### 4.3. Artikel 2

Sette B.J.G.; *Development of a new Robust Velocity Pressure Probe for Heat Release Applications; Fire and Materials*<sup>[60]</sup>

Uit voor recensie: 1 Februari 2005

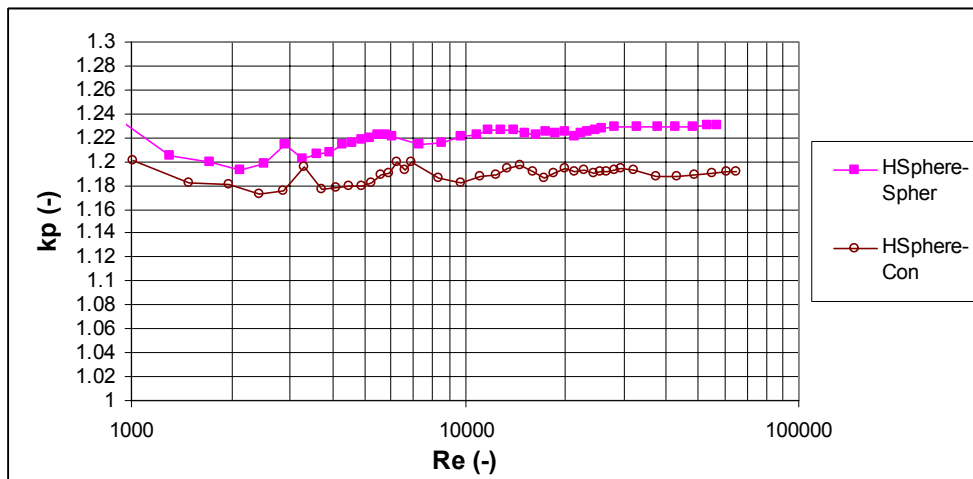
Aanvaard voor publicatie: 30 Maart 2005

Dit artikel bouwt voort op het voorgaande artikel en gaat op zoek naar alternatieven voor de bestaande bi-directionele sonde. Na evaluatie van een aantal mogelijke ontwerpen wordt het ontwerp van Figuur 9.b weerhouden. Het betreft een hemisferische sonde die met haar open zijde stroomopwaarts gericht wordt.



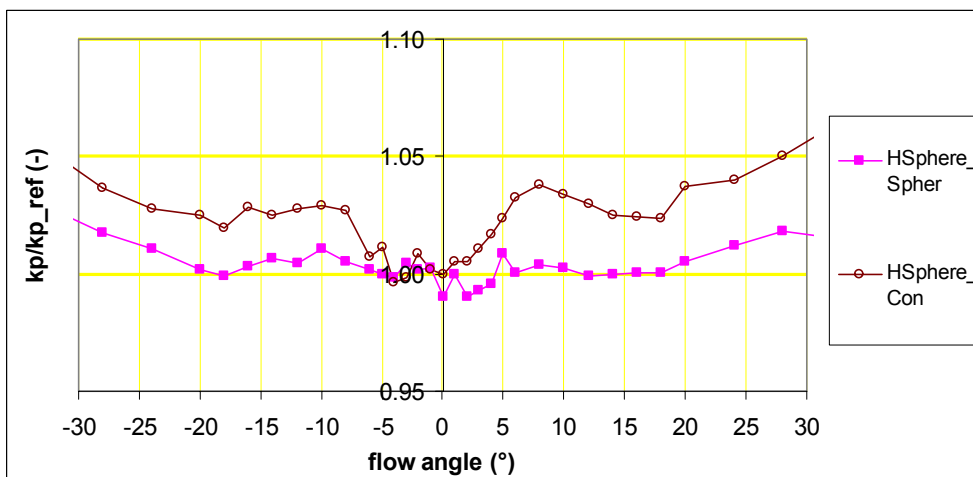
Figuur 9. a. bi-directionele sonde; b. Hemisferische sonde

Zoals getoond in Figuur 10 blijft de ijkfactor van de hemisferische sonde met hemisferische inlaat (HSphere-Spher) nagenoeg constant in een gebied van  $Re = 5\ 000$  tot  $60\ 000$ .



Figuur 10. Ijfactor voor de hemisferische sonde met sferische en met conische inlaat

Bovendien vertoont de sonde een z er grote ongevoeligheid voor hoekverdraaiingen t.o.v. de stroming in een bereik van  $\pm 20^\circ$ .



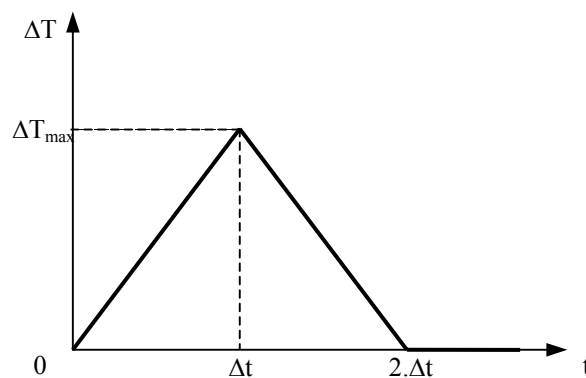
Figuur 11. Hoekafhankelijkheid ijfactor voor sferische en conische inlaat

#### 4.4. Artikel 3

Sette, B., Theuns E., Merci B., *Temperature effects on the mass flow rate in the SBI and similar Heat Release Rate Test Equipment, Fire and Materials*<sup>[61]</sup>

Uit voor recensie: 7 December 2004

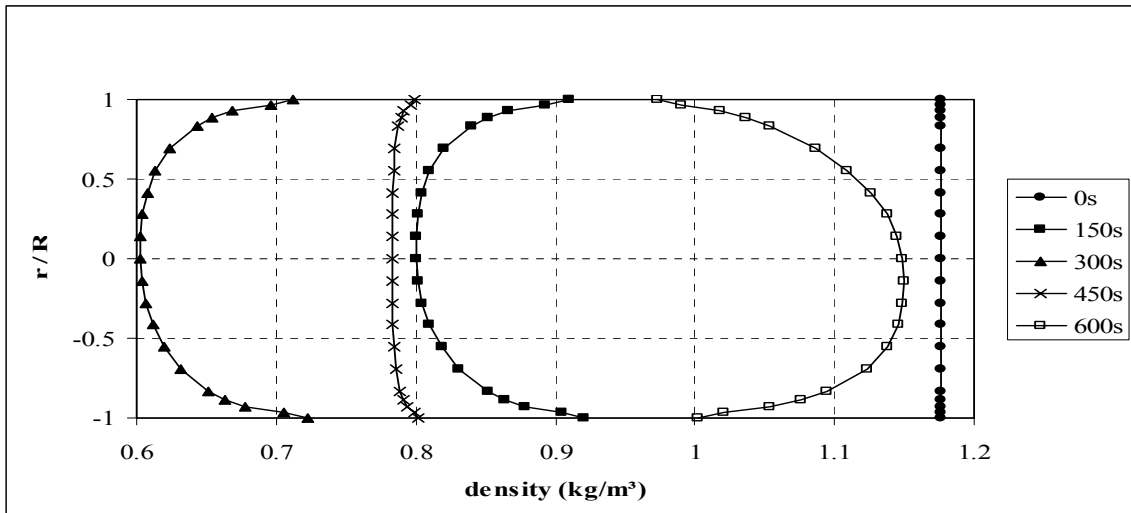
Aan de hand van een snelheids- en temperatuursmeting op de as van de rookgasbuizen wordt het massadebiet van de rookgassen bepaald op basis van het snelheidsprofiel over de buissectie. Door de sterke temperatuursverandering over het verloop van een test en door thermische traagheid van de rookgasbuizen zullen zowel het snelheidsprofiel als de densiteit van de rookgassen over de buissectie variëren in functie van de tijd en temperatuur (Figuur 13).



Figuur 12. Variatie van de temperatuur van de inkomende stroming

Langs numerische weg (CFD) wordt een schatting gemaakt van de fout die gemaakt wordt op de bepaling van het massadebiet. Dit gebeurt aan de hand van een aantal opgelegde temperatuursveranderingen aan de ingang van de buis (Figuur 12). De fout verschilt naargelang men werkt bij constant volumedebiet of constant massadebiet.





Figuur 13. Verandering van de dichtheid in de meetsectie i.f.v. de tijd.

#### 4.5. Artikel 4

*Merci B., Theuns E., Sette B., Vandeveld P.; Numerical Investigation of the Influence of Gas Heating and Cooling on the Velocity Profile Correction Factor in the SBI-Configuration; Fire and Materials<sup>[55]</sup>*

Uit voor recensie: 7 December 2004

Artikel 4 sluit aan bij artikel 3 en merkt op dat er géén éénduidig verband meer is tussen het snelheidsprofiel en het Reynoldsgetal en dit door de sterke temperatuur- en dichtheidveranderingen.

Er wordt een effectief Reynoldsgetal gedefinieerd waarbij de viscositeitsterm  $\mu$  vervangen wordt door een effectieve viscositeit  $\mu_{\text{eff}} = \mu + \mu_t$ .  $\mu_t$  is hierbij de turbulente viscositeit. Door dit te doen wordt het éénduidig verband tussen het snelheidsprofiel en het effectieve Reynoldsgetal hersteld.

## **5 Dynamisch gedrag**

### **5.1. Bandbreedte**

In hoofdstuk 5 wordt het begrip bandbreedte ingevoerd, een begrip dat welbekend is in o.a. de elektronica en de procescontrole. De bandbreedte zoals in dit werk gebruikt, is per definitie die frequentie waaronder eeningangssignaal zo goed als onvervormd doorgelaten wordt zowel in amplitude als in fase. Signalen die door een systeem gestuurd worden waarvan de bandbreedte lager is dan deze van de signalen, worden uitgesmeerd over de tijd.

In voorafgaande studies werd het dynamische gedrag van het testtoestel en van de meetinstrumenten steeds achterwege gelaten. Ofwel lag de focus van de onderzoekers op het zoveel mogelijk verkleinen van de responstijden. Deze doctoraalscriptie toont aan dat deze maatregelen ontoereikend zijn en dat dynamische aspecten in rekening dienen gebracht te worden.

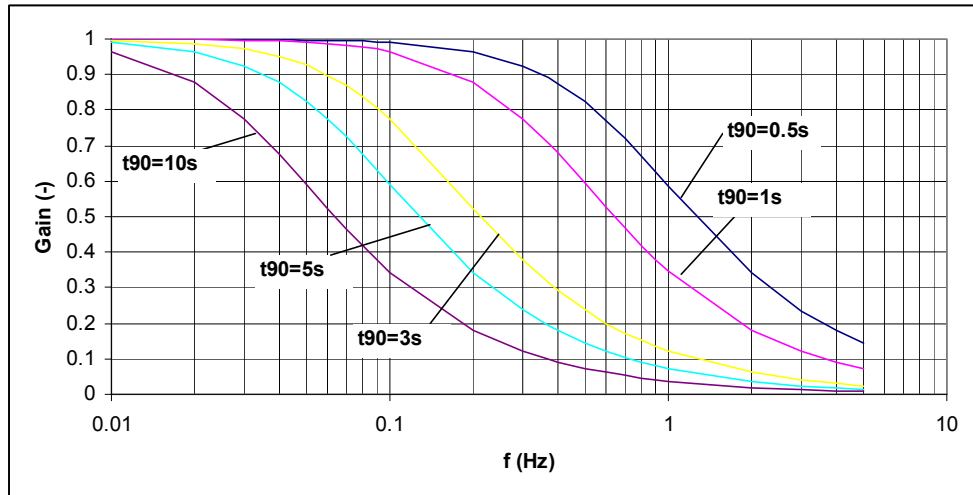
Hiertoe wordt eerst de bandbreedte bepaald van de verschillende meetinstrumenten evenals van het data-acquisitiesysteem en van de massadebietregelaar voor het sturen van de branders. Bijkomend wordt de bandbreedte bepaald van de parameteriseerbare filters die aanwezig zijn op sommige van de meetinstrumenten. Vermits weinig informatie beschikbaar wordt gesteld door de producent, is het vermoedelijke gedrag van de filters gesimuleerd via convolutie.

	$\tau$ (s)	BW (Hz)	dode tijd (s)
<b><i>Ingangsignaal</i></b>			
MFC (mg/s)	4	0.25	
<b><i>Uitgangsignaal</i></b>			
O <sub>2</sub> (Vol%)	3.5	0.29	12
CO <sub>2</sub> (Vol%)	3.5	0.29	12
$\Delta p$ (Pa)	0.5	2	3
T <sub>gas</sub> (°C)	1.15	0.87	3
T <sub>wall</sub> (°C)	220	0.0045	9
	1200	0.0008	
<b><i>Data acquisitie</i></b>			
DAQ		22	
<b><i>Elektronische demping</i></b>			
t <sub>90%</sub> = 0,5	0.22	0.7	
t <sub>90%</sub> = 1	0.43	0.3	
t <sub>90%</sub> = 3	1.30	0.1	
t <sub>90%</sub> = 5	2.17	0.07	
t <sub>90%</sub> = 10	4.34	0.03	

Tabel 1. Overzichtstabel bandbreedtes

## 5.2. Filters

Een veel voorkomend filtertype is de exponentiële filter. Deze filter wordt onder andere gebruikt in de gasanalyseapparatuur en de verschildrukopnemer. Uitzetten van de filterkarakteristieken leert ons echter dat deze filter frequenties tot ver beneden de bandbreedte beroert. Exponentiële filters hebben dus met andere woorden geen steile filterkarakteristiek.



Figuur 14. Versterking bij exponentiële filters

Verder wordt onderzocht hoe door het combineren van verschillende filters, de bandbreedte van de verschillende meetcomponenten zoveel als mogelijk gelijkgetrokken kan worden.

Ook wordt de glijdend gemiddelde filter geëvalueerd. Deze filter wordt toegepast op de HRR data alvorens FIGRA te berekenen en dit om zoveel als mogelijk ruis te onderdrukken. Deze ‘vlakke’ filter vertoont echter zwakke filterkarakteristieken en een ander type filter dringt zich op.

Er wordt een beroep gedaan op een in het vakgebied van de economie veel gebruikte glijdende filter die werkt op basis van gewogen gemiddelden. De wegingscoëfficiënten worden zo gekozen dat ze voldoende variatie overlaten om een derdegraadspolynoom te reconstrueren. De besproken filters zijn Henderson filters van verschillende orde. De orde stemt overeen met het aantal termen dat men nodig heeft in de berekening. Henderson filters met 9, 11, 13, 23 en 111 termen worden besproken en vergeleken met de vlakke filter zoals actueel gebruikt in de SBI.

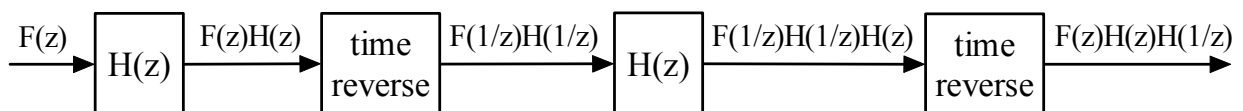
	S	bias	variance	LMSE	$1/f_c$
S11	<b>0.020</b>	0.50	0.10	0.35	$22.8 t_s$
H9	0.068	-0.10	<b>0.28</b>	0.29	$7 t_s$
H11	<b>0.022</b>	<b>-0.04</b>	<b>0.24</b>	<b>0.24</b>	$8.4 t_s$
H13	<b>0.008</b>	<b>0.04</b>	<b>0.20</b>	<b>0.20</b>	$9.8 t_s$
H23	<b>0.001</b>	0.33	0.12	<b>0.23</b>	$16.3 t_s$

Tabel 2. Vergelijk van verschillende glijdende filters

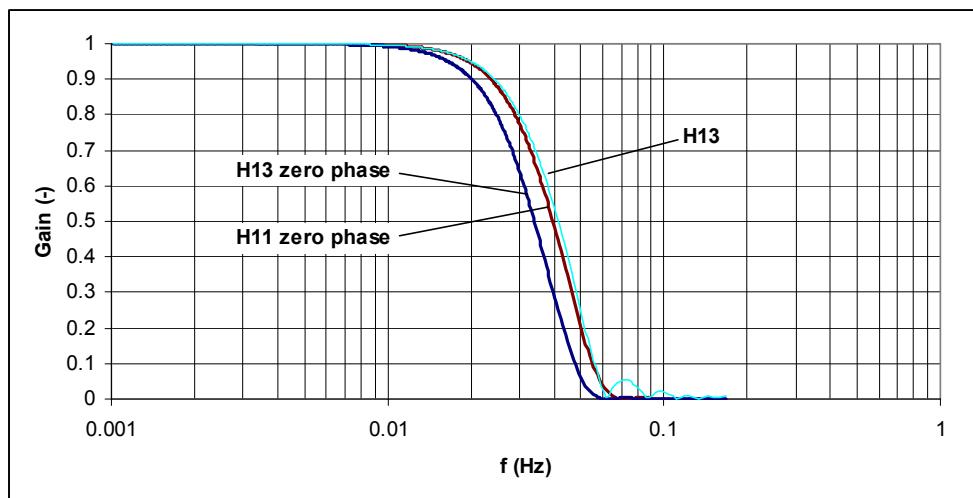
waarbij:

- $S$  een maat is voor de demping;
- bias een maat is voor de lokale fout die gemaakt wordt;
- variance een maat is voor de lokale variantie;
- LMSE de mate aangeeft waarin de locale wegingscoëfficiënten doorwegen op de berekende waarde of niet.

Verder wordt de mogelijkheid besproken om de filter tweemaal toe te passen, dit om faseverschuivingen te voorkomen. Ten dien einde dient het tijdsverloop van de data, na de eerste filterdoorgang, omgedraaid te worden zodat het laatste punt het eerste wordt enzoverder. Na de tweede filterdoorgang krijgt de data weer zijn juiste chronologische volgorde.



Uiteindelijk wordt er voor de filtering van de SBI data ( $t_s = 3$  s) gekozen voor een Henderson filter met 11 termen die tweemaal toegepast wordt (H11 ZP) om faseverschuivingen te vermijden.



Figuur 15. Versterking voor de *H13*, *H13ZP* en *H11 ZP* filters @  $t_s = 3$  s

Bij het verkleinen van de bemonsteringsperiode tot  $t_s = 0.1$  s wordt er geopteerd voor een Henderson filter met 111 termen (H111 ZP).

De keuze van de filters heeft te maken met de gewenste doorlaatfrequentie. Bij een bemonsteringsperiode van  $t_s = 3$  s verkiezen we de laagdoorlaatfilter zo te kiezen dat de

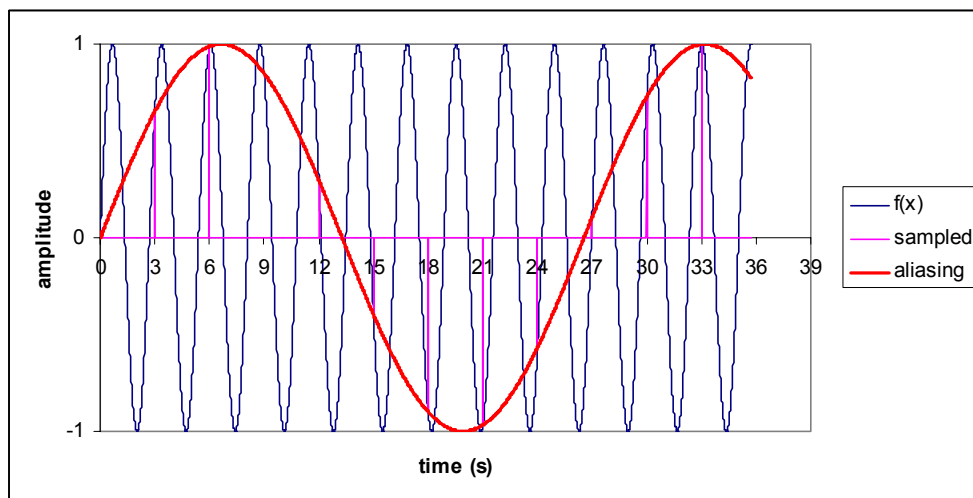
doorlaatfrequentie rond 1/30 Hz ligt. Hierbij de vuistregel indachtig dat men best minstens tien maal sneller bemonstert dan de hoogst beoogde frequentie die men tracht te capteren.

Bij een bemonsteringsperiode van  $t_s = 0.1$  s wordt gekozen de doorlaatfrequentie rond 1/10 Hz te leggen. De idee hierachter is dat gebeurtenissen met een periodiciteit die lager liggen dan 10 s niet relevant zijn voor de beoordeling van materialen op hun brandgedrag in de SBI test.

Filter	$1/f_c$
H13	$9.8 t_s$
H11 zero phase	$10.2 t_s$
H13 zero phase	$11.9 t_s$
H111 zero phase	$90 t_s$

Tabel 3. Doorlaatfrequenties

Teneinde frequentiespiegeling (aliasing) te vermijden wordt voorgesteld een analoge Butterworth filter met een doorlaatfrequentie van 1 Hz toe te passen op de inkomende signalen. Frequentiespiegeling is het fenomeen dat frequenties boven de halve bemonsteringsfrequentie worden weergegeven als lagere frequenties.



Figuur 16. Voorbeeld van frequentiespiegeling

Er wordt geopteerd voor een Butterworth filter vermits deze een vlakke versterking heeft van 1 (= ongewijzigd) onder de doorlaatfrequentie en een steile val kent voor frequenties boven de doorlaatfrequentie.

### 5.3. Voorgestelde wijzigingen

Vermits verschillende meetinstrumenten verschillende tijdsconstanten hebben en vermits tussen laboratoria onderling eveneens grote verschillen van het dynamisch gedrag der meetinstrumenten kunnen voorkomen, worden drie mogelijke pistes tot wijziging van de standaard voorgesteld.

De focus ligt hierbij op het gelijktrekken van de bandbreedtes van de meetinstrumenten en dit over alle testlaboratoria heen.

voorgestelde veranderingen	benaderde bandbreedte BW	filter
voorstel 1	1 / 30 Hz	H11 ZP @ $t_s = 3$ s
voorstel 2	1 / 10 Hz	H111 ZP @ $t_s = 0.1$ s
voorstel 3	1 Hz	inverse filter

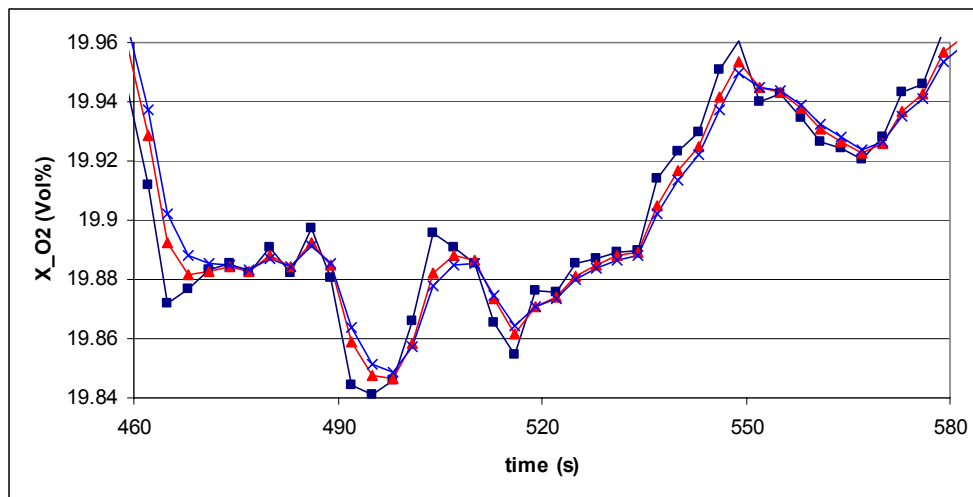
Tabel 4. benaderde bandbreedte BW van drie mogelijk veranderingspistes

Een eerste optie bestaat hierin de bandbreedte te beperken tot 1/30 Hz.

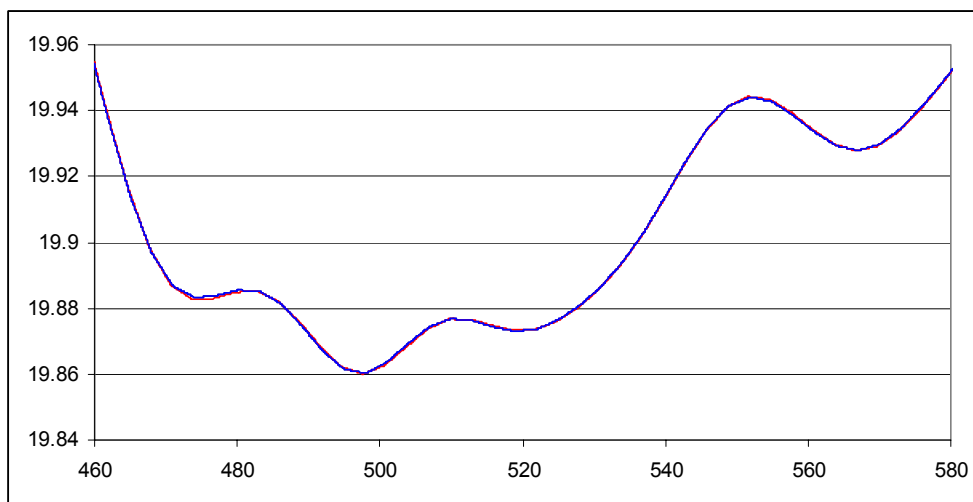
Kort samengevat wordt hiervoor als volgt tewerk gegaan.

- Digitale en/of analoge filters trekken de tijdsconstante van de tijdsveranderlijke meetcomponenten op tot een zeker niveau  $\tau$  dat gelijk is voor alle meetcomponenten.  $\tau$  is hierbij groter dan de individuele tijdsconstanten doch zo klein mogelijk.
- Een H11 ZP filter wordt toegepast op alle data ( de SBI 'running average filter' wordt achterwege gelaten).
- Data worden gesynchroniseerd gebruik makende van de maximalisatie van de Pearson correlatie coëfficiënt.

Deze maatregelen leiden tot meer dan bevredigende resultaten doch ten koste van het verlies van enige bandbreedte. Bij wijze van voorbeeld geven de volgende twee grafieken data voor en na de behandeling weer.



Figuur 17. identieke data doorheen systemen met verschillende tijdsconstanten  $\tau_1 = 0.5$  s,  $\tau_2 = 3$  s,  $\tau_3 = 5.5$  s



Figuur 18. Data na behandeling en beperking van de bandbreedte tot 1/30 Hz

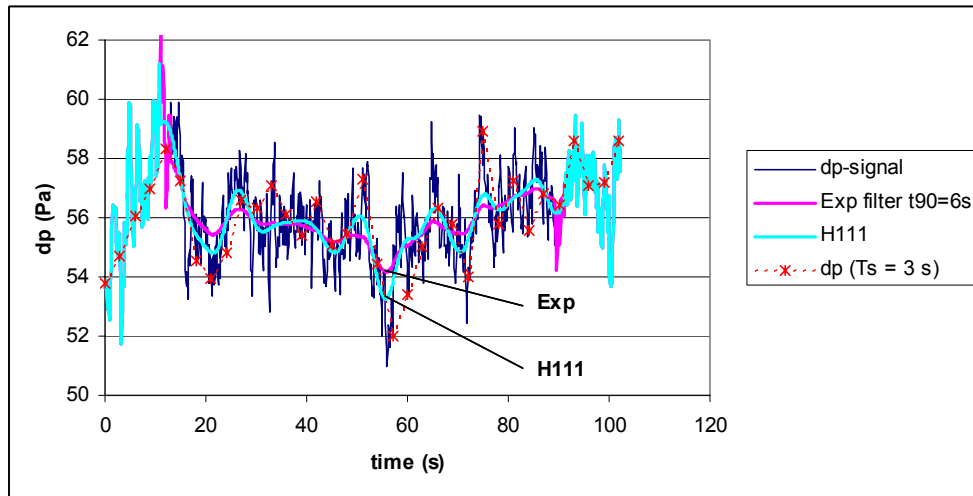
Een tweede optie bestaat erin de bandbreedte te beperken tot 1/10 Hz.

Kort samengevat wordt hiervoor als volgt tewerk gegaan:

- Alle demping op de meetinstrumenten wordt uitgeschakeld.
- Er wordt een analoge Butterworth filter toegepast met doorlaatfrequentie van 1 Hz op de inkomende data.
- De bemonsteringsfrequentie wordt opgetrokken tot 10 Hz.
- Er wordt een H111 ZP filter toegepast op alle data. Hierbij worden alle data met frequentie boven 1/10 Hz weggefilterd.

Onderstaand voorbeeld laat zien hoe deze maatregelen de data kunnen verbeteren. Hierbij wordt ook een vergelijk gemaakt met een veelgebruikte exponentiële filter.

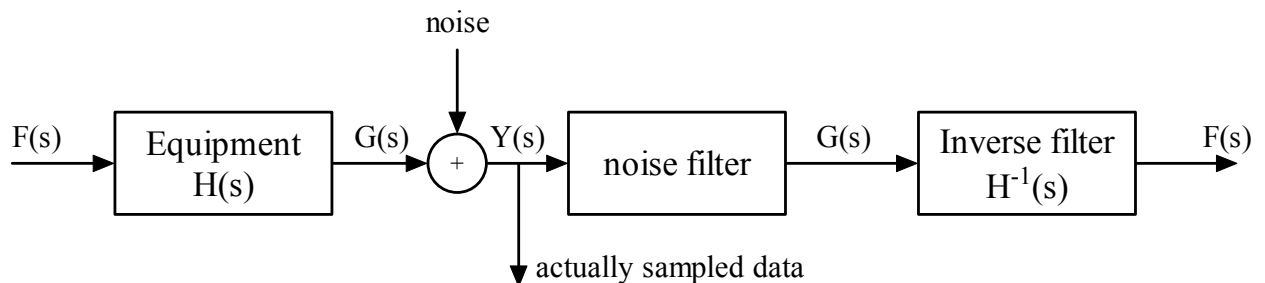




Figuur 19. Originele data, gefilterde data (*H111 ZP* and *EXP6s ZP*) en bemonsterde data ( $t_s=3s$ )

Een derde optie bestaat eruit de bandbreedte op te drijven tot 1 Hz. Vermits de bandbreedte van de gasanalysatoren lager is, dienen inverse filters toegepast te worden.

De techniek kan kort als volgt geschetst worden.

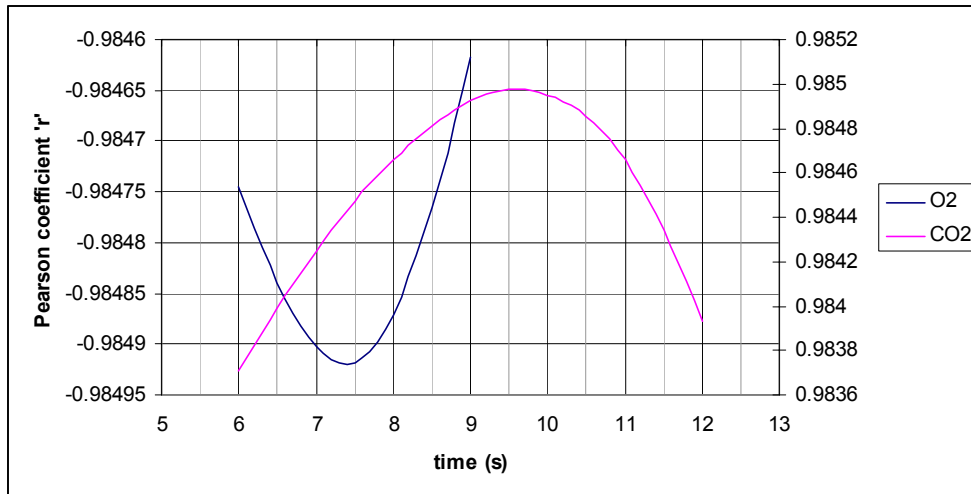


Figuur 20. Principe van een ideale inverse filter

Het grootste probleem echter bij het toepassen van deze techniek is de aanwezigheid van ruis.

Uiteindelijk wordt er gekozen voor optie twee vermits: deze ons garandeert dat frequentiespiegeling niet optreedt, deze in staat is fenomenen met een periodiciteit van 10 s te capteren, deze een betere demping en synchronisatie van de data toelaat met als resultaat een betere herhaalbaarheid en reproduceerbaarheid van de testmethode.

Tenslotte wordt er nog een alternatieve techniek voorgesteld voor het synchroniseren van data. Deze maakt gebruik van de maximalisatie van de Pearson correlatiecoëfficiënt. Onderstaande figuur geeft de Pearson coëfficiënt weer in functie van de tijdsverschuiving van de O<sub>2</sub>-data en de CO<sub>2</sub>-data.



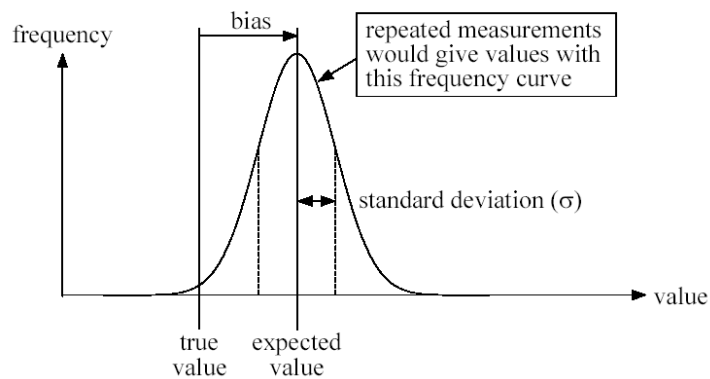
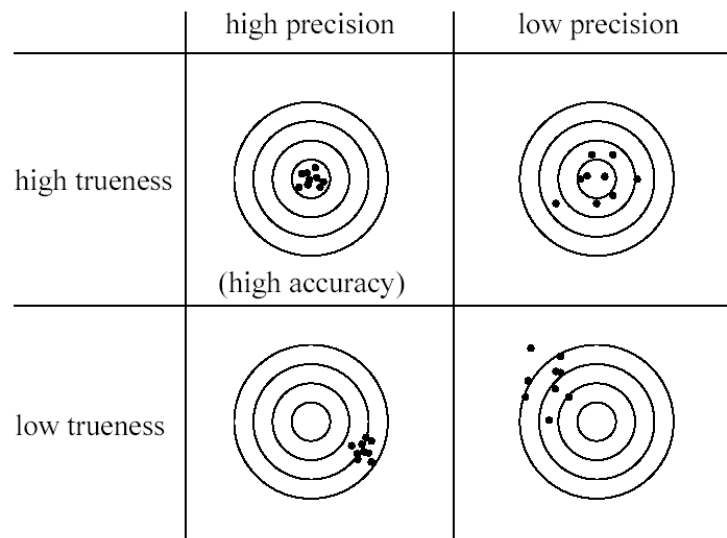
Figuur 21. Synchronisatie van data d.m.v. maximalisatie van de Pearson coëfficiënt

## 6 Onzekerheid

Overeenkomstig EN ISO 17025<sup>[9]</sup>, *Algemene vereisten omtrent de competenties van test- en kalibratielaboratoria*, en ISO 10012-1<sup>[14]</sup>, *omtrent het verzekeren van de kwaliteit van meetapparatuur*, dienen onzekerheden op de metingen opgenomen te worden in zowel de test als kalibratierapporten. De algemene principes voor het evalueren en het rapporteren van onzekerheden worden beschreven in de Richtlijn tot het bepalen van onzekerheden op metingen, GUM<sup>[13]</sup>, maar dienen geïnterpreteerd en toegepast te worden op brandtesten.

Het kwalitatieve concept van echtheid (accuracy) wordt gekwantificeerd door de onzekerheid (uncertainty). Beiden zijn invers proportioneel met elkaar. Echtheid omhelst zowel juistheid (trueness) als betrouwbaarheid (precision) zoals getoond op onderstaande figuur. De juistheid wordt numeriek weergegeven door de systematische fout (bias) terwijl de betrouwbaarheid voorgesteld wordt door de standaard afwijking (standard deviation).

Er wordt van de laboratoria verwacht dat men systematische fouten uitschakelt. Echter, indien de systematische fout niet gekwantificeerd kan worden, mag ze beschouwd worden als een willekeurige (random) fout. Random fouten resulteren in een spreiding van de waarden en kunnen meestal verkleind worden door het aantal observaties te verhogen. De verwachte waarde voor random fouten is nul.



Figuur 22. Concept van echtheid (onzekerheid), juistheid en betrouwbaarheid

Volgens de GUM dient ieder rapport omtrent onzekerheid een volledige lijst te bevatten van de componenten die gebruikt werden om tot de onzekerheid te komen. De componenten worden veelal in twee categorieën onderverdeeld naargelang de wijze waarop ze geëvalueerd worden:

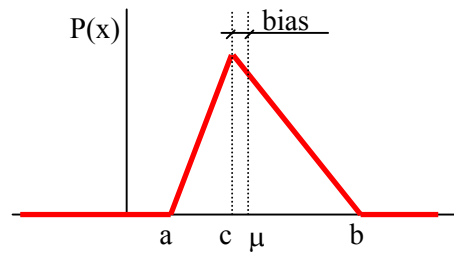
Type A De componenten in categorie A worden gekarakteriseerd door de geschatte varianties  $s_i^2$  of door de geschatte standaard afwijking  $s_i$  en dit gebruik makende van statistische methoden.

Voor dergelijke componenten wordt de standaard onzekerheid  $u_i = s_i$ .

Type B De componenten in categorie B worden geschat op basis van specificaties, kalibraties, literatuur, ervaring, etc. en worden voorgesteld door  $u_j$ . De numerieke waarde wordt bekomen door middel van een onderstelde probabiliteitsdistributie.

Waar nodig dienen ook covarianties in beschouwing genomen te worden.

De distributies beschouwd in deze doctoraalscriptie zijn de normale distributie, de rechthoekige distributie en de triangulaire distributie. Verder worden er ook asymmetrische distributies beschouwd, waarvan hieronder een voorbeeld is gegeven.



Figuur 23. Asymmetrische triangulaire distributie

Voor asymmetrische distributies wordt het verschil tussen de gemiddelde waarde  $\mu$  en  $c$  beschouwd als een systematische fout. Overeenkomstig GUM wordt hiervoor dus gecorrigeerd.

In deze doctoraalscriptie worden covarianties tussen de signalen van de zuurstofanalyse, koolstofdioxide analyse, verschilddrukopnemer en thermokoppels in rekening gebracht. De wenselijkheid hiervoor kan eenvoudig ingezien worden door het beschouwen van volgend voorbeeld:



Bij verbranding van propaan wordt voor ieder molair volume verbruikte zuurstof, 3/5 mol koolstofdioxide geproduceerd. Er bestaat in voorgaand geval dus een perfecte negatieve correlatie tussen deze twee. Ook zal door de verbranding de temperatuur stijgen en de volumestroom verhogen (bij constant massadebiet) wat resulteert in een negatieve correlatie tussen zuurstof en temperatuur enerzijds en tussen zuurstof en verschilddruk anderzijds. Onderstaande tabel geeft de correlatiecoëfficiënten weer voor een brandtest op een vezelplaat.

		O2-raw	CO2-raw	Tms-raw	dp-raw
O2-raw	Pearson Correlation	1	-.996**	-.985**	-.912**
	Sig. (2-tailed)	.	.000	.000	.000
	N	16676	16676	16676	16676
CO2-raw	Pearson Correlation	-.996**	1	.985**	.912**
	Sig. (2-tailed)	.000	.	.000	.000
	N	16676	16676	16676	16676
Tms-raw	Pearson Correlation	-.985**	.985**	1	.930**
	Sig. (2-tailed)	.000	.000	.	.000
	N	16676	16676	16676	16676
dp-raw	Pearson Correlation	-.912**	.912**	.930**	1
	Sig. (2-tailed)	.000	.000	.000	.
	N	16676	16676	16676	16676

\*\* . Correlation is significant at the 0.01 level (2-tailed).

Tabel 5. Correlaties tussen  $XO_2$ ,  $XCO_2$ ,  $T_{ms}$  en  $\Delta p$  voor een test op een vezelplaat

Indien niet kan gecorrigeerd worden voor systematische fouten bijvoorbeeld omwille van achterwaartse compatibiliteit van testdata, kan men het onzekerheidsinterval uitbreiden. Over hoe dergelijke gevallen behandeld dienen te worden, blijft de GUM in gebreke. Er wordt voorgesteld de techniek voorgesteld door Phillips et al<sup>[58]</sup> te volgen omwille van zijn conservatieve benadering. Deze methode telt de systematische fout op bij de geëxpandeerde onzekerheid U tenzij de systematische fout groter is:

$$Y = y_{-U}^{+U} \quad [ 6.2 ]$$

waarbij

$$U^+ = \begin{cases} ku_c - \delta & \text{if } ku_c - \delta > 0 \\ 0 & \text{if } ku_c - \delta \leq 0 \end{cases} \quad [ 6.3 ]$$

en

$$U^- = \begin{cases} ku_c + \delta & \text{if } ku_c + \delta > 0 \\ 0 & \text{if } ku_c + \delta \leq 0 \end{cases} \quad [ 6.4 ]$$

De gecombineerde standaard onzekerheid wordt dan uitgewerkt voor HRR evenals de hiervan afgeleide classificatieparameters. Dit vereist een cascade van onzekerheidsbepalingen die eindigt bij de samenstellende componenten.

Een uitgebreide studie werd gedaan ter bepaling van de onzekerheid van de samenstellende componenten. Dit resulteerde, naast een schatting van de onzekerheid van de verschillende componenten, in een reeks van vier artikels zoals weergegeven in hoofdstuk 4.

Nieuw in deze doctoraalscriptie was het in rekening brengen van covarianties, het in rekening brengen van transiënte fenomenen en het in rekening brengen van de onzekerheid op de synchronisatie van data.

Verder worden de onzekerheden bepaald in functie van de tijd vermits ze vaak afhankelijk zijn van de hoeveelheid warmte die wordt vrijgesteld.

Voorts worden er verschillende suggesties gegeven tot verbetering van de onzekerheid op de verschillende individuele componenten:

- Door gebruik te maken van een RTD weerstand ter bepaling van de omgevingstemperatuur i.p.v. een thermokoppel, kan de onzekerheid op de temperatuurbepaling teruggedrongen worden met een factor 10.
- Door een parameter (c) werkelijk te gaan berekenen i.p.v. haar constant te onderstellen kan een winst geboekt worden op de onzekerheid van een factor 10 of meer. De geboekte winst is afhankelijk van omgevingsvoorwaarden zoals druk, temperatuur en vochtigheid.
- Door roetaanslag en thermische vervormingen kan er een systematische fout optreden bij het bepalen van de doorsnede van de rookgasbuizen. Er wordt voorgesteld deze systematische fout te elimineren.
- Een sterke vermindering van de onzekerheid op de verschildruksondefactor kan verkregen worden door een wijziging aan het bestaande ontwerp. Twee voorstellen worden hier geformuleerd. Ofwel wordt er teruggegrepen naar een oudere versie van de sonde, ofwel – en dit geniet de voorkeur – wordt de sonde vervangen door de nieuw ontwikkelde hemi-sferische sonde zoals beschreven in hoofdstuk 4.
- Door gebruik te maken van afgeschermd thermokoppels in de rookgaskanalen kan een verbetering van om en bij de 30% gerealiseerd worden op de onzekerheid van deze temperatuursmeting.

## 7 Evaluatie en resultaten van het Analytisch Model

### 7.1. Inleiding

In dit hoofdstuk wordt alle informatie van de vorige hoofdstukken samengebracht in één analytisch onzekerheidsmodel. Het model omvat de cascade van alle onzekerheden.

Vermits verschillende van de samenstellende onzekerheden direct of indirect afhankelijk zijn van de warmtevrijstelling in de test, is de globale onzekerheid functie van de tijd en dus niet te vatten in één enkel getal. In dit hoofdstuk wordt het model daarom toegepast op werkelijke test data.

Vooreerst wordt het model geëvalueerd op basis van vergelijkingen met de resultaten van SBI RR2. Dit ringonderzoek is een alternatieve, onafhankelijke methode ter bepaling van de onzekerheid. De vergelijking gebeurt op basis van de *herhaalbaarheidslimiet*<sup>[15]</sup> van de classificatieparameters FIGRA en THR600s.

Vervolgens wordt het model aangewend om de suggesties tot wijziging van de norm, zoals voorgesteld in hoofdstukken 5 en 6, te evalueren.

### 7.2. Evaluatie van het Model

Onderstaande tabel geeft de herhaalbaarheidslimiet  $r/m$  weer van drie producten zoals ze getest werden in het kader van SBI RR2. Negen laboratoria voerden in totaal 27 tests uit per product ter bepaling van de onderstaande waarden.

	<b>P1: Faced glass wool</b>		<b>P2: MDF board</b>		<b>P3: Plastisol coated steel</b>	
	Figra (W/s)	THR <sub>600s</sub> (MJ)	Figra (W/s)	THR <sub>600s</sub> (MJ)	Figra (W/s)	THR <sub>600s</sub> (MJ)
<b>SBI RR2 test resultaten van 9 laboratoria</b>						
m (gemiddelde)	17	1.0	455	25	257	1.8
r	9	0.2	31	1	41	0.3
<b>r/m</b>	<b>52 %</b>	<b>22 %</b>	<b>7 %</b>	<b>4 %</b>	<b>16 %</b>	<b>17 %</b>

Tabel 6. Herhaalbaarheidslimieten voor producten P1-P3 via ringonderzoek

Vergelijken we dit met de herhaalbaarheidslimiet verkregen langs analytische weg zoals uiteengezet in deze doctoraalscriptie, dan bekomen we onderstaande tabel. Om de resultaten met elkaar te kunnen



vergelijken werden de onzekerheden tengevolge van transiënte fenomenen genegeerd evenals de systematische fouten zoals besproken in hoofdstuk 6.

Dit maakt dat de verwachting is dat de herhaalbaarheidslimiet uit het ringonderzoek hoger zal zijn dan deze die volgt uit het analytische model.

	<b>P1: Faced glass wool</b>		<b>P2: MDF board</b>		<b>P3: Plastisol coated steel</b>	
	Figra (W/s)	THR <sub>600s</sub> (MJ)	Figra (W/s)	THR <sub>600s</sub> (MJ)	Figra (W/s)	THR <sub>600s</sub> (MJ)
<b>Analytisch model (onderstelling: glijdend gemiddelde op HRR reduceert onzekerheid)</b>						
<b>r/m (Sample 1)</b>	<b>36.8 %</b>	<b>14.3 %</b>	<b>5.5 %</b>	<b>1.4 %</b>	<b>12.6 %</b>	<b>12.2 %</b>
<b>r/m (Sample 2)</b>	<b>79.6 %</b>	<b>34.4 %</b>	<b>5.9 %</b>	<b>1.7 %</b>	<b>12 %</b>	<b>10 %</b>
<b>r/m (Sample 3)</b>	<b>33 %</b>	<b>14.8 %</b>	<b>5.5 %</b>	<b>1.4 %</b>	<b>16.5 %</b>	<b>13.3 %</b>
<b>Analytisch model (onderstelling: glijdend gemiddelde op HRR reduceert onzekerheid niet)</b>						
r/m (Sample 1)	120.3 %	15.1 %	17.4 %	1.6 %	48.6 %	13 %
r/m (Sample 2)	259.2 %	35.4 %	18.1 %	1.7 %	39.2 %	10 %
r/m (Sample 3)	108.9 %	15.8 %	16.3 %	1.4 %	51.6 %	13.3

Tabel 7. Herhaalbaarheidslimieten voor producten P1-P3 via analytische modellering

De herhaalbaarheidslimiet  $r/m$  zoals berekend door het model ligt in de lijn van de resultaten van het ringonderzoek. Over het algemeen is de herhaalbaarheidslimiet van het model iets lager dan van het ringonderzoek. Dit kan redelijkerwijs verklaard worden doordat enerzijds transiënte fenomenen verwaarloosd werden zoals hierboven kort besproken en anderzijds door de kwalitatief goede data van het Gentse testlaboratorium. De brandafdeling van de Universiteit Gent heeft steeds een voortrekkersrol gespeeld in de ontwikkeling en verbetering van op zuurstofdepletie gebaseerde testtoestellen.

Deze resultaten suggereren dat het analytische model gebruikt kan worden ter schatting van het onzekerheidsinterval bij routinematige testen. Merk hierbij op dat het model voor iedere individuele test een onzekerheidsanalyse kan uitvoeren, dit in tegenstelling tot het grootschalige ringonderzoek dat een groot aantal laboratoria en tests vereist.

Bijkomend dient er opgemerkt te worden dat er een zeer grote spreiding is op de resultaten, bekomen uit het ringonderzoek bij het testen van verschillende materialen. Dit wordt weergegeven in onderstaande tabel die overgenomen werd uit het SBI RR2 project.

	FIGRA <sub>0,2MJ</sub>	FIGRA <sub>0,4MJ</sub>	THR <sub>600s</sub>
Aantal producten	9	9	9
Bereik r /m	7 - 70 %	7 - 93 %	4 - 35 %
Gemiddelde r /m	32 %	38 %	23 %
Aantal producten *	5	4	2
Bereik r /m *	7 - 29 %	7 - 35 %	4 - 27 %
Gemiddelde r /m *	16 %	20 %	16 %

\*: producten met een zeer lage gemiddelde waarden – die minder relevant zijn voor de classificatie – werden uitgesloten

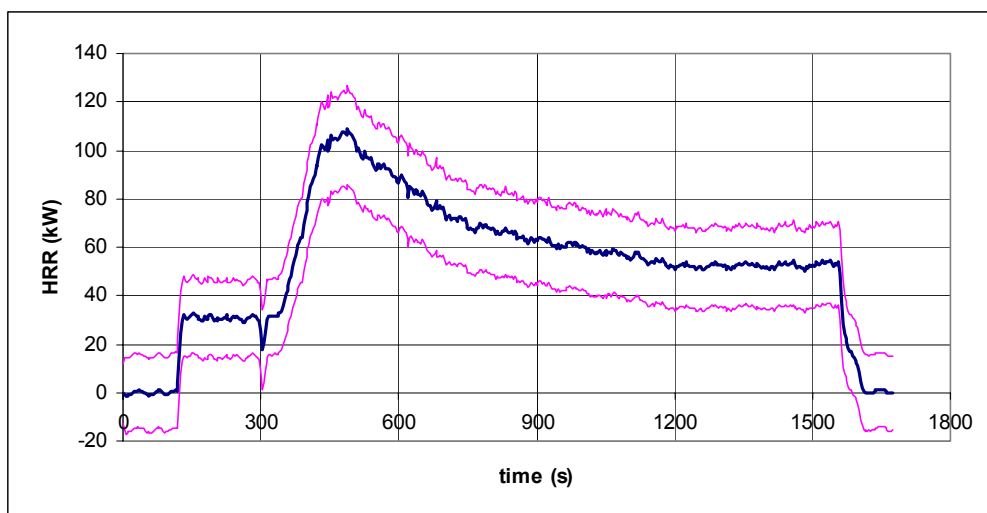
Tabel 8. Herhaalbaarheidslimieten uit het ringonderzoek SBI RR2

### 7.3. Gebruik van het model ter verbetering van de testmethode

In deze sectie worden zes cases besproken die gaan van zéér conservatieve benaderingen ter bepaling van de meetonzekerheid, tot geoptimaliseerde meet- en berekenmethoden ter verbetering van de meetonzekerheid.

Alle berekeningen werden uitgevoerd op eenzelfde gegevensset.

**Case 1** gaat uit van de meest conservatieve onderstellingen wat betreft de bepaling van de onzekerheid op transiënte fenomenen. De onzekerheid op de transiënt wordt vast verondersteld en wordt bepaald op basis van een ‘worst case scenario’. De standaard onzekerheid op de warmte vrijstelling bij 30 kW wordt geschat op 26%. Onderstaande figuur geeft de warmte vrijstelling in functie van de tijd tezamen met een 95% confidentialiteitsinterval.



Figuur 24. HRR curve met 95% confidentieinterval ( $k = 2$ ) (case 1)

De grootste bijdrage tot de onzekerheid van om en bij de 22% wordt geleverd door de meting van het zuurstofgehalte in de rookgassen.

De tweede grootste bijdrage wordt geleverd door de verschildruksonde.

**Case 2** bekijkt de onzekerheid indien een aantal vrij eenvoudig te implementeren verbeteringen aangebracht zouden worden.

- Door gebruik te maken van een RTD weerstand ter bepaling van de omgevingstemperatuur i.p.v. een thermokoppel kan de onzekerheid op de temperatuurbepaling terug gedrongen worden met een factor 10.
- Door een parameter (c) werkelijk te gaan berekenen i.p.v. van haar constant te houden kan een winst geboekt worden op de onzekerheid van een factor 10 of meer. De geboekte winst is afhankelijk van omgevingsvoorwaarden zoals druk, temperatuur en vochtigheid.
- Door roetaanslag en thermische vervormingen kan er een systematische fout optreden bij het bepalen van de doorsnede van de rookgasbuizen. Er wordt voorgesteld deze systematische fout te elimineren.
- Een sterke vermindering van de onzekerheid op de verschildruksondefactor kan verkregen worden door een wijziging aan het bestaande ontwerp. Twee voorstellen worden hier geformuleerd. Ofwel wordt er teruggesproken naar een oudere versie van de sonde, ofwel – en dit geniet de voorkeur – wordt de sonde vervangen door de nieuw ontwikkelde hemi-sferische sonde zoals beschreven in hoofdstuk 4.
- Door gebruik te maken van afgeschermd thermokoppels in de rookgaskanalen kan een verbetering van om en bij de 30% gerealiseerd worden op de onzekerheid van deze temperatuursmeting.

De bijdrage tot de onzekerheid bij een niveau van 30 kW vermindert van 7.2% tot 3%. De meest efficiënte maatregelen hiertoe zijn in volgorde van belangrijkheid:

- de vervanging van de bi-directionele verschildruksonde;
- het berekenen van de constant onderstelde parameter 'c';
- het elimineren van de systematische fout op de sectiebepaling van de rookgasleiding;
- het gebruik van een RTD weerstand ter bepaling van de omgevingstemperatuur;
- het gebruik van afgeschermd thermokoppels in de rookgaskanalen.

Deze laatste maatregel heeft slechts een verwaarloosbaar effect en kan zodoende achterwege gelaten worden.

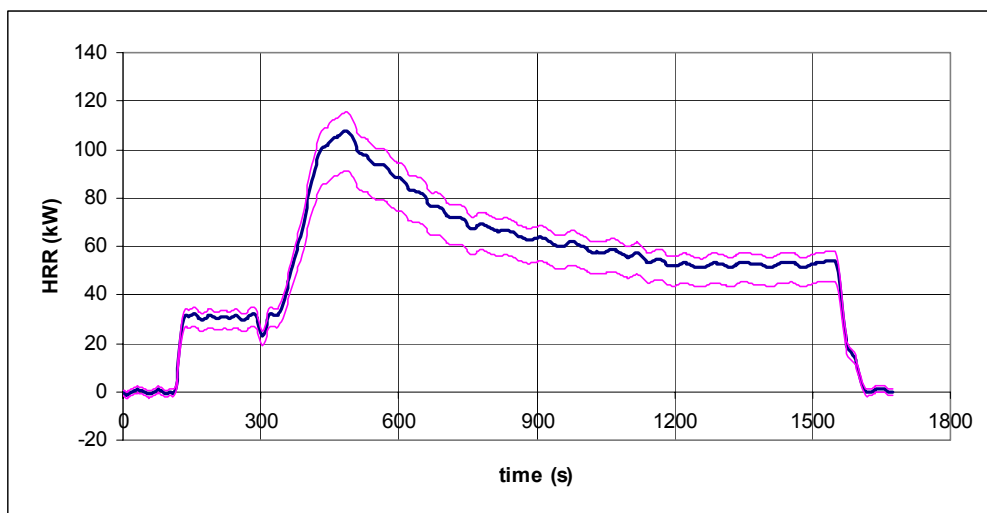
**Cases 3 en 4** voeren de voorgestelde veranderingen ter beperking van de bandbreedte door zoals besproken in hoofdstuk 5. Case 3 behandelt het geval waarbij de bandbreedte beperkt wordt tot 1/30 Hz, terwijl Case 4 het geval behandelt waarbij de bandbreedte beperkt wordt tot 1/10 Hz.

In beide gevallen vermindert de bijdrage tot de onzekerheid van de depletiefactor bij een niveau van 30 kW van 23% tot minder dan 2%.

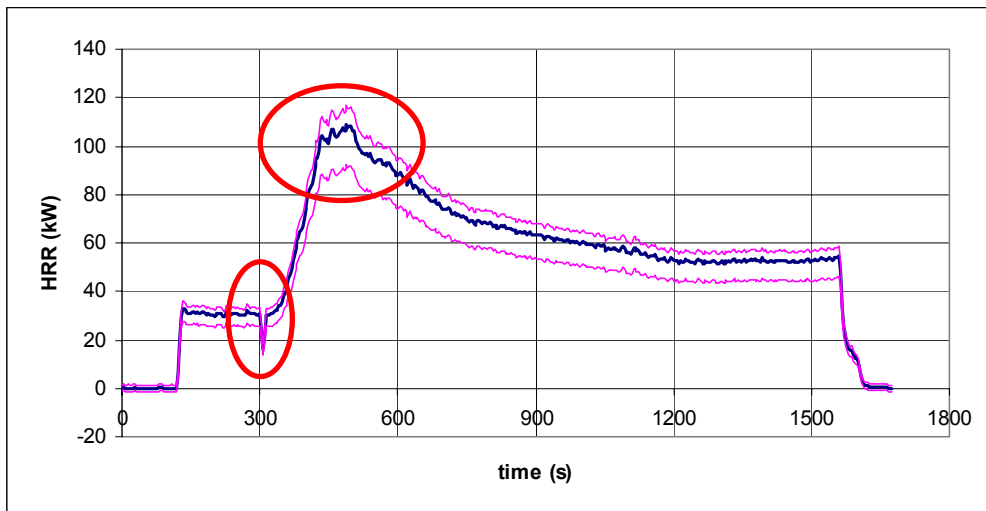
Het verschil tussen de twee cases zit niet zozeer in de reductie van de onzekerheid, doch in de verbetering van de kwaliteit van de meting en dit in:

- de verhoging van de bandbreedte (de verhoging van de bandbreedte van 1/30 Hz tot 1/10 Hz heeft tot gevolg dat er meer detail, meer variatie overblijft in de data zoals zichtbaar bij het vergelijken van de twee onderstaande figuren);
- het volledig verwijderen van mogelijke frequentiespiegeling (frequentiespiegeling introduceert schijnbare variaties op de data die in werkelijkheid niet bestaan);
- de betere mogelijkheden tot correct synchroniseren van de data.

Vanuit het oogpunt van de meting worden met case 4 betere herhaalbaarheden en reproduceerbaarheden gehaald.



Figuur 25. HRR curve met 95% confidentie interval ( $k = 2$ ) (case 3)

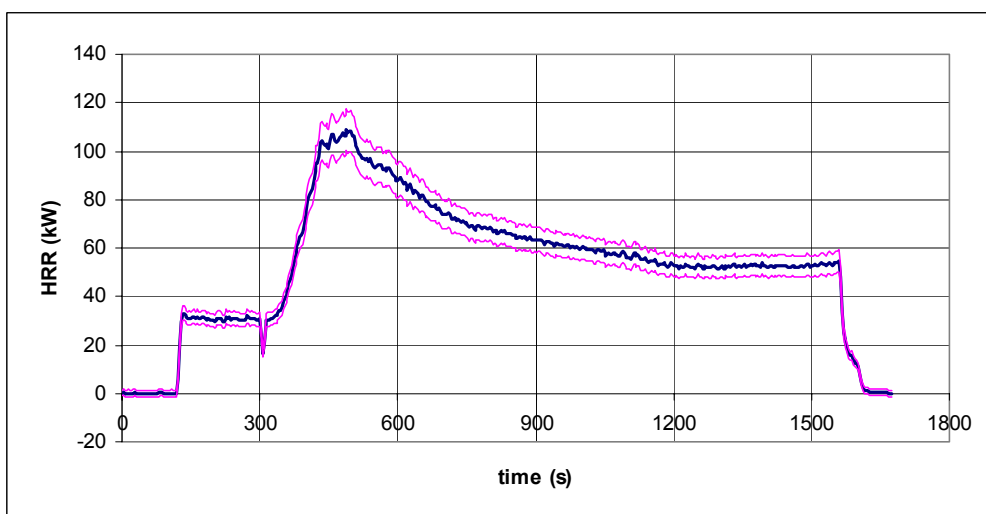


Figuur 26. HRR curve met 95% confidentie interval ( $k = 2$ ) (case 4)

**Cases 5 en 6** combineren cases 3 respectievelijk 4 met de verandering voorgesteld in case 2. Dit resulteert voor case 6 tenslotte in een standaard onzekerheid van om en bij de 5% voor het 30 kW niveau i.p.v. de 26% voor case 1.

Verder zakt de herhaalbaarheidslimiet  $r/m$  op FIGRA van 15 % naar 5.4 % en op THR600s van 4.2 % naar 1.4 %.

Een en ander wordt weergegeven in onderstaande grafiek en tabellen.



Figuur 27. HRR curve met 95% confidentie interval ( $k = 2$ ) (case 6)

top level (relevant voor HRR)	sub-level (relevant voor $X_i$ )	bijdrage tot $u(X_i)$	bijdrage tot $u(\text{HRR}_{30\text{kW}})$
Grootheid $X_i$	Grootheid $x_i$	$c(x_i).u(x_i)/X_i$ (%)	$c(X_i).u(X_i)/\text{HRR}$ (%)
$V_{\text{Droog}}$			3.47372
	c	0.71429	
	A	0.5646	
	$k_r$	1.75234	
	$k_n$	1.94444	
	$\Delta n$	0.76359	
	$T_{\text{me}}$	0.5179	
$\phi$			1.66269
	X $O_2$	1.45348	
	X $CO_2$	0.73567	
	X $O_2^\circ$	0.30545	
	X $CO_2^\circ$	0.16023	
E			2.55814
$X_{O_2}^{\text{D}}$			0.10913
	X $O_2^\circ$	0.00348	
	H	0.03003	
	n bar	0.00092	
	T room	0.10486	
$\alpha$			0.08648
standaard onzekerheid op HRR (exclusief crosscorrelaties)			<b>4.22624</b>
standaard onzekerheid op HRR (inclusief crosscorrelaties)			<b>4.48484</b>

Tabel 9. Onzekerheidsanalyse bij HRR = 30kW (case 6)

k = 2 (95%)	m	U+(m)	U-(m)	U+/m	U-/m	r/m
FIGRA (W/s)	517.4	19.7	19.7	3.8 %	3.8 %	5.4 %
THR600s (MJ)	27.14	0.26	0.26	1 %	1 %	1.4 %
MARHE (kW)	49.48	0.6	0.6	1.2 %	1.2 %	1.7 %

Tabel 10. Onzekerheidsanalyse op de classificatieparameters and MARHE value (k = 2) (case 6)

Naast de onzekerheidsbepaling op de classificatieparameters FIGRA en THR600s werd er ook een onzekerheidsbepaling gedaan op de parameter MARHE. Hoewel MARHE noch vereist noch beschreven staat in de SBI norm werd de onzekerheid op deze parameter toch mee geschat vermits dit een wezenlijke bijdrage kan leveren in de gaande discussie of FIGRA al dan niet vervangen dient te worden door een andere parameter, eventueel MARHE.

Louter en alleen gebaseerd op de onzekerheidsbepaling genieten de parameters MARHE en THR600s de voorkeur op FIGRA. Verder onderzoek in hoeverre MARHE correleert met resultaten uit het

grootschalige referentiescenario is echter noodzakelijk en weegt zwaarder door dan de merkelijk betere schatting van de onzekerheid.

## 8 Besluiten

De SBI testmethode is ontwikkeld als resultaat van de tenuitvoerlegging van de Bouwproductenrichtlijn (CPD) 89/106/CE in Europa en wordt nu gebruikt om de reactie bij brand performantie van bouwproducten, exclusief bevloeringen, in de Europese Unie te beoordelen.

De ontwikkeling van de SBI testmethode werd bevolen door de Europese Commissie en werd uitgevoerd onder directe begeleiding van de Groep van Regelgevers i.v.m. brandzaken. Een consortium van negen test laboratoria werd opgericht. Het doel was een testmethode te ontwikkelen waarvan de resultaten representatief zijn voor het gedrag van bouwproducten wanneer deze blootgesteld worden aan typisch één enkel brandend voorwerp, b.v. een brandende papiermand in de hoek van een kamer.

Een grootschalig ringonderzoek toonde aan dat de SBI testmethode in staat is de vereiste brandkenmerken op een herhaalbare en reproduceerbare manier te bepalen en dit op een aanvaardbaar niveau. Er werd echter wel geëist dat er gezocht zou worden naar enkele technische verbeteringen.

Daarnaast maakt de internationale norm EN ISO 17025:1999<sup>[9]</sup> die algemene eisen stelt ten aanzien van de bekwaamheid van test- en kalibratielaboratoria de rapportering van onzekerheid op testresultaten verplichtend.

Deze twee factoren vormen de directe aanleiding voor deze doctoraalscriptie.

Tot dusver werden slechts enkele studies uitgevoerd ter bepaling van de onzekerheid op testtoestellen gebaseerd op de zuurstofdepletie techniek. Deze studies vertonen bovendien een aantal zwakke punten.

Deze doctoraalscriptie levert een significante bijdrage in de ontwikkeling van een methode ter bepaling van de onzekerheid in HRR metingen langs analytische weg. Het brengt de algemene aanbevelingen van de 'ISO Guide to the Expression of Uncertainty in Measurement' (GUM)<sup>[13]</sup> in uitvoering.

De doctoraalscriptie schenkt aandacht aan dynamische effecten, covarianties, etc., effecten die voorheen verwaarloosd werden. Verder brengt deze studie fenomenen onder de aandacht zoals het effect van thermische inertie van de rookgaskanalen op het snelheids- en dichtheidsprofiel, evenals de Reynoldsafhankelijkheid van de SBI verschuldruksonde en de hoekafhankelijkheid van alle sondes momenteel in gebruik in middel- en grootschalige brandtesten.

Aansluitend op de deelname aan de ontwikkeling van de SBI en het daaropvolgende ringonderzoek, heeft de auteur het werk aangaande het onderhavige document aangevat.



### ***Evaluatie van de SBI verschildruksonde***

Uit een gedetailleerde studie ter bepaling van de onzekerheden op de verschillende meetcomponenten, werd duidelijk dat de verschildruksonde ter bepaling van het volumedebiet in de rookgaskanalen Reynoldsafhankelijk is en dat de ijkfactor hoger is dan deze vermeld in de norm. De oorzaak hiervoor kon toegewezen worden aan de fixeersaaf toegevoegd aan de originele sonde.

De aanbeveling luidt ofwel de kalibratie in functie van het Reynoldsgetal op te nemen of de fixeersaaf achterwege te laten.

### ***Evaluatie van de McCaffrey & Heskestad sonde***

De originele McCaffrey & Heskestad verschildruksonde heeft een ijkfactor die constant ondersteld kan worden voor Reynoldsgetalen boven 2 500. Dit stemt overeen met het maximale bereik dat praktisch gesproken verwacht kan worden in de ISO Room Corner test, de SBI test en vergelijkbare testen. Wanneer men metingen beoogt in een brandstadium voorbij vlamoverslag, dient men rekening te houden met de variabiliteit van de ijkfactor in functie van het Reynoldsgetal.

Het grootste nadeel van de McCaffrey & Heskestad verschildruksonde is haar hoekafhankelijkheid. Hoekverdraaiingen ten opzichte van de as van de rookgasbuis leiden tot fouten in de orde van 2 tot 4% (2% bij 3°; 4% bij 5°).

Deze eigenschap kan echter wel gebruikt worden om de sonde uit te lijnen en dit door te zoeken naar het lokale minimum.

Aan de hand van windtunnelexperimenten werd een ijkfactor van 1.046 gevonden voor een lengte/breedte verhouding van de sonde gelijk aan  $L/B = 2$ . De standaard onzekerheid hierop werd geschat op +0.009 en -0.011. Wijziging van de lengte/breedte verhouding vereist een herkalibratie van de sonde.

### ***Ontwikkeling van een hemisferische verschildruksonde***

Metingen in rookgassen zouden gebaat zijn met een geoptimaliseerde verschildruksonde waarbij speciaal gelet wordt op de hoekafhankelijkheid, echter zonder te raken aan de voordelen van de huidige sonde.

Deze vaststelling was de aanleiding voor verder onderzoek. Het heeft uiteindelijk geleid tot de ontwikkeling van een nieuwe hemisferisch gevormde verschildruksonde die een grote ongevoeligheid vertoont voor hoekverdraaiingen en Reynoldsafhankelijk is in een ruim bereik.

De ijkfactor van de sonde wordt geschat op  $1.224 \pm 0.008$  voor Reynoldsgetallen in het bereik 5 000 tot 60 000. Dit stemt overeen met een drukwinst van om en bij de 50 % ten opzichte van een Pitot-static sonde. De sonde is ongevoelig voor hoekverdraaiingen in een bereik van minstens  $\pm 20^\circ$ .

Verder wordt er verwacht dat de sonde zich minstens even goed gedraagt in rookgassen als de huidige bi-directionele sonde. De eerste uitgevoerde experimenten zien er veelbelovend uit.

Het gebruik van de hemisferische verschildruksonde is niet beperkt tot metingen in buizen noch tot brandproeven. Ze kan toegepast worden in een brede waaier van toepassingen waar relatieve snelheden van fluïda t.o.v. objecten dienen gemeten te worden.

### ***Introductie van het begrip ‘bluff-body blockage’ in brandproeven***

Wanneer stompe lichamen in een stroming geplaatst worden, zullen zij de stroomlijnen van de onverstoorde stroming wijzigen. In afgesloten kanalen is deze verstoring echter veel belangrijker dan men op het eerste gezicht zou vermoeden op basis van de verhouding van de doorsnede van het object tot de doorsnede van het kanaal.

De ijkfactor  $k_p$  dient daarom gecorrigeerd te worden wanneer de sonde gebruikt wordt in buizen met beperkte diameter. De toe te passen correctiefactor wordt besproken in secties 4.2 en 4.3 van het Engelstalige document.

### ***Effect van thermische inertie van de rookafvoerbuizen op de warmte vrijstelling***

De thermische tijdsconstante van de SBI rookafvoerbuizen is in de orde van 220 s. Dit leidt tot een onderschatting van het massadebiet dat voor plotse hoge warmte vloeiden geschat wordt op 1.4% bij een toestel dat werkt bij constant massadebiet. In de onderstelling dat hier een triangulaire distributie van toepassing is, resulteert dit in een standaard onzekerheid van 0.6 %.

Bij een toestel dat werkt bij constante volumestroom, reduceert de standaard onzekerheid tot 0.3 % in het geval van de SBI

### ***Analyse van de onzekerheid met inbegrip van de classificatieparameters***

In hoofdstuk 6 werd er een schatting gemaakt van de onzekerheid op de classificatieparameters FIGRA en THR<sub>600s</sub>, evenals van MARHE. Voor de berekeningen werden de richtlijnen van de ISO richtlijn ter bepaling van de onzekerheid bij metingen (GUM) gebruikt.

Voor zover bekend is deze doctoraalscriptie de eerste studie die zichzelf niet beperkt tot het bepalen van de onzekerheid op het warmte vrijstellingsvermogen (HRR) doch eveneens aandacht schenkt aan de afgeleide parameters FIGRA en THR<sub>600s</sub>.

### ***Behandeling van transiënte fenomenen, eliminatie van systematische fouten, etc.***

In tegenstelling tot eerdere studies worden hier asymmetrische distributies gebruikt waar nodig, worden er correlaties tussen de zuurstof, koolstofdioxide, verschildruk en temperatuursmetingen in rekening gebracht en wordt er een methode voorgesteld om systematische fouten te elimineren.

Ook behandelt deze doctoraalscriptie voor het eerst de onzekerheid geassocieerd met transiënte fenomenen en met de synchronisatie van data.

### ***Gedetailleerde studie van de onzekerheid van de verschillende samenstellende componenten***

Er werd een gedetailleerde studie gemaakt van de onzekerheid van de verschillende samenstellende componenten van de globale onzekerheid. Deze studie omvat ondermeer:

- een schatting van de verbrandingswaarde  $E$  voor pure substanties zoals propaan en n-heptaan;
- een onzekerheidsbepaling op de zuurstof- en koolstofdioxide concentraties in functie van de warmteafgifte;
- een onzekerheidsbepaling op de dwarsdoorsnede van de afvoerbuï voor rookgassen;
- een onzekerheidsbepaling op de ijkfactor  $k_p$  van de verschildruksensor;
- een onzekerheidsbepaling op het snelheidsprofiel gekarakteriseerd door de factor  $k_t$ .

### ***Introductie van het concept ‘bandbreedte’ in brandproeven***

In hoofdstuk 5 wordt het concept *bandbreedte* ingevoerd. Hoewel dit begrip sterk aanwezig is in disciplines als elektronica en procescontrole is het nieuw in de context van brandproeven. De bandbreedte is per definitie die frequentie waaronder een ingangssignaal zo goed als onvervormd doorgelaten wordt zowel in amplitude als in fase. Signalen die door een systeem gestuurd worden waarvan de bandbreedte lager is dan de frequentie van de signalen, worden uitgesmeerd over de tijd. Het concept blijkt belangrijk.

Piekwarmte vrijstellingen worden vaak gebruikt in regelgevingen betreffende brand. Deze piekwaarden zijn echter waardeloos zo zij niet vergezeld zijn van een verklaring i.v.m. de bandbreedte van het testtoestel.

Ter illustratie werd de bandbreedte van het instrumentarium van het SBI testtoestel in het brandlaboratorium van de UGent bepaald.

### ***Hoe om te gaan met bandbreedte in brandproeven***

Door verschillen in bandbreedte van instrumentaria in en tussen laboratoria kunnen meetresultaten sterk verschillen. Om dit probleem te verhelpen wordt er voorgesteld om de bandbreedte te beperken tot ofwel 1/30 Hz, ofwel 1/10 Hz. Een derde mogelijkheid behelst een verruiming van de bandbreedte tot 1 Hz doch dit vereist inverse filtertechnieken die zéér gevoelig zijn voor storende invloeden zoals ruis.

Uiteindelijk wordt er gekozen voor de beperking van de bandbreedte tot 1/10 Hz. Dit garandeert dat frequentiespiegeling niet optreedt, dat fenomenen met een periodiciteit van 10 s gecaptureerd worden en dat er een betere demping en synchronisatie van de data mogelijk is, met als resultaat een betere herhaalbaarheid en reproduceerbaarheid van de testmethode.

#### ***Introductie van een alternatieve synchronisatiemethode***

Een alternatieve techniek voor het synchroniseren van data wordt voorgesteld. Deze techniek maakt gebruik van de maximalisatie van de Pearson correlatiecoëfficiënt.

#### ***Introductie van een Henderson glijdend gemiddelde filter in brandproeven***

Vlakke glijdend gemiddelde filters zijn populair om data te dempen. Hoewel deze filters gemakkelijk in gebruik en eenvoudig te verstaan zijn, dempen zij niet alleen hogere storende frequenties, doch ook lagere waardevolle frequenties. Dit resulteert in een hoge lokale systematische fout en een zwakke lokale variantie.

Er wordt een beroep gedaan op een in het vakgebied van de economie veel gebruikte glijdende filter die werkt op basis van gewogen gemiddelden. De wegingscoëfficiënten worden zo gekozen dat ze voldoende variatie overlaten om een derdegraadspolynoom te reconstrueren. De besproken filters zijn Henderson filters van verschillende orde. De orde stemt overeen met het aantal termen dat men nodig heeft in de berekening. Er wordt voorgesteld nulfase Henderson filters te gebruiken van orde 11 voor bemonsteringsfrequenties van 1/3 Hz en van orde 111 voor bemonsteringsfrequenties van 10 Hz.

#### ***Ontwikkeling van een analytisch computermodel ter schatting van onzekerheden***

De theoretische beschouwingen uit hoofdstukken 5 en 6 werden geïmplementeerd in een computer model. Een eerste vergelijking van de resultaten van dit model met SBI RR2 data geeft aan dat dit model naar alle waarschijnlijkheid onzekerheden op een behoorlijke wijze schat. Schattingen kunnen gemaakt worden op de classificatieparameters FIGRA en  $THR_{600s}$  en alle tussenliggende resultaten.

#### ***Voorgestelde wijzigingen aan het data-acquisitiesysteem***

Er wordt voorgesteld de bemonsteringsfrequentie op te drijven van 1/3 Hz tot 10 Hz. De hoofdredenen zijn een verruiming van de bandbreedte en het vermijden van frequentiespiegeling.

#### ***Andere voorgestelde veranderingen aan de testmethode***

Naast een beperking van de bandbreedte tot een gelijk niveau voor alle laboratoria, zijn de meest efficiënte maatregelen voor de beperking van de onzekerheid, in volgorde van belangrijkheid:

- de vervanging van de bi-directionele verschildruksonde;
- het berekenen van de constant onderstelde parameter 'c';
- het elimineren van de systematische fout op de sectiebepaling van de rookgasleiding;
- het gebruik van een RTD weerstand ter bepaling van de omgevingstemperatuur;

#### ***Voldaan aan de eisen van EN ISO 17025***

Deze doctoraalscriptie resulteerde in een analytisch model ter schatting van de onzekerheid op de metingen in het SBI testtoestel en dit op een volledige en betrouwbare manier in lijn met de eisen gesteld in EN ISO 17025.

**Een substantiële bijdrage werd geleverd in de ontwikkeling van een methode voor het berekenen van de betrouwbaarheid in testtoestellen gebaseerd op de zuurstofdepletietechniek .**

**De bijdragen geleverd in dit werk zijn van belang en relevant voor al diegenen die actief zijn in het domein van brandproeven, fire engineering, kwaliteitscontrole en accreditatie.**

**De bijdrage geleverd met het ontwikkelen van een nieuwe verschildruksonde is van belang en relevant voor al diegenen die werken met stromingen, snelheid van stromingen en dies meer en is niet beperkt tot brandtoepassingen.**

## Referenties

- [1] \*\*\*\*\* NORMEN \*\*\*\*\*
- [2] European Standard - Reaction to fire tests for building products - Building products excluding floorings exposed to the thermal attack by a single burning item. EN 13823:2002. CEN Central Secretariat, Brussels 2002
- [3] European and International Standard – Fire classification of construction products and building elements – Part 1: Classification using test data from reaction to fire tests. EN 13501-1:2002; CEN Central Secretariat, Brussels (2002)
- [4] International Standard – Reaction-to-fire tests – Heat release, smoke production and mass loss rate – Part 1 : Heat release rate (cone calorimeter method) ; ISO 5660-1:2002
- [5] EGOLF/R4; Accreditation of Fire Test Laboratories – Interpretation of the European Standard EN ISO/IEC 17025:1999 when applied to Fire Test Laboratories; EGOLF / R4:2001
- [6] International Standard – Fire tests – Full-scale room test for surface products; ISO 9705:1993; International Organisation for Standardisation, Geneva, 1993
- [7] European Standard – Common test methods for cables under fire conditions – Heat release and smoke production measurement on cables during flame spread test – Part 1: Apparatus; prEN 50399-1; CENELEC project 15315
- [8] European Standard - Railway applications - Fire protection on railway vehicles; prEN 45545; CENELEC project 12281
- [9] European and International Standard – General requirements for the competence of testing and calibration laboratories. EN ISO/IEC 17025:2000.; CEN Central Secretariat, Brussels (2000) and International Organisation for Standardisation, Geneva (1999)
- [10] European Standard – General criteria for the operation of testing laboratories; EN 45001:1989; CEN Central Secretariat, Brussels 1989
- [11] International Standard – Thermocouples – Part 2: Tolerances; IEC 60584-2; International Electrotechnical Commission, Geneva, 1982
- [12] European Standard – Fire resistance tests - Part 1: General requirements; EN 1363-1:1999; CEN Central Secretariat, Brussels 1999
- [13] GUM, Guide to the expression of uncertainty in measurement; BIPM/IEC/IFCC/ISO/IUPAC/OIML; ISBN 92-67-10188-9
- [14] International Standard – Quality assurance requirements for measuring equipment – Part 1: Metrological confirmation system for measuring equipment. ISO 10012-1:1992; International Organisation for Standardisation, Geneva (1992)
- [15] International Standard – Accuracy (trueness and precision) of measurement methods and results – ISO 5725 Parts 1 to 6; International Organisation for Standardisation, Geneva, 1996-1998
- [16] European and International Standard – General requirements for the competence of testing and calibration laboratories. EN ISO/IEC 17025:2000.; CEN Central Secretariat, Brussels (2000) and International Organisation for Standardisation, Geneva (1999)
- [17] Thermocouples, International Reference Tables. Temperatures according to IPTS-68
- [18] Aardolieproducten - Brandstoffen (klasse F) - Vloeibaar gemaakt petroleumgas – Specificaties; NBN T 52-706:2004
- [19] JANAF Thermochemical Tables, 2<sup>nd</sup> Edn. NSRDS-NBS 37, National Bureau of Standards, Washington, DC, 1971
- [20] Chase M.W., NIST-JANAF Thermochemical Tables, 4<sup>th</sup> Edn., American Institute of Physics, Woodbury, New York, 1998
- [21] The Construction Products Directive; Council Directive 89/106/EEC of 21 December 1988 on the approximation of laws, regulations and administrative provisions of the Member States relating to construction products; European Commission, Enterprise, 1989
- [22]
- [23] \*\*\*\*\* BOEKEN \*\*\*\*\*
- [24] Atomic Weights of the Elements 1997; IUPAC Compendium of Chemical Terminology; Pure Appl. Chem., Vol. 71, No. 8, pp. 1593-1607, 1999.

- [25] Arts T., et al. ; Measurement Techniques in Fluid Dynamics – An Introduction ; von Karman Institute for Fluid Dynamics ; Sint-Genesius-Rode, Belgium, 1994
- [26] Babrauskas V.; Heat of combustion and potential heat; Heat release in fires; Babrauskas V., Grayson S.J., Eds; pp. 207-223, Elsevier Science Publishers Ltd, London, UK, 1992
- [27] Babrauskas V.; Ignition Handbook; Fire Science Publishers, Fire Science and Technology Inc., Issaquah, 2003
- [28] Boyce W.E. and DiPrima R.C; Elementary Differential Equations and Boundary Value Problems, Fourth Edition; John Wiley & Sons, Singapore, 1986
- [29] Brigham E.O. (1988); The Fast Fourier Transform and its applications; Prentice-Hall International, London
- [30] Drysdale D.D.; Thermochemistry; SFPE Handbook of Fire Protection Engineering; DiNunno, et al.; Eds. The National Fire Protection Association, USA 1995
- [31] Fox R.W. and McDonald A.T.; Introduction to fluid mechanics; John Wiley & Sons, New York 1985
- [32] Holman J.P.; Heat Transfer; McGraw-Hill Book Company, Singapore 1989
- [33] Janssens M., Parker W.J.; Oxygen Consumption Calorimetry; Heat release in fires; Babrauskas V., Grayson S.J., Eds; pp. 31-59, Elsevier Science Publishers Ltd, London, UK, 1992
- [34] Jones F.E.; Techniques and Topics in Flow Measurements; CRC Press, Boca Raton, FL, 1995
- [35] Keithley Instruments, Inc. (2001); Data Acquisition and Control Handbook, A Guide to Hardware and Software for Computer-Based Measurement and Control; Keithley Instruments, Inc.; Cleveland, Ohio, USA
- [36] Macrae J.C.; An Introduction to the Study of Fuel; Elsevier Publishing Company, London, 1966
- [37] Özisik M.N.; Finite Difference Methods in Heat Transfer; CRC Press, Boca Raton, Florida, 1994
- [38] Schoukens J. and Pintelon R. (1991); Identification of Linear Systems – A practical guideline to accurate modelling; Pergamon Press Oxford
- [39] Tewarson A.; Generation of heat and chemical compounds in fires; SFPE Handbook of Fire Protection Engineering; DiNunno, et al.; Eds. The National Fire Protection Association, USA 1995
- [40] Wonnacott T.H. and Wonnacott R.J.; Introductory Statistics for Business and Economics; fourth edition; John Wiley & Sons, Inc., Singapore, 1990
- [41] Zhu Y.C. and A.C.P.M. Backx (1993); Identification of Multivariable Industrial Processes: for Simulation, Diagnosis and Control; Springer-Verlag London
- [42] Netwerktheorie
- [43]
- [44] \*\*\*\*\* CURSUSSEN \*\*\*\*\*
- [45] An Introductory Course on Time Series Analysis – Electronic Delivery; Australian Bureau of Statistics; January 2005
- [46]
- [47] \*\*\*\*\* ARTIKELS \*\*\*\*\*
- [48] Dagum E.B. and Luati A.; Relationship between Local and Global Nonparametric Estimators Measures of Fitting and Smoothing; Studies in Nonlinear Dynamics & Econometrics, vol. 8, n. 2; The Berkeley Electronic Press, 2004
- [49] Dagum E.B. and Luati A.; Global and Local Statistical Properties of Fixed-Length Nonparametric Smoothers; Statistical Methods and Applications, vol. 11, n. 3, pp.313-333
- [50] Enright P., and Fleischmann C.; Uncertainty of Heat Release Rate Calculation of the ISO 5660-1 Cone Calorimeter Standard Test Method; Fire Technology, Vol. 35, 1999, pp. 153-169
- [51] Henderson R.; Note on Graduation by Adjusted Average; Transaction of the Actuarial Society of America, 17, pp. 43-48, 1916
- [52] Huggett C.; Estimation of Heat release rate by Means of Oxygen Consumption Measurements; Fire and Materials, Vol. 4, N°. 2, p. 61-65, 1980
- [53] Janssens M.; Variability in Oxygen Consumption Calorimetry Tests; Thermal Measurements: The Foundation of Fire Standards, ASTM STP 1427, ASTM International, West Conshohocken, PA, 2002

- [54] McCaffrey B.J. and Heskestad, G.; A Robust Bidirectional Low-Velocity Probe for Flame and Fire Application; *Combustion and Flame* 26, 125-127 (1976)
- [55] Merci B., Theuns E., Sette B., Vandeveld P.; Numerical Investigation of the Influence of Gas Heating and Cooling on the Velocity Profile Correction Factor in the SBI-Configuration; *Fire and Materials*; Under review
- [56] Messerschmidt B. and Van Hees P.; Influence of Delay Times and Response Times on Heat Release Measurements; *Fire and Materials* 24 (2), pp 121-130, 2000
- [57] Parker W. J. (1982); Calculation of the heat release rate by oxygen consumption for various applications; U.S. Department of Commerce, Washington DC
- [58] Phillips S.D., Eberhardt K.R. and Parry B.; Guidelines for Expressing the Uncertainty of Measurement Results Containing Uncorrected Bias; *Journal of Research of the National Institute of Standards and Technology*, Vol. 102, Number 5, 1997
- [59] Sette B.J.G.; Critical considerations on the use of a bi-directional probe in heat release measurements; *Fire and Materials*; In press
- [60] Sette B.J.G.; Development of a new Robust Velocity Pressure Probe for Heat Release Applications; *Fire and Materials*; In press
- [61] Sette, B., Theuns E., Merci B., Temperature effects on the mass flow rate in the SBI and similar Heat Release Rate Test Equipment, *Fire and Materials*, Under review
- [62] Thornton W.; The Relation of Oxygen to the Heat of Combustion of Organic Compounds; *Philosophical Magazine and Journal of Science*, Vol. 33, No. 196, 1917
- [63]
- [64] \*\*\*\*\* RAPPORTEN \*\*\*\*\*
- [65] Axelsson J., Andersson P., Lönnermark A. and Van Hees P.; Uncertainty in Measuring Heat and Smoke Release Rates in the Room/Corner Test and the SBI; SP Report 2001:04; Swedish National Testing and Research Institute, Borås, Sweden, 2001
- [66] Bryant R.A. et al; The NIST 3 Megawatt Quantitative Heat Release Rate Facility – Description and Procedures, NISTIR 7052; National Institute of Standards and Technology, Washington, September 2004
- [67] Dahlberg M.; Error Analysis for Heat Release Rate Measurements with the SP Industry Calorimeter; SP Report 1994:29; Swedish National Testing and Research Institute, Borås, Sweden, 1994
- [68] Enright T.; Heat Release and the Combustion Behaviour of Upholstered Furniture; *Fire Engineering Research Report 99/17*; ISSN 1173-5996; University of Canterbury, Christchurch, New Zealand, 1999
- [69] Plastics; A material of choice in building and construction, APME, figures of 1995
- [70] Official Laboratories Group; Development of the Single Burning Item Test – Results of the SBI Round Robin tests – Regulators Group document RG N115 (1997)
- [71] Sundström B., P. Van Hees and P. Thureson; Result and Analysis from Fire Tests of Building Products in ISO 9705, the Room/Corner Test, SP Report 2001:04, Borås (2001)
- [72] Project for the European Commission: Enterprise Directorate-General; “SBI (Single Burning Item) Second Round Robin”; Call Identifier ENTR/2002/CP11; Applicant: EGOLF
- [73]
- [74] \*\*\*\*\* CATALOGI \*\*\*\*\*
- [75] KEITHLEY Instruments, Inc. ; Model 2000 Multimeter – User’s Manual; Document Number: 2000-900-01 Rev. D; Cleveland, Ohio, U.S.A., 1995
- [76] MERCK KGaA; Chemical Reagents; Darmstadt, 1999/2000
- [77] SIEMENS AG; SIMATIC Komponenten für Totally Integrated Automation; Katalog ST 70 - 1999, Nürnberg, 1999
- [78] SIEMENS AG; Oxymat 6, Ultramat 6 - Analysatoren für IR-absorbierende Gase und Sauerstoff; C79000-G5200-C143-03, Karlsruhe, 1998
- [79]
- [80] \*\*\*\*\* WEBSITES \*\*\*\*\*
- [81] <http://users.pandora.be/peterulenaers/WEERGRAFIEKEN.HTM> December 2004
- [82] <http://webbook.nist.gov/chemistry/>; February 2005



- [83] <http://www.chemdat.de/> August 2004
- [84] [http://www.devosenergie.be/nl/tf\\_propaangas.aspx](http://www.devosenergie.be/nl/tf_propaangas.aspx); August 2004
- [85] [http://www.kauffman-gaz.com/cadre\\_neerlandais.htm](http://www.kauffman-gaz.com/cadre_neerlandais.htm); August 2004
- [86] Weisstein E.W.; "Triangular Distribution." From MathWorld--A Wolfram Web Resource. <http://mathworld.wolfram.com/TriangularDistribution.html>; February 2005
- [87] <http://www.webelements.com/webelements/scholar/properties/definitions/atomic-weight.html>; February 2005



**DEEL 2: ENGELSTALIGE VERSIE**  
**PART 2: ENGLISH VERSION**



## Contents

### PART 1

Dutch summary

### PART 2

English version

Contents.....	61
List of Symbols and Abbreviations.....	66
Abstract.....	70
<b>1 Introduction .....</b>	<b>72</b>
1.1. Brief outline of fire testing in Europe.....	72
1.2. The reaction to fire classification system.....	73
1.3. Development of the initial SBI test.....	75
1.4. Recent developments .....	78
1.5. Evaluating and reporting uncertainty .....	81
1.6. Research topics .....	83
1.7. Strategy followed .....	87
<b>2 Measurement principle and calculation procedures.....</b>	<b>89</b>
2.1. General.....	89
2.2. Calculation procedure.....	92
<b>3 Gas Analysis.....</b>	<b>99</b>
3.1. Introduction .....	99
3.2. Optimising.....	99
<b>4 Mass flow rate.....</b>	<b>105</b>
4.1. Introduction .....	105
4.2. Article 1 .....	106
4.3. Article 2 .....	108
4.4. Article 3 .....	110

4.5.	Article 4 .....	111
5	Dynamic behaviour .....	112
5.1.	Introduction .....	112
5.2.	Identification of the measurement components.....	112
5.3.	Filters.....	129
5.4.	Recommended filters.....	141
5.5.	Inverse filters .....	149
5.6.	Elimination of delay time.....	150
5.7.	Conclusions .....	152
6	Uncertainty .....	154
6.1.	Introduction .....	154
6.2.	Elaboration of terms and concepts .....	156
6.3.	Combined standard uncertainties.....	167
6.4.	Standard uncertainty on the different components.....	179
6.5.	Conclusions .....	227
7	Evaluation and results of the Analytical Model.....	228
7.1.	Introduction .....	228
7.2.	Comparing the model with the SBI RR2 results .....	228
7.3.	Using the model to improve the test method.....	233
7.4.	Conclusions .....	250
8	Conclusions .....	251
8.1.	Introduction .....	251
8.2.	Recommended changes specific to the SBI standard .....	259
8.3.	General recommendations to all Heat Release Rate based test facilities .....	261
8.4.	Main contribution of this work to the measuring technique .....	262
8.5.	Further research.....	264
	References .....	265
A	Annex.....	273

<b>A.1.</b>	<b>Article 1 .....</b>	<b>273</b>
<b>A.2.</b>	<b>Article 2 .....</b>	<b>299</b>
<b>A.3.</b>	<b>Article 3 .....</b>	<b>327</b>
<b>A.4.</b>	<b>Article 4 .....</b>	<b>349</b>
<b>B</b>	<b>Annex.....</b>	<b>371</b>
<b>B.1.</b>	<b>Desiccant.....</b>	<b>371</b>
<b>B.2.</b>	<b>Time constant thermocouples.....</b>	<b>373</b>
<b>B.3.</b>	<b>Time constant duct system.....</b>	<b>376</b>
<b>B.4.</b>	<b>Time constant hood .....</b>	<b>378</b>
<b>B.5.</b>	<b>Radiation effect thermocouples.....</b>	<b>379</b>
<b>B.6.</b>	<b>Chemical composition of commercial grade propane .....</b>	<b>381</b>
<b>B.7.</b>	<b>Estimation of uncertainty on Heats of combustion .....</b>	<b>383</b>
<b>B.8.</b>	<b>Uncertainty analysis on the gas analyser.....</b>	<b>386</b>
<b>B.9.</b>	<b>Uncertainty analysis on the oxygen analyser .....</b>	<b>388</b>
<b>B.10.</b>	<b>Uncertainty analysis on the carbon dioxide analyser.....</b>	<b>389</b>
<b>B.11.</b>	<b>Transient error first order system .....</b>	<b>391</b>
<b>B.12.</b>	<b>Conversion factor upper to lower heat of combustion .....</b>	<b>393</b>
<b>B.13.</b>	<b>Composition Heptane.....</b>	<b>394</b>
<b>B.14.</b>	<b>Electronic damping O<sub>2</sub> and CO<sub>2</sub> analysers .....</b>	<b>396</b>
<b>B.15.</b>	<b>Cross sensitivity of the Oxymat 6E analyser<sup>[76]</sup> .....</b>	<b>397</b>





Graceful for the beauty of Live

I do want to thank  
my wife and children,  
my parents and in-laws,  
my manager Prof. Paul Vandavelde and promoter Prof. Erik Dick.

I also want to thank for gained insight  
Prof. Jean-Pierre Martens and Prof. Robin De Keyser from UGent  
and Prof. Jeroen van Beeck of the Von Karman Institute, Sint-Genesius-Rode.

For joined articles written on the subject I also want to thank  
Ir. Rudolf Van Mierlo of TNO, Delft,  
Prof. Bart Merci and Dr. Erwin Theuns from UGent.

Furthermore I wish to thank each and everyone who have helped me in one way or another  
and I especially want to thank  
Mrs. Marthe Vandavelde and Mrs. Els Van Gysel,  
Prof. Gilbert De Mey, Dr. Saïd Dhimdi, Ir. Pjotr Kawka, Ir. Mihaela Sbarciog, Ir. Wim Meeus,  
Mr. Patrick Ysebie, Mr. Martin Cambier, Mrs. Leen De Clippel, Mr. Patrick Depue,  
Mr. Pascal De Jonge and Mr. Jurgen Delamper.

## List of Symbols and Abbreviations

A	cross sectional area exhaust duct	[m <sup>2</sup> ]
c	$\sqrt{2T_{298}/\rho_{298}} \cong 22.4$	[K.m <sup>3</sup> /kg] <sup>1/2</sup>
$c_x^y$	sensitivity coefficient of x with respect to y	
$c_p$	heat capacity	[J/kg.K]
D	diameter	[m]
e	error	
E	heat of combustion per unit volume of oxygen (at 298 K) consumed	[MJ/Nm <sup>3</sup> O <sub>2</sub> ]
E'	heat of combustion per unit mass of oxygen consumed	[MJ/kg O <sub>2</sub> ]
$f_s$	sampling frequency	[Hz]
F	view factor	[-]
G( $\omega$ )	gain function in the frequency domain	[-]
h	convective heat transfer coefficient	[W/m <sup>2</sup> .K]
$\Delta h_c$	heat of combustion	[kJ/kg]
H	enthalpy	[kJ/kg]
Im{x}	imaginary part of x	
j	imaginary operator ( $j^2 = -1$ )	
k	coverage factor	[-]
k	thermal conductivity	[W/m.K]
$k_t$	velocity profile correction factor (relation between mean velocity and velocity on axis)	[-]
$k_p$	pressure probe factor	[-]
L	length	[m]
£	Laplace operator	
m	mean value	
$\dot{m}$	mass flow	[kg/s]
n or N	number of samples	
Nu	Nusselt number	[-]
O()	order of	
p	barometric pressure	[Pa]
P(x)	probability function	
Pr	Prandtl number	[-]
$\dot{Q}$	heat release rate	[kW]

$r$	repeatability limit	
$r(x_i, x_j)$	Pearson correlation coefficient	[-]
$Re$	Reynolds number	[-]
$Re\{x\}$	real part of $x$	
$s$	operator of the Laplace transform	
$s$	estimated standard deviation	
$s^2$	estimated variance	
$s_r$	standard deviation estimates on repeatability	
$s_R$	standard deviation estimates on reproducibility	
$t$	time	[s]
$t_s$	sampling interval	[s]
$T$	temperature	[K]
$u(x)$	standard uncertainty on $x$	
$U$	expanded uncertainty	
$v$	velocity	[m/s]
$V$	volume	[m <sup>3</sup> ]
$\dot{V}_{D298}$	volume flow through the duct (298 K)	[m <sup>3</sup> /s]
$w_i$	weighing factor	
$\bar{x}$	estimated mean value	
$X_{O_2}$	Concentration of, in this case $O_2$ , in the gas considered	[Vol%]
$X_{O_2}^{D^\circ}$	Initial oxygen concentration in the exhaust duct	[Vol%]
$X_{O_2}^{A^\circ}$	Initial oxygen concentration as measured by the analyser	[Vol%]
$X_{O_2}^A$	Actual oxygen concentration as measured by the analyser	[Vol%]
$z$	operator of the Z-transform	

### Greek symbols

$\alpha$	expansion factor	
$\delta$	bias	
$\Delta$	difference operator	
$\varepsilon$	emissivity	[-]
$\mu$	mean value	
$\nu$	kinematic viscosity	[m <sup>2</sup> /s]
$\rho$	density	[kg/m <sup>3</sup> ]
$\sigma$	standard deviation	

$\sigma^2$	variance	
$\tau$	time constant	[s]
$\varphi$	relative humidity	[%]
$\phi$	depletion factor	
$\Phi(\omega)$	phase shift in the frequency domain	
$\omega$	circular frequency	[rad/s]

### Subscripts

$A^\circ$	initial analyser value
atm	atmosphere
av	average
b	bias
c	combined
$D^\circ$	initial value measured in the duct
eff	effective
f	formation
ms	measuring section
rect	rectangular
st.dev.	standard deviation
trap	trapezoidal
trian	triangular

### Superscripts

$^\circ$	initial
l	lower
u	upper

### List of abbreviations

ABS	Absolute
ARHE	Average Rate of Heat Emission
BW	Bandwidth
CEN	European Committee for Standardisation
CPD	Construction Products Directive; 89/106/CE

DAQ	Data acquisition system
DMM	Digital Multi Meter
EGOLF	The European Group of Organisations for Fire testing, Inspection and Certification
EN	European Standard
FIGRA	Fire Growth Rate
FS	Full Span
GUM	Guide to the expression of uncertainty in measurement <sup>[13]</sup>
HRR	Heat Release Rate
ISO	International Organisation for Standardisation
LMSE	Local Mean Square Error
MARHE	Maximum Average Rate of Heat Emission
MAX	Maximum of
MDF	Medium Density Fibreboard
MR	Measuring Range
PLC	Power Line Cycle
PLC	Programmable Logic Controller
ppm	Parts per million
PVDF	Polyvinylidene fluoride
REL	Relative
RC	Room corner test; ISO 9705 <sup>[6]</sup>
RTD	Resistive Temperature Detector
SBI	Single Burning Item test; EN13823 <sup>[2]</sup>
SBI RR1	First round robin exercise on the SBI held in 1997
SBI RR2	Second round robin exercise on the SBI held in 2003 – 2004
SMOGRA	Smoke Growth Rate
SPR	Smoke Production Rate
THR600s	Total heat released over the first 10 minutes
TSP600s	Total smoke production over the first 10 minutes

## **Abstract**

In its aim to establish a 'common market' amongst its members for construction products, the European Union has established the Construction Products Directive (CPD) 89/106/CE. In this a new test and classification system EN 13501<sup>[1]</sup> for both Reaction to Fire and Resistance to Fire has been established. This EUROCLASSES system has become operational and results in the year 2002 in the first construction products carrying the CE-mark. With this CE-mark products are free to circulate within the European Union.

In the field of reaction to fire an entirely new classification system based on six different test methods has been developed. Wherever possible or politically acceptable, existing ISO or national test methods have been used, however it was considered necessary to develop a new intermediate scale test method, the Single Burning Item (SBI) EN13823<sup>[2]</sup>, named after the fire conditions it is expected to simulate. The SBI is the key method in the new classification system.

The SBI generates dynamic fire data like Heat Release Rate and Smoke Production Rate which are considered essential for evaluating the reaction to fire performance of products.

According to EN ISO 17025<sup>[9]</sup>, General requirements for the competence of testing and calibration laboratories, and ISO 10012-1<sup>[4]</sup>, Quality assurance requirements for measuring equipment, uncertainties are to be reported in both testing and calibration reports. The general principles for evaluating and reporting uncertainties are given in the Guide to the expression of uncertainty in measurement, GUM<sup>[3]</sup>, but need to be interpreted and applied to the specific case of fire testing.

Several authors have tried to quantify uncertainty associated with the calculation of Heat Release Rate and Smoke Production Rate<sup>[65][62][45][64]</sup> for heat release rate based test facilities. However, out of a review of all major round robins, Janssens<sup>[50]</sup> found that the results suggest that the uncertainty is much greater than the theoretically deduced values, in particular for intermediate and large-scale tests. Technical reasons for this discrepancy are investigated, changes are proposed to the model and SBI apparatus, and a time dependant analytical uncertainty model is developed.

Furthermore, this work fills up the gaps left open by the GUM.

Two round robin exercises, in which the author participated, have been organised in an international context and the data have been analysed, resulting in an experimentally determined uncertainty of the test method. The before mentioned analytical uncertainty model has been checked against the experimental data.

A key element in the determination of the dynamic fire data is the accurate measurement of the volume flow of the combustion gases. To date the SBI uses a bi-directional low-velocity probe<sup>[65]</sup> for this purpose. This dissertation however demonstrates that the probe constitutes an essential component in the measurement uncertainty.

A custom made pressure probe for measuring unidirectional flows in exhaust ducts has been developed which leads to better, more accurate, results with a lower uncertainty.

Due to the dynamic nature of the parameters measured, the dynamics of the apparatus have a major effect on the end result. They have been investigated in dept and proposals are formulated how to deal with them.

As an outcome of this work, recommendations are forwarded to CEN TC127 in order to modify the standard. This work has increased the insight in the SBI test method and other fire testing equipment using similar measuring techniques. It also provides a tool for EGOLF, the *European Group of Organisations for Fire testing, Inspection and Certification*, to deal with the problem of evaluating and reporting uncertainty in fire testing.

Key words: reaction to fire, SBI, heat release rate, mass flow rate, flow velocity, pressure probe, uncertainty, dynamic behaviour

# 1 Introduction

## 1.1. Brief outline of fire testing in Europe

The SBI test method has been developed as a result of the implementation of the *Construction Products Directive* (CPD) 89/106/CE in Europe and is used now to assess the reaction to fire performance of construction products, excluding floorings, in the European Union.

Through the use of harmonized technical specifications, thus removing technical barriers between Member States, the CPD aims to create a single European market. It applies to all construction products that are produced for, or incorporated within, building and civil engineering construction works. It harmonises all the technical characteristics of construction products subject to regulatory controls as a basis for CE marking purposes.

The CPD defines six *Essential Requirements*, from which one is the *Safety in case of fire*. While in other Directives the essential requirements are directed to the products themselves, the CPD relates to the essential requirements of the works. The link between the requirements of the works and the technical specifications for building products is established through the *Interpretative Documents*. One of the fire characteristics for construction products to assess is the reaction to fire performance.

The CPD provides for a *Standing Committee on Construction* (SCC), which assists the European Commission in its implementation. The SCC members are representatives of the Member States. In general the SCC is a consulting body to the Commission, but for certain items indicated in the CPD it is a regulatory body. The SCC has set up a technical working group to assist in the interpretation of the Directive in fire safety related matters: the *Fire Regulators Group* (FRG), recently re-established and named *Experts Group on Fire issues under the CPD* (EGF).

One of the characteristics for construction products to assess is the reaction to fire performance. This characteristic is present in the national regulations of all European member states and plays an important role in evaluating possible uses of building products. The philosophy for the European reaction to fire classification, the EUROCLASSES, was put in place in 1993 by the Fire Regulators Group. The classification system was based on the performance of products under different fire conditions: the attack of a small flame; exposure to a fully developed fire; and some level in between. Due to the nature of fire under the influence of gravity forces (hot gases tend to rise), two basic applications of products were distinguished: products applied on a floor and all other products.



All but one of the tests needed in this new classification system were known international standard test methods (ISO). One test method, including the apparatus, representing the scenario of a Single Burning Item - to test building products excluding floor coverings - had to be designed from scratch. The apparatus soon got called the SBI.

The SBI test method, a medium scale test, was planned to assess or predict the fire performance of building products in a (real scale) room corner scenario. The ISO 9705 Room corner test<sup>[6]</sup>, a full-scale test method evaluating the contribution to fire growth by surface products in a room, was put forward as the reference test for this scenario. The main development objective therefore was that the product ranking in the SBI would have a high correlation with the ranking obtained in the ISO Room corner test. The second development objective followed from the requirement that the method had to be capable of measuring the required characteristics in a repeatable and reproducible way.

## **1.2. The reaction to fire classification system**

The basis for the European reaction to fire classification, the EUROCLASSES, was put in place in 1993 by the Fire Regulators Group. The classification of building products excluding floorings is assessed using four test methods. Three classifications apply: a main classification related to heat production (classes A1, A2, B, C, D, E or F, where A1 represents the highest level (“no contribution to fire”) and F has no requirements or “no performance determined”), and additional classifications for smoke production (s1, s2 or s3, where s1 is the best, s3 has no requirements) and for flaming droplets and particles (d0, d1, d2, where d0 is the best, d2 has no requirements). The SBI test method is relevant for the main classes A2 up till and including D and the additional classes on smoke and droplets/particles in these classes.

The fire characteristics evaluated in the SBI are: an index representing the *Fire Growth Rate* (FIGRA), the *total heat released* over the first 10 minutes (THR600s), a simple *lateral flame spread* to the end of the specimen (LFS<sub>edge</sub>), an index representing the *Smoke Growth Rate* (SMOGRA), the *total smoke produced* over the first 10 minutes (TSP600s), and a parameter defining three levels of *flaming droplets and particles* (FDP).

Due to differences in national regulatory needs the characteristics are combined in the three separate classifications mentioned earlier: a main, heat release based, classification, valid for all member states, a smoke production classification and a classification of falling flaming droplets and particles for only a part of the member states.

The FIGRA and SMOGRA indices use threshold values for total heat release and smoke production below which they are set to zero by definition. This in order to eliminate some ambiguous and

irrelevant results obtained with very small release rates in the first tens of seconds in the test. To further stabilise the classification system, different levels of thresholds were introduced for FIGRA in different classes, leading to FIGRA0,2MJ and FIGRA0,4MJ.

A compilation of the SBI criteria in the various classes is given in Table 1. The sub classifications on smoke and droplets/particles are independent from the main classification. Other criteria from other tests apply, and this in function of the classification.

Main classification		Smoke classification		Flaming droplets/particles classification	
<b>A1</b>	FIGRA <sub>0,2MJ</sub> ≤ 20 W/s LFS < specimen edge THR <sub>600s</sub> ≤ 4,0 MJ s1 & d0	<b>s1</b>	SMOGR <sub>A</sub> ≤ 30 m <sup>2</sup> /s <sup>2</sup> TSP <sub>600s</sub> ≤ 50 m <sup>2</sup>	<b>d0</b>	No flaming droplets/part.
<b>A2</b> & <b>B</b>	FIGRA <sub>0,2MJ</sub> ≤ 120 W/s LFS < specimen edge THR <sub>600s</sub> ≤ 7,5 MJ	<b>s2</b>	SMOGR <sub>A</sub> ≤ 180 m <sup>2</sup> /s <sup>2</sup> TSP <sub>600s</sub> ≤ 200 m <sup>2</sup>	<b>d1</b>	No flaming droplets/part. persisting > 10 s
<b>C</b>	FIGRA <sub>0,4MJ</sub> ≤ 250 W/s LFS < specimen edge THR <sub>600s</sub> ≤ 15 MJ	<b>s3</b>	No requirement	<b>d2</b>	No requirement
<b>D</b>	FIGRA ≤ 750 W/s				

Table 1. SBI criteria in the various classes

### 1.3. Development of the initial SBI test

The SBI test simulates a *single burning item* in a corner of a room. The test apparatus is presented in Figure 1. The total exposed specimen surface area is 1,5 m x 1,5 m. The specimen consists of two parts (height 1,5 m, width 0,5 and 1,0 m) which form a right-angled corner. Possible corner joints as applied in end-use conditions form part of the product under test. A triangular shaped propane diffusion gas burner running at 30kW acts as heat and ignition source. It is placed at the basis of the specimen corner. The performance of the specimen is evaluated during 20 minutes. There is a floor in the test configuration but no ceiling. Floor, specimen and burner are installed on a trolley that can be removed from the room for easy mounting of the specimens. The combustion gases are collected in a hood and transported through a duct. The duct contains a measurement section with a differential pressure probe, thermocouples, a gas sampling probe and a smoke measurement system, to measure heat and smoke release rate.

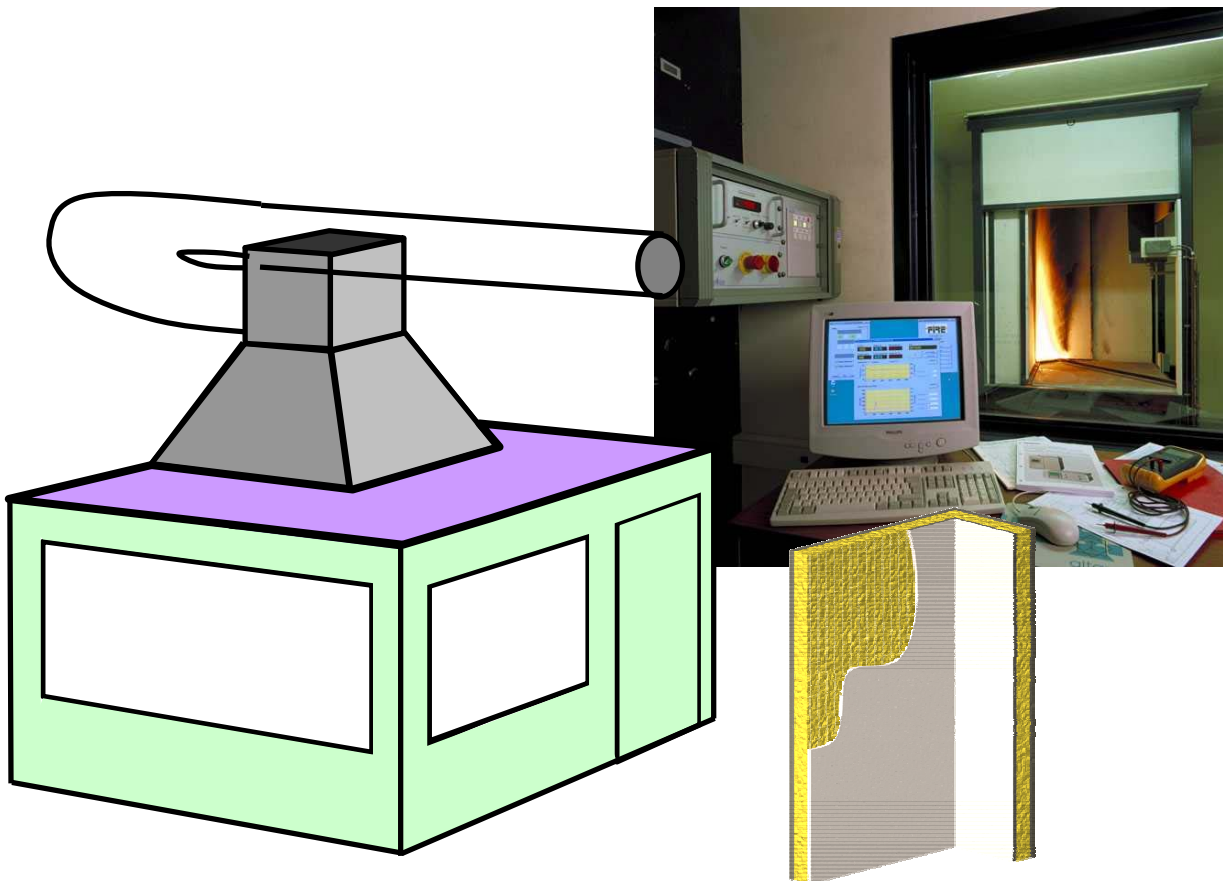


Figure 1. SBI: test apparatus and typical specimen

The development of the SBI test method was ordered by the European Commission and carried out under direct guidance of the Fire Regulators Group. A consortium of seven, later nine, fire testing laboratories from an equal number of EU member states was formed in 1993 with the task to develop the method. The chairmanship was with professor Paul Vandeveldel (UGent). The aim was to develop a test method that produces results representative for the behaviour of building products when exposed to typically one single burning object, e.g. a litter basket on fire, placed in the corner of a room. A specific incident irradiance level was specified by the Fire Regulators Group.

Many design aspects were considered in the early stages, the aim of which it was to optimise the simulation of the specified scenario. The major ones being: the type of heat source, an open or closed test arrangement, the inclusion or not of a ceiling in the specimen arrangement.

It was decided to use the oxygen depletion principle for the heat release rate measurement. The oxygen depletion measurement technique and accompanying instrumentation were based on the ISO 9705 Room Corner and ISO 5660<sup>[4]</sup> Cone Calorimeter design.

The successful finalisation of the project was of extraordinary political importance, because considered to be the major remaining obstacle for the application of the Construction Products Directive itself. The test method under development was therefore continuously thoroughly scrutinised, as well by the European Commission, ordering the development of the method, as well as by all parties seeing (commercial) advantages in postponing the Common Market for construction products.

As a consequence, not only the design of the apparatus received much attention, but also the test, calibration and calculation procedures were examined and specified in great detail. Unlike the more global description of the calculations in many other fire test standards, the calculations were introduced in great detail to facilitate the writing of calculation software without (much) further technical understanding of the measurement techniques.

After acceptance of the design and prototypes by the Fire Regulators Group, the Standing Committee on Fire and the European Commission, some twenty test apparatuses were build and installed all over Europe in just a few months to perform a large interlaboratory round robin project (SBI RR1). The round robin started in May 1997 with 20 laboratories, testing 30 building products in threefold. Fifteen laboratories managed to perform the tests in the required very tight time schedule. All 30 products were also tested in the full scale Room Corner reference scenario in order to find a good correlation with full scale fires. The result of the round robin was accepted by the Standing Committee in December 1997, as sufficient proof of the ability of the SBI test method to measure the required

characteristics in a repeatable and reproducible way, however under the condition of some further improvements.

A further one year of development work resulted in improvements of the smoke measurement system, the velocity profile in the exhaust duct and the calculation and calibration procedures:

- Smoke measurement system improvements concern practical aspects such as the prevention of soot deposit on the lenses; a reduction of vibration in the optical system; and simplification of the positioning of calibration filters.
- The velocity profile in the exhaust duct at the pressure probe position derived essentially from the profile of a fully developed flow. Three changes were introduced to the exhaust duct: a shift of the guide vanes further away from the probe position, the introduction of a small orifice immediately behind the guide vanes and the introduction of 0,5 meter additional duct length. The result was a nearly flat profile approaching much better a fully developed flow.
- Calculation procedures: two improvements were introduced:
  - Automatic synchronisation of gas analyses data: Since the measurement of the exhaust flow rate on the one hand and oxygen and carbon dioxide concentration on the other hand, needed to calculate the heat release, have different delay times, a synchronization is needed. A fully automated procedure was introduced to exclude human interpretation.
  - Introduction of a series of validity checks for all measurements, failure of which invalidates the test result.
- Calibration procedures: all calibration procedures were reconsidered and more extensively specified; some new procedures were introduced.

After five and a half years of development under direct guidance of the Fire Regulators Group and the European Commission, the draft method was handed over to CEN in spring 1999. There the method was transferred into a draft CEN standard without fundamental design changes.

The SBI method was accepted in CEN as a European test method in the Autumn of 2001 and published in 2002 as EN 13823:2002<sup>[2]</sup>, *Reaction to fire tests for building products - Building products excluding floorings exposed to the thermal attack by a single burning item*.

The related classification standard EN 13501-1:2002<sup>[3]</sup>, *Fire classification of construction products and building elements – Part 1: Classification using test data from reaction to fire tests*, was published in that same year.

This test method is now referenced in already over 30 European product standards and implemented in the national regulations of nearly all European member states, including the new members.

## 1.4. Recent developments

Since its introduction the SBI test has been used extensively in a large number of European fire test laboratories and considerable experience has been acquired. The European building sector is now working with the SBI test method to provide their products with a reaction to fire classification, and the particularities of the method have become increasingly apparent ever since.

Several organisations have started to further examine the method. EGOLF, the European Group of Organisations for Fire testing, Inspection and Certification, has identified ambiguous and insufficiently defined (parts of) procedures and proposed common interpretations for them to harmonise the way of working with the method between its members. These proposals, “recommendations” in EGOLF, are not changes to, but only further detailed specifications or interpretations of the current standard. The Fire Sector Group of Notified Bodies (FSG) works along the same lines to support the work of the notified laboratories. Both EGOLF and the FSG send requests for changes in EN 13823 to CEN TC127. This CEN committee has now just started the formal review of the method. An extensive list of potential work items has been drafted by TC127. Most purely technical issues which will not ‘change’ the test results have already been solved. Some remaining items however, might lead to more or less fundamental changes of the method.

As major weakness of the method (e.g. in terms of repeatability and reproducibility) the importance of the mounting and fixing of specimens could be mentioned. However, this is a direct consequence of the CPD principle to test products in their end use application and to test specimen of considerable size where mechanical deformation behaviour plays an important role.

Real weaknesses are recognized in issues like:

- Fallen debris blocking the burner and/or closing the gas supply by blocking the visibility of the flames by the flame detector. The use of a grid to protect the burner only solves part of the problem; it will give no improvement for fluid debris.
- The oxygen analyser is used at the border of its specifications. Regular calibrations, day-to-day checks, good pre-measurement filtering and conditioning of the combustion gases and good maintenance are essential but do not solve all the problems here.
- The verification of the thermal attack on the specimen is considered insufficient. Some think this could be improved using a heat flux measurement or by specifying a reference test on a reference material. But the actual proposals are not reliable enough to replace the actual propane gas supply specification.

The remaining questions in relation to the method have led to a joint initiative of EGOLF and CEPMC (Council of European Producers of Materials for Construction) to organise a second round

robin (SBI RR2) with financial support by the Commission. The round robin was formally set up “to verify the efficiency of the various modifications previously made to the test method and the test procedure after the first round robin in 1997 and to investigate any further remaining deficiencies”. The results were reported only recently<sup>[70]</sup> and can be summarized as follows:

- The repeatability and reproducibility of the values used for classification (FIGRA0,2MJ, FIGRA0,4MJ, THR600s, SMOGRA and TSP600s), represented by the ratio of the standard deviation estimates ( $s_r$  and  $s_R$ ) to the mean value of the parameters ( $m$ ), are between 11% and 20% for  $s_r/m$  and between 21% and 34% for  $s_R/m$ , when very low mean values are excluded. General proof of improvement of the accuracy of the method in comparison to the first round robin could not be found. Only the reproducibility of the smoke measurements shows some improvement.
- All laboratories show sufficient proof to measure heat release related data in an acceptable way; 90% of them do this acceptably for smoke production related data as well. It takes many laboratories however much longer than expected to comply with the calibration requirements. This creates concern about the abilities and level of training of the laboratories/operators.
- Overall the current specified calibration procedure is able to evaluate a laboratory’s capability to measure heat release rate and smoke production rate in an accurate way. The procedure also helps to highlight problems and to locate them. The round robin shows that there is room for improvement of the calibration procedure and it is recommended to revise them. Furthermore it is recommended to further develop the calibration of the optical system and to make it normative.
- The results of the visual observations indicate that the set of products used may be a poor discriminator to check the ability of the method to assess the visual observation related parameters. The results however already indicate that large differences in interpretation of visual observations do exist.

The round robin clearly shows the benefit of having good calibration procedures, but only if the laboratory personnel knows how to act when criteria are not satisfied, i.e. if the operators fully understand the measuring technique.

The eagerness of construction products industry and fire test laboratories to obtain information about the reliability of the test results is not the only drive for further research and development. Accreditation bodies are increasing the pressure on fire test laboratories to include well founded statements of measurement uncertainty in the test report.

According to EN ISO 17025:1999<sup>[16]</sup>, which sets out the general requirements for the competence of testing and calibration laboratories, and ISO 10012-1<sup>[14]</sup>, which specifies the requirements for assuring the quality of measuring equipment, uncertainties are to be reported in both testing and calibration

reports. Accreditation of fire test laboratories according to EN ISO 17025 is becoming a condition for acceptance of test reports across the country borders as well as for EGOLF membership.

In response to these international standards EGOLF has published EGOLF/R4<sup>[5]</sup> in 2001. This document provides guidelines by which EGOLF members should interpret and implement EN ISO 17025. It includes the criteria by which EGOLF members should be inspected and accredited by accreditation authorities.

Unlike EN 45001:1989<sup>[10]</sup> which preceded EN ISO 17025, the latter makes the estimation and declaration of uncertainty of test results mandatory. Till the release of EN ISO 17025, EGOLF considered that reporting uncertainty on fire test results was practically speaking not possible, taking into account the nature of fire tests and the complex functional relationship between a series of different types of measurements and the ultimate fire test ‘result’. This position is still reflected in the actual document EGOLF/R4 but is under revision now. More recent initiatives in EGOLF try to develop means to evaluate uncertainty of measurement for each individual method or family of methods. Provisionally all uncertainty declarations are based on limited round robin exercises.

The results of the present work should be considered as a contribution to the long and complex process of the scientific evaluation of uncertainty of measurements for heat and smoke release rates in fire tests.

In the mean time EGOLF uses the results of round robin exercises as a basis for demonstration of competence of its member laboratories. This method however has several disadvantages and shortcomings:

- It does not differentiate between the sources of the uncertainty: the apparatus, the operator, the product under test, etc.;
- It is costly and time consuming to organise them;
- The results are based on some ‘representative’ products; in practice however the spread in results may be different.

A round robin finally results in a repeatability and reproducibility limit. The repeatability limit is defined as *the value less than or equal to which the absolute difference between two test results obtained under repeatability conditions may be expected to be with a probability of 95%.*<sup>[15]</sup>

On the other hand, fairly recently, some individual organisations have tried to quantify uncertainty associated with the calculation of heat release rate and smoke production rate<sup>[47][62][64][65][66]</sup> on a theoretical basis. However, out of a review of all major round robins, Janssens<sup>[50]</sup> found that the results suggest that the uncertainty is much greater than the theoretically found values, in particular for intermediate and large-scale tests.



So one of the biggest challenges for the fire community in the coming years is to elaborate, for the different test methods, means to evaluate uncertainty of measurement. Due to the European harmonisation of fire testing, and its economical consequences both for fire test laboratories and construction products manufacturers, this is becoming even more important.

## 1.5. Evaluating and reporting uncertainty

The general principles for evaluating and reporting uncertainties are given in the ISO *Guide to the Expression of Uncertainty in Measurement* (GUM<sup>[13]</sup>). They need to be adapted to the specific case of fire testing. Till today, on the international scene, few studies exist which address the uncertainty of heat release rate measurements by oxygen consumption calorimetry. The studies vary in apparatus and in detail of analysis. Enright and Fleischmann<sup>[47]</sup> performed an analytical estimate of the heat release rate measurement uncertainty for the Cone Calorimeter. They estimated a relative expanded uncertainty ranging from 10 % to 12 %, depending on the heat release rate. The main sources of uncertainty identified were, the heat of combustion factor, the combustion expansion factor and the oxygen concentration measurement. Axelsson et al.<sup>[62]</sup> estimated the uncertainties related to heat and smoke release rates in both the Room Corner test<sup>[6]</sup> and the SBI test<sup>[2]</sup>. The relative expanded uncertainty estimates for the Room Corner ranged from 7 % to 11 %, depending on the heat release rate. For the SBI test at the 35 kW level, respectively 50 kW level, the relative expanded uncertainty was estimated at 13.5 %, respectively 10 %. The main sources of uncertainty identified were, the oxygen concentration measurement, followed by the heat of combustion factor and the mass flow rate measurement. Bryant et al.<sup>[64]</sup> performed an analytical estimate of the heat release rate measurement uncertainty for their large scale 3 Megawatt test facility. The relative expanded uncertainty was estimated at 11 % for fire sizes larger than 400 kW. The major source of uncertainty identified were the bi-directional pressure probes used to compute the exhaust duct volume flow rate.

In view of the pressure exercised by accreditation authorities, there is an increasing interest of testing laboratories worldwide in the subject.

Despite the initiatives taken, there is still an important way to go before reporting uncertainty along the lines of the GUM document.

The weak points in the work done so far are that:

- Not all relevant phenomena are taken into account, often because people are not aware of them or because they believe they can be neglected. Examples of these are the Reynolds dependence of the velocity pressure probe in the SBI, used to obtain the mass flow of the exhaust gases, and the angular dependence of that same probe.

- The ‘guesses’ made on uncertainties on the different components where the required statistical information is not readily available. Example of this is that the uncertainty on a gas concentration measurement by one group of researchers is taken as the sum of noise and drift of that gas analyser over half an hour period.
- Dynamic effects of the apparatus have not been taken into account in the analysis of the results. Due to non negligible time constants of some measuring devices, a transient error is introduced. This error cannot be neglected especially not when considering momentary values like peaks and dips. This is the case in the SBI where the main classification criterion, FIGRA, is defined as the maximum of the ratio of Heat Release Rate to time elapsed to reach that level. To partially eliminate this effect the SBI standard prescribes that the heat release rate firstly should be smoothed by means of a running average filter over half a minute period.
- Covariances between the different measurands have been neglected. This is not justifiable as can easily be understood from the following example. Suppose a pure substance like for example propane is burnt,



we know that for every mole of oxygen consumed, 3/5 moles of carbon dioxide will be formed. So there is a perfect negative correlation between the oxygen consumed and the carbon dioxide produced ( $r = -1$ ).

- Synchronisation errors have been neglected. Due to different lag times of the instrumentation, data needs to be synchronised in a post-processing phase. This synchronisation can't be any better than the data scan interval used, which is usually in the order of 3 s (SBI) to 5 s.

## 1.6. Research topics

Several possibilities for further improvement of the method still remain. The most important categories are: representativeness of product performance in practice, good control of the test conditions and determination and limitation of measurement uncertainties. Items from all three categories have been discussed from the beginning of the development of the method, but with an emphasis on the first two. As discussed earlier, research topics in that area have been listed already by CEN, FSG and EGOLF.

Little attention has been paid to the third category on measurement uncertainty and its improvement. Due to the recent uncertainty discussions in relation to EN 17025, this however has become more important. The major research topics in this area are discussed below and will be dealt with in this work. Gaining a better insight in the oxygen depletion measurement technique and identifying its pitfalls, greatly improves the accuracy of the method and allows a reliable estimation of the uncertainty interval.

In a nutshell, the measurement technique used, the oxygen depletion technique, is based on the observation that, in general, the heats of combustion per unit mass of oxygen consumed are approximately the same for most fuels commonly encountered in fires (Huggett<sup>[49]</sup>). The mass flow together with the oxygen concentration in the extraction system suffices to continuously calculate the amount of heat released. Some corrections can be introduced if additionally CO<sub>2</sub> and/or CO are measured. The technique is further explained in chapter 2.

The time dependence of the different measurands also requires to consider the dynamic aspects of the measuring technique.

### 1.6.1 Gas analysis

The oxygen concentration is one of the most important measurands when measuring heat release rate. Evenly important as the concentration measurement itself is the gas sampling and preparation. This includes the sampling, filtering, transport over several meters distance and dehydration.

The uncertainty related to the oxygen concentration measurement itself includes the calibration method, the calibration gas, ambient conditions like barometric pressure and room temperature, damping, vibrations, etc. The challenge here is to measure variations in concentration of the order of 50 ppm in the range from 17 to 21 Vol.%. These variations are in the same order as the allowed noise level. Although damping of the signal allows elimination of a great part of the noise, it results in higher response times.

Determination of the uncertainty on the measurement requires much more than for example taking the sum of noise and drift as proposed by Enright<sup>[66]</sup>.

## 1.6.2 Mass flow rate

So far only limited effort has been invested in the accurate determination of the mass flow rate and/or in the improvement of the extraction system (duct diameter, guide vanes, ...). Only a limited number of people within the fire testing community seems to be aware of the impact of the mass flow on the accuracy of the overall heat release rate and smoke release rate measurement. Prove of this are the pre-standards prEN 50399-1<sup>[7]</sup>, for the assessment of the reaction to fire performance of cables, and prEN 45545-2<sup>[8]</sup>, for the assessment of the reaction to fire performance of materials for railway vehicles. Especially in the second standard, where heat release rates as low as 7 kW and variations of heat release rate smaller than 1 kW are envisaged using hardware designed to cope with fires releasing up to 1 MW (Duct  $\phi = 400$  mm; extraction rate 1.5 m<sup>3</sup>/s at 298 K). The oxygen depletion at the 1 kW level under the given circumstances is only 35 ppm, which disappears in the measurement noise.

In general, there is a high degree of ‘copy-pasting’ from other standards, i.e. ISO 9705, into new developed standards without re-evaluating the method in these new circumstances. ISO 9705 is a full-scale test method intended to evaluate the contribution to fire growth provided by a surface product applied in a room. It goes for itself that appropriate downscaling and adaptation for small and intermediate scale test methods and, in particular for this work, the SBI test is necessary if an acceptable uncertainty is envisaged.

### 1.6.2.1 Velocity profile – The effect of heating and cooling

The technique for measuring mass flow rate  $\dot{m}$  currently used in intermediate to large scale calorimeter tests consists of measuring the velocity on the axis of the duct  $v_{axis}$  and to multiply this with a correction factor  $k_t$  to obtain the mean velocity. This mean velocity is then multiplied with the mean density  $\bar{\rho}$  and the surface area  $A$  to obtain the mass flow rate.

$$\dot{m}(t) = \bar{\rho} k_t v_{axis}(t) A \quad [ 1.2 ]$$

$k_t$  is the velocity profile correction factor and is defined as

$$k_t(t) = \frac{\int v(t) dA}{v_{axis}(t)A} \quad [1.3]$$

Since the distribution of the velocity is not known,  $k_t$  is approximated and taken as a constant over time. If we knew the velocity distribution, the mass flow rate could be approximated by

$$\dot{m}(t) = \bar{\rho} \int_A v(t) dA \quad [1.4]$$

which is only correct when the density is uniform over the measuring section. Ideally we would want to measure

$$\dot{m}(t) = \int_A \rho(t)v(t) dA \quad [1.5]$$

So far, all uncertainty studies have disregarded the error made by assuming the density is constant.

Bryant et al. however, for their 3 Megawatt test facility use a series of *velocity pressure probe – thermocouple* pairs to more accurately measure the mass flow which is of course a good solution.

### 1.6.2.2 The velocity measurement

The velocity measurement is made by means of a so called bi-directional pressure probe which is based on the pitot-static tube principle. The bi-directional probe<sup>[51]</sup> was originally designed for measuring the low velocity of (buoyancy-driven) fire induced flows associated with small to medium size fires. It has been ‘copy-pasted’ into various international test standards and is considered to be the state of the art for measuring mass flows in combustion gases.

Although the probe is suited to work both in sooty environments and at elevated temperatures, this dissertation revealed that it overestimates the measured velocity by approximately 1% per degree pitch or yaw angle initially<sup>[56]</sup>. This can be caused by improper alignment of the probe with the flow or by a radial velocity component in the exhaust flow. It also reveals that the probe used in the SBI standard, which has a slightly modified design, is less angle sensitive but is, in contradiction with the standard bi-directional probe, Reynolds dependant. Due to the ever changing temperatures of the combustion

gases in time and the varying velocity of those gases, the Reynolds number related to the probe outside diameter will, in the SBI, vary in the range from  $3 \cdot 10^3$  to  $3 \cdot 10^4$  approximately.

So far, these effects have been disregarded resulting in an underestimation of the uncertainty interval.

### 1.6.2.3 Transient error

An additional source of error is introduced by the response times of the measuring devices. The gas analysis system – from sampling to analysis – has a non negligible time constant  $\tau$ . This introduces a transient error which, in the case of oxygen, equals

$$e = \tau \frac{dX_{O_2}}{dt} \quad [ 1.6 ]$$

Inverse techniques may help to restore the ‘real’ variation of oxygen concentration over time. This however needs further investigation and, if used, a general agreed consensus on how to do it.

In a nutshell the procedure is as follows. The gas analysis system is considered to work as a (first order) low pass filter with transfer function  $H(s)$ . Taking the inverse in the Laplace domain  $H(s)^{-1}$  allows to restore the original signal. However, high frequency disturbances like noise tend to disturb the process. Indeed, the inverse system  $H(s)^{-1}$  works as an amplifier for the high frequencies.

So inverse techniques should only be used with great care and require appropriate filters to remove the high frequency noise from the measured signal. They also require a complete redesign of the data acquisition procedure applied now, i.e. one sample taken every three seconds.

## 1.7. Strategy followed

As outlined in the previous paragraph, this work highlights three major research topics: the analysis of combustion gases, the mass flow through the exhaust duct of those same gases and the dynamic aspects of instruments, processes and measuring equipment.

Contiguous, their influence on the global uncertainty is investigated and means to decrease this uncertainty and to remove systematic errors are proposed.

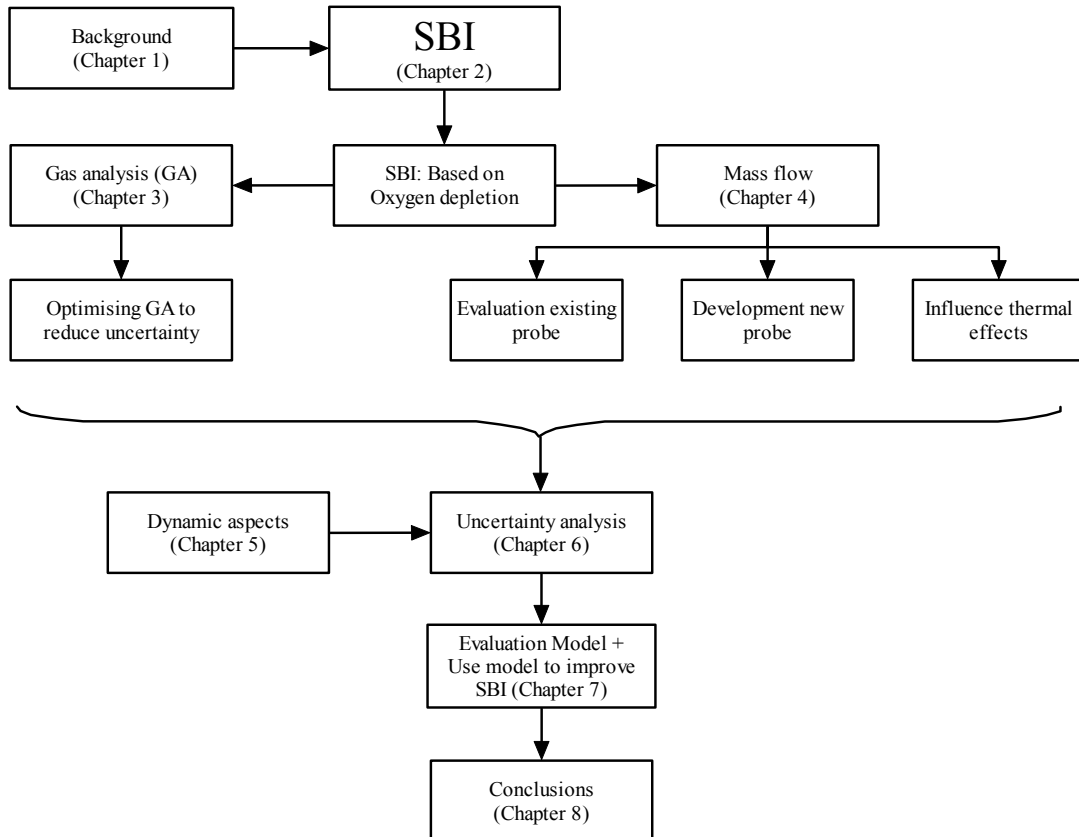


Figure 2. General overview

In chapter II the measurement principle is explained and the main calculation procedures presented.

Chapter III focuses on the gas sampling which includes the complete train from sampling till analysis.

Chapter IV discusses the mass flow rate measurement and contains one of the major contributions of this work: after an evaluation of the existing velocity pressure probes, where some major drawbacks are first identified, a high performance pressure probe has been designed that overcomes the shortcomings of the existing probes and improves on the other aspects. Furthermore, the probe factor of both the existing probes and the new developed probe, together with an estimate on the standard deviation, have been obtained. The results have been summarised in papers which have been accepted for publication and will be published soon.

A further two papers on the influence of thermal effects on the velocity profile of duct flows and, more general, on the mass flow are out for review. Those two papers have been prepared in close collaboration with two colleagues of the same department.

The main focus was on the estimation of uncertainty due to thermal effects on the mass flow<sup>[58]</sup>, and the relationship between the transient (due to thermal inertia) velocity profile and a newly defined effective Reynolds number<sup>[52]</sup>.

Chapter V deals with the dynamic aspects of the test instruments, the process and the data acquisition. It also evaluates the, currently used, ‘flat’ *moving average filter* and proposes the use of a more efficient Henderson filter.

Furthermore it raises questions like ‘what is the bandwidth (fastest process) we’re interested in’, gives guidance on this and proposes three possible levels of alternative measuring methods. It also discusses the possibility of using inverse filters to increase the bandwidth.

Although all of the concepts are known to specialists in the field, they are virgin territory to the fire testing community.

Chapter VI discusses uncertainty and any related aspects in great detail. After elaboration of some general concepts, the combined standard uncertainty for heat release measurements in the SBI has been worked out. This analytical model requires the input of estimates of uncertainty on the different components which are discussed in a next section.

New with respect to previous attempts to estimate the uncertainty is: the use of asymmetric distributions, the use of correlated input quantities, the inclusion of transient errors, the inclusion of uncertainty related to synchronisation and, last but not least, the detailed study on the estimation of the different uncertainty components.

In chapter VII the model is checked using round robin results and some recommendations are given to improve the test method.

Chapter VII brings us to the conclusions and recommendations.

Annex A groups four articles that have gone out for review. Two of them have been accepted for publication in the mean time, while the other two are in the process of reviewing.

Annex B groups some intermediate results, some correspondence with manufacturers, etc.



## 2 Measurement principle and calculation procedures

### 2.1. General

The measuring technique of the SBI test instrument is based on the observation that, in general, the heats of combustion per unit mass of oxygen consumed are approximately the same for most fuels commonly encountered in fires (Huggett<sup>[49]</sup>). The mass flow together with the oxygen concentration in the extraction system suffices to continuously calculate the amount of heat released. Some corrections can be introduced if additionally CO<sub>2</sub>, CO and/or H<sub>2</sub>O are measured.

The specimen under test consists of two parts mounted in a corner configuration. The dimensions of the parts are 1500mm by 1000mm and 1500mm by 500mm, with a maximum thickness of 200mm. After mounting on a trolley sample holder, the specimen is placed underneath a hood.

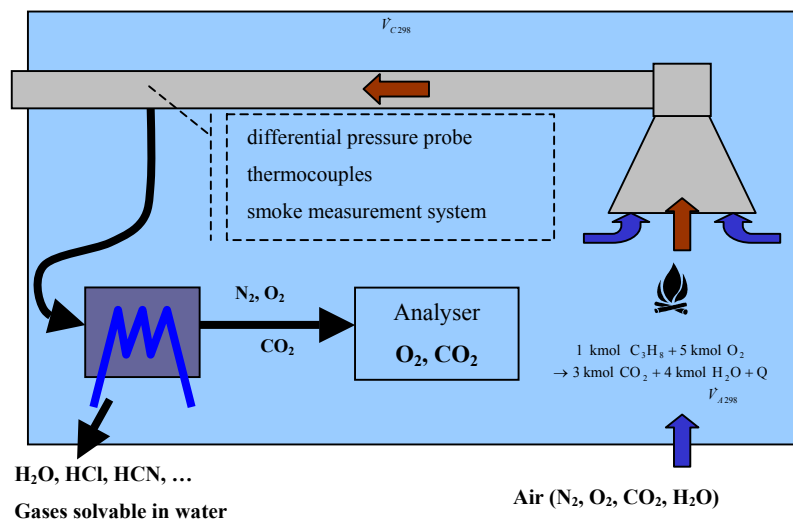


Figure 3. Schematic of the working principle of the oxygen depletion technique

The thermal attack – that simulates a single burning item like a paper basket on fire – onto the specimen is achieved using a triangular shaped diffusion type burner, fired with propane. The main burner is placed at a distance of 40mm from both sides of the specimen.

A ‘primary burner’ – installed at a safe distance from the specimen – that burns for three minutes prior to the attack of the specimen, allows to subtract the contribution of the burner afterwards.

The test sequence is:

- -60s - 0s: Registering of pre-test conditions;
- 0s - 120s: Registering of zero-reference and drift while burner is kept off;
- 120s - 300s: Registering 30kW-reference and drift with primary burner turned on;
- 300s - 1560s: Actual test with main burner turned on at 300 s;

- Registering end of test conditions for O<sub>2</sub>, CO<sub>2</sub> and light obscuration after the sample has been removed (check drift).

The main signals that are registered every 3 seconds during the test are (see Table 2):

- the propane mass flow to the burner system [mg/s];
- the oxygen concentration in the exhaust gases [Vol%];
- the carbon dioxide concentration in the exhaust gases [Vol%];
- the carbon monoxide concentration in the exhaust gases [Vol%] (optional);
- the pressure difference over a bi-directional probe [Pa];
- the temperature at the height of the bi-directional probe [K];
- the light transmittance through the exhaust gases [%].

i/o	Signal	symbol	Units	kW		
				0	30*	92.7*
y <sub>1</sub>	Paramagnetic oxygen analyser	X <sub>O<sub>2</sub></sub>	Vol%	20.95	20.67	20.06
y <sub>2</sub>	Non-dispersive IR CO <sub>2</sub> -analyser	X <sub>CO<sub>2</sub></sub>	Vol%	0.04	0.23	0.63
y <sub>3</sub>	Temperature measurement MS (K-type)	T <sub>MS</sub>	K	290	318	376
y <sub>4</sub>	Bi-directional pressure probe	Δp	Pa	61	67	79
y <sub>5</sub>	Smoke opacity measurement	I	%	100	97	96
u <sub>1</sub>	Propane Mass Flow Controller	MFC	mg/s	0	647	2000
<b>Derived data</b>						
	Volume flow exhaust gases (at 25°C)	V <sub>298</sub>	m <sup>3</sup> /s	0.65	0.65	0.65
	Heat Release Rate	HRR	KW	0	30	92.7
	Total Heat Release (in first 600 s)	THR <sub>600s</sub>	MJ	0	NA	NA
	Fire Growth Rate	FIGRA	W/s	0	NA	NA
	Smoke Production Rate	SPR	m <sup>2</sup> /s	0	0.06	0.08
	Total Smoke Production (in first 600 s)	TSP <sub>600s</sub>	m <sup>2</sup> /s <sup>2</sup>	0	NA	NA
	Smoke Growth Rate	SMOGRA	m <sup>2</sup> /s <sup>2</sup>	0	NA	NA
<b>* approximate values for the Ghent premises running at a constant mass flow</b>						

Table 2. Main SBI signals and derivatives

Figure 4 shows the ‘raw’ data of a ‘typical’ SBI test. The peak observed around 300 s finds its origin in the switching between *primary* and *main* burner. This peak is used to synchronise the data afterwards.

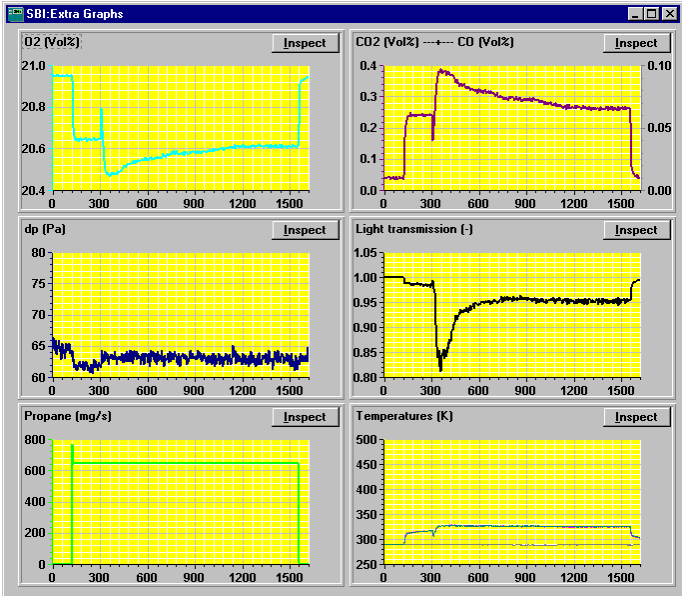


Figure 4. Example of SBI raw data

The volume flow referenced to 298 K together with the oxygen and carbon dioxide concentration results in the global heat release rate (burner + specimen) (Figure 5.a). The heat release in the period from 150 s to 270 s (primary burner burning) serves as a basis to subtract the heat release contribution of the burner. A ‘flat’ running average filter now smoothes the heat release contribution of the specimen (Figure 5.b).

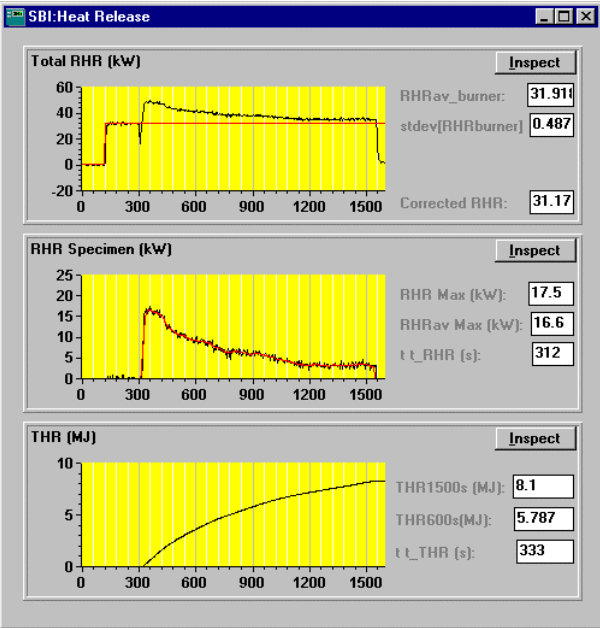


Figure 5. Heat release rate and derivatives

Out of the (undampened) heat release rate (HRR) the total heat release rate in the first 600 s of the test (THR600s; 300 – 900 s) is calculated and out of the dampened HRR the FIre Growth RAte (FIGRA) is calculated. FIGRA is proportional to the maximum of the ratio of the HRR (running average HRR) contribution of the specimen to the time required to reach this HRR level.

The FIGRA index in the context of the SBI test method was first introduced in 1997<sup>[69]</sup> as a result of the analysis of the first round robin exercise<sup>[68]</sup> held by fifteen leading European Fire test laboratories including the Fire department of the Ghent University.

The idea behind the FIGRA (SMOGRA) index is to penalise heat release rate (smoke production rate) – i.e. contribution to the development of the fire – in the initial stage of a fire for this is the time when people try to make their ways out of the building.

(\*) Some threshold values apply:

$$\text{HRR} < 3\text{kW} \Rightarrow \text{FIGRA} = 0$$

$$\text{THR} < 0,2 \text{ or } 0,4\text{MJ} \Rightarrow \text{FIGRA} = 0$$

## **2.2. Calculation procedure**

### **2.2.1 Introduction**

The main calculation procedures for obtaining the HRR and its derived parameters are summarised here for convenience. The formulas will be used in the next chapters and especially in the chapter on uncertainty.

The calculations and procedures can be found in full detail in the SBI standard<sup>[2]</sup>.

### **2.2.2 Synchronization of data**

The measured data are synchronised making use of the dips and peaks that occur in the data due to the switch from ‘primary’ to ‘main’ burner around  $t = 300$  s, i.e. at the start of the thermal attack to the test specimen. Synchronisation is necessary due to the delayed response of the oxygen and carbon dioxide analysers. The filters, long transport lines, the cooler, etc. in between the gas sample probe and the analyser unit, cause this shift in time.

After synchronisation, all data are shifted such that the ‘main’ burner ignites – by definition – at time  $t = 300$  s.

## 2.2.3 Heat output

### 2.2.3.1 Average heat release rate of the specimen (HRR<sub>30s</sub>)

A first step in the calculation of the heat release rate contribution of the specimen is the calculation of the *global heat release rate*. The global HRR is constituted of the HRR contribution of both the specimen and the burner and is defined as

$$\text{HRR}_{\text{total}}(t) = E' \dot{V}_{D298}(t) x_{a\_O2} \left( \frac{\phi(t)}{1 + 0,105\phi(t)} \right) \quad [2.1]$$

where:

- HRR<sub>total</sub>(t) is the total heat release rate of the specimen and burner [kW];
- E' is the heat release per unit volume of oxygen consumed at 298 K, = 17 200 [kJ/m<sup>3</sup>];
- $\dot{V}_{D298}(t)$  is the volume flow rate of the exhaust system, normalized at 298 K [m<sup>3</sup>/s];
- x<sub>a\_O2</sub> is the mole fraction of oxygen in the ambient air including water vapour;
- $\phi(t)$  is the oxygen depletion factor.

The last two terms x<sub>a\_O2</sub> and  $\left( \frac{\phi(t)}{1 + 0,105\phi(t)} \right)$  express the amount of moles of oxygen, per unit volume, that have chemically reacted into some combustion gases. Multiplication with the volume flow gives the amount of moles of oxygen that have reacted away. Finally this value is multiplied with the 'Huggett' factor. Huggett stated that regardless of the fuel burnt roughly a same amount of heat is released.

The volume flow of the exhaust system, normalized at 298 K,  $\dot{V}_{D298}(t)$  is given by

$$\dot{V}_{D298}(t) = cA \frac{k_t}{k_p} \sqrt{\frac{\Delta p(t)}{T_{ms}(t)}} \quad [2.2]$$

where:

- c =  $\sqrt{(2T_0/\rho_0)} = 22,4$  [K<sup>0.5</sup>·m<sup>1.5</sup>·kg<sup>-0.5</sup>]
- A is the area of the exhaust duct at the general measurement section [m<sup>2</sup>];

- $k_t$  is the flow profile correction factor; converts the velocity at the height of the bi-directional probe in the axis of the duct to the mean velocity over the cross section of the duct
- $k_p$  is the Reynolds number correction for the bidirectional probe, taken as 1,08;
- $\Delta p(t)$  is the pressure difference over the bi-directional probe [Pa];
- $T_{ms}(t)$  is the temperature in the measurement section [K].

The oxygen depletion factor  $\phi(t)$  is defined as

$$\phi(t) = \frac{\bar{x}O_2(30s...90s)\{1 - xCO_2(t)\} - xO_2(t)\{1 - \bar{x}CO_2(30s...90s)\}}{\bar{x}O_2(30s...90s)\{1 - xCO_2(t)\} - xO_2(t)} \quad [2.3]$$

where:

- $xO_2(t)$  is the oxygen concentration in mole fraction;
- $xCO_2(t)$  is the carbon dioxide concentration in mole fraction;
- $Ys...Zs$  mean taken over interval Y s to Z s.

The mole fraction of oxygen in ambient air, taking into account the moisture content, is given by

$$x_{a_{O_2}} = \bar{x}O_2(30s...90s) \left[ 1 - \frac{H}{100p} \exp \left\{ 23,2 - \frac{3816}{\bar{T}_{ms}(30s...90s) - 46} \right\} \right] \quad [2.4]$$

where:

- $xO_2(t)$  is the oxygen concentration in mole fraction;
- $H$  is the relative humidity [%];
- $p$  is the ambient pressure [Pa];
- $T_{ms}(t)$  is the temperature in the general measurement section [K].

Since we are interested in the HRR contribution of the specimen only, the HRR contribution of the burner needs to be subtracted. An estimate of the burner contribution  $HRR_{burner}(t)$  is taken as the  $HRR_{total}(t)$  during the base line period preceding the thermal attack to the specimen. A mass flow controller assures an identical heat release rate through the burners before and after switching from primary to the main burner. The average HRR of the burner is calculated as the average  $HRR_{total}(t)$  during the base line period with the primary burner on ( $210 s \leq t \leq 270 s$ ):

$$\text{HRR}_{\text{av\_burner}} = \overline{\text{HRR}}_{\text{total}}(210 \text{ s} \dots 270 \text{ s}) \quad [ 2.5 ]$$

where:

$\text{HRR}_{\text{av\_burner}}$  is the average heat release rate of the burner [kW];

$\text{HRR}_{\text{total}}(t)$  is the total heat release rate of specimen and burner [kW].

### ***HRR of the specimen***

In general, the heat release rate of the specimen is taken as the global heat release rate  $\text{HRR}_{\text{total}}(t)$  minus the average heat release rate of the burner  $\text{HRR}_{\text{av\_burner}}$ :

For  $t > 312$  s:

$$\text{HRR}(t) = \text{HRR}_{\text{total}}(t) - \text{HRR}_{\text{av\_burner}} \quad [ 2.6 ]$$

where:

$\text{HRR}(t)$  is the heat release rate of the specimen [kW];

$\text{HRR}_{\text{total}}(t)$  is the global heat release rate of specimen and burner [kW];

$\text{HRR}_{\text{av\_burner}}$  is the average heat release rate of the burner [kW].

During the switch from the primary to the main burner at the start of the exposure period, the total heat output of the two burners is less than  $\text{HRR}_{\text{av\_burner}}$  (it takes some time for the gas to be directed from one burner to the other). Equation [2.6] then gives negative values for  $\text{HRR}(t)$  for at most 12 s (burner switch response time). Such negative values and the value for  $t = 300$  s are set to zero, as follows:

For  $t = 300$  s:

$$\text{HRR}(300) = 0 \text{ kW} \quad [ 2.7 ]$$

For  $300 \text{ s} < t \leq 312 \text{ s}$ :

$$\text{HRR}(t) = \max. \{ 0 \text{ kW}, \text{HRR}_{\text{total}}(t) - \text{HRR}_{\text{av\_burner}} \} \quad [ 2.8 ]$$

where:

$\max.[a, b]$  is the maximum of two values  $a$  and  $b$ .

### **Calculation of $HRR_{30s}$**

In view of the calculation of the FIGRA index, the HRR data are smoothed with a ‘flat’ 30 s running average filter using 11 consecutive measurements:

$$HRR_{30s}(t) = \frac{0,5HRR(t-15) + HRR(t-12) + \dots + HRR(t+12) + 0,5HRR(t+15)}{10} \quad [2.9]$$

where:

$HRR_{30s}(t)$  is the average of  $HRR(t)$  over 30 s [kW];

$HRR(t)$  is the heat release rate at time  $t$  [kW].

More information on the behaviour of this filter is given in section 5.3.1.

### **2.2.3.2 Calculation of $THR(t)$ and $THR_{600s}$**

The total heat release of the specimen  $THR(t)$  and the total heat release of the specimen in the first 600 s of the exposure period ( $300 \text{ s} \leq t \leq 900 \text{ s}$ ),  $THR_{600s}$ , are calculated as follows:

$$THR(t_a) = \frac{1}{1000} \sum_{300s}^{t_a} HRR(t) \times 3 \quad [2.10]$$

$$THR_{600s} = \frac{1}{1000} \sum_{300s}^{900s} HRR(t) \times 3 \quad [2.11]$$

whereby the factor 1000 is introduced to convert the result from kJ into MJ and the factor 3 stands for the time interval in-between two consecutive measurements,

and where:

$THR(t_a)$  is the total heat release of the specimen during the period  
 $300 \text{ s} \leq t \leq t_a$  [MJ];

$HRR(t)$  is the heat release rate of the specimen [kW];

$THR_{600s}$  is the total heat release of the specimen during the period  $300 \text{ s} \leq t \leq 900 \text{ s}$   
[MJ]; [equal to  $THR(900)$ ].



### 2.2.3.3 Calculation of FIGRA<sub>0,2MJ</sub> and FIGRA<sub>0,4MJ</sub> (Fire growth rate indices)

The FIGRA is defined as the maximum of the ratio  $HRR_{av}(t)/(t - 300)$ , multiplied by 1 000. The ratio is calculated only for that part of the exposure period in which the threshold levels for  $HRR_{av}$  and THR have been exceeded. If one or both threshold values are not exceeded during the exposure period, FIGRA is equal to zero. Two combinations of threshold values are used, resulting in FIGRA<sub>0,2MJ</sub> and FIGRA<sub>0,4MJ</sub>.

a) The average of HRR,  $HRR_{av}$ , used to calculate the FIGRA is equal to  $HRR_{30s}$ , with the exception of the first 12 s of the exposure period. For data points in the first 12 s, the average is taken only over the widest possible symmetrical range of data points within the exposure period:

$$\text{For } t = 300 \text{ s: } HRR_{av}(300 \text{ s}) = 0 \quad [ 2.12 ]$$

$$\text{For } t = 303 \text{ s: } HRR_{av}(303 \text{ s}) = \overline{HRR}(300 \text{ s} \dots 306 \text{ s}) \quad [ 2.13 ]$$

$$\text{For } t = 306 \text{ s: } HRR_{av}(306 \text{ s}) = \overline{HRR}(300 \text{ s} \dots 312 \text{ s}) \quad [ 2.14 ]$$

$$\text{For } t = 309 \text{ s: } HRR_{av}(309 \text{ s}) = \overline{HRR}(300 \text{ s} \dots 318 \text{ s}) \quad [ 2.15 ]$$

$$\text{For } t = 312 \text{ s: } HRR_{av}(312 \text{ s}) = \overline{HRR}(300 \text{ s} \dots 324 \text{ s}) \quad [ 2.16 ]$$

$$\text{For } t \geq 315 \text{ s: } HRR_{av}(t) = HRR_{30s}(t) \quad [ 2.17 ]$$

b) Calculate FIGRA<sub>0,2MJ</sub> for all  $t$  where:

$$(HRR_{av}(t) > 3 \text{ kW}) \text{ and } (THR(t) > 0,2 \text{ MJ}) \text{ and } (300 \text{ s} < t \leq 1\,500 \text{ s});$$

and calculate FIGRA<sub>0,4MJ</sub> for all  $t$  where:

$$(HRR_{av}(t) > 3 \text{ kW}) \text{ and } (THR(t) > 0,4 \text{ MJ}) \text{ and } (300 \text{ s} < t \leq 1\,500 \text{ s});$$

both using:

$$FIGRA = 1000 \times \max \left( \frac{HRR_{av}(t)}{t - 300} \right) \quad [ 2.18 ]$$

where:

FIGRA is the fire growth rate index

$HRR_{av}(t)$  is the average of  $HRR(t)$  as specified in a) [kW];

As a consequence, specimens with a  $HRR_{av}$  not exceeding 3 kW during the total test have FIGRA values  $FIGRA_{0,2MJ}$  and  $FIGRA_{0,4MJ}$  equal to zero. Specimens with a THR not exceeding 0,2 MJ over the total test period have a  $FIGRA_{0,2MJ}$  equal to zero and specimen with a THR not exceeding 0,4 MJ over the total test period have a  $FIGRA_{0,4MJ}$  equal to zero.

#### 2.2.3.4 Calculation of (M)ARHE

The MARHE parameter, which stands for *Maximum Average Rate of Heat Emission*, is a value that is not used for classification purposes nor is it required by the SBI standard. It has however been included in this document since it is discussed internationally. The present work limits itself to the evaluation of the uncertainty related to this parameter.

The MARHE value is defined as the maximum of the ARHE curve which is given by ( $n = 1, 2, \dots$ ):

$$ARHE(t_n) = \left( \frac{t_1 - t_0}{t_n - t_0} \right) \left( \sum_{i=0}^n HRR(t_i) - \frac{HRR(t_n)}{2} \right) = \frac{1}{n} \left( \sum_{i=0}^n HRR(t_i) - \frac{HRR(t_n)}{2} \right) \quad [ 2.19 ]$$

This formula assumes that the initial heat release contribution of the specimen (at the start of the test) is zero ( $HRR(t_0) = 0$  kW) and further uses the trapezoidal integration scheme.

## **3 Gas Analysis**

### **3.1. Introduction**

In view of the importance of a correct oxygen depletion measurement and the automation of the measuring process, an optimised gas analysis rack – from sampling till analysis – has been developed in collaboration with Siemens Belgium and Siemens Karlsruhe.

In heat release rate (HRR) related measurements, the oxygen concentration is one of the most important properties. Although the technique for measuring gas concentrations is known, the system has been optimised for heat release rate measurement applications in terms of sample preparation, precision and robustness of the gas analysis rack.

The design of the analysis rack is such that it cannot only be used for the SBI, but also for the room corner test, the cone calorimeter test and similar test methods based on the oxygen depletion technique. In the mean time well over twenty laboratories are using this analysis rack in a wide variety of heat release test instruments.

### **3.2. Optimising**

In the previous chapter and in the SBI standard the oxygen depletion technique is described for the specific case of the SBI. For a more general discussion, a good description is given by Parker<sup>[54]</sup>. In this paper distinction is made between four different cases:

1. The gas concentrations of O<sub>2</sub>, CO<sub>2</sub>, CO and H<sub>2</sub>O are measured.
2. The gas concentrations of O<sub>2</sub>, CO<sub>2</sub> and CO are measured. H<sub>2</sub>O is removed from the sample gas prior to analysing the gas concentrations.
3. The gas concentrations of O<sub>2</sub> and CO<sub>2</sub> are measured. H<sub>2</sub>O is removed from the sample gas prior to analysing the gas concentrations and the CO concentration is neglected.
4. Only the O<sub>2</sub> concentration is measured. Both H<sub>2</sub>O and CO<sub>2</sub> are removed from the sample gas because they push aside the O<sub>2</sub> molecules thus reducing the O<sub>2</sub> concentration. The concentration of CO is neglected.

The presence of a water vapour analyser further improves the accuracy of the measurement but has proven to be somewhat cumbersome and difficult to implement successfully. The entire gas sampling train must be heated in order to avoid condensation. Since the inclusion of water vapour measurements

requires a completely different approach from the other three cases, all efforts are concentrated on cases 2 till 4.

The use of a carbon dioxide analyser eliminates the need for removal of CO<sub>2</sub> out of the gas sample. This is mainly of practical importance as the scrubbing agent – which is a chemical absorbent – used to remove CO<sub>2</sub> usually requires careful handling and is rather expensive.

Measuring heat release by oxygen concentration only thus requires an additional chemical recipient over cases 2 and 3.

Because the oxygen depletion technique is applied in a wide variety of standards ranging from small <sup>[4]</sup>, over intermediate <sup>[2][7][8]</sup> to large scale tests <sup>[6]</sup>, the challenge was to design one gas analysis unit that can be interchanged easily between different applications.

Other requirements imposed on the design are:

- filtering the gas for particles directly after the gas sampling;
- avoid condensation of water vapour and/or corrosive gases like HCl etc. in the transport lines;
- provide dry gas, free of particles to the gas analysers;
- pressure compensation on the oxygen analyser;
- keep temperature variations to within a minimum;
- reduce the amount of consumables to a minimum;
- robustness;
- limited size;
- minimum maintenance;
- plug and play;
- limit the cost.

In a first stage the focus is on the gas analysers and especially on the oxygen analyser where the following improvements are obtained:

- The use of selected measuring cells increases the stability of the analyser. All analyser cells are checked by Siemens for some minimum requirements on performance and stability. Based on the outcome of this check, they are subdivided into three categories ranging from highly stable to acceptable performance. Since stability of the analyser is of outmost importance, the requirement is to only use those measuring cells with best stability performance.
- The oxygen analyser makes use of the fact that when two gases with different oxygen concentration meet in a magnetic field, a pressure difference is produced between them. So besides the measured gas, a reference gas is needed. Most Siemens systems use Nitrogen as

reference gas. By introducing ambient air as a reference gas, several advantages could be introduced:

- The measuring range can be narrowed from 0-21Vol% to 17-21Vol% increasing the resolution of the output signal and lowering the uncertainty on the output.
- The analyser works close to its point of equilibrium. Indeed, initially the analysed gas has the same concentration as the reference gas, i.e. 20.95Vol%, and, as heat release increases, remains close to equilibrium (>17 Vol%).
- Note that the room corner test (ISO 9705) requires the full range 0-21Vol%. For those cases, Nitrogen will be used as a calibration gas instead of 17Vol% of oxygen. The reference gas and the rest of the analysis system however remains unchanged.
- The cost of nitrogen consumption as a reference gas and the renting of two nitrogen bottles (one spare) is saved.

Alternatively to using ambient air as a reference gas, synthetic air containing for example 21 Vol% of oxygen could be used. In the first case, a chemical desiccant is needed to remove any water vapour, while in the second case, the consumption of gas and the renting of bottles should be taken into account.

- The oxygen measuring cell together with the carbon dioxide and carbon monoxide cells are combined in one 19" housing. Since the oxygen analyser works on the paramagnetic principle and the other two analysers on the infrared principle, they have never been combined into one unit. By doing so the following advantages are obtained:
  - Cost and space savings.
  - One user interface for all three gas analysers.
  - Less pipe work resulting in faster response times.
  - Possibility to correct for the interference of the CO<sub>2</sub> gas on the O<sub>2</sub> measurement. Due to diamagnetism and paramagnetism of residual gases there is a deviation on the measured oxygen concentration. If pure carbon dioxide were to be introduced into the oxygen analyser, the analyser would have a reading of -0.30Vol% of oxygen. This deviation only becomes significant for high heat release rates when high concentrations of carbon dioxide are reached.

In a second stage the focus is on the reduction of the delay and response time of the gas analysis system. Commercial gas analysers are mostly designed to operate in steady state or to measure 'slowly' changing signals. The following measures were taken:

- Limiting the inside diameter pipe work to 4 mm. This choice introduces as a consequence:
  - Filtering of the hot sample gas. Just after the gas sample probe, a temperature controlled filter is installed. The re-useable heated ceramic filter is kept at a

temperature of 200°C in order to prevent the pores to get saturated too quickly by condensing gases. The filter eliminates particles down to a size of 3µm.

- Heating of the gas sampling line connecting the measurement point to the gas analysis rack. The heated sampling line (9m) has a replaceable PVDF core heated to 120°C to prevent condensation of combustion gases which would result in blockage of the pipework.
- The use of a high capacity membrane pump that extracts the gas at a rate of 16 litres/minute. This high extraction rate reduces the transport time of the gas through the heated filter, the heated sampling line and through the cooler to a minimum. The analysers only need 2 litres/minute which makes that the excess gas is blown off just after the pump. This however implies that:
  - The heated filter must be sized correspondingly;
  - The capacity of the cooler needs to be upscaled by a factor 8.
- All pipe work after the membrane pump is kept to a strict minimum. This is achieved by:
  - Reducing the size of the gas analysis rack. This was only possible after combining the three gas analysers into one unit.
  - Adequate positioning of the remaining components (water absorbent, filter, valves)
- Reduction of the electronic damping on the analyser signal to a strict number. This is only acceptable when highly stable gas analysers are used, and confirms once more the need for the 'selected' oxygen measuring cells.

In a third stage the focus was on the gas conditioning, and more in particular the removal of H<sub>2</sub>O. Since one of the assumptions in the calculations is that the gas coming into the analyser consists of O<sub>2</sub>, CO<sub>2</sub>, (CO) and N<sub>2</sub> only, all water vapour (and water soluble components such as HCl, HCN, etc.) needs to be removed from the sample gas. This is achieved in two steps:

1. A gas sample cooler brings down the temperature of the sample gas to approximately 3°C. The saturation pressure at this temperature is approximately 770 Pa. Leaving this water vapour in the gas sample introduces an error at two levels:
  - a. the measured oxygen depletion will be smaller and the error amounts approximately 1% of the depletion.
  - b. variations on the dew point of the gas cooler as a consequence of cooler temperature variations lead to a different saturation pressure with corresponding error. Due to temporary higher water vapour concentrations in the exhaust gases, the dew point may vary. For a dew point increase of 2°C to 5°C the saturation pressure increases with 110 Pa approximately with a resulting difference in oxygen concentration of 230ppm.

2. This is why a desiccant is used to remove the remaining water vapour. Nowadays laboratories use Anhydrous Calcium Sulfate (Drierite) for this purpose. A more ample discussion on desiccants can be found in annex B.1.

A consequence is that also the reference gas for the oxygen analyser, which is ambient air, needs to pass through a desiccant. As mentioned before, synthetic air could be used as an alternative which eliminates the use to 'dry' the reference gas.

In the final stage some additional features are introduced to:

- increase the user friendliness:
  - all user interfaces are located at the front and at an ergonomic height;
  - pumps, valves, heating of filters and sampling lines are controlled by illuminated pushbuttons
  - status of cooler, analyser, reference gas pump, heated filter, heated sampling line, breaker tripping are checked and available to the user
  - the rack can be controlled remotely to run for example calibrations or tests without intervention of the operator. This allows a complete control of the test instrument through the software with status reporting, auto calibration, etc.
- increase the interchangeability between different fire test instruments (cone calorimeter, SBI, room corner, etc.):
  - mounted on wheels
  - eyebolts on the top
  - all signals (both digital and analogue) and power supply brought to four connectors mounted on the top of the rack
  - Plug and Play
- Robustness and other features:
  - 19" Rittal housing
  - Front door protects the instrumentation and helps to keep dust out
  - Temperature controlled
  - Filtered cooling air



Figure 6. Front and backside (in a cone calorimeter unit) of the gas analysis rack



## **4 Mass flow rate**

### **4.1. Introduction**

So far only limited effort has been invested in the accurate determination of the mass flow rate and/or in the improvement of the extraction system. This is surprising since the heat release rate (HRR) is proportional to it.

The mass flow rate in the circular exhaust duct is obtained by a one point velocity measurement in a cross section. This requires an accurate measurement of velocity on the duct axis and a knowledge of both the velocity profile and density profile over the cross-section of the duct. So far in fire test applications, the probe factor is almost always taken constant over time and the effect of non-uniform density over the duct is disregarded.

The velocity measurement is made by means of a Pitot like differential pressure probe adapted for measuring bi-directional flows in fires<sup>[51]</sup>. Bi-directional probes are designed to measure flow speed in fire conditions where the direction of the flow is not necessary known nor constant. For example mounted in a doorway, in function of the height there may first be entrainment of air to the fire while later on in the test, hot combustion gases may leave that same doorway as the hot smoke layer increases and lowers.

The design has been copied for use in HRR test applications for its robustness and assumed angle and Reynolds independence without thoroughly investigating the drawbacks of the probe. Nevertheless, these are for the SBI application a non negligible sensitivity to pitch and yaw angle variations and a Reynolds dependence.

This chapter focuses, by means of papers, on the above aspects and estimates the corresponding uncertainty. A high performance pressure probe design that overcomes the shortcomings of the existing probes and improves on other aspects is introduced and the probe factor of both the existing probes and the new developed probe are estimated.

**The papers can be found in Annex A and form an essential part of this dissertation.**

## 4.2. Article 1

Sette B.J.G.; *Critical considerations on the use of a bi-directional probe in heat release measurements; Fire and Materials*<sup>[56]</sup>

Out for review: 5 October 2004

Accepted for publication: 21 December 2004

This article evaluates the bi-directional pressure probe that is used in the SBI and other fire tests. The probe that is used in the SBI differs from the probes used in other fire tests in so far that it has a positioning rod welded to it (Figure 7.c).

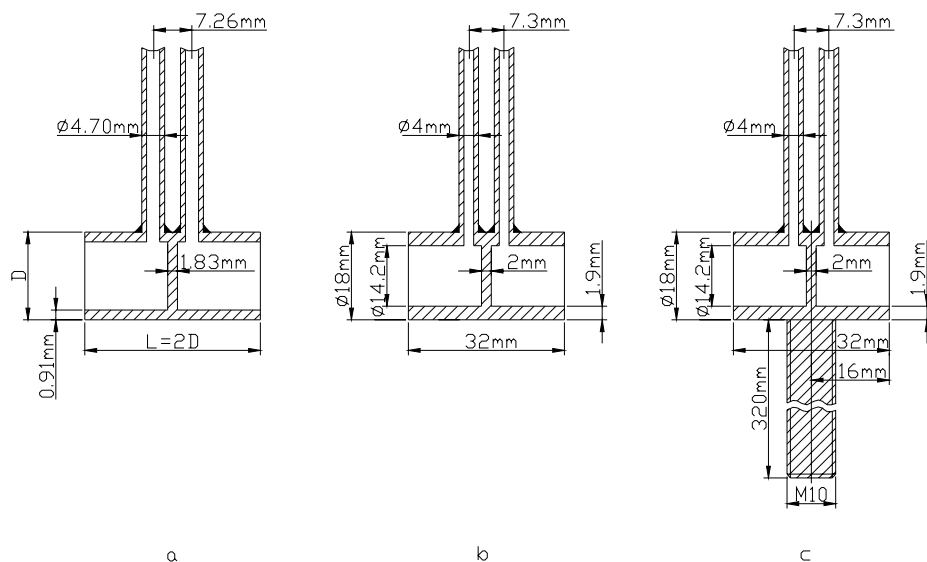


Figure 7. bi-directional pressure probes

The introduction of the positioning rod has a big impact on the probe's behaviour. The probe no longer is Reynolds independent (Figure 8/1.c). This results in a spectacular increase of the uncertainty related to the mass flow measurement if one keeps the probe factor  $k_p$  constant as indicated by the SBI standard.

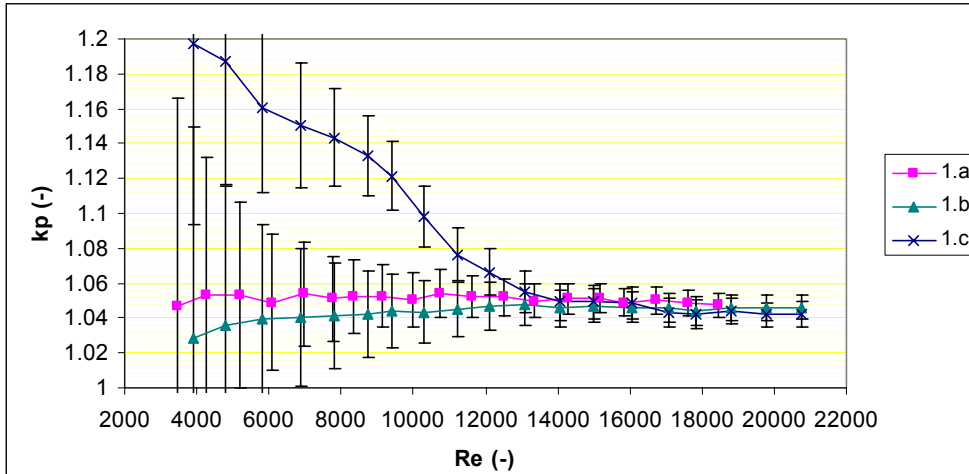


Figure 8. probe factor  $k_p$  as function of Re (95% confidence interval)

Furthermore, the original design (Figure 7.a) is evaluated. Although the original probe is Reynolds independent over a large range, its probe factor changes with pitch and/or yaw angle variations (Figure 9/1.a).

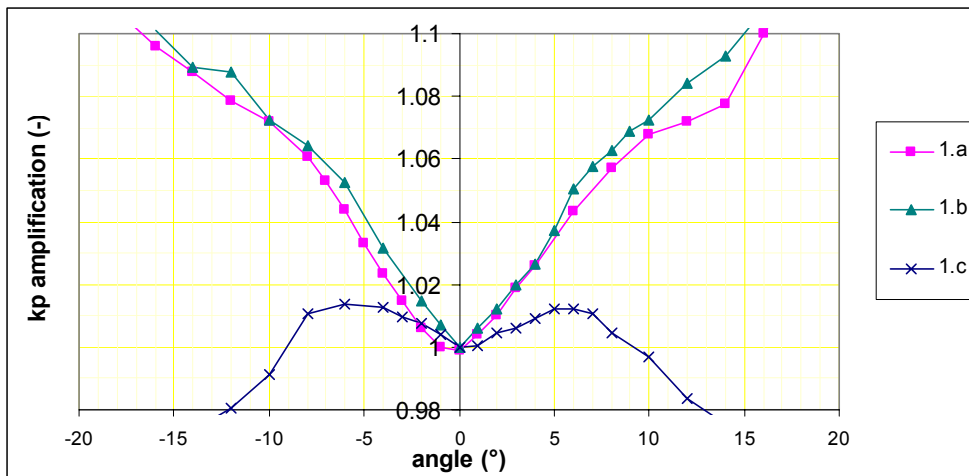


Figure 9. Pitch/yaw angle dependence ( $Re \approx 10\ 000$ )

It is proposed to develop an improved differential pressure probe design that combines Reynolds independence with a low sensitivity to angular variations.

### 4.3. Article 2

Sette B.J.G.; *Development of a new Robust Velocity Pressure Probe for Heat Release Applications; Fire and Materials*<sup>[57]</sup>

Out for review: 1 February 2005

Accepted for publication: 30 March 2005

This article builds on the previous article and looks for alternatives for the existing bi-directional probes. After evaluation of a few possible designs, the design of Figure 10.b is retained. It concerns a hemispherical probe with its open side facing the incoming flow.

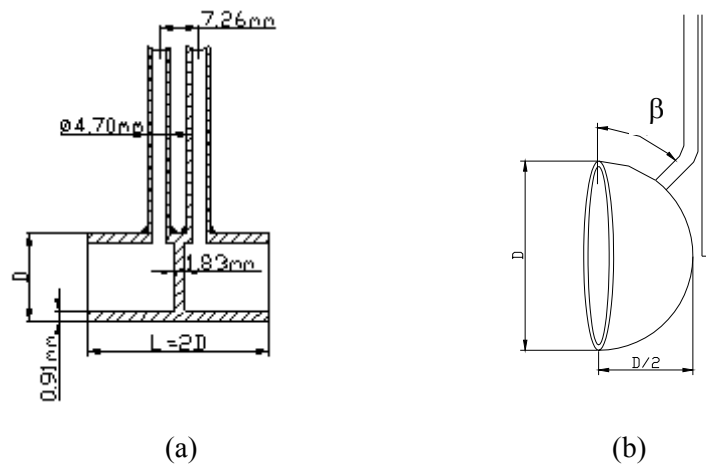


Figure 10. a. bi-directional probe; b. Hemispherical probe

The probe factor for the hemispherical probe with hemispherical inlet (HSphere-Spher) is almost constant in a range from  $Re = 5\,000$  till  $60\,000$  as shown in Figure 11.

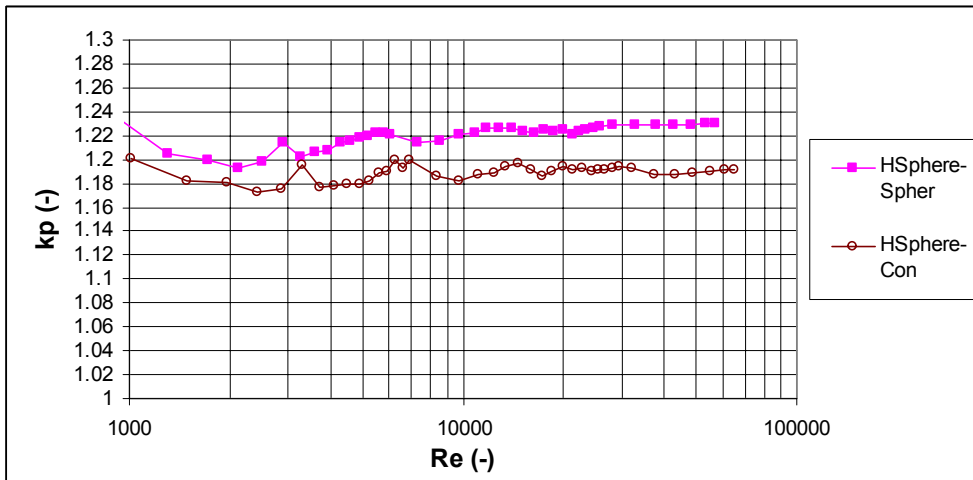


Figure 11. Probe factor for the hemispherical probe with spherical and with conical inlet

In addition the probe shows a low sensitivity to pitch and/or yaw angle variations in a range of  $\pm 20^\circ$ .

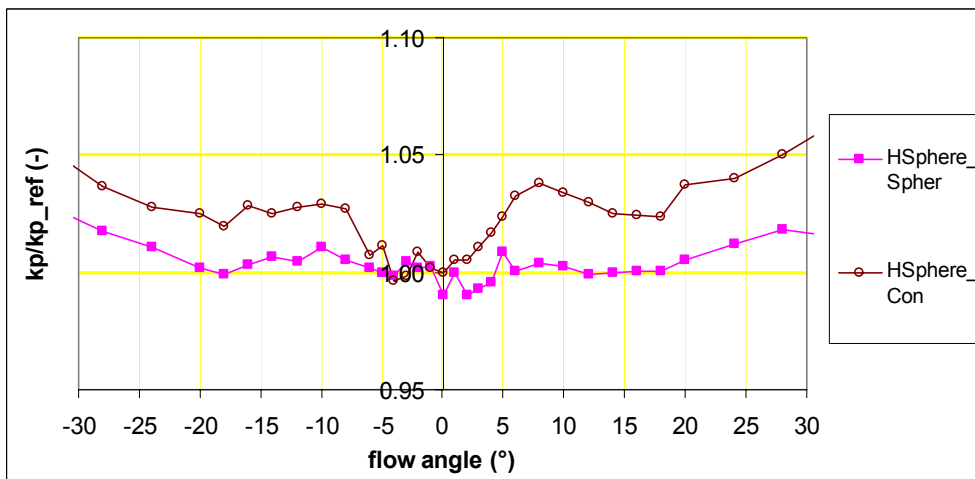


Figure 12. Sensitivity to angular variations for a spherical and a conical inlet

#### 4.4. Article 3

*Sette, B., Theuns E., Merci B., Temperature effects on the mass flow rate in the SBI and similar Heat Release Rate Test Equipment, Fire and Materials<sup>[58]</sup>*

Out for review: 7 December 2004

The mass flow of combustion gases extracted is measured by means of a temperature and velocity measurement on the axis of the exhaust duct in combination with the velocity profile over the duct section. Due to fast temperature changes over a test run and due to thermal inertia of the exhaust duct, both the velocity and density profile over the cross section vary as a function of time and temperature (Figure 14).

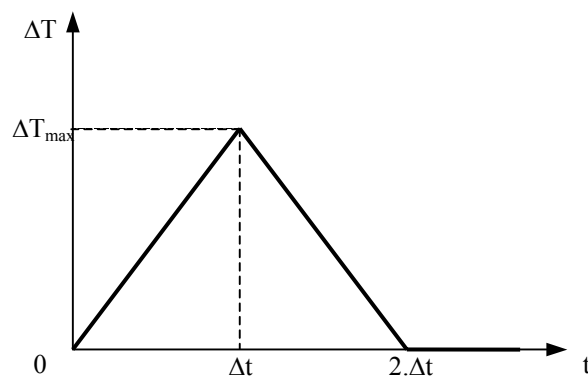


Figure 13. Variation of the fluid temperature at the inlet

An estimation of the error on the mass flow is made through numerical simulation (CFD). This is made by means of some imposed temperature variations at the inlet of the exhaust duct (Figure 13). The error seems to depend on whether working at constant volume flow or constant mass flow.

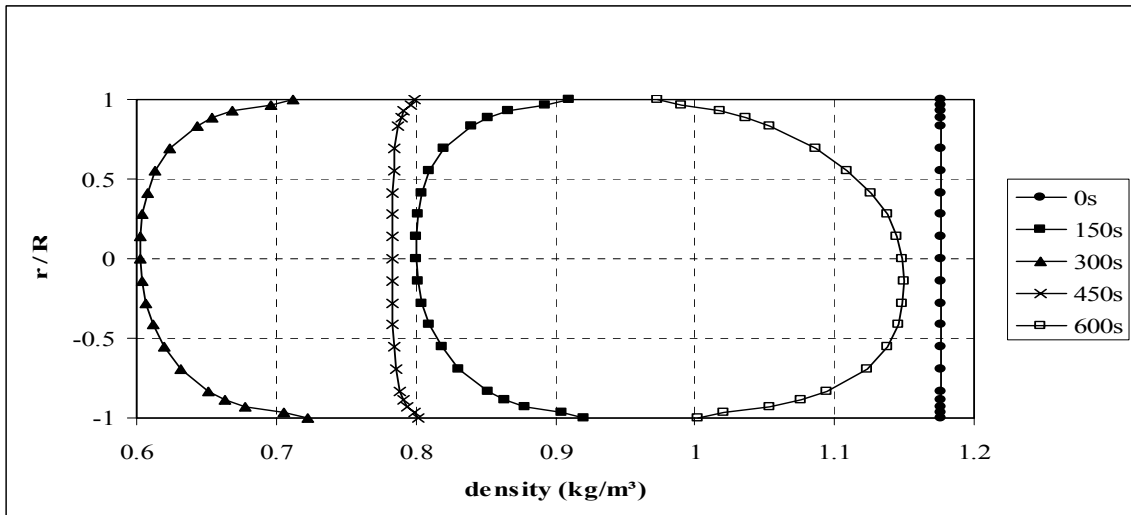


Figure 14. Evolution in time of density in the measurement section for test cycle II.

#### 4.5. Article 4

*Merci B., Theuns E., Sette B., Vandeveld P.; Numerical Investigation of the Influence of Gas Heating and Cooling on the Velocity Profile Correction Factor in the SBI-Configuration; Fire and Materials<sup>[52]</sup>*

Out for review: 7 December 2004

Article 4 builds on article 3. In this paper it is noticed that there is no longer a one-to-one correspondence between the velocity profile shape and the instantaneous Reynolds number, due to the time-dependent temperature and density profile evolution in the exhaust duct.

By defining an ‘effective’ Reynolds number, based on the effective viscosity, i.e. the sum of the molecular and the turbulent viscosity, a one-to-one relation is recovered.

## 5 Dynamic behaviour

### 5.1. Introduction

Chapter V deals with the dynamic aspects of the process, the test instruments and the data acquisition. It also evaluates the, currently used, ‘flat’ *moving average filter* used to smooth the HRR data prior to calculating FIGRA and proposes the use of a more efficient Henderson filter.

Furthermore it considers questions like ‘what is the bandwidth (fastest process) we’re interested in’, gives guidance on this and proposes three alternative measuring methods with an increasing level of bandwidth (BW) but also complexity. One of them is the use of inverse filters.

Finally it also proposes an alternative data synchronisation method.

### 5.2. Identification of the measurement components

In order to better understand the SBI test equipment we need information on:

- the bandwidth of the different measuring devices;
- the identification of the built in filter on some of the devices;
- the bandwidth of the data acquisition system;
- the bandwidth of the mass flow controller (input signal).

The bandwidth (BW) is the frequency below which an input signal is transferred without substantial distortion in amplitude and/or phase-shift.

#### 5.2.1 Bandwidth of the data acquisition system

Voltage measurement during data acquisition relies on a process known as analog-to-digital (A/D) conversion. The mainstream A/D conversion methods for data acquisition and measurement instruments include *successive approximation*, *integrating*, *flash converters* and *sigma-delta converters*. Each conversion method offers a different combination of performance and price that makes it suitable for a specific set of data acquisition applications<sup>[34]</sup>.

Both data acquisition systems (Siemens Simatic PLC and Keithley 2000 series) that are currently used at the Ghent premises make use of the Integrating A/D principle. The general operating principle of the integrating A/D converter is based on the charging and discharging of a capacitor by an unknown



signal and a reference voltage. The capacitor is charged first by the unknown signal for a set time interval. Next, the capacitor is discharged back to zero at a fixed rate and the time needed to discharge the capacitor is measured. This time is a measure of the integrated input voltage and can be used to deduce the unknown voltage.

The benefit of the integrating A/D conversion process is that it can average out noise over time, which results in good noise rejection. Also the integration time can be selected to match the frequency of a known noise source.

In our case the integration time is set to 20ms which corresponds to one so called Power Line Cycle at 50Hz. This will eliminate any periodic noise caused by the electric net.

The integration process works as a low pass filter with – in case of an integration time of 20ms – a cutoff frequency (-3dB) of 22Hz.

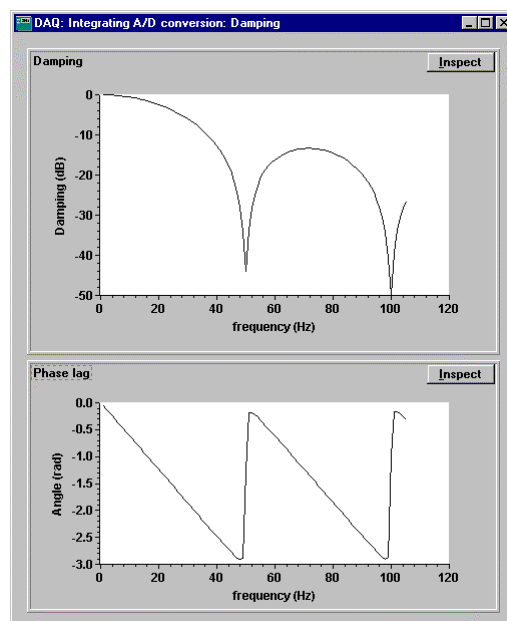


Figure 15. Gain and Phase lag of an Integrating A/D principle DAQ system @ 1PLC / 50Hz

## 5.2.2 Bandwidth of the measuring devices

The response times and delay times mentioned in the next section always refer to the whole measuring chain. For example with *the response time of the O<sub>2</sub>-analyser* is not only mentioned the response time of the device itself, but also the influence of filters, transport lines etc. are taken into account.

This makes that the times found are different from the ones found in the specifications from the manufacturer.

### **Background**

The purpose of the measurement is to find the Heat Release Rate (kW) of a burning sample in function of time. Therefore, four signals need to be monitored:

1. A differential pressure measurement is a measure for the velocity of the combustion gases in the exhaust duct, and thus for the volume flow.
2. The volume flow is referenced to a temperature of 25°C (mass flow) and therefore the recording of the temperature of the exhaust gases is needed.
3. Besides temperature, the reaction chemistry makes that the CO<sub>2</sub>-concentration and the volume of the incoming air increases after combustion and therefore a correction on the measured O<sub>2</sub>-concentration, by means of CO<sub>2</sub>-concentration, is needed.
4. Finally, the O<sub>2</sub>-concentration together with the volume flow through the system gives the required heat release rate. The assumption is that for every cubic metre of oxygen consumed 17,2MJ of heat will be released. This assumption holds within an uncertainty from 5 to 10%<sup>[26][49][30][39]</sup> for most materials that are commonly used in the building and construction industry.

A first point of interest is to find out the error made not taking into account the dynamic aspects of the different devices. This transient error  $e_x$  on measurand X can be quantified for a first order system by

$$e_x = \tau \frac{dX}{dt} \quad [ 5.1 ]$$

whereby  $\tau$  is the time constant of the system.

The thermocouples and pressure transducer have fairly different response times from the gas analysers but today their signals are used in the formulas without any data pre-treatment, thus neglecting any dynamic effect.

Furthermore, there is an interest to know what the cutoff frequency is of the overall system for burning processes.

In a second stage there is a need to define specifications on data pre-treatment and on the scan rate of the data acquisition system.

The main target however is to identify the process such that the input (burning process) can be regenerated out of the four above mentioned measurements in a more accurate way.

A further step down the road would be to investigate the possibility to replace the gas analysis measurement (measurements 3 and 4) by a temperature + heat flux measurement.

## *Estimation of the bandwidth*

### **5.2.2.1 Differential pressure-signal**

The differential pressure device is model P92 from HALSTRUP, with a measuring range from 0 to 250 Pa.

The data acquisition is done by means of a Keithley2000 multimeter at a sampling rate of 50Hz. The integration time was set to 0,1 PLC (Power Line Cycle).

All electronic damping on the pressure difference device was turned off.

A stepwise change is introduced by suddenly taking away the pressure on one of the input ports. This makes that the sensor sees a sudden pressure change from about 75Pa to 0Pa. All tubing and probes were connected while measuring.

A response time of 0,5s (exponential curve in Figure 16) is obtained for the pressure difference device.

According to the manufacturer the electronics contain a first order analogue filter on the output, which explains the 'slow' response time. Usually we would expect response times in the order of tens of milliseconds. If so desired, the capacitor responsible for this damping could be replaced to modify the response time.

Besides the analogue low pass filter, the unit has a built in digital filter with selectable time constants between 1 s and 40 s. More information on this digital filter is given in section 5.2.3.

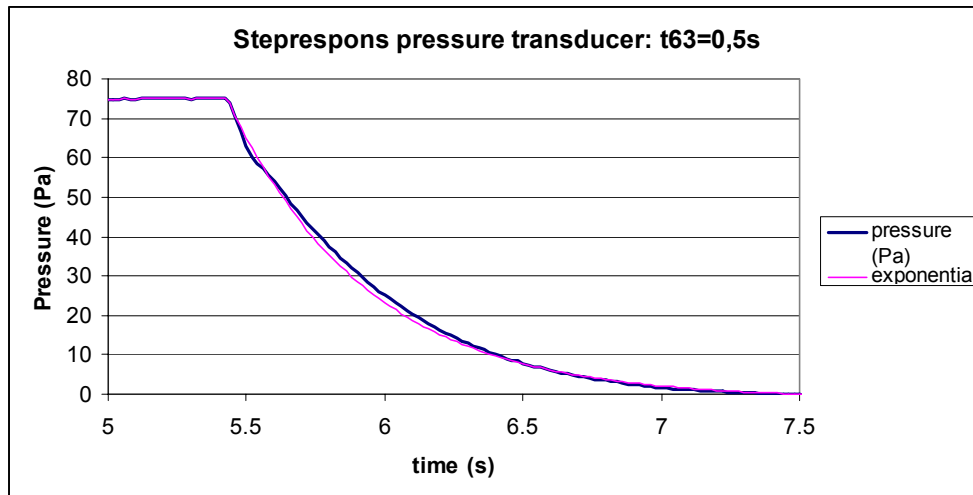


Figure 16. Step response pressure transducer Halstrup P92

### 5.2.2.2 Thermocouple-signal ( $T_{\text{gas}}$ )

The volume flow is referenced to a temperature of 25°C (mass flow) and therefore the recording of the temperature of the exhaust gases is needed. The sensing element is a K-type insulated thermocouple ( $\phi = 0,5\text{mm}$ ) that is placed perpendicular to the gas flow with an approximate velocity of 8m/s.

The convective heat transfer between the free stream gas and the solid thermocouple tip governs the temperature evolution of the thermocouple. A correction for radiative losses may be introduced afterwards.

The estimated time constant for the thermocouple is  $(1.15 \pm 0.15)$  s at temperatures of around 300 K and velocities of 8 m/s, decreasing to 0.8 s in the limit case of 600 K and 16 m/s. (Annex B.2).

The time constant of the thermocouple will be taken as 1.15 s with a standard uncertainty of 0.15 s. For higher temperatures, this results in a slight overestimation of the transient error on the temperature measurement as will be discussed further.

### 5.2.2.3 CO<sub>2</sub>-signal

The data acquisition is done by means of a Keithley2000 multimeter at a sampling rate of 10Hz. The integration time was set to 1 PLC (Power Line Cycle; 20ms when AC=50Hz) thus eliminating any 50Hz interference.

All electronic damping on the CO<sub>2</sub>-analyser that can be set by the user was turned off.

In a first test a stepwise change is realised by turning on a propane burner (30kW) after 10s.

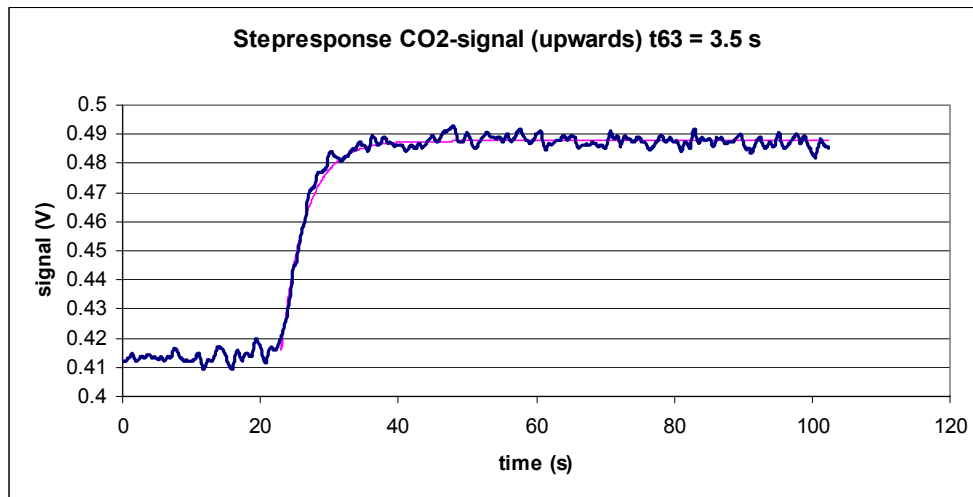


Figure 17. Step response carbon dioxide analyser + sampling

A second test looks at the step response when turning the burner off after 10s.

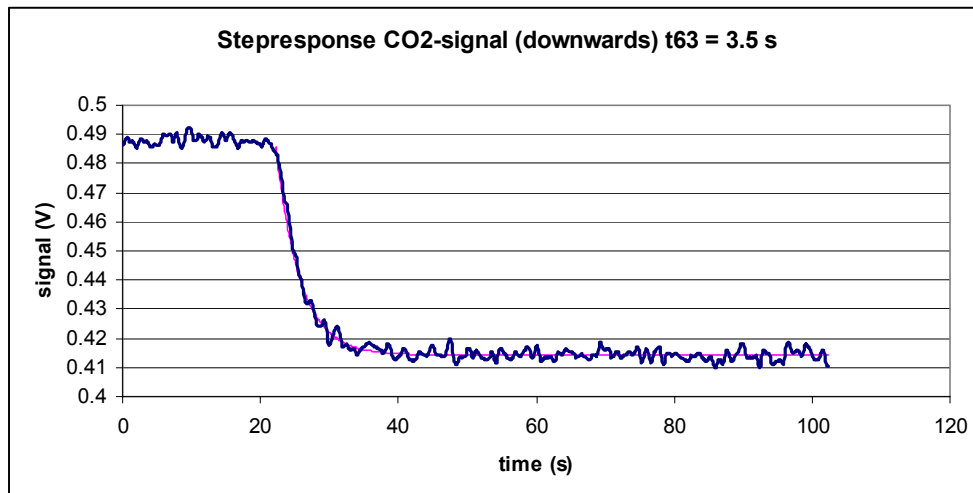


Figure 18. Step response carbon dioxide analyser + sampling

Observations:

- some disturbances are observed on the signal (see below)
- there is a death time of approximately 12 s before the analyser starts to react

- the response time of the CO<sub>2</sub>-gas analysis system (includes transport lines/ filters/cooler/...) is approximately 3.5 s

Note that the system delay and response time is the result of an extraction duct flow time (from flame to sample probe), a gas sample flow time (from sample probe to the gas analyser) and the instrument response time. So both delay and response times may change when one of these changes.

In the assumption that the time constant lies within the interval  $(3.5 \pm 0.2)$  s (= rectangular distribution with width 0.2 s; see 6.2), the standard uncertainty on the time constant is estimated at 0.12 s.

In a third test, data is logged without any forced external disturbance.

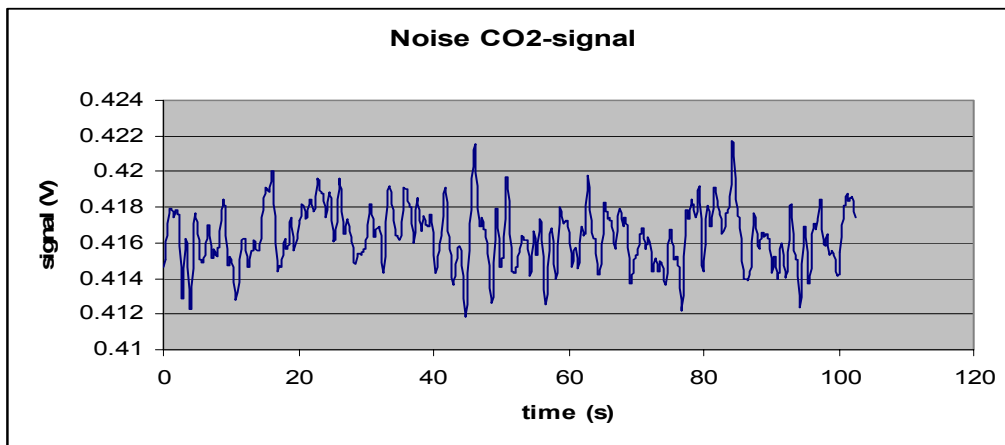


Figure 19. Noise signal carbon dioxide analyser

A FFT-analysis reveals some low order disturbances with frequencies mainly below 1Hz which can be categorised as 'noise'. No specific disturbance at one frequency is observed.

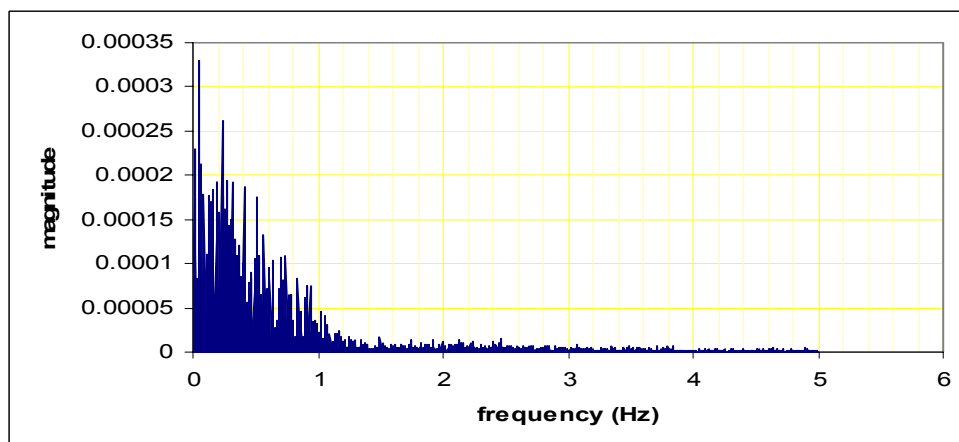


Figure 20. Frequency response noise signal CO<sub>2</sub> analyser

#### 5.2.2.4 O<sub>2</sub>-signal

As for the CO<sub>2</sub> signal, the data acquisition is run at a sampling rate of 10 Hz with an integration time of 1 PLC. All electronic damping on the O<sub>2</sub>-analyser that can be set by the user was turned off.

In a first test a stepwise change is realised by turning on a propane burner (30kW) after 10s.

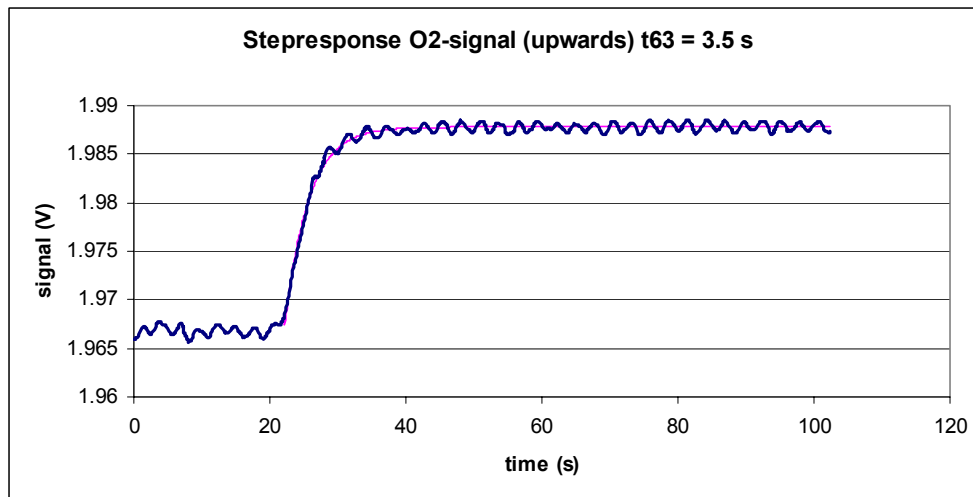


Figure 21. Step response oxygen analyser + sampling

A second test looks at the step response when turning the burner off after 10s.

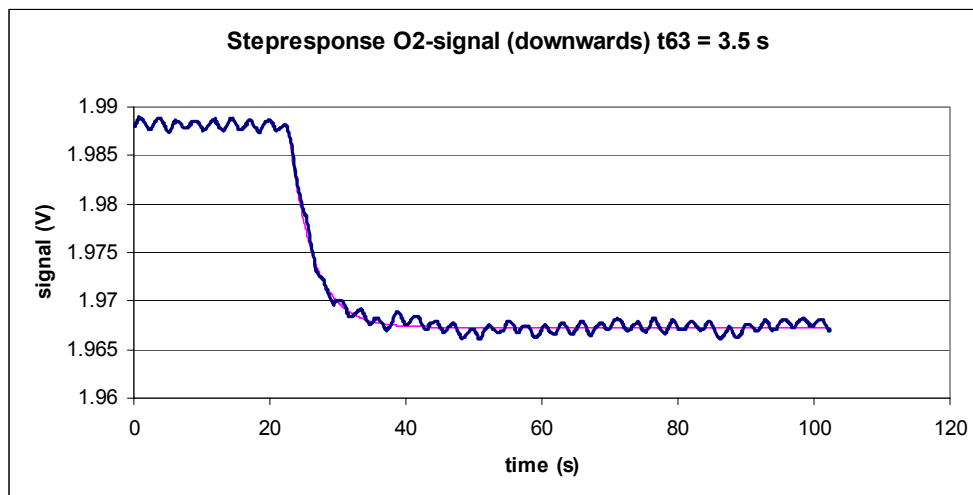


Figure 22. Step response oxygen analyser + sampling

Observations:

- an important periodic disturbance can be seen on the signal (see below)
- a death time of approximately 12s exists before the analyser starts to react
- the response time of the O<sub>2</sub>-gas analysis system (includes transport lines/ filters/cooler/...) is approximately 3.5 s

In the assumption that the time constant lies within the interval  $(3.5 \pm 0.2)$  s (= rectangular distribution with width 0.2 s; see 6.2), the standard uncertainty on the time constant is estimated at 0.12 s.

In a third test, data is logged without any forced external disturbance.

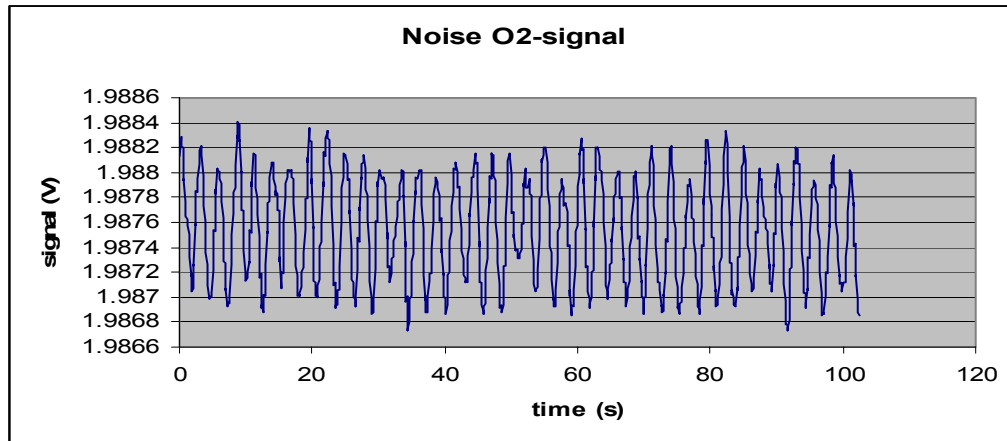


Figure 23. Noise signal oxygen analyser

A FFT-analysis reveals a periodic disturbance with a frequency of around 0.37 Hz.

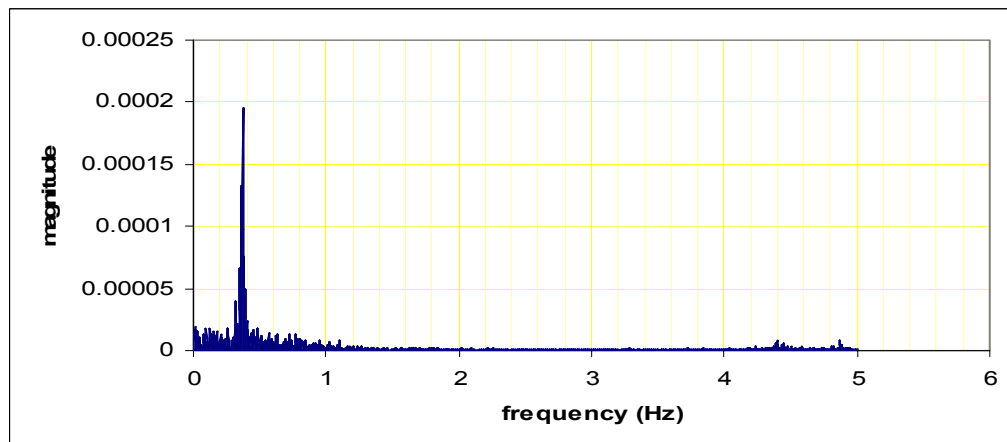


Figure 24. Step response oxygen analyser + sampling

Apart from this periodic 0.37 Hz disturbance with a peak-to-peak value of approximately 1.5 mV or 1000 ppm, the signal looks very stable. A value of 1000 ppm is unacceptably high. Remember that the standard prescribes noise & drift values of maximum 100 ppm.

This disturbance has been identified as being caused by pressure fluctuations and mechanical vibrations induced by the membrane pump in the gas analysis rack. Apparently the oxygen analyser, which is in the same housing as the carbon dioxide analyser, is more sensitive to vibrations and pressure fluctuations. This most probably can be attributed to the different measurement principles used, i.e. paramagnetism for the oxygen analyser while infrared absorption for the carbon dioxide analyser.



Eliminating the mechanical vibrations and damping the pressure fluctuations using an air damper, the signal improves considerably as shown in Figure 25.

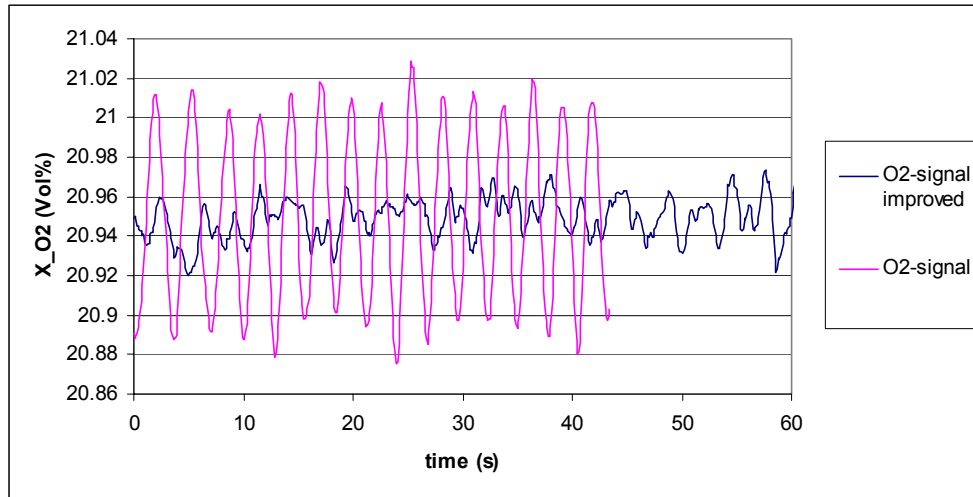


Figure 25. Effect of eliminating disturbances (pressure fluctuations & vibrations)

Alternatively to eliminating the disturbance, filtering techniques can be used. Different filter types will be discussed further in this chapter.

Using the built in electronic damping of the analyser, with a time constant  $\tau_{90\%}$  of for example 5 s, the disturbance will be damped by approximately -14 dB (20% of original signal). Setting  $\tau_{90\%}$  to 6 s reduces the amplitude of the disturbance to 16%.

A preferred solution however is to apply a 111 term Henderson anti-causal filter, H111, on the data sampled at 10 Hz which completely removes the 0.37 Hz disturbance. An anti-causal filter is looking both forward and backward in time, as opposed to a causal filter which only depends on the past.

Both the exponential smoothing filters and the Henderson filters will be discussed in section (5.3).

Filter type	specification	amplitude of distortion
Exponential smoothing (Exp5)	$\tau_{90\%} = 5$ s	20 %
Exponential smoothing (Exp 6)	$\tau_{90\%} = 6$ s	16 %
Henderson (H111 ZP)	111 term zero phase	0 %

Table 3. Efficiency of different filters to remove a 0.37 Hz disturbance

Applying the Exp6 filter and the H111 filter on the original O<sub>2</sub>-data and the improved O<sub>2</sub>-data results in the time series shown in the next two figures.

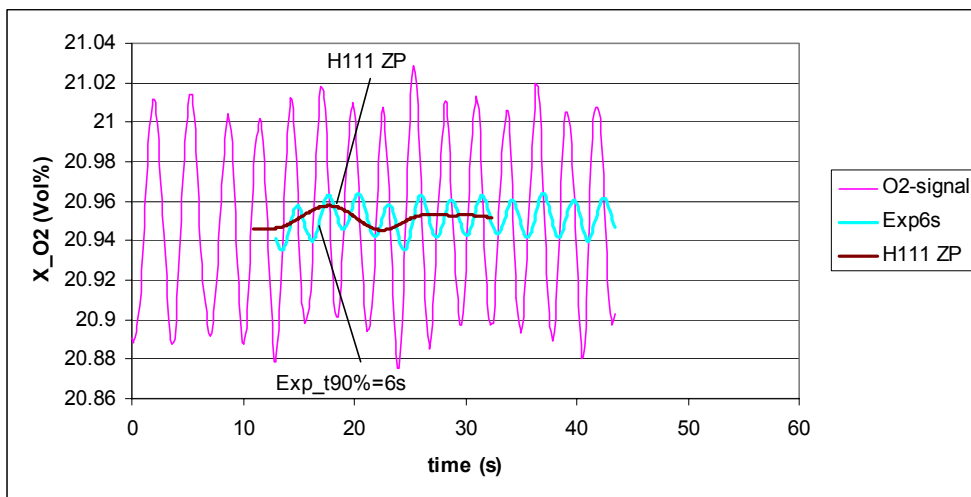


Figure 26. Effect of *Exp6* en *H111 ZP* filters on the raw O<sub>2</sub>-signal

Figure 26 shows that the *Exp6s* filter only partly removes the periodic disturbance while it introduces a phase shift. The *H111 ZP* filter eliminates completely the periodic disturbance and follows the longer term variations.

Note that for the *H111 ZP* filter there is no filtered data available for the first 110 samples (11s) of the two tails. Asymmetric filters could be used, if desired, in the tails.

When starting from the improved data – which required some extra measures to the gas analysis system – both filters have a good noise rejection, but only the *H111 ZP* filter is in phase with the original data.

Also note that the filtered (*H111 ZP*) data does not improve when the O<sub>2</sub>-data improves. This means that this filter also eliminates the disturbances introduced by the pressure fluctuations and vibrations of the membrane pump.

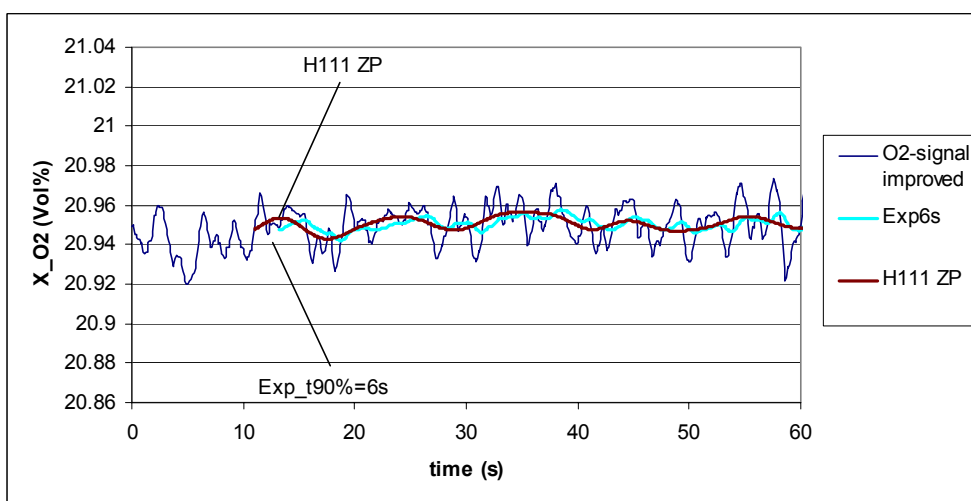


Figure 27. Effect of *Exp6* en *H111 ZP* filters on the improved O<sub>2</sub>-signal

#### **5.2.2.5 Thermocouple-signal ( $T_{wall}$ )**

The time constant related to the 'slow heating' of the exhaust duct is estimated to be in the order of 220 s (Annex B.3).

A third 'temperature' time constant can be associated with the slow heating of the exhaust gas collection hood. The time constant related to the heating of the hood is estimated to be in the order of 1200s (Annex B.4).

### 5.2.3 Identification of built in filter

Some of the available measuring devices have a built in damping with a parameterisable electric time constant. In order to better understand the behaviour of this equipment, the characteristics and behaviour of the filter will be investigated.

In total three measuring devices make use of this same type of filter being:

- Siemens Oxymat 6E oxygen analyser;
- Siemens Ultramat 6E carbon dioxide analyser;
- Halstrup Walcher Delta\_P P92 differential pressure transducer.

In both the Siemens and Halstrup manuals, the damping is characterised by an electric time constant. Additional information has been requested from both manufacturers (Annex B.14)

Out of the vague description, it is assumed that the filters behave as follows:

- The signal is sampled at an interval  $t_s$  (Siemens:  $t_s = 240\text{ms}$ ) and consecutive values are stored in a temporary memory;
- The outgoing signal is the mean value of the  $n$  last data points weighted with an exponential decaying function with time constant  $\tau$  ( $t_{90\%}$  can be specified by the user).

The sampling frequency  $f_s = 4^{1/6}$  Hz ( $t_s = 240\text{ms}$ ) apparently is half the frequency of the electromagnetic field of the measuring head of the oxygen analyser ( $f_{ef} = 8^{1/3}$  Hz). By doing so, one eliminates any aliasing effect (spurious data introduced by scanning at a too low frequency; see section 6.4.3) that would be introduced by the electromagnetic field.

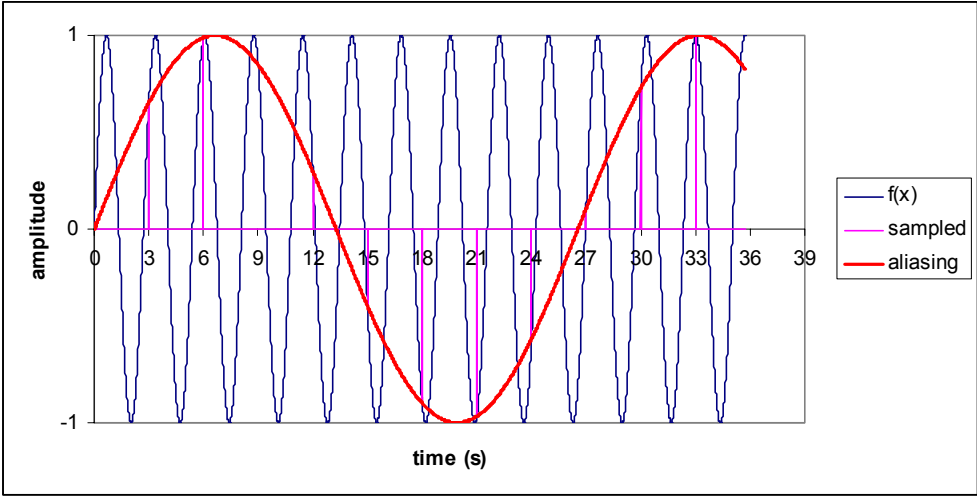


Figure 28. Example of aliasing effect

Since none of the manufacturers is clear about the exact functioning of the filter an experiment is run whereby:

- no external excitation is introduced;
- data is logged at a scanrate of 10Hz during 100s
- In a first period of 50s all damping (electric time constant is zero) is turned off
- In a second period of 50s damping is introduced with an electric time constant  $t_{90\%}$  of 3s ( $\tau=1.3s$ ).

The obtained experimental data  $X(t)$  (Graph 1; Figure 29) is now smoothed by calculating the convolution integral with an exponentially decaying function  $Y(t)$  (Graph 2) with time constant  $\tau=1.3s$ .

Comparing (Graph 4) the calculated smoothed experimental data in the period 0-50s (Graph 3) with the data smoothed by the analyser in period 50-100s (Graph 1) it is reasonable to assume that the filter has the above described behaviour.

*The experiment and the conclusions have been double checked making use of different time constants ( $t_{90\%} = 5s$  and  $1s$ )*

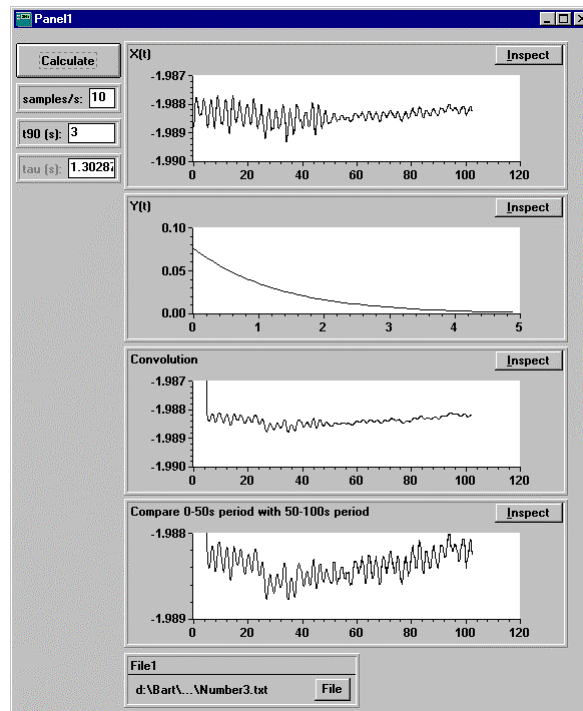


Figure 29. Comparison of simulation and real behaviour of the built in digital filter

This behaviour corresponds to that of an exponential smoothing filter as will be discussed in the next section. The exponential filter can easily be implemented on a real time process and only requires the temporary storage of one value.

## 5.2.4 Bandwidth of the Mass Flow Controller

The mass flow controller (Bronkhorst F112AC-FA-55-V / F-004AC) is used throughout this research as a known and variable input source. It controls the amount of propane (mg/s) that flows to the burner, which is directly related to the amount of heat released ( $H_0$  propane = 46.360kJ/kg).

The frequency response of the mass flow controller, obtained by applying sine variations on the input, reveals a cutoff frequency of 0.25Hz approximately.

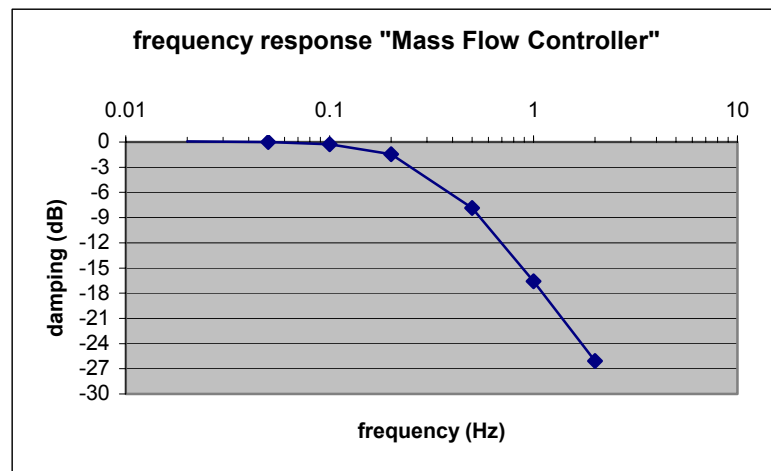


Figure 30. Gain of the Mass Flow Controller

Note that the response of the switching on of the burner is almost immediately ( $\tau_{90} < 1$  s). The turning on of the burner is controlled by means of an electromagnetic valve. Since prior to the opening of the valve the flow is zero, the mass flow controller opens its valve completely resulting in a very fast initial reaction.

### 5.2.5 Summary table

This table gives an overview of the response and delay times for the instrumentation used. The delay times are taken from the time of igniting the burner (opening the gas supply by means of an electromagnetic valve). This explains the high delay times of both the pressure transducer (bi-directional probe) and the thermocouples (duct measuring section). Delay times are rounded off to the nearest second.

	$\tau$ (s)	BW (Hz)	delay time (s)
<b><i>input signal</i></b>			
MFC (mg/s)	4	0.25	
<b><i>output signals</i></b>			
O <sub>2</sub> (Vol%)	3.5	0.29	12
CO <sub>2</sub> (Vol%)	3.5	0.29	12
$\Delta p$ (Pa)	0.5	2	3
T <sub>gas</sub> (°C)	1.15	0.87	3
T <sub>wall</sub> (°C)	220	0.0045	9
	1200	0.0008	
<b><i>Data acquisition</i></b>			
DAQ		22	
<b><i>Electronic damping</i></b>			
t <sub>90%</sub> = 0,5	0.22	0.7	
t <sub>90%</sub> = 1	0.43	0.3	
t <sub>90%</sub> = 3	1.30	0.1	
t <sub>90%</sub> = 5	2.17	0.07	
t <sub>90%</sub> = 10	4.34	0.03	

Table 4. Bandwidth of different components



## 5.3. Filters

### 5.3.1 Introduction

In this section first some digital filters are discussed like: the *exponential smoothing filter*, as used in the gas analysis equipment and in the pressure transducer, the *SBI running average filter*, as applied on the HRR data prior to calculating FIGRA, and the *Henderson filter* as an alternative to the previous two.

Since the data can be processed offline, the anti-causal versions of the above filters are preferred since they do not introduce any phase lag. This technique requires to time reverse the data which explains why it can't be used in a real time process.

Next, an analogue Butterworth filter is described that could be used to remove any aliasing effect (spurious data introduced by scanning at a too low frequency; see section 6.4.3).

Inverse filtering techniques allow to (partially) restore any damping introduced by the measuring devices thus increasing the bandwidth of the system. Some guidance is given on how to implement them.

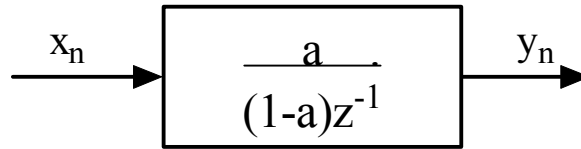
Finally an alternative data synchronisation method is proposed.

### 5.3.2 Exponential smoothing filter

The behaviour of an exponential smoothing filter corresponds with an analogue first order filter with time constant

$$\tau = \frac{t_s}{\ln\left(\frac{1}{1-a}\right)} \quad [5.2]$$

whereby  $t_s$  represents the sampling period and 'a' is a filter parameter ( $0 \leq a \leq 1$ ). 'a' follows out of  $\tau$  when the sampling interval  $t_s$  is known.



This filter only requires to memorise one value and can easily be implemented using the formula

$$y_n = (1 - a)y_{n-1} + ax_n \quad [ 5.3 ]$$

The electronic damping works like a low pass filter with the following cutoff frequencies (-3dB)

damping ( $t_{90\%}$ ) (s)	time constant $\tau$ (s)	cutoff freq (Hz)
0,5	0,22	0,7
1	0,43	0,3
3	1,30	0,1
5	2,17	0,07
10	4,34	0,03

Table 5. Cutoff frequencies for different settings of the digital filter

The gain and phase shift of the filters in Table 5 are shown in Figure 31 and in Figure 32.

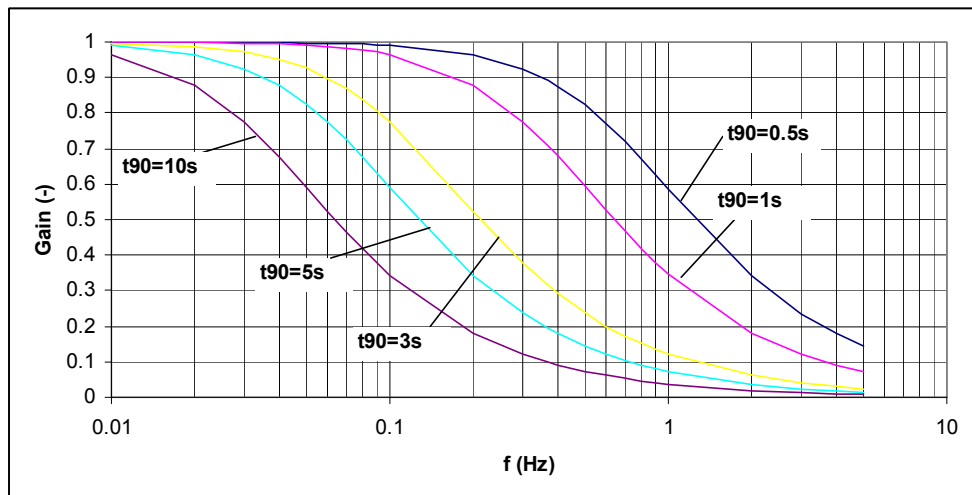


Figure 31. Gain of the exponential smoothing filter

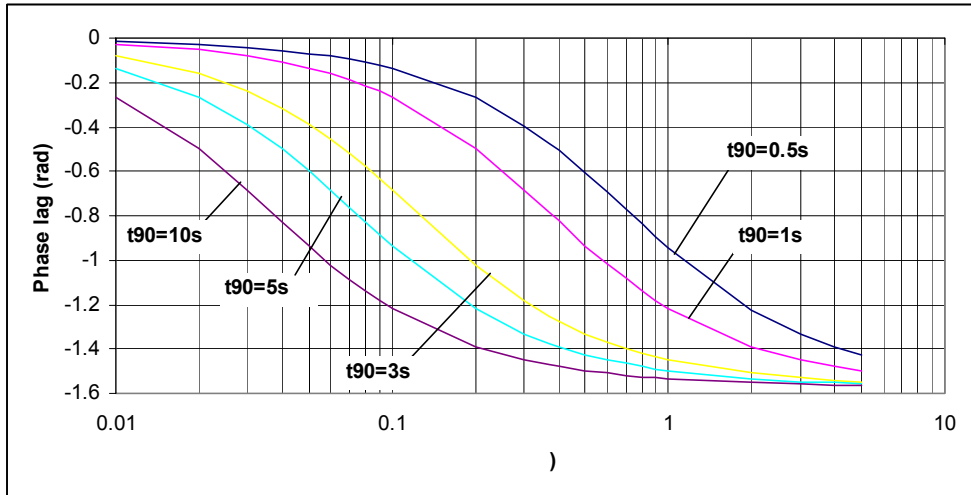


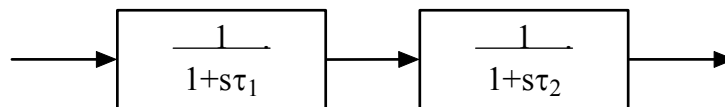
Figure 32. Phase shift of the exponential smoothing filter

Passing for example a sine wave with periodicity of 10 s through a  $t_{90} = 5$  s filter, the damping will be some 41% while the phase lag is  $54^\circ$ .

*How to deal with differences in time constants?*

Different measurands have different response times and even a single measurand may have different response times from laboratory to laboratory. In view of better controlling the dynamic behaviour of different measurements in different laboratories, we want to obtain similar time constants irrespective of what and where we are measuring.

Applying an exponential filter with time constant  $\tau_2$  to a first order system having a time constant  $\tau_1$  corresponds approximately (in the pass band) with the behaviour of a first order system with an apparent time constant of  $\tau = \sqrt{\tau_1^2 + \tau_2^2}$  :



with gain

$$G(\omega) = \frac{1}{\sqrt{1 + (\omega\tau_1)^2}} \frac{1}{\sqrt{1 + (\omega\tau_2)^2}} \cong \frac{1}{\sqrt{1 + (\omega\tau)^2}} \quad \omega\tau \ll 1$$

Combining, by way of example, an oxygen analyser ( $\tau_1 = 3.5 \text{ s}$ ) with an exponential filter  $t_{90\%} = 5 \text{ s}$  ( $\tau_1 = 2.17\text{s}$ ), the resulting apparent time constant is  $\tau = 4.12 \text{ s}$  (see Figure 33).

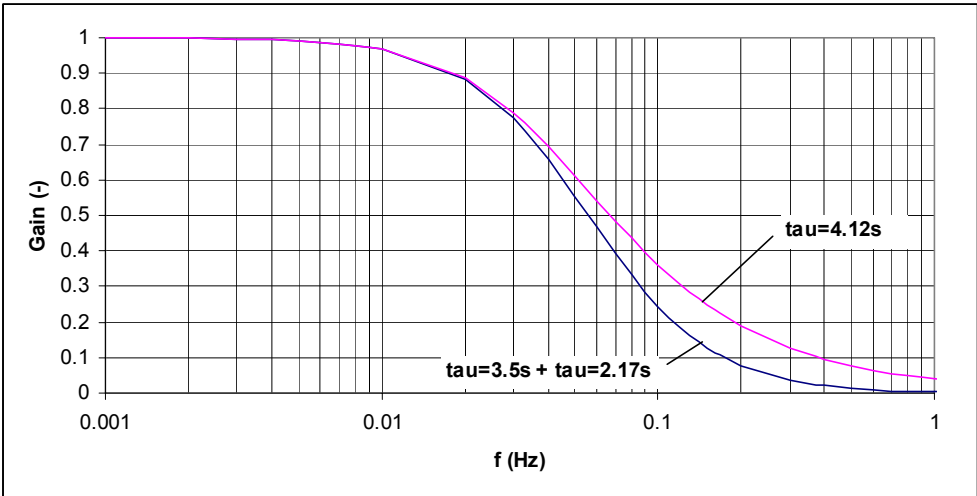


Figure 33. Gain of combined first order systems & gain of apparent combined system

Combining this further with a *Henderson 11 term zero phase filter* (@ a sampling frequency of 1/3 Hz), as will be discussed in the next section, the frequency response curve becomes:

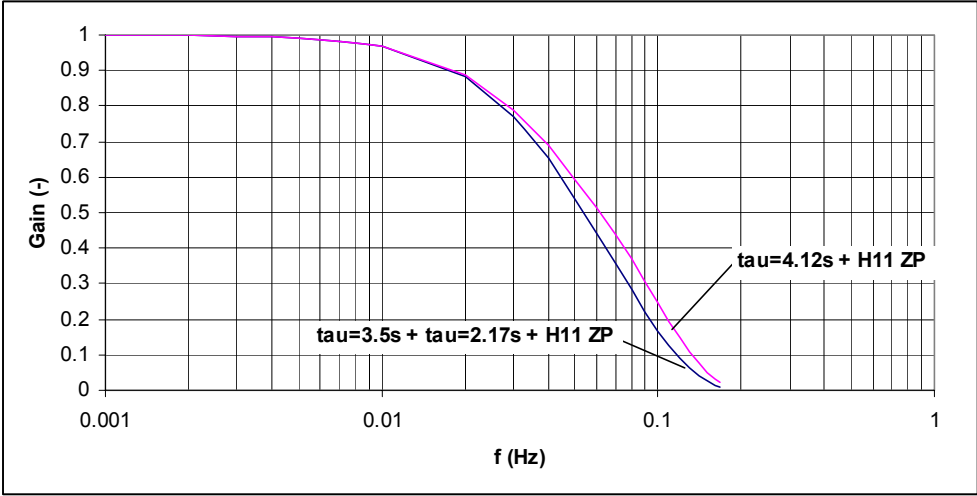


Figure 34. Above figure combined with a Henderson 11 term zero phase filter

By using this technique, it is now possible to give all measurement components an almost equal dynamic behaviour.

### 5.3.3 Moving average filters

Moving averages (or linear filters) successively average a shifting time span of data and are often used to explore time series with seasonal characteristics like economics. Depending on their weighting structure, they can either be used to eliminate cycles or to smooth data. They work on the assumption that the trend and cyclic components are stochastic (the future is only partly determined by past values) and not deterministic.

Moving averages are often applied to smooth out irregularities in a series to obtain an estimate of the trend.

Often distinction is made between symmetric and asymmetric filters. Asymmetric filters are used to provide trend estimates of the most recent data points in real time analysis and of the endpoints of a time series.

Since in the SBI no real time trend analysis is needed nor a trend analysis of the two tails is essential, only symmetric moving average filters will be discussed further.

#### Definitions

Define a set of filter weights of length  $m_1 + m_2 + 1$  as

$$w_{-m_1}, w_{-(m_1-1)}, \dots, w_{-1}, w_0, w_1, \dots, w_{m_2} \quad [5.4]$$

A symmetric filter satisfies the conditions  $m = m_1 = m_2$  and  $w_i = w_{-i}$ . Only symmetric filters will be considered further.

For an observed time series  $y_t$ , a filtered series  $z_t$  can be calculated using

$$z_t = \sum_{i=-m}^m w_i y_{t+i} \quad [5.5]$$

Theoretically, the properties of these filters can be identified by studying the Fourier transform<sup>[62]</sup>

$$f(\omega) = \sum_{i=-m}^m w_i e^{i\omega j} = \sum_{i=-m}^m w_i \cos(i\omega) + j \sum_{i=-m}^m w_i \sin(i\omega) \quad [5.6]$$

The gain function of this symmetric filter is given by

$$G(\omega) = \sqrt{\text{Re}^2\{f(\omega)\} + \text{Im}^2\{f(\omega)\}} = \left| w_0 + 2 \sum_{k=1}^m w_k \cos(\omega k) \right| \quad [5.7]$$

while the phase shift is given by

$$\Phi(\omega) = \arctan\left(\frac{\text{Im}\{f(\omega)\}}{\text{Re}\{f(\omega)\}}\right) = \arctan\left(\frac{0}{\text{Re}\{f(\omega)\}}\right) = \begin{cases} 0 & \text{if } \text{Re}\{f(\omega)\} > 0 \\ \pi & \text{if } \text{Re}\{f(\omega)\} < 0 \end{cases} \quad [5.8]$$

whereby  $\text{Re}\{f(\omega)\}$  and  $\text{Im}\{f(\omega)\}$  represent respectively the *real* and *imaginary* part of the function  $f(\omega)$ .

### **SBI filter**

The moving average filter used in the SBI (see formula 2.9) is a symmetric filter with  $m = 5$  and a weighing pattern as given in Table 6.

The filter is applied on the HRR time series prior to calculating the FIGRA time series.

### **Henderson filter**

Henderson moving averages<sup>[48]</sup> are a commonly used filter to smooth data. They have the property that they are able to track a cubic polynomial without distortion. To obtain the weights, a compromise was struck between two of the characteristics that are generally expected of a trend series; i.e. that the trend should be able to reproduce or represent a wide range of curvatures, and that it should be as smooth as possible. They can be used, for example, to obtain estimates of trend by smoothing a series containing trend and irregular components. Henderson moving averages are used in preference to simpler moving averages as they can reproduce polynomials up to degree three. This means that they are able to adequately capture trend turning points and points of inflection.<sup>[62]</sup>

The weighing pattern for often used Henderson filters is given in Table 6.

Weighing pattern for some symmetric filters	
11 Term SBI (S11)	(0.05, 0.1, 0.1, 0.1, 0.1, <b>0.1</b> , 0.1, 0.1, 0.1, 0.1, 0.05)
9 Term Henderson (H9)	(-0.041, -0.010, 0.119, 0.267, <b>0.330</b> , 0.267, 0.119, -0.010, -0.041)
13 Term Henderson (H13)	(-0.019, -0.028, 0.0, 0.066, 0.147, 0.214, <b>0.240</b> , 0.214, 0.147, 0.066, 0.0, -0.028, -0.019)
23 Term Henderson (H23)	(-0.004, -0.011, -0.016, -0.015, -0.005, 0.013, 0.039, 0.068, 0.097, 0.122, 0.138, <b>0.148</b> , 0.138, 0.122, 0.097, 0.068, 0.039, 0.013, -0.005, -0.015, -0.016, -0.011, -0.004)

Table 6. Weighing pattern for some symmetric filters

### Choice of filter

A first way to compare the different filters is by comparing their gain function. Figure 35 sets out the gain for a sample interval (scan rate) of  $t_s = 3$  s.

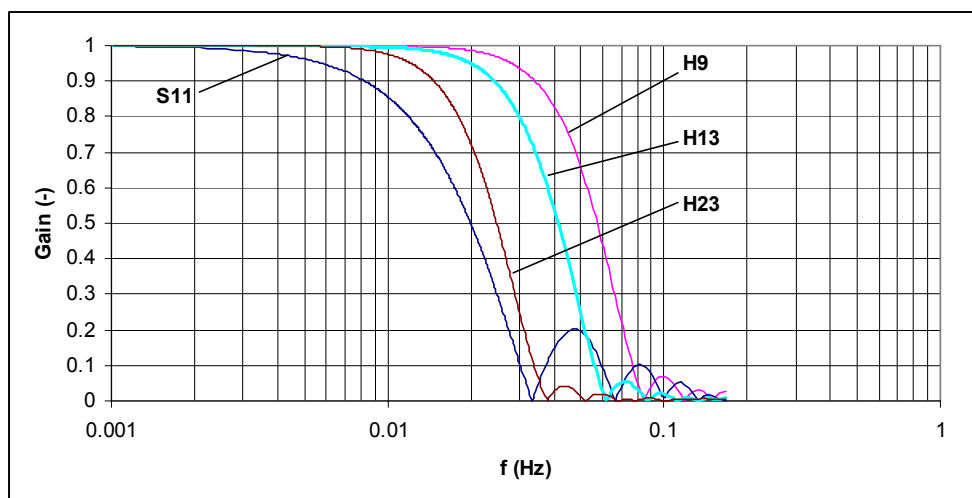


Figure 35. Gain functions of four moving average filters @  $t_s = 3$  s

The corresponding phase shift for the SBI filter S11 is shown below.

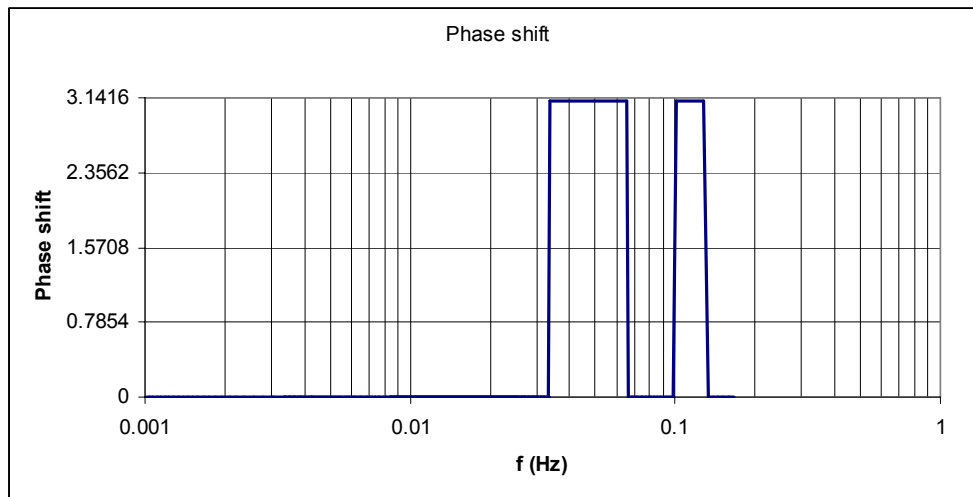


Figure 36. Phase shift for filter S11 @  $t_s = 3$  s

All three Henderson filters are efficient low pass filters with a good noise rejection (higher frequencies). The SBI filter (S11) is less favourable since it also partially dampens out the lower frequencies with a resulting bias on the result.

To further evaluate the different filters, a measure for smoothing developed by Henderson<sup>[48]</sup> and a local mean square error (LMSE), variance and bias developed by Dagum and Luati<sup>[45][46]</sup> will be used.

The *Henderson measure of smoothing* ( $S$ ) is defined by the sum of squares of the third differences of the weights

$$S = \sum_{i=-m}^{m+3} (\Delta^3 w_i)^2$$

Higher  $S$  values mean that more noise will be present in the filtered data point.

The *local bias* is defined as

$$1 - \sum_{i=-2}^2 w_i$$

while the *local variance* is, according to Dagum and Luati, expected to be well approximated by



$$\sum_{i=-m}^m w_i^2.$$

The theoretical weight-based *local mean square error (LMSE)* is defined as

$$LMSE = \left(1 - \sum_{i=-2}^2 w_i\right)^2 + \sum_{i=-m}^m w_i^2$$

And finally the *cutoff frequency*,  $f_c$ , is defined as the frequency above which the gain drops below  $1/\sqrt{2}$  (approx. 71%). This corresponds with an attenuation of  $-3$  dB.

	S	bias	variance	LMSE	$1/f_c$
S11	<b>0.020</b>	0.50	0.10	0.35	22.8 $t_s$
H9	0.068	-0.10	<b>0.28</b>	0.29	7 $t_s$
H11	<b>0.022</b>	<b>-0.04</b>	<b>0.24</b>	<b>0.24</b>	8.4 $t_s$
H13	<b>0.008</b>	<b>0.04</b>	<b>0.20</b>	<b>0.20</b>	9.8 $t_s$
H23	<b>0.001</b>	0.33	0.12	<b>0.23</b>	16.3 $t_s$

Table 7. Comparison of moving average filters

Table 7 shows that H13 is an excellent smoother with a low bias and acceptable variance. Its local mean square error is low with a good distribution between bias and variance. Its cutoff frequency for a sampling rate of 3 s is approximately 1/30 Hz ( $1 / 9.8 t_s$ ). This is inline with the rule of thumb to measure 10 times faster than the highest frequency of interest and to filter out all higher frequencies.

Note that, with this respect, H13 will always be the preferred filter independent from the scanrate since the wavelength of the cutoff frequency is approximately 10 times (9.8) the sampling period.

### Local variance

In analogy with the local bias and local variance associated with the filter, a local variance on the measurement signal is defined for use in the next chapter:

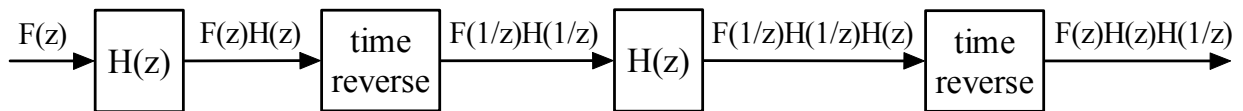
$$s_l^2 = \frac{1}{4} \sum_{i=-2}^2 (y_{t+i} - z_{t+i})^2$$

### 5.3.4 Anti-Causal, Zero-Phase Filter Implementation

All filters described above have a phase lag of  $\pi$  in some periods where  $\text{Re}\{f(\omega)\}$  becomes negative. In order to remove this phase lag, an *anti-causal filter* can be used instead. An anti-causal filter uses the information in the signal at points in time before and after the current point, in essence “looking into the future”, to eliminate phase distortion. This type of processing cannot be done in real-time, but must be done after a signal is captured by post-processing methods for it requires to time reverse the data ( $y_1, y_2, \dots, y_n \rightarrow y_n, y_{n-1}, \dots, y_1$ )

The technique consists of:

1. filtering once the data;
2. the output is then time reversed;
3. filter the time reversed data;
4. time reverse the data filtered twice.



The technique implies the complete removal of any phase shift  $\Phi(\omega)$  and results in a squared gain  $G(\omega)$ .

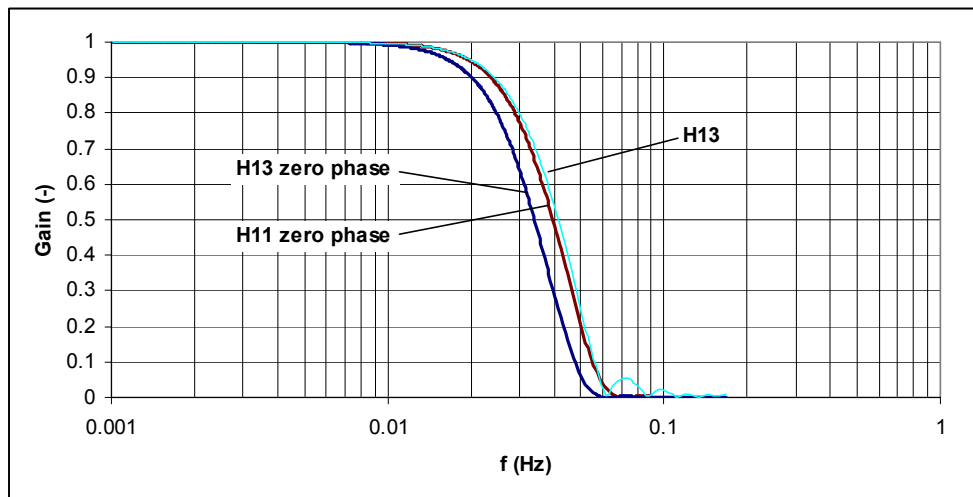


Figure 37. Gain functions of the *H13* and *H13 zero phase* filters @  $t_s = 3$  s

Note that the *H11 zero phase* filter best approaches a cutoff frequency of 10 times the sampling period for the zero phase filters.

Filter	$1/f_c$
H13	$9.8 t_s$
H11 zero phase	$10.2 t_s$
H13 zero phase	$11.9 t_s$
H111 zero phase	$90 t_s$

Table 8. cutoff frequencies

It is therefore recommended to use a *H11 zero phase* (H11 ZP) filter in this work since it removes any phase shift and has a cutoff frequency of 10 times the sampling period.

In some cases, as will be discussed later in this chapter, higher order filters like the *H111 ZP* filter are useful. The gain function of this filter on data sampled at 10 Hz is given in Figure 38 and its cutoff frequency in Table 8.

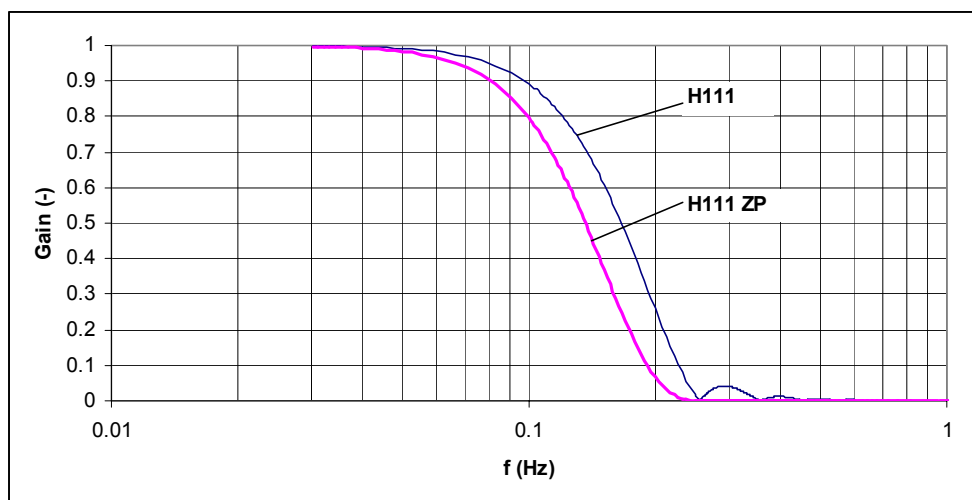


Figure 38. Gain function of the *H111 zero phase* filter @  $t_s = 0.1$  s

### 5.3.5 Chebychev and Butterworth filters

In order to prevent aliasing effects, an analogue filter should be used prior to the D/A converter of the data acquisition system. Most commercial low pass filters have cutoff frequencies down to 1 Hz. Below this frequency, the signal is often considered to be a DC signal.

In general, filters can be described as function of their transfer-function:

$$H(s) = \frac{b_m s^m + \dots + b_1 s + b_0}{a_m s^m + \dots + a_1 s + a_0} = \frac{b_m (s - n_m)(s - n_{m-1}) \dots (s - n_1)}{a_m (s - p_m)(s - p_{m-1}) \dots (s - p_1)}$$

$H(s)$  is the Laplace transform of the impulse response  $h(t)$ :

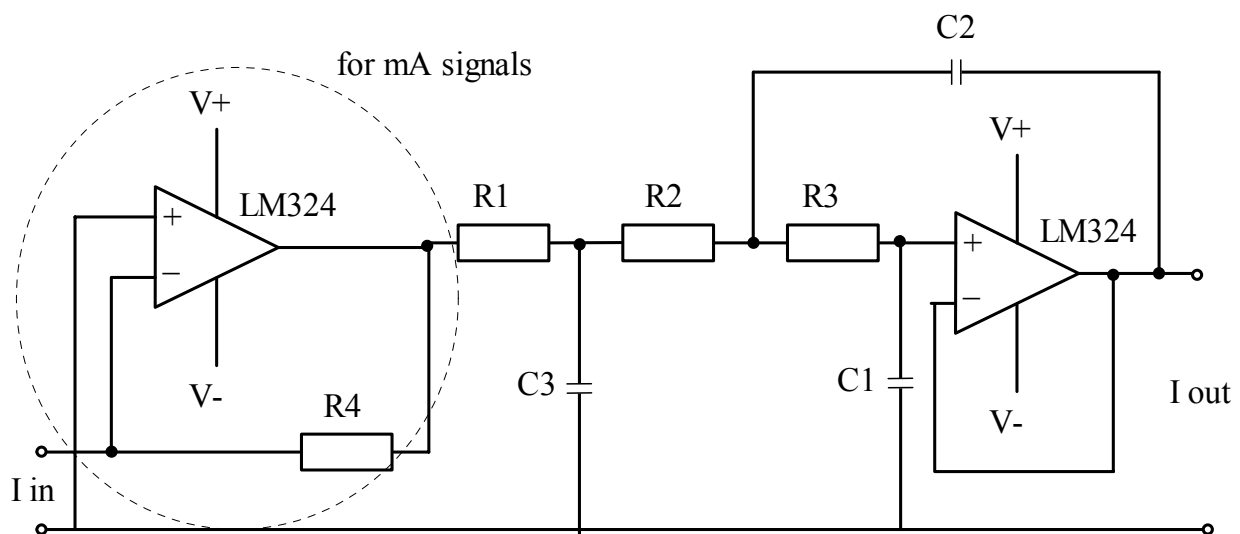
$$H(s) = \mathcal{L}\{h(t)\}$$

Nodes are values of  $s$  whereby the nominator becomes zero, while poles are values whereby the denominator becomes zero.

The Butterworth filter is a low-pass filter common to many applications that require a response that is flat in the passband, but cuts-off as sharply as possible afterwards. It requires arranging poles of a low pass filter with equal spacing around a semi-circular locus.

By bringing poles closer to the axis, the Chebychev filter's frequency cutoff is steeper than the Butterworth filter. Chebychev filter derives from a Butterworth filter by moving each pole closer to the axis in the same proportion so that the poles lie on an ellipse. The Chebychev filter offers a trade-off between ripple and cutoff. In this respect, the Butterworth filter, in which passband ripple has been set to zero, is a special case of the Chebychev filter.

Figure 39 sketches a low pass Butterworth filter of the third order with a cutoff frequency of 1 Hz<sup>[40]</sup> (damping of -60 dB/decade)



$$R1=R2=R3=X \Omega; R4 = 500 \Omega; C1 = 0.322/X \text{ mF}; C2 = 5.644/X \text{ mF}; C3 = 2.216/X \text{ mF}$$

Figure 39. Low pass Butterworth filter of the third order

whereby X is a scaling factor that can be used to end up with some practical values for the capacitances and resistances.

## 5.4. Recommended filters

As may have become clear from the previous sections the use and/or lack of analogue and digital filters substantially influences the measured signal in so far that it may have repercussion on the values used for classification and thus classification result.

This section proposes changes to the data handling in the SBI standard at three possible levels. A *first level* only requires minor changes to the calculation procedures (software) while a *second level* requires substantial changes to both the calculation procedures and the data acquisition system (software and hardware). A third level requires the introduction of inverse filters to recover some BW and requires the careful optimisation of the gas analysis rack.

The three different levels result in three different bandwidths (BW).

changes	approximate BW	filtering
level 1	1 / 30 Hz	H11 ZP @ $t_s = 3$ s
level 2	1 / 10 Hz	H111 ZP @ $t_s = 0.1$ s
level 3	1 Hz	inverse filtering

Table 9. Approximate BW of different alternative measurement methods

Note that if a signal is passed through a filter whose BW is less than that of the signal, the result is a smearing or broadening of the input waveform.

### 5.4.1 First level changes

The first level changes aim at getting qualitative measurements under the limitations of the SBI standard.

#### *Actual specifications on the gas analysers*

The standard prescribes to measure with a 3 s sampling interval which immediately limits the BW according to the Nyquist criterion to 0.16667 Hz ( $1/[2*3s]$ ). This criterion says that the fastest event that can be restored out of a measurement at a sampling rate of  $f_s = 1/t_s$  has a periodicity of  $2*t_s$ .

Furthermore, there are no stringent limitations on the damping of the gas analysers. The only requirement is that the response time  $\tau_{SBI}$  of the overall system is limited to 12 s as described in section C.2.1 of the standard. In the field, values between 7 s and 12 s are reported. The relationship between the time constant  $\tau$  and  $\tau_{SBI}$  (time between a 10% and 90% change) for a first order system is given by

$$\tau_{SBI} = t_2 - t_1 = (-\tau \ln(0.9)) - (-\tau \ln(0.1)) \cong 2.2\tau \quad [ 5.9 ]$$

Combining this with the time constants found in section 5.2.2, the  $\tau_{SBI}$  value for both gas analysers at the Ghent premises is  $\tau_{SBI} = 7.7$  s.

#### *Actual specifications on the pressure transducer*

The limitation on the response time of the pressure transducer is that *it shall have a 90% response time of 1 s or better*. This corresponds to a time constant (first order system) of  $\tau = 0.43$  s ( $1/2.303$ ) or better.

This requirement, because not accompanied with other measures, has a negative influence on the quality of the measurement result. Indeed, pressure fluctuations induced by chimney pressure fluctuations would typically have frequencies in the order of 1 Hz or lower. Since they are not dampened out by the pressure transducer and since the scan rate is limited to 3 s only, spurious data will occur on the measurement result due to the aliasing effect (see 6.4.3) for almost any disturbing frequency between 0.1667 Hz and 1 Hz.

A better choice, in the given circumstances, would be to dampen the pressure signal (most often pressure transducers have a parameterisable damping system) with a same time constant as for the gas analysers.

#### *First level changes*

In view of:

- different time constants for the different measuring devices,
- different time constants of equipment of different laboratories,
- the limited scanrate,
- the rule of thumb to measure 10 times faster than the highest frequency of interest and to filter out all frequencies above this frequency,

the proposal is to apply:

1. an exponential digital or analogue filter on the pressure transducer, O<sub>2</sub> and CO<sub>2</sub> signal such that the output has a time constant  $\tau = \beta$  s (this signal is then fed into the data acquisition system),
2. an exponential digital filter in the software with time constant  $\tau_2$  on the temperature signal such that the combined time constant  $\tau = \beta$  s ( $\tau_2 = \sqrt{\tau^2 - \tau_1^2}$ ) ( $\tau_1$  is the time constant of the undampened signal),
3. a *H11 zero phase* (11 term Henderson) on all sampled data and to no longer use the *SBI running average* filter on the heat release data (HRR),
4. eliminate delay time by synchronising data using maximisation of Pearson's correlation coefficient as discussed further in section 5.6.

### *Effect of first level changes*

As discussed in section 5.3.4 this will dampen all frequencies above 1/30 Hz equally for all channels without additional phase distortion. This allows to accurately synchronise the data and removes differences between laboratories caused by different time constants at the cost of some loss of BW.

The value of  $\beta$  should be taken as low as practically possible and would typically have a value of 3.5 to 4 s, certainly not more than 5 s (refer to 5.3.2 for the effects of exponential filters).

By way of example a same data source is passed through three systems with different time constants, being  $\tau_1 = 0.5$  s,  $\tau_2 = 3$  s,  $\tau_3 = 4$  s. The system with time constant  $\tau_1$  can typically be a pressure transducer while a system with time constant  $\tau_3$  can be that same system in combination with a digital exponential filter. Another example is an oxygen analyser with a fast response time  $\tau_2$  (fastest response time reported in the second SBI round robin) or with a more moderate response time  $\tau_3$ .

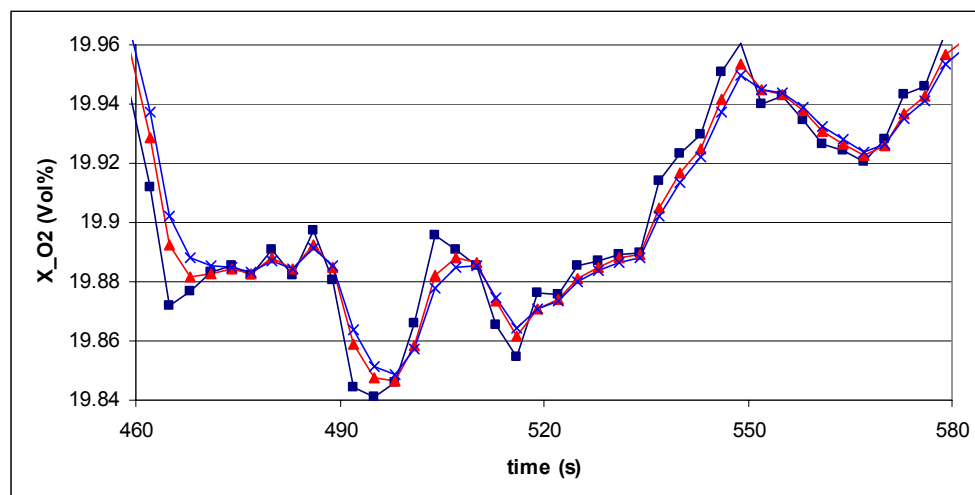


Figure 40. same data passed through systems with time constants  $\tau_1 = 0.5$  s ( $\square$ ),  $\tau_2 = 3$  s ( $\nabla$ ),  $\tau_3 = 5.5$  s ( $\times$ )

Two things that catch the eye are that local differences can be important especially for equipment with big differences in response time and that phase shifting occurs.

In order to better match the data with each other, the signals of the ‘fast’ systems 1 and 2 can be passed through a digital exponential smoothing filter with a time constant  $\tau_{ES}$ . The resulting *apparent* time constant  $\tau$  equals the time constant of for example the slowest system  $\tau_3$  ( $\tau_{ES,i} = \sqrt{\tau^2 - \tau_i^2}$   $i=1,2$ ).

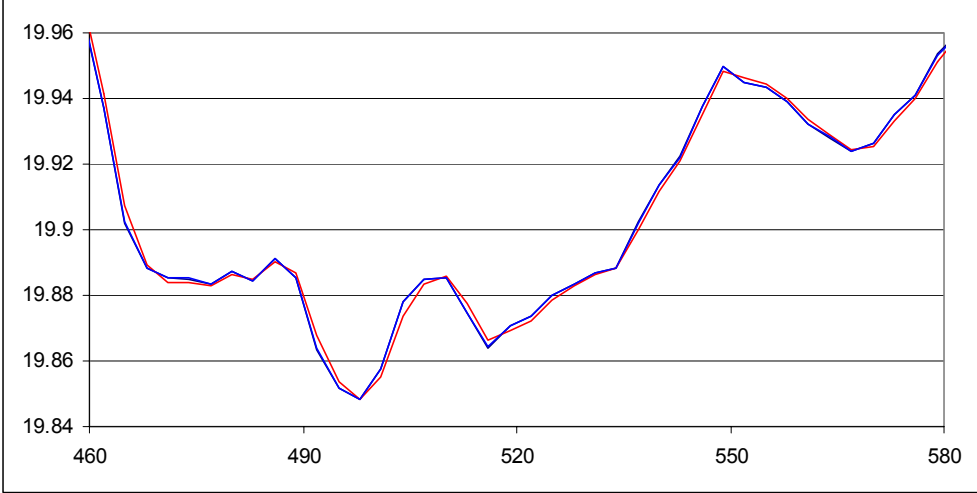


Figure 41. application of an exponential smoothing filter

The frequency response of the combined system (system + smoothing filter) would typically have a shape as displayed in Figure 33, and can further be improved by combining this with a Henderson 11 term zero phase filter ( $t_s = 1/3$  Hz) as shown in Figure 34 and Figure 42.

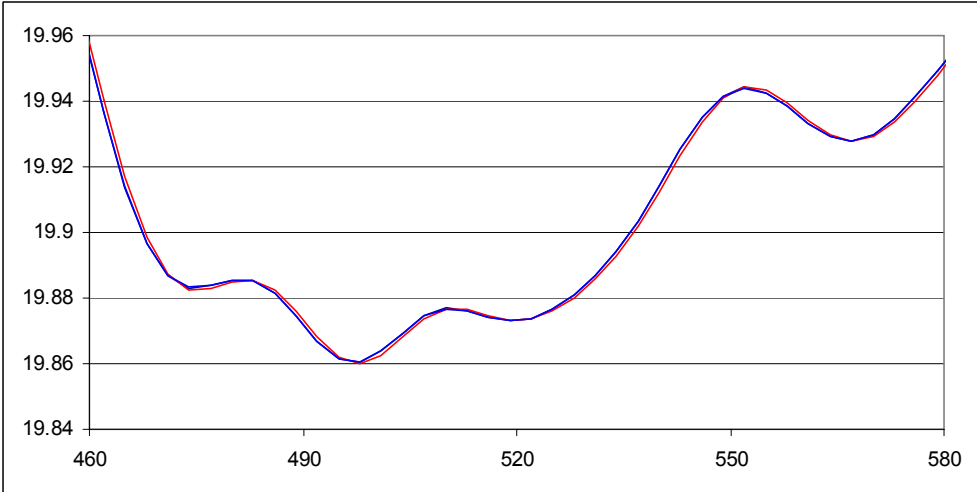


Figure 42. applying a Henderson 11 term zero phase filter in addition

Due to different phase shifts of the different exponential filters used, there still remains a time shift between the different data sets. In this specific case, the time shift is approximately 0.35 s as found by re-sampling the data at 20 Hz (linear interpolation between data points sampled at 1/3 Hz) and by maximising Pearson’s correlation coefficient as explained further in section 5.6.



The results, after correction for this time shift, are displayed in Figure 43.

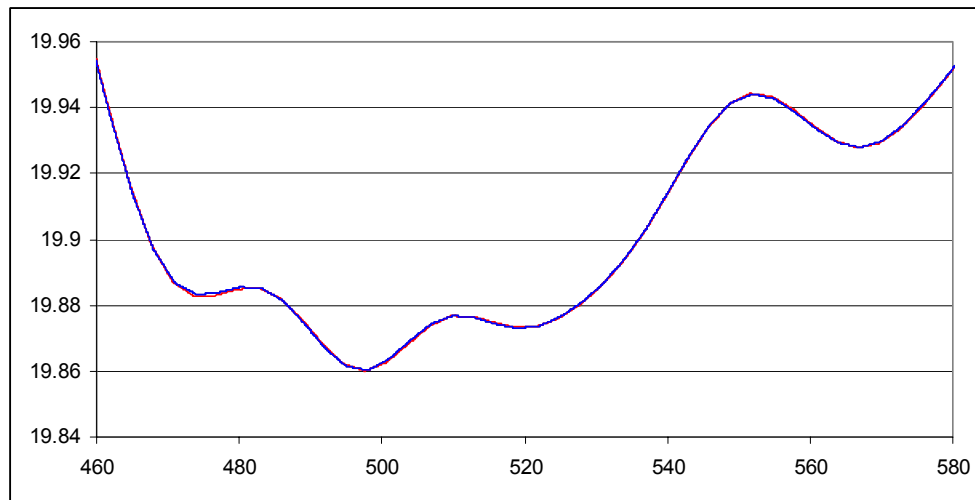


Figure 43. further synchronisation (re-sampling & maximising 'r' coefficient)

The measures presented will improve the reproducibility of test results between test laboratories.

*Effect of differences in time constants (actual situation)*

Indeed, Figure 44 shows the results for the Figra value (used for classification) for two virtual laboratories, one with an assumed response time on the oxygen analyser (according to the definition of the SBI standard) of 7.7 s and the second with a response time of 13.2 s. As a side remark the above numbers are, according to the standard, rounded to the nearest integer of the series (0, 3, 6, 9, 12, ...) to the numbers 9 s and 12 s respectively, so they are within tolerance and still match the recommendations of Messerschmidt and Van Hees<sup>[53]</sup> to fall within a window of 9s to 12s. This in order to minimise the tendency of differing labs to rate a product differently.

The results are based on 30 different data sets, each representing a test on a same MDF board as further explained. A test was run on a MDF board (product P2, fourth sample, SBI RR2) with the data acquisition running at 10 samples a second (10 Hz). Then the data set was reduced to 30 different data sets by taking every 30th data point starting with element  $i$  ( $i = 1 \dots 30$ ). In this way, it is as if we have thirty different data sets at a scanrate of 1/3 Hz (as required by the standard) from a same test. Ideally all thirty data sets should produce the same result, which clearly they don't.

The test results should be compared in pairs (each case separately). The graph shows that, for this specific case and test, the differences in the classification parameter FIGRA vary from 0 to 3%.

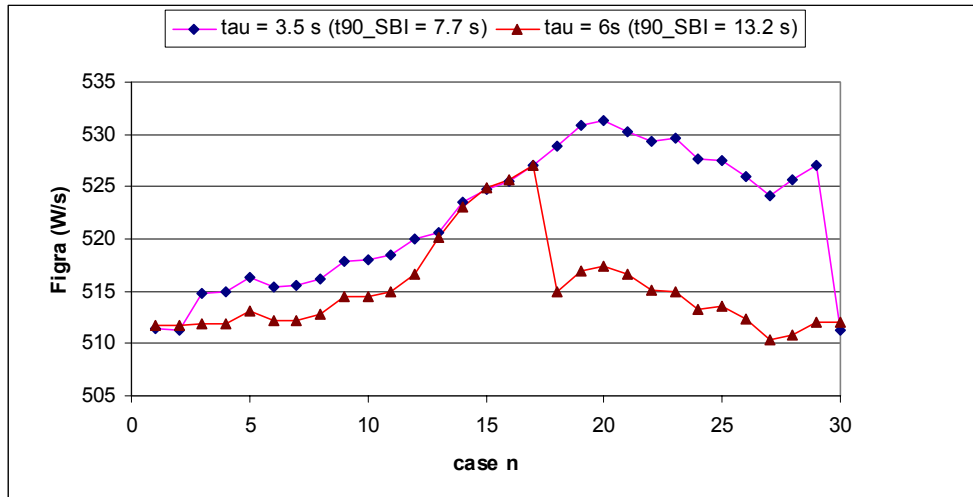


Figure 44. Example of different classification result due to different response times

This example highlights the need for managing the dynamic behaviour of all time variable data.

### 5.4.2 Second level changes

One may argue that the SBI should be able to capture faster events without smearing out events over time. The limit of the fastest event we want to capture could be taken arbitrarily as *sustained flaming* as defined in the Cone Calorimeter test<sup>[4]</sup>. In the Cone Calorimeter standard, distinction is made between:

- flashes, where a flame on or over the surface of the specimen exists for periods of less than 1s,
- transitory flaming, where a flame on or over the surface of the specimen exists for periods of between 1 s and 10 s,
- sustained flaming, where a flame on or over the surface of the specimen exists for periods of over 10 s.

Bryant et al<sup>[64]</sup> also raise the question as to how rapid a HRR fluctuation matters in the context of a 3 Megawatt heat release rate test facility. They say that there may not be a unique answer to that and they plan research on the subject at NIST. They further suggest that it may be in the order of 5 s to 15 s.

#### *Second level changes*

Assuming the fastest event we want to capture is in the order of 10 s, this requires:

- the turning off of any damping on the measuring equipment,
- the use of an analogue filter with a cutoff frequency at 1 Hz (to avoid aliasing),
- a scan rate of 10 Hz (to avoid aliasing),

- the application of a *H111 zero phase* (111 term Henderson) filter on the sampled data (to remove any disturbance with frequency above 1/10 Hz).

*Effect of second level changes*

An example of how level two changes can improve the DAQ is shown in Figure 45. Besides the original sampled differential pressure data (10 Hz), the graph shows the filtered data making use of either a zero phase Henderson filter or a zero phase exponential filter (please disregard the tails where no filtering is applied). By way of example, one of thirty possible data sets at a sampling rate of  $t_s = 3$  s is shown in the same graph.

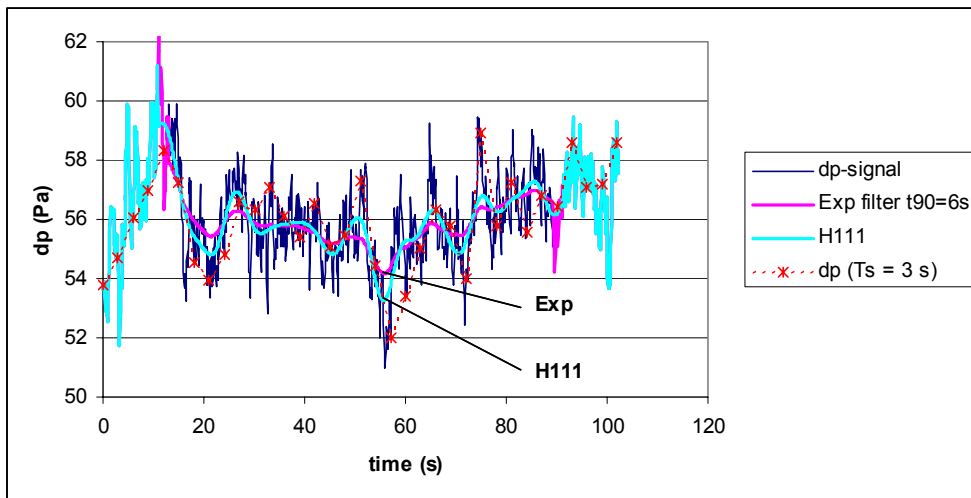


Figure 45. Original data, filtered data (*H111 ZP* and *EXP6s ZP*) and sampled data ( $t_s=3s$ )

In order to better understand the behaviour of, and the differences between the filters, the next three figures show a Fast Fourier Transform (FFT) on the three data sets (original, Exp filtered, H111 filtered).

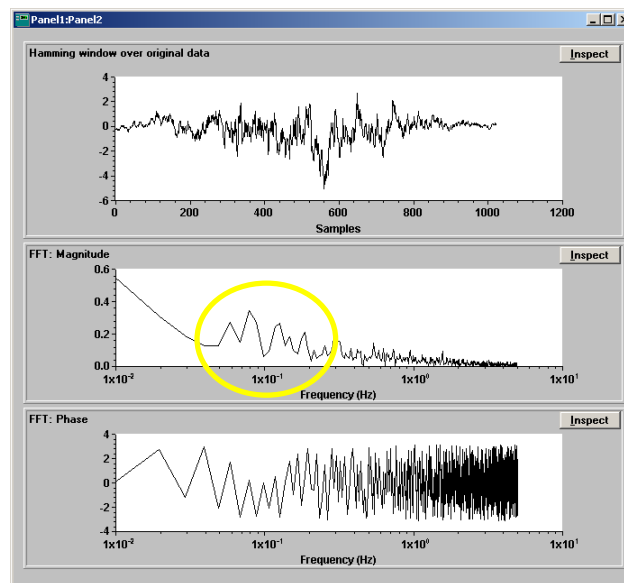


Figure 46. FFT on the original data

Comparing the magnitude of the frequency spectra, it is clear that the exponential filter not only dampens out frequencies above 0.1 Hz, but also changes the spectrum below 0.1 Hz.

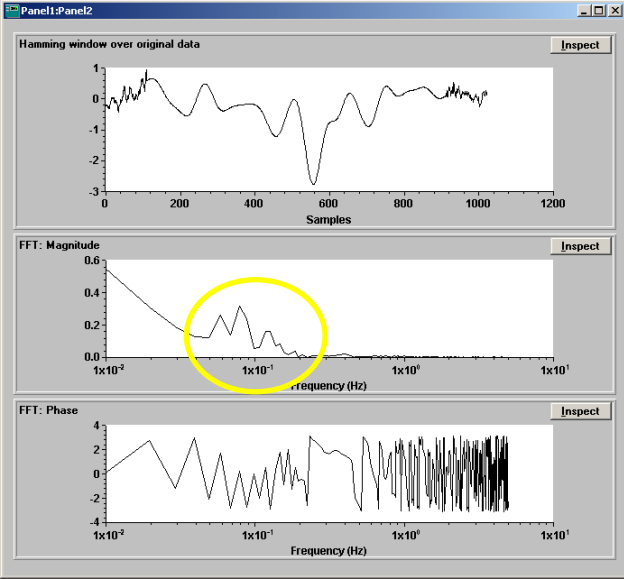


Figure 47. FFT on the filtered data (*H111 ZP*)

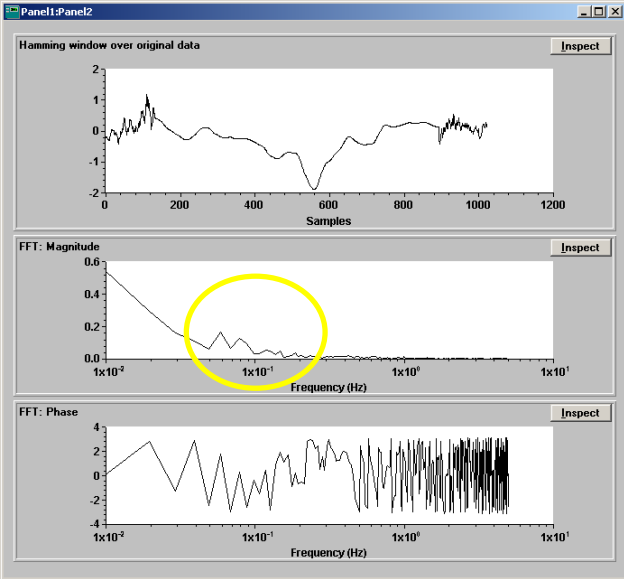


Figure 48. FFT on the filtered data (*Exp6s ZP*)

The second level technique could be used to capture events up to 1/5 Hz (with an adapted Henderson filter). Above this frequency, not only the data acquisition system needs to be replaced but also the gas analysis system and pressure transducer need careful design to allow for inverse filtering.

### 5.4.3 Third level changes

If one wants to capture faster events like transitory flaming or even flashes, inverse filters need to be applied. This is not recommended for the SBI test but could be useful for small scale research equipment like the Cone Calorimeter.

Inverse filtering is discussed briefly in the next section.

### 5.5. Inverse filters

All four major measurement components ( $O_2$ ,  $CO_2$ , temperature and differential pressure) have time constants ranging from 0.5 s to 3.5 s. This means that we are only able to capture events with a time constant exceeding 3.5 s.

For most intermediate and large scale fire applications like the room corner test and the SBI, this does not pose any problem since the fastest events of interest would have a periodicity of at least 5 to 15 seconds as discussed earlier.

However, if we would want to measure events like surface flashes ( $T < 1$  s) or transitory flaming ( $T < 10$  s), we hit the limits of the actual measurement devices.

By applying inverse filters  $H^{-1}(s)$  on the individual measurement signals, we can remove the damping effect  $H(s)$  of the internal system thus restoring the ‘real’ signal.

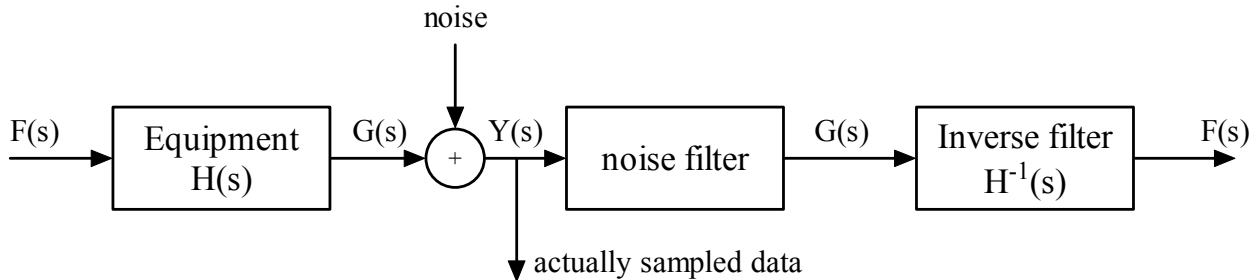


Figure 49. Principle of an ideal inverse filter set-up

One major drawback of this technique is however that the inverse filter acts as an amplifier for the higher frequencies including noise on the measurement signal. The inverse filter therefore needs to be designed such that it only amplifies frequencies in the narrow BW we want to restore.

Suppose we want to increase the BW to 1Hz, instead of the actual 0.29 Hz, this would require the following steps:

1. Improve the gas analysis equipment to eliminate (or suppress sufficiently) any disturbance with frequency below 1 Hz
2. Introduce an analogue filter with cutoff frequency of 1 Hz in order to avoid any aliasing effect and to remove higher frequencies that are of no interest
3. Increase the sampling rate to 10Hz (10 times higher than the highest frequency of interest)
4. Apply the inverse filter

A Butterworth type filter is recommended as analogue filter since it shows no ripple in the pass band.

The maximum achievable BW is 2 Hz since the internal sampling rate of the electronics in the gas analysers is working at  $t_s = 240$  ms ( $f_s \cong 4$ Hz). Indeed, according to the Nyquist criteria the maximum perceptible frequency is half the sampling frequency.

However, when applying this technique, one may encounter other limiting effects like pressure fluctuations, vibrations, etc.

## 5.6. Elimination of delay time

Since the differential pressure measurement, the temperature measurement, the oxygen and carbon dioxide concentration measurements, needed to calculate the heat release, have different delay times, a synchronization of data is needed. In general, there is a delay time of several seconds (9 s to 15 s in most labs) in-between the sampling of the combustion gases and the actual gas concentration measurement. A fully automated procedure is given in the SBI standard to exclude human interpretation

The measured data are synchronised in time making use of the dips and peaks that occur in the data due to the switch from 'primary' to 'main' burner around  $t = 300$  s. Synchronisation is necessary due to the delayed response of the oxygen and carbon dioxide analysers that can easily reach values from 6 s to 15 s and even higher (the standard allows 30 s delay). The filters, long transport lines, the cooler, etc. in between the gas sample probe and the analyser unit, cause this delay time.

After synchronisation, all data are shifted such that the 'main' burner ignites – by definition - at time  $t=300$ s

Since synchronisation can have such a big impact on the classification results, a scientifically more sound method is proposed based on correlations.

Correlation can be used to compare the similarity of two sets of data. Correlation computes a measure of similarity of two input signals as they are shifted by one another. The correlation result reaches a maximum at the time when the two signals match best. If the two signals are identical, this maximum is reached at  $t = 0$  (no delay). If the two signals have similar shapes but one is delayed in time and possibly has noise added to it then correlation is a good method to measure that delay.

The Pearson coefficient 'r' is a single correlation value that reflects the degree of linear relationship between two data sets. Its value is between -1 and +1. A value of +1 means that there is a perfect positive linear relationship between the two data sets. A value of -1 means that there is a perfect negative linear relationship, and a value of 0 means there is no linear relationship at all between the data sets.

Pearson's coefficient is calculated as

$$r = \frac{\sum_n (X_n - \bar{X})(Y_n - \bar{Y})}{\sqrt{\sum_n (X_n - \bar{X})^2} \sqrt{\sum_n (Y_n - \bar{Y})^2}} \quad [ 5.10 ]$$

Synchronising the data would then mean to maximise the absolute value of Pearson's coefficient. Applying this by way of example on a *particle board* data set sampled at 10 Hz a delay time of 7.4 s for the oxygen concentration data set is found while 9.6 s is found for the carbon dioxide data set. In analogy with the standard, the data sets have been synchronised with respect to the temperature data set.

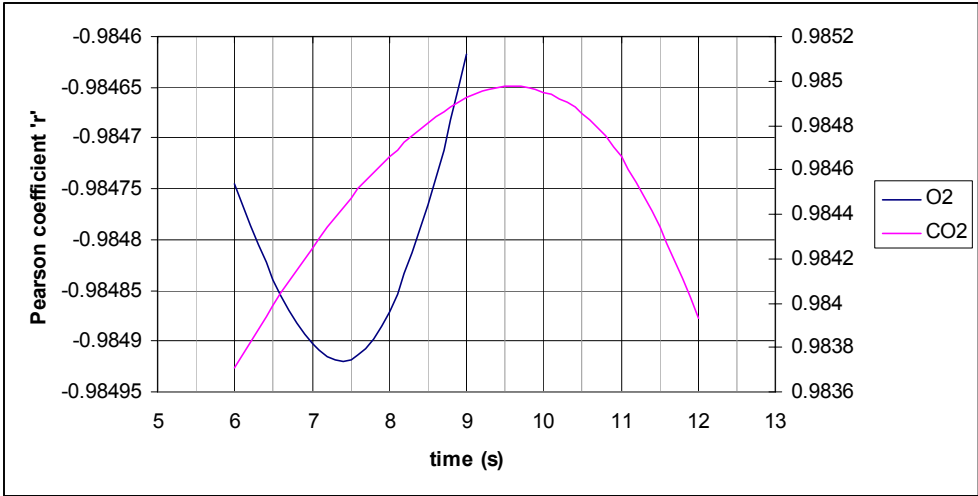


Figure 50. Data synchronisation by means of maximising correlation (Pearson)

## 5.7. Conclusions

In this chapter, the concept of bandwidth (BW) – well known in electronic engineering and process control – has been introduced. The BW is the frequency below which an input signal is transferred without substantial distortion in amplitude and/or phase-shift. If a signal is passed through a filter whose BW is less than that of the signal, the result is a smearing or broadening of the input waveform.

Peak heat release rate values, which are often used in fire regulations, are meaningless if not accompanied with the BW of the test instrumentation. The consequence for the European classification system is that test results for products that did not go to flashover in the Room Corner test end up with a high uncertainty interval because based on peak heat release rate divided by the time to reach this peak.

The BW of the different measuring devices, mass flow controller and data acquisition system of the Ghent premises have been identified together with the behaviour of the built in adjustable filters in some of the measuring devices.

Due to differences in BW between instrumentation and in-between laboratories, measurement results can vary substantially. In order to overcome the tendency of differing labs to rate products differently three possible levels of changes to the standard have been proposed. A first level only requires some minor changes to the software calculation procedures and results in an approximate BW of 1/30 Hz. A second level involves substantial changes to both the calculation procedures and the data acquisition system and results in an approximate BW of 1/10 Hz. This is our preferred option because: it guarantees the complete elimination of any possible aliasing effect, it is able to capture events with a periodicity down to 10 s, it allows for a better smoothing and synchronisation of the data with a resulting better repeatability and reproducibility.

A third level requires the introduction of inverse filters and potentially allows to recover some BW up to 1 Hz. Since the periodicity of events of interest in the SBI test method is in the order of 10 s or higher the proposal is to not follow this route for intermediate and large scale heat release rate test equipment. The technique may be of interest in small scale tests like the Cone Calorimeter. It needs to be stressed however that this method is very sensitive to noise and that it requires a complete redesign and optimisation of the gas analysis train to eliminate any disturbing noise.

Also an alternative automatic synchronisation method based on the maximisation of a correlation coefficient has been proposed. Contrary to the actual method, which is based on the synchronisation of times when signals surpass a certain limit value after a stepwise burner change, the method does take differences in dynamic behaviour of the different components into account.



Flat running average filters are popular for smoothing data over time. Although they are easy to understand and implement, they not only dampen out the higher frequencies but they also disturb the lower frequencies which are of interest to us. This results in a high local bias and a poor local variance. The concept of weighted, Henderson moving average filters is introduced. Henderson filters are often used as trend filters in economics. The Henderson filters can reproduce polynomials up to degree three which enables them to adequately capture trend turning points and points of inflection.

The same or similar filter techniques can be applied for the smoke measurement.

## 6 Uncertainty

### 6.1. Introduction

According to EN ISO 17025<sup>[9]</sup>, which sets out the general requirements for the competence of testing and calibration laboratories, and ISO 10012-1<sup>[14]</sup>, which sets out the requirements for assuring the quality of measuring equipment, uncertainties are to be reported in both testing and calibration reports.

The general principles for evaluating and reporting uncertainties are given in the ISO Guide to the Expression of Uncertainty in Measurement (GUM)<sup>[13]</sup>, but need to be applied to the specific case of fire testing. Due to the harmonisation of fire testing in the European Community (EUROCLASSES; EN 13501-1<sup>[1]</sup>) and the pressure on testing laboratories to operate under accreditation, this is becoming even more important.

It is of common knowledge that measurement results are never perfectly accurate. In practice the sources of systematic and random errors which can affect the results of measurement are numerous, even for the most careful operators. To describe this lack of perfection, the term "uncertainty" is used. Although the concept of uncertainty may be related to a "doubt", in the real sense the knowledge of uncertainty implies increased confidence in the validity of results.

The qualitative concept of accuracy is quantified by the uncertainty which varies inversely 'proportioned' to it. Accuracy consists of both trueness and precision as shown in Figure 51. A numerical measure for precision is the standard deviation, while trueness is expressed numerically by the systematic error or the bias.

It is considered good practice to eliminate any systematic errors. However, if the value of a systematic error is unknown it may be regarded as a random error. Random errors result in a spread of the values and can usually be reduced by increasing the number of observations. Its expectation or expected value is zero.

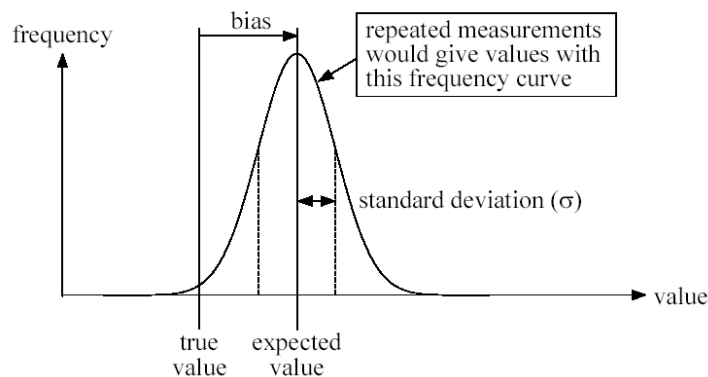
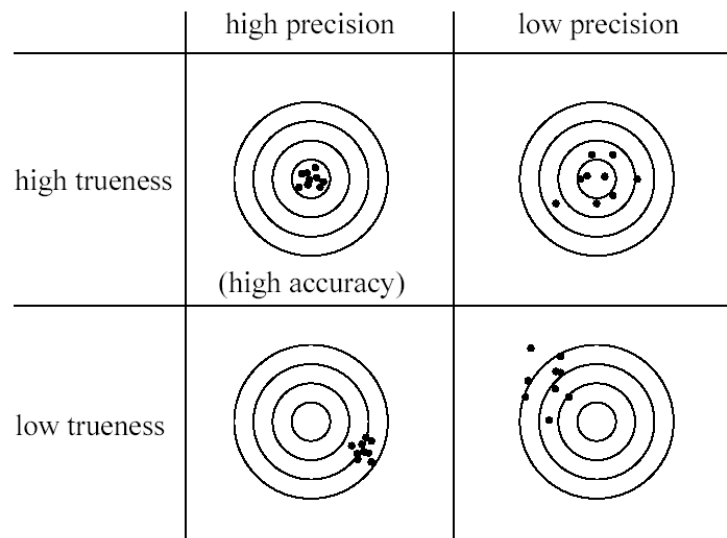


Figure 51. Concepts of accuracy (uncertainty), precision (standard deviation) and trueness (bias)

In general, the result of a measurement is only an approximation or estimate of the value of the specific quantity subject to measurement, that is, the measurand, and thus the result is complete only when accompanied by a quantitative statement of its uncertainty.

Without knowledge of the accuracy (trueness and precision) of measurement methods and/or the uncertainty of measurement results, it may appear very easy to make decisions. But, in practice, these decisions may be incorrect and sometimes lead to serious consequences, if the measurement uncertainty is not taken into account.

For example, in fire testing, when rejecting instead of accepting a good product during a certification process or, conversely, when accepting a bad product by error. So, it is vital to quantify the reliability of the measurement results to greatly reduce any disputes and adverse consequences of legal proceedings. This is of particular importance if we consider the growing number of cases of litigation in Europe and the liability problems of manufacturers in case of accidents.

NOTE – The difference between error and uncertainty should always be borne in mind. For example, the result of a measurement after correction can unknowably be very close to the unknown value of the measurand, and thus have negligible error, even though it may have a large uncertainty.

## 6.2. Elaboration of terms and concepts

### 6.2.1 Mean and variance

A population with a ‘normal’ probability density function is characterised by its mean value  $\mu$  and its variance  $\sigma^2$ :  $N(\mu, \sigma^2)$ . When both  $\mu$  and  $\sigma^2$  are unknown, they can be estimated by taking a number  $n$  of samples and by calculating the estimated mean  $\bar{x}$ , the estimated variance  $s^2$  and the estimated standard deviation  $s$ .

$$\bar{x} = \frac{1}{n} \sum_{i=1}^n x_i \quad [ 6.1 ]$$

$$s^2 = \frac{1}{n-1} \sum_{i=1}^n (x_i - \bar{x})^2 \quad [ 6.2 ]$$

If a covariance exists between two variables  $x$  and  $y$ , it is given by

$$s_{ij}^2 = \frac{1}{n-1} \sum_{i=1}^n (x_i - \bar{x})(y_i - \bar{y}) \quad [ 6.3 ]$$

### 6.2.2 Estimation of the confidence interval for the population mean<sup>[40]</sup>

Often the standard deviation  $\sigma$  is unknown. To evaluate the confidence interval, some estimate of  $\sigma$  must be made. The most obvious candidate is the sample standard deviation  $s$ . But the use of  $s$  introduces an additional source of unreliability, especially if the sample is small. To retain the confidence interval, we must therefore widen the interval. We do so by using the  $t$  distribution instead of the standard normal distribution. For a sample size larger than 100, the  $t$ -distribution approaches the

normal distribution. For a 95% (two tails of 2.5%) confidence interval – which we strive for – the uncertainty is estimated by

$$t_{0.025} \frac{s}{\sqrt{n}} \quad [ 6.4 ]$$

The value  $t_{0.025}$  depends on the amount of information used in calculating  $s^2$ , i.e. on the degrees of freedom. For large sample sizes,  $t_{0.025}$  approaches 1.96 which is the value for a normal distribution. For a normal distribution, a coverage factor 2 (1.96) corresponds to a 95% confidence interval (see 6.2.6).

### 6.2.3 Sources of uncertainty

According to GUM any detailed report of the uncertainty should consist of a complete list of the components, specifying for each the method used to obtain its numerical value. The components may be grouped into two categories based on their method of evaluation:

Type A            The components in category A are characterized by the estimated variances  $s_i^2$  or by the estimated standard deviation  $s_i$  derived from data by statistical methods. Where appropriate the covariance  $s_{ij}^2$  should be given. For such a component, the standard uncertainty is  $u_i = s_i$ .

Type B            The standard uncertainty of a Type B evaluation is approximated based on specifications, calibrations, handbooks, experience, judgements etc. and is represented by a quantity  $u_j$ . It is obtained from an assumed probability distribution based on all the available information.

Where appropriate the covariance should be given and should be treated in a similar way.

The ‘type’ classification does not indicate any difference in the nature of the components resulting from the two types of evaluation. Both are based on probability distributions, and the uncertainty components resulting from either type are quantified by standard deviations. It should be recognized that a Type B evaluation of standard uncertainty can be as reliable as a Type A evaluation.

The standard deviation of a Type B evaluation is based on the shape of the distribution. Distributions used in this dissertation are the rectangular, the triangular, the trapezoidal and the normal distribution. For the rectangular and triangular also asymmetric distributions are discussed.

## 6.2.4 Standard uncertainties for different distributions

### *Normal distribution*

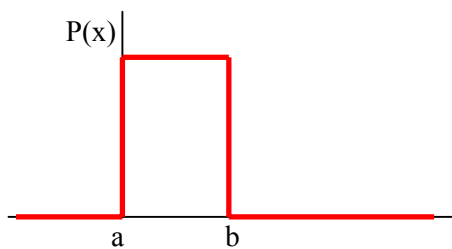
Often calibration certificates, handbooks, manufacturer's specifications, etc. state a particular multiple of a standard deviation. In this case, a normal distribution is assumed to obtain the standard uncertainty.

### *Rectangular distribution*

In other cases the probability that the value of  $X_i$  lies within the interval  $a^-$  to  $a^+$  for all practical purposes is equal to one and the probability that  $X_i$  lies outside this interval is essentially zero. If there is no specific knowledge about the possible values of  $X_i$  within the interval, a uniform or rectangular distribution of values is assumed. The associated standard deviation is function of the width of the distribution as:

$$u_{rect} = \frac{a}{\sqrt{3}} \quad [6.5]$$

Indeed, for a rectangular distribution, the variance is obtained as follows. Given the probability function of the rectangular distribution



$$P(x) = \begin{cases} 0 & x < a \\ \frac{1}{b-a} & a < x < b \\ 0 & x > b \end{cases} \quad [6.6]$$

This can be written in terms of the Heaviside step function  $H(x)$  as

$$P(x) = \frac{H(x-a) - H(x-b)}{b-a} \quad [6.7]$$

This makes that the variance  $\sigma^2$  with population mean  $\mu$  for an asymmetric distribution becomes

$$\mu = \int_{-\infty}^{\infty} P(x)x dx = \int_a^b \frac{x}{(b-a)} dx = \frac{b+a}{2} \quad [6.8]$$

$$\sigma^2 = \int_{-\infty}^{\infty} P(x)(x-\mu)^2 dx \quad [6.9]$$

$$\sigma^2 = \int_{-\infty}^{\infty} \frac{H(x-a) - H(x-b)}{b-a} \left(x - \frac{a+b}{2}\right)^2 dx \quad [6.10]$$

$$\sigma^2 = \int_a^b \frac{\left(x - \frac{a+b}{2}\right)^2}{b-a} dx = \frac{(a+b)^2}{12} \quad [6.11]$$

So for a symmetric rectangular interval  $a^-$  to  $a^+$ , the variance reduces to

$$\sigma^2 = \frac{a^2}{3}. \quad [6.12]$$

The sample estimate of the standard deviation thus is:

$$u_{rect} = \frac{a}{\sqrt{3}}. \quad [6.13]$$

The rectangular distribution is a reasonable default model in the absence of any other information. But if it is known that values of the quantity in question near the centre of the limits are more likely than values close to the limits, a triangular or a normal distribution may be a better model.

#### *Triangular and trapezoidal distribution*

In many cases it is more realistic to expect that values near the bounds are less likely than those near the midpoint. It is then reasonable to replace the symmetric rectangular distribution by a symmetric

trapezoidal distribution having equal sloping sides, a base of width  $2a$  and a top of width  $2a\beta$  where  $0 \leq \beta \leq 1$ . Similar as for a rectangular distribution, for a trapezoidal distribution the standard deviation becomes:

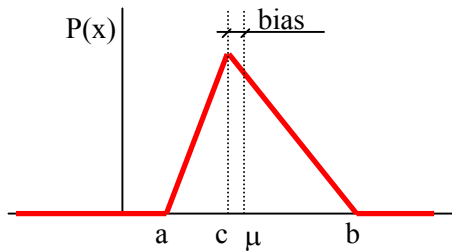
$$u_{trap} = \frac{a\sqrt{(1 + \beta^2)}}{\sqrt{6}} \quad [6.14]$$

As  $\beta$  goes to 1 this trapezoidal distribution approaches the rectangular distribution while for  $\beta=0$  it is a triangular distribution.

$$u_{trian} = \frac{a}{\sqrt{6}} \quad [6.15]$$

### *Asymmetric distributions*

For an asymmetric triangular distribution the mean value and standard deviation become<sup>[84]</sup>



$$\mu = \frac{1}{3}(a + b + c) \quad [6.16]$$

$$u_{asymmetric\_triangular} = \sqrt{\frac{1}{18}(a^2 + b^2 + c^2 - ab - ac - bc)} \quad [6.17]$$

For the limit case of a 'one sided triangular distribution ( $a=c=0$ ;  $b=b$ ) this reduces to

$$\mu = \frac{b}{3} \quad [6.18]$$

$$u_{asymmetric\_triangular} = \frac{b}{3\sqrt{2}} \quad [6.19]$$



The limit case of a 'one sided rectangular distribution (a=0; b=b) reduces to (formulas 6.8 & 6.11)

$$\mu = \frac{b}{2} \quad [ 6.20 ]$$

$$u_{\text{asymmetric\_rectangular}} = \frac{b}{\sqrt{12}} \quad [ 6.21 ]$$

For asymmetric distributions the difference between the mean value  $\mu$  and  $c$  will be considered as a bias and, as recommended by the GUM, we will correct for it.

## 6.2.5 Combined uncertainty

### 6.2.5.1 Uncorrelated input quantities

The standard uncertainty of  $y$ , where  $y$  is the estimate of the measurand  $Y$  and thus the measurement, is obtained by appropriately combining the standard uncertainties of the input estimates  $x_i$ . In case all input quantities are independent, this combined standard uncertainty  $u_c(y)$  is the positive square root of the combined variance  $u_c^2(y)$  and is given by

$$u_c = \sqrt{\sum_{i=1}^N [c_i u(x_i)]^2} \quad [ 6.22 ]$$

where the sensitivity coefficient is given by

$$c_i = \frac{\partial y}{\partial x_i} \quad [ 6.23 ]$$

### 6.2.5.2 Correlated input quantities

The above equation is only valid when the input quantities  $X_i$  are independent or uncorrelated. When the input quantities are correlated, the appropriate expression for the combined variance  $u_c^2(y)$  associated with the result of the measurement is

$$u_c = \sqrt{\sum_{i=1}^N [c_i u(x_i)]^2 + 2 \sum_{i=1}^{N-1} \sum_{j=i+1}^N c_i c_j u(x_i) u(x_j) r(x_i, x_j)} \quad [6.24]$$

whereby the degree of correlation between  $x_i$  and  $x_j$  is characterised by the estimated correlation coefficient (Pearson)

$$r(x_i, x_j) = \frac{u(x_i, x_j)}{u(x_i)u(x_j)} \quad -1 \leq r(x_i, x_j) \leq +1 \quad [6.25]$$

If the estimates  $x_i$  and  $x_j$  are independent,  $r(x_i, x_j) = 0$ , and a change in one does not imply an expected change in the other. Pearson's coefficient reflects the degree of linear relationship between two data sets. Its value is between -1 and +1. A value of +1 means that there is a perfect positive linear relationship between the two data sets. A value of -1 means that there is a perfect negative linear relationship, and a value of 0 means there is no linear relationship at all between the data sets. Please refer to section 5.6 for additional information.

The measurands  $E^2$ ,  $p_{atm}$ ,  $T_{room}$ ,  $\phi$ ,  $\alpha$ ,  $c$ ,  $A$ ,  $k_t$  and  $k_p$ , as defined in sections 2.2.3.1 and 6.4, are constant or can be considered constant throughout the test. They are treated as independent input quantities. However, the oxygen concentration ( $XO_2$ ), the carbon dioxide concentration ( $XCO_2$ ), the exhaust gas temperature in the measurement section ( $T_{ms}$ ) and the differential pressure over the velocity probe ( $\Delta p$ ) are significantly correlated the one to the others as can be seen, by way of example, in Table 10.

		O2-raw	CO2-raw	Tms-raw	dp-raw
O2-raw	Pearson Correlation	1	-.996**	-.985**	-.912**
	Sig. (2-tailed)	.	.000	.000	.000
	N	16676	16676	16676	16676
CO2-raw	Pearson Correlation	-.996**	1	.985**	.912**
	Sig. (2-tailed)	.000	.	.000	.000
	N	16676	16676	16676	16676
Tms-raw	Pearson Correlation	-.985**	.985**	1	.930**
	Sig. (2-tailed)	.000	.000	.	.000
	N	16676	16676	16676	16676
dp-raw	Pearson Correlation	-.912**	.912**	.930**	1
	Sig. (2-tailed)	.000	.000	.000	.
	N	16676	16676	16676	16676

\*\* . Correlation is significant at the 0.01 level (2-tailed).

Table 10. Correlation between  $XO_2$ ,  $XCO_2$ ,  $T_{ms}$  and  $\Delta p$  for a *particle board* test.

Besides the correlation coefficients, Table 10 shows the 2 tailed significance level of the hypotheses

$H_0$  = “variable x and variable y are uncorrelated”. A significance level of 0.05 or lower indicates that there is a 95% chance or higher that the variables are correlated.

This can also be explained intuitively. Suppose a pure substance like for example propane is burnt,



we know that for every mole of oxygen consumed, 3/5 moles of carbon dioxide will be formed. So there is a perfect negative correlation between the two ( $r = -1$ ).

Furthermore, when there is oxygen consumption, there is heat release and temperature of the exhaust gases will rise with a resulting negative correlation. This negative correlation is also true for the differential pressure, which will increase due to an increased velocity in the exhaust duct when running the equipment at constant mass flow rate (see by way of example Table 2, p. 90).

The correlation coefficients  $r(x_i, x_j)$  used throughout this dissertation will be calculated based on the data of the test under consideration.

## 6.2.6 Expanded uncertainty

Although the combined standard uncertainty  $u_c$  is used to express the uncertainty of a wide variety of applications, what is often required is a measure of uncertainty that defines an interval about the measurement result  $y$  within which the value of the measurand  $Y$  can be confidently asserted to lie. The measure of uncertainty intended to meet this requirement is termed expanded uncertainty,  $U$ , and is obtained by multiplying  $u_c(y)$  by a *coverage factor*  $k$ . Thus  $U = k u_c(y)$  and it is confidently believed that  $Y$  is greater than or equal to  $y - U$ , and is less than or equal to  $y + U$ , which is commonly written as  $Y = y \pm U$ .

In general, the value of the coverage factor  $k$  is chosen on the basis of the desired level of confidence to be associated with the interval defined by  $U = k u_c$ . Typically,  $k$  is in the range 2 to 3. When the normal distribution applies and  $u_c$  is a reliable estimate of the standard deviation of  $y$ ,  $U = 2 u_c$  (i.e.,  $k = 2$ ) defines an interval having a level of confidence of approximately 95 % (95.44%), and  $U = 3 u_c$  (i.e.,  $k = 3$ ) defines an interval having a level of confidence greater than 99 % (99.73%).

Throughout this dissertation, we will work with standard deviations to express the uncertainty of individual measurands and combined standard uncertainties, and with a coverage factor of 2 to express the confidence interval on the estimate of the overall uncertainty.

On occasion, a self defined *apparent standard deviation* defined as the uncertainty for a 95% interval divided by 1.96 will be used. This is useful when for example using t-distributions since for this distribution the expanded uncertainty  $U(k=1.96) \neq 1.96 \cdot U(k=1)$ . Since we know that we finally want to end up with a 95% confidence interval but we are working with standard deviations, t-distributions will be calculated based on a 95% confidence interval divided by 1.96.

This allows us to work with standard deviations all the time and to, at the end, multiply with the coverage factor of  $k = 1.96$ .

$$U_{95\%}(x) = 1.96 \sqrt{\left(c_{x1} \frac{U(x_1)}{1.96}\right)^2 + \left(c_{x2} \frac{U(x_2)}{1.96}\right)^2 + \dots} \quad [ 6.27 ]$$

### 6.2.7 Uncorrected bias

Although it is recommended (and strongly preferred) practice of correcting for all known bias effects, in view of backwards compatibility of test results for example, an increased uncertainty interval may be the preferred option.

Unfortunately, the GUM does not deal directly with the situation where a known measurement bias is present but is uncorrected.

Several proposed methods of treating uncorrected bias are available. We propose to follow the guidelines of Phillips et al<sup>[55]</sup> because of its conservative approach. This method algebraically sums the signed bias  $\delta$  with the expanded uncertainty, unless the bias is larger:

$$Y = y_{-U^-}^{+U^+} \quad [ 6.28 ]$$

where

$$U^+ = \begin{cases} ku_c - \delta & \text{if } ku_c - \delta > 0 \\ 0 & \text{if } ku_c - \delta \leq 0 \end{cases} \quad [ 6.29 ]$$

and

$$U^- = \begin{cases} ku_c + \delta & \text{if } ku_c + \delta > 0 \\ 0 & \text{if } ku_c + \delta \leq 0 \end{cases} \quad [ 6.30 ]$$

Note that the expanded uncertainty must be re-computed if the coverage factor is changed, and in particular, that  $U_{\pm}(k=2) \neq 2 \cdot U_{\pm}(k=1)$ .

The combined standard uncertainty  $u_c$  is calculated out of the standard uncertainty associated with the bias  $u_b$  and the standard uncertainty  $u$  that accounts for the combination of all other uncertainty sources not directly associated with the bias.

$$u_c = (u^2 + u_b^2)^{1/2} \quad [ 6.31 ]$$

The proposed approach can somewhat overestimate the uncertainty. In the case of a coverage factor  $k=2$ , the method maintains the 95% confidence interval until the ratio of the bias to the combined standard uncertainty becomes larger than the coverage factor. For such large bias values, the method produces uncertainty intervals that are slightly conservative.

Note that the sign of the sensitivity coefficient is important to know the effect on the global uncertainty. As an example, suppose  $x_1$  and  $x_2$  both have uncorrected bias and the expanded uncertainty is given by

$$x_{1-U^{1+}} \quad [ 6.32 ]$$

$$x_{2-U^{2+}} \quad [ 6.33 ]$$

The uncertainty interval on  $x$  defined as

$$x = \frac{x_1}{x_2} \quad [ 6.34 ]$$

then becomes

$$\frac{u(x)}{x} = \begin{cases} + \sqrt{\left(\frac{U^{1+}}{x_1}\right)^2 + \left(\frac{U^{2-}}{x_2}\right)^2} \\ - \sqrt{\left(\frac{U^{1-}}{x_1}\right)^2 + \left(\frac{U^{2+}}{x_2}\right)^2} \end{cases} \quad [ 6.35 ]$$

assuming  $x_1 \neq 0$  and  $x_2 \neq 0$ .

An underestimation of  $x_1$  leads to an underestimation of  $x$ , while an underestimation of  $x_2$  leads to an overestimation of  $x$ .

## 6.3. Combined standard uncertainties

### 6.3.1 Combined standard uncertainty on sums

Since the discussion on the uncertainty of a data acquisition system often requires the standard uncertainty on the sum of  $N$  independent variables/measurements, a short review is given below.

Assume the sum

$$y = a \sum_i^N x_i \quad [ 6.36 ]$$

Taking the partial derivative to the different components  $x_i$  results in the corresponding sensitivity coefficients  $c_i = a$ .

The standard uncertainty of  $y$  is obtained by appropriately combining the standard uncertainties of the input estimates  $x_i$ . This combined standard uncertainty  $u_c(y)$  is the positive square root of the combined variance  $u^2_c(y)$  and is given by

$$u_c(y) = \sqrt{\sum_{i=1}^N [c_i u(x_i)]^2} = a \sqrt{\sum_{i=1}^N u^2(x_i)} \quad [ 6.37 ]$$

Note that for correlated measurements this is no longer true as will be discussed in the next section.

### 6.3.2 Combined standard uncertainty on averages

If  $x_i$  is a repetitive independent measurement of a measurand  $X$ , the uncertainty on the average is given by

$$u_c(x) = \frac{\sqrt{\sum_{i=1}^N u^2(x_i)}}{N} = \frac{\sqrt{N u^2(x_i)}}{N} = \frac{u(x_i)}{\sqrt{N}} \quad [ 6.38 ]$$

If however the uncertainty of a component is related to an effect with periodicity exceeding the weighing interval ( $t_N - t_1 \ll T_{\text{effect}}$ ), the uncertainty on the average is more likely to be

$$u_c(x) = \overline{u(x_i)} \quad [6.39]$$

One could say that the measurement results are highly correlated ( $r = 1$ ) such that formula 6.24 becomes ( $c_i = 1/N$ )

$$u_c = \sqrt{\sum_{i=1}^N [c_i u(x_i)]^2 + 2 \sum_{i=1}^{N-1} \sum_{j=i+1}^N c_i c_j u(x_i) u(x_j)} = \frac{\sum_{i=1}^N u(x_i)}{N} = \overline{u(x_i)} \quad [6.40]$$

When for example calculating the 30 second running average of the heat release rate (formula 2.9) this should be kept in mind. The running average will reduce the uncertainty associated with noise, but will not for example eliminate the uncertainty related to daily cycle temperature variations.

The following graph may illustrate this by way of example. Suppose a cyclic phenomenon with periodicity  $t_s = 360$  s introduces an uncertainty of 500 ppm. Noise on the signal introduces an uncertainty estimated at 100 ppm.

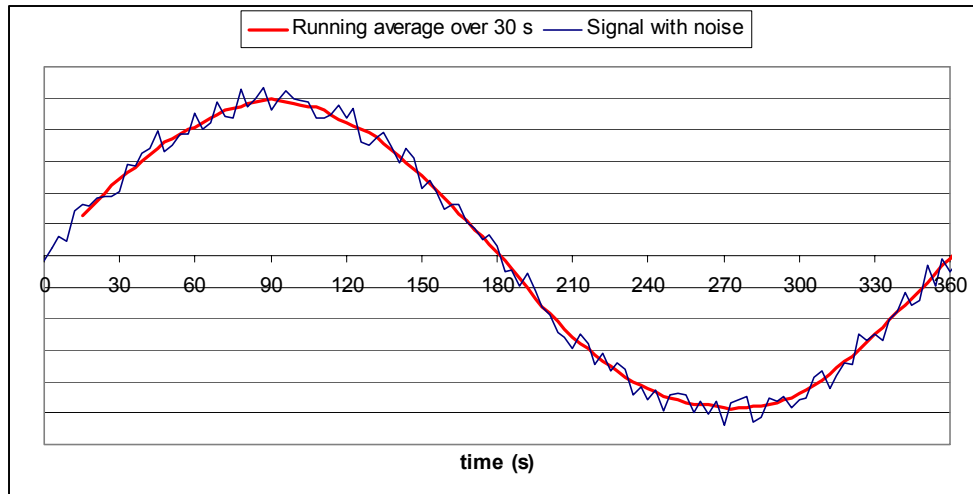


Table 11. Effect of averaging on uncertainty (function of periodicity)

From this example it is clear that the running average over 10 samples (30 s) may reduce the uncertainty associated with noise with a factor  $\sqrt{10}$ , but does not affect the uncertainty related to longer term variations ( $t_s \gg 30$  s).



A similar statement is true for the calculation of the total heat release in the first ten minutes of a test (600 s). Suppose the measurements are perfectly correlated ( $r = 1$ ) the uncertainty on the sum becomes ( $c_i = 1$ ):

$$u_c = \sqrt{\sum_{i=1}^N [c_i u(x_i)]^2 + 2 \sum_{i=1}^{N-1} \sum_{j=i+1}^N c_i c_j u(x_i) u(x_j)} = \sum_{i=1}^N u(x_i) \quad [6.41]$$

which is higher than formula 6.33. In this case, events with a periodicity of approximately ten minutes or less will be dampened out while events with a longer periodicity will not be dampened out ( $r$  goes to 1).

For parameters like MARHE, which is also based on total heat release, the behaviour with respect to uncertainty will depend upon the integration time which is variable.

On the other hand however, uncertainties related to very slow processes ( $\tau > 10$  times test run) hardly contribute to the uncertainty on the oxygen depletion since it is a relative measurement, i.e. the actual status is compared with the initial status at the start of the test.

The proposal therefore is to consider measurements as being independent, include the uncertainty related to slow processes ( $\tau > 10$  times test run) in the *zero calibration* (= daily calibration of zero points), include the uncertainty related to drift over one test run in the uncertainty related to the actual measurement point.

### 6.3.3 Combined standard uncertainty of a product and a division

Throughout the work, often the uncertainty has to be calculated for a product and for a division.

Starting from the general form

$$y = ax_1 x_2 \quad [6.42]$$

The partial derivative to the variables  $x_1$  and  $x_2$  is given by

$$\frac{\partial y}{\partial x_1} = ax_2 = \frac{y}{x_1} \quad (\text{if } x_1 \neq 0) \quad [6.43]$$

$$\frac{\partial y}{\partial x_2} = ax_1 = \frac{y}{x_2} \quad (\text{if } x_2 \neq 0) \quad [ 6.44 ]$$

Thus the combined standard uncertainty on y is estimated out of

$$\frac{u(y)}{y} = \sqrt{\left(\frac{u(x_1)}{x_1}\right)^2 + \left(\frac{u(x_2)}{x_2}\right)^2} \quad (\text{if } x_1 \neq 0 \text{ and } x_2 \neq 0) \quad [ 6.45 ]$$

This formula holds for a division. Indeed, taking the partial derivatives of the general form

$$y = a \frac{x_1}{x_2} \quad [ 6.46 ]$$

$$\frac{\partial y}{\partial x_1} = \frac{a}{x_2} = \frac{y}{x_1} \quad (\text{if } x_1 \neq 0) \quad [ 6.47 ]$$

$$\frac{\partial y}{\partial x_2} = -\frac{ax_1}{x_2^2} = -\frac{y}{x_2} \quad (\text{if } x_2 \neq 0) \quad [ 6.48 ]$$

Note: The statement (if  $x_i \neq 0$ ) will be omitted from now on if it can reasonably be assumed that  $x_i$  will always fulfil this requirement in a practical sense.

### 6.3.4 Combined standard uncertainty on the heat release rate (Q)

The heat release rate ( $Q = \text{HRR}_{\text{total}}$ ) is given by (Formula 2.1)

$$\underline{Q} = \frac{\phi}{\{1 + (\alpha - 1)\phi\}} E' X_{O_2}^{D^\circ} \dot{V}_{D298} \quad [6.49]$$

Substituting the volume flow  $\dot{V}_{D298}$  (§6.3.7) this becomes

$$\underline{Q} = \frac{\phi}{\{1 + (\alpha - 1)\phi\}} E' X_{O_2}^{D^\circ} c_A \frac{k_t}{k_p} \sqrt{\frac{\Delta p(t)}{T_{\text{ms}}(t)}} \quad [6.50]$$

Taking the partial derivative of  $\underline{Q}$  to the different components  $x_i$  results in the corresponding sensitivity coefficients  $c_i$ :

$$c_\phi^Q \equiv \frac{\partial \underline{Q}}{\partial \phi} = \frac{E' X_{O_2}^{D^\circ} \dot{V}_{D298} - (\alpha - 1)\underline{Q}}{[1 + (\alpha - 1)\phi]} \quad [6.51]$$

$$c_{X_{O_2}^A}^Q = c_\phi^Q c_{X_{O_2}^A}^\phi \quad \text{see also 6.3.5} \quad [6.52]$$

$$c_{X_{CO_2}^A}^Q = c_\phi^Q c_{X_{CO_2}^A}^\phi \quad \text{see also 6.3.5} \quad [6.53]$$

$$c_{E'}^Q \equiv \frac{\partial \underline{Q}}{\partial E'} = \frac{\underline{Q}}{E'} \quad [6.54]$$

$$c_\alpha^Q \equiv \frac{\partial \underline{Q}}{\partial \alpha} = \underline{Q} \left[ \frac{-\phi}{1 + (\alpha - 1)\phi} \right] \quad [6.55]$$

$$c_{X_{O_2}^{D^\circ}}^Q \equiv \frac{\partial \underline{Q}}{\partial X_{O_2}^{D^\circ}} = \frac{\underline{Q}}{X_{O_2}^{D^\circ}} \quad [6.56]$$

$$c_{\dot{V}_D}^Q \equiv \frac{\partial \underline{Q}}{\partial \dot{V}_D} = \frac{\underline{Q}}{\dot{V}_D} \quad [6.57]$$

$$c_c^Q = c_{\dot{V}_D}^Q c_c^{V_D} \quad \text{see also 6.3.7} \quad [6.58]$$

$$c_A^Q = c_{V_D}^Q c_A^{V_D} \quad \text{see also 6.3.7} \quad [6.59]$$

$$c_{k_t}^Q = c_{V_D}^Q c_{k_t}^{V_D} \quad \text{see also 6.3.7} \quad [6.60]$$

$$c_{k_p}^Q = c_{V_D}^Q c_{k_p}^{V_D} \quad \text{see also 6.3.7} \quad [6.61]$$

$$c_{\Delta p}^Q = c_{V_D}^Q c_{\Delta p}^{V_D} \quad \text{see also 6.3.7} \quad [6.62]$$

$$c_{T_{ms}}^Q = c_{V_D}^Q c_{T_{ms}}^{V_D} \quad \text{see also 6.3.7} \quad [6.63]$$

$$c_{XO_2^A}^Q = c_\phi^Q c_{XO_2^A}^\phi + c_{XO_2^D}^Q c_{XO_2^A}^{XO_2^D} \quad \text{see also 6.3.5 and 6.3.6} \quad [6.64]$$

$$c_{XCO_2^A}^Q = c_\phi^Q c_{XCO_2^A}^\phi \quad \text{see also 6.3.5} \quad [6.65]$$

and to the combined standard uncertainty

$$u(\dot{Q}) = \left[ \begin{aligned} & \left( c_{XO_2^A}^Q u(XO_2^A) \right)^2 + \left( c_{XCO_2^A}^Q u(XCO_2^A) \right)^2 + \left( c_E^Q u(E) \right)^2 + \left( c_\alpha^Q u(\alpha) \right)^2 \\ & + \left( c_{XO_2^D}^Q u(XO_2^D) \right)^2 + \left( c_c^Q u(c) \right)^2 + \left( c_A^Q u(A) \right)^2 + \left( c_{k_t}^Q u(k_t) \right)^2 \\ & + \left( c_{k_p}^Q u(k_p) \right)^2 + \left( c_{\Delta p}^Q u(\Delta p) \right)^2 + \left( c_{T_{ms}}^Q u(T_{ms}) \right)^2 \\ & + \left( c_{XO_2^A}^Q u(XO_2^A) \right)^2 + \left( c_{XCO_2^A}^Q u(XCO_2^A) \right)^2 \\ & + 2c_{XO_2^A}^Q c_{XCO_2^A}^Q u(XO_2^A) u(XCO_2^A) r(XO_2^A, XCO_2^A) \\ & + 2c_{XO_2^A}^Q c_{T_{ms}}^Q u(XO_2^A) u(T_{ms}) r(XO_2^A, T_{ms}) \\ & + 2c_{XO_2^A}^Q c_{\Delta p}^Q u(XO_2^A) u(\Delta p) r(XO_2^A, \Delta p) \\ & + 2c_{XCO_2^A}^Q c_{T_{ms}}^Q u(XCO_2^A) u(T_{ms}) r(XCO_2^A, T_{ms}) \\ & + 2c_{XCO_2^A}^Q c_{\Delta p}^Q u(XCO_2^A) u(\Delta p) r(XCO_2^A, \Delta p) \\ & + 2c_{T_{ms}}^Q c_{\Delta p}^Q u(T_{ms}) u(\Delta p) r(T_{ms}, \Delta p) \end{aligned} \right]^{1/2} \quad [6.66]$$

### 6.3.5 Combined standard uncertainty on the depletion factor ( $\phi$ )

The depletion factor in the exhaust duct is given by

$$\phi = \frac{X_{O_2}^{A^\circ} - X_{O_2}^A \frac{1 - X_{CO_2}^{A^\circ}}{(1 - X_{CO_2}^A)}}{X_{O_2}^{A^\circ} \left( 1 - \frac{X_{O_2}^A}{(1 - X_{CO_2}^A)} \right)} \quad [ 6.67 ]$$

Taking the partial derivative to the different components  $x_i$  results in the corresponding sensitivity coefficients  $c_i$ :

$$c_{X_{O_2}^A}^\phi \equiv \frac{\partial \phi}{\partial X_{O_2}^A} = \frac{1}{(1 - X_{CO_2}^A - X_{O_2}^A)} \left[ \phi + \frac{(X_{CO_2}^{A^\circ} - 1)}{X_{O_2}^{A^\circ}} \right] \quad [ 6.68 ]$$

$$c_{X_{CO_2}^A}^\phi \equiv \frac{\partial \phi}{\partial X_{CO_2}^A} = \frac{\phi - 1}{(1 - X_{CO_2}^A - X_{O_2}^A)} \quad [ 6.69 ]$$

$$c_{X_{O_2}^{A^\circ}}^\phi \equiv \frac{\partial \phi}{\partial X_{O_2}^{A^\circ}} = \frac{(1 - X_{CO_2}^A) - (1 - X_{CO_2}^A - X_{O_2}^A)\phi}{(1 - X_{CO_2}^A - X_{O_2}^A)X_{O_2}^{A^\circ}} \quad [ 6.70 ]$$

$$c_{X_{CO_2}^{A^\circ}}^\phi \equiv \frac{\partial \phi}{\partial X_{CO_2}^{A^\circ}} = \frac{X_{O_2}^A}{(1 - X_{CO_2}^A - X_{O_2}^A)X_{O_2}^{A^\circ}} \quad [ 6.71 ]$$

### 6.3.6 Combined standard uncertainty on the initial O<sub>2</sub>-concentration (X<sup>D°</sup><sub>O<sub>2</sub></sub>)

The initial concentration of oxygen in the exhaust duct is function of the relative humidity, temperature and absolute pressure and is given by

$$X_{O_2}^{D^\circ} = X_{O_2}^{A^\circ} \left[ 1 - \frac{\varphi}{100p} \exp \left\{ 23,2 - \frac{3816}{T_{room} - 46} \right\} \right] \quad [ 6.72 ]$$

Taking the partial derivative to the different components x<sub>i</sub> results in the corresponding sensitivity coefficients c<sub>i</sub>:

$$c_{X_{O_2}^{A^\circ}}^{X_{O_2}^{D^\circ}} \equiv \frac{\partial X_{O_2}^{D^\circ}}{\partial X_{O_2}^{A^\circ}} = \frac{X_{O_2}^{D^\circ}}{X_{O_2}^{A^\circ}} \quad [ 6.73 ]$$

$$c_{\varphi}^{X_{O_2}^{D^\circ}} \equiv \frac{\partial X_{O_2}^{D^\circ}}{\partial \varphi} = \frac{1}{\varphi} (X_{O_2}^{D^\circ} - X_{O_2}^{A^\circ}) \quad [ 6.74 ]$$

$$c_p^{X_{O_2}^{D^\circ}} \equiv \frac{\partial X_{O_2}^{D^\circ}}{\partial p} = -\frac{1}{p} (X_{O_2}^{D^\circ} - X_{O_2}^{A^\circ}) \quad [ 6.75 ]$$

$$c_{T_{room}}^{X_{O_2}^{D^\circ}} \equiv \frac{\partial X_{O_2}^{D^\circ}}{\partial T_{room}} = \left( \frac{3816}{(T_{room} - 46)^2} \right) (X_{O_2}^{D^\circ} - X_{O_2}^{A^\circ}) \quad [ 6.76 ]$$

and to the combined standard uncertainty

$$u(X_{O_2}^{D^\circ}) = \sqrt{\left( c_{X_{O_2}^{A^\circ}}^{X_{O_2}^{D^\circ}} u(X_{O_2}^{A^\circ}) \right)^2 + \left( c_{\varphi}^{X_{O_2}^{D^\circ}} u(\varphi) \right)^2 + \left( c_p^{X_{O_2}^{D^\circ}} u(p) \right)^2 + \left( c_{T_{room}}^{X_{O_2}^{D^\circ}} u(T_{room}) \right)^2} \quad [ 6.77 ]$$

### 6.3.7 Combined standard uncertainty on the volume flow rate ( $V_{D298}$ )

The volume flow rate – referenced to 298K – in the exhaust duct is given by

$$V_{D298}(t) = cA \frac{k_t}{k_p} \sqrt{\frac{\Delta p(t)}{T_{ms}(t)}} \quad [ 2.2 ]$$

Taking the partial derivative to the different components  $x_i$  results in the corresponding sensitivity coefficients  $c_i$ :

$$c_c^{V_D} \equiv \frac{\partial \dot{V}_{D298}}{\partial c} = \frac{\dot{V}_{D298}}{c} \quad [ 6.78 ]$$

$$c_A^{V_D} \equiv \frac{\partial \dot{V}_{D298}}{\partial A} = \frac{\dot{V}_{D298}}{A} \quad [ 6.79 ]$$

$$c_{k_t}^{V_D} \equiv \frac{\partial \dot{V}_{D298}}{\partial k_t} = \frac{\dot{V}_{D298}}{k_t} \quad [ 6.80 ]$$

$$c_{k_p}^{V_D} \equiv \frac{\partial \dot{V}_{D298}}{\partial k_p} = -\frac{\dot{V}_{D298}}{k_p} \quad [ 6.81 ]$$

$$c_{\Delta p}^{V_D} \equiv \frac{\partial \dot{V}_{D298}}{\partial \Delta p} = \frac{1}{2} \frac{\dot{V}_{D298}}{\Delta p} \quad [ 6.82 ]$$

$$c_{T_{ms}}^{V_D} \equiv \frac{\partial \dot{V}_{D298}}{\partial T_{ms}} = -\frac{1}{2} \frac{\dot{V}_{D298}}{T_{ms}} \quad [ 6.83 ]$$

### 6.3.8 Combined standard uncertainty on the air density ( $\rho_{air}$ )

The molecular weight of air is significantly affected by the presence of water vapour. Jones<sup>[34]</sup> gives an extensive development and comes to the equation below for density of air as a function of temperature (K), pressure (Pa) and relative humidity ( $\varphi$ ):

$$\rho_{air} = \left( \frac{0.0034847}{T} \right) \left[ p - 0.003796 * 1.7526^{E+11} \varphi \exp\left( \frac{-5315,56}{T} \right) \right] \quad [ 6.84 ]$$

Taking the partial derivative to the different components  $x_i$  results in the corresponding sensitivity coefficients  $c_i$ :

$$c_T^{\rho_{air}} \equiv \frac{\partial \rho_{air}}{\partial T} = \frac{1}{T^3} \left[ -0.0034847 * p * 5315,56 + \rho_{air} T (5315,56 - T) \right] \quad [ 6.85 ]$$

$$c_p^{\rho_{air}} \equiv \frac{\partial \rho_{air}}{\partial p} = \frac{0.0034847}{T} \quad [ 6.86 ]$$

$$c_\varphi^{\rho_{air}} \equiv \frac{\partial \rho_{air}}{\partial \varphi} = -\frac{0.0034847}{T} 0.003796 * 1.7526^{E+11} \exp\left( \frac{-5315,56}{T} \right) \quad [ 6.87 ]$$

and to the combined standard uncertainty

$$u(\rho_{air}) = \sqrt{\left( c_T^{\rho_{air}} u(\rho_{air}) \right)^2 + \left( c_p^{\rho_{air}} u(p) \right)^2 + \left( c_\varphi^{\rho_{air}} u(\varphi) \right)^2} \quad [ 6.88 ]$$



### 6.3.9 Combined standard uncertainty on specimen heat release rate ( $\dot{Q}_{\text{specimen}}$ )

The specimen heat release rate is defined as the global heat release rate minus the heat release rate contribution of the burner (see 2.2.3.1). The contribution of the burner is calculated as the mean heat release rate measured in the time interval 210 – 270 s.

The uncertainty contribution of the burner is given by

$$u(\dot{Q}_{\text{burner}}) = \frac{1}{21} \sqrt{\sum_{i=210\text{s}}^{270\text{s}} [u(\dot{Q}(t_i))]^2} \quad [ 6.89 ]$$

and of the specimen heat release rate by

$$u(\dot{Q}_{\text{specimen}}) = \sqrt{u(\dot{Q}_{\text{burner}})^2 + u(\dot{Q}_{\text{total}})^2} . \quad [ 6.90 ]$$

Despite the relatively short time interval (60 s; 21 measurements @  $f_s = 1/3$  s) to calculate the burner contribution, all 21 measurements will be considered independent from each other ( $r = 0$ ) as discussed in 6.3.2.

### 6.3.10 Combined standard uncertainty on the average heat release rate ( $\dot{Q}_{\text{av}}$ )

The average heat release rate is based on a running average over 30 s of the specimen heat release rate contribution.

Although this filtering dampens out higher frequency events such as noise, thus removing the uncertainty contribution of noise, one could argue that it hardly changes anything to the global uncertainty so that  $u(\dot{Q}_{\text{av}}) \cong u(\dot{Q}_{\text{specimen}})$ .

As discussed in paragraph 6.3.2 however we will further assume the measurements to calculate this running average as independent. This is confirmed by the SBI RR2 results as will be discussed in chapter 6.

### 6.3.11 Combined standard uncertainty on FIGRA

The combined standard uncertainty on FIGRA is composed of the uncertainty related to the average heat release rate  $u(Q_{av})$  and the uncertainty related to the time elapsed for reaching this heat release rate level  $u(t)$ . Since the value  $Q_{av}(t)$  could be reached anywhere in the interval  $[t - t_s/2 ; t + t_s/2]$ , the uncertainty distribution on 't' will be assumed rectangular with a resulting standard uncertainty

$$u(t) = \frac{t_s}{2\sqrt{3}} = \frac{\sqrt{3}}{2} \quad [6.91]$$

The uncertainty on FIGRA now becomes

$$u(FIGRA) = \frac{1}{t - 300} \sqrt{(1000 \cdot u(Q_{av}))^2 + (FIGRA \cdot u(t))^2} \quad [6.92]$$

### 6.3.12 Combined standard uncertainty on THR600s

The combined standard uncertainty on the total heat release in the first 600 s of the test will be estimated out of:

$$u(\text{THR}_{600s}) = \frac{3}{1000} \sqrt{\sum_{300s}^{900s} (u(Q_{specimen}))^2} \quad [6.93]$$

The assumption is that this time interval includes enough variation to justify the assumption of independent measurements.

### 6.3.13 Combined standard uncertainty on MARHE

The combined standard uncertainty on the Maximum Average Rate of Heat Emission (MARHE) of the test will be estimated out of:

$$u(\text{MAHRE}) = \frac{1}{n} \sqrt{\sum_{i=0}^n (u(Q_{specimen}(t_i)))^2 - \left(\frac{1}{2} u(Q_{specimen}(t_n))\right)^2} \quad [6.94]$$

The assumption is that this time interval includes enough variation to justify the assumption of independent measurements.

## 6.4. Standard uncertainty on the different components

### 6.4.1 Uncertainty on the Data Acquisition (DAQ)

Not only the measuring sensors contribute to the overall uncertainty, also the DAQ system introduces an uncertainty.

Two different types of data acquisition systems are currently used in reaction to fire applications at the Ghent University, Siemens Simatic S7 PLC and Keithley 2000 DMM. The Keithley digital multimeter has been used on the SBI device from its introduction in 1997 till 2001, while the PLC has been used from 2001 on since it allowed automation of the test method. The calculations in chapter 6 are based on the PLC data acquisition system which, in terms of uncertainty contribution, is less favourable.

#### a) Siemens Simatic S7 PLC

The system SIMATIC S7-300 is a modular automation system that builds around a central processing unit. The modules include, but are not limited to, digital input and output modules and analogue input and output modules. Depending on the module, the analogue signals can handle different types of signals (volt, mAmps, ...) in different resolutions.

The processor units used in our department are either model 'CPU 314 IFM' or model 'CPU 313c'. The analogue I/O-cards used have the following specifications<sup>[75]</sup>:

I/O card	Specification manufacturer		'error' (%)
6ES7 331-7SF00-0AB0 for <i>temperature</i> and <i>resistance</i> measurements	Resolution	15-bit	0.003 1
	'error' at 25°C	±0.1% of MR	0.1
	additional 'error' in range 0-60°C	±0.09% of MR	0.09
6ES7 331-7NF00-0AB0 for <i>volt</i> measurements	Resolution	15-bit	0.003 1
	'error' at 25°C	±0.05% of MR	0.05
	'error' in range 0-60°C	±0.1% of MR	0.1
6ES7 331-7NF00-0AB0 for <i>current</i> measurements	Resolution	15-bit	0.003 1
	'error' at 25°C	±0.05% of MR	0.05
	'error' in range 0-60°C	±0.3% of MR	0.3

Table 12. PLC analogue I/O card specifications

Assuming that:

- the Measuring Range (MR) for a K-type thermocouple is approximately 1300K (-50°C/+1250°C)
- ‘error’ stands for an interval within which the result may be confidently supposed to lie at any time
- the distribution is Rectangular
- ‘errors’ are independent from each other
- the PLC works in the range 0-60°C,

and knowing that:

- the MR for a RTD (Pt-100) measurement is 150Ω
- the MR for a Volt measurement is 10V
- the MR for a Current measurement is 16mA (4 to 20mA),

the estimated standard uncertainties associated with the PLC system are (Table 13)

Measurand	‘error’ (%)	probability distribution	standard uncertainty (%)	standard uncertainty
Temperature by means of T/C	0.135	rectangular	0.078	1.0 K
Temperature by means of RTD (Pt-100)	0.135	rectangular	0.078	0.117 Ω 0.3 K
Volt	0.10	rectangular	0.058	5.8 mV
Current	0.30	rectangular	0.173	0.028mA

Table 13. Estimated standard uncertainties associated with the PLC system

Remark: According to the specifications the maximum length allowed of the thermocouple cable is 200m of shielded cable and 50m for RTD. It is therefore further assumed that any voltage differences between the compensation leads (9 m) and the thermocouples has been included in the specifications.

#### b) Keithley 2000 DMM

The Keithley Model 2000 is a 6<sup>1/2</sup>-digits high performance digital multimeter that can cope with a large variety of input signals in broad measurement ranges (MR).

According to the manufacturer's specifications<sup>[73]</sup> the following applies, where FS stands for Full Scale:

Measurement Range	conditions	reading + FS (ppm $\equiv$ 0.000 1%)	Resolution
0 – 100 mV	1 year; 23°C $\pm$ 5	$\pm(50 + 35)$	0.1 $\mu$ V
	1 year; 0-50°C	$\pm(52 + 41)$	0.1 $\mu$ V
0 – 10 V	1 year; 23°C $\pm$ 5	$\pm(30 + 5)$	1.0 $\mu$ V
	1 year; 0-50°C	$\pm(32 + 6)$	1.0 $\mu$ V
0 – 1 000 $\Omega$	1 year; 23°C $\pm$ 5	$\pm(100 + 10)$	1 m $\Omega$
	1 year; 0-50°C	$\pm(108 + 11)$	1 m $\Omega$

Table 14. Keithley DMM specifications

Assuming that:

- the distribution is Rectangular
- errors are independent from each other
- the instrument works in the range 0-50°C
- the voltage differences between the compensation lead & connectors and the thermocouple wires are less than 5 $\mu$ V
- the temperature differences between the RTD and the contacts in the isothermal box remain limited to  $\pm 0.2$ K,

and knowing that:

- the MR for a RTD (Pt-100) measurement is 150 $\Omega$
- the MR for a Volt measurement is 10V
- the MR for a Temperature measurement is 100 mV
- the voltage measured over a K-type thermocouple with its hot junction at 300°C and with a reference temperature of 0°C is 12.207 mV<sup>[17]</sup>,

the estimated standard uncertainties associated with the Keithley system are given by Table 15. The standard uncertainty related to a temperature measurement by means of a thermocouple (T/C) reduces to less than 0.2K.

Measurand	'error'	probability distribution	standard uncertainty	standard uncertainty
Temp. by means of T/C ( $\Delta T \cong 0$ K)	41 ppm 0.004 1 mV	rectangular	24 ppm 0.002 4 mV	0.062 K
Temp. by means of T/C ( $\Delta T \cong 300$ K)	0.004 735 mV	rectangular	0.002 73 mV	0.070 K
Temperature by means of RTD (Pt-100) ( $R \cong 110 \Omega$ )	0.022 9 $\Omega$	rectangular	0.013 2 $\Omega$	0.034 K
Compensation leads +connectors (0-40°C)	0.005 mV	rectangular	0.0029 mV	0.074 K
Isothermal box	0.2 K	rectangular	0.12 K	0.12 K
Absolute temperature by means of T/C + RTD + cables + box ( $\Delta T \cong 300$ K)				0.16 K
Volt (0 – 10 V) ( $V = 10$ V)	0.000 38 V	rectangular	0.000 22 V	0.22 mV

Table 15. Estimated standard uncertainties associated with the Keithley system

#### 6.4.2 Transient error

Due to the response times of the gas analysis system, the thermocouples and the differential pressure system, which are – or at least can be approximated by – first order systems (see 5.2.2) with time constant  $\tau$ , an error  $e(t)$  for each component is introduced equal to (see B.11)

$$e(t) = \tau \frac{dy(t)}{dt}. \quad [ 6.95 ]$$

whereby  $y(t)$  is the measured output.

There are three different ways to deal with this error. One is to estimate the error and to correct for it. A second option is not to correct for the transient error, but instead increase the uncertainty interval. A

third option is to reduce the bandwidth (reduce highest frequency of interest) considering not relevant fast events.

#### 6.4.2.1 Estimate error and correct for it

##### a) Use data as is

An estimate of this bias can be obtained by means of for example a *central difference discretisation* scheme

$$e(t) = \tau \frac{y^{i+1} - y^{i-1}}{2\Delta t} \quad [ 6.96 ]$$

This finite difference representation of the first order derivative, which is based on Taylor's series expansion, has an associated *truncation error* because higher order terms are neglected. The truncation error of the lowest order term for this central difference scheme is  $O(\Delta x) = \frac{1}{6}(\Delta t)^2 y'''$  [37]. This error is proportional to the squared scan interval and gives a first indication of the necessity to increase the scan rate.

Intuitively it can easily be understood that the estimated error is very sensitive to noise on the measurement  $y(t)$ . Due to noise, the forward, backward, central or higher order discretisation formulas will lead to substantially different results. This problem, which is inherent to inverse filters as discussed in 5.5, can be made less relevant by removing higher frequencies from the measured data.

This brings us back to the large scan interval of  $\Delta t = 3$  s which will only allow us to reconstruct, and eliminate if desired, signals with a periodicity of 6 s and higher ( $f = 0.1667$  Hz). Any signal with a frequency between  $f = 0.1667$  Hz (1/6 s) and the cutoff frequency of the DAQ ( $f = 22$  Hz) or the measuring device (see 5.2), whichever is the lowest, will give rise to aliasing. Aliasing introduces, as explained in §6.4.3, phantom data; things are seen that are not there!

A good remedy to this problem are the so called *level two changes* as discussed in 5.4.2.

The standard uncertainty related to formula 6.24 is given by

$$u(e) = \sqrt{2\left(\frac{\tau \cdot u(y)}{2\Delta t}\right)^2 + \left(\frac{e \cdot u(\tau)}{\tau}\right)^2} \quad [ 6.97 ]$$

As an estimate for the uncertainty  $u(y)$  the noise level on the output signal  $y(t)$  in the period 120 s – 300 s will be taken.

From Figure 52 – that represents the transient error estimate of the oxygen signal for a test on a MDF board (Medium Density Fibre board; Product 2 in the SBI RR2) – we see that the noise level in the first 120 s of the test, this is when no heat is released, is much lower than when the auxiliary burner is ignited (120 s – 300 s). The standard uncertainty on the oxygen concentration from 0 – 120 s is 33 ppm for this specific test, while for the period 120 – 300 s it is 69 ppm.

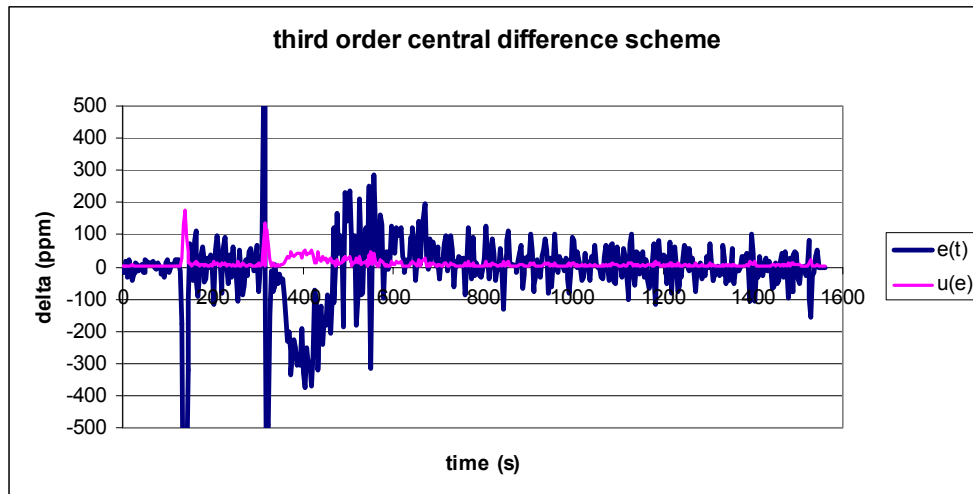


Figure 52. Transient error and standard uncertainty estimate on raw data

The fluctuations in  $e(t)$  are too high to confidently apply the correction in bias to the result. In the next section it is shown how this ‘noise’ can be reduced while still capturing the global trend.



**b) Filter out high frequency events**

By first applying a 11-point Henderson zero phase filter (see 5.3.1) to the measured data (sampled at  $f = 1/3$  Hz), the cutoff frequency lowers to approximately  $f = 1/30$  Hz.

Figure 53 represents the estimated transient error and corresponding standard uncertainty calculated with a central differencing scheme on the filtered data (same data as above). The standard uncertainty  $u(y)$  will be estimated in a different way as above.

For estimation of the standard uncertainty  $u(y)$  a *local variance* on the measurement signal is defined (see 5.3.1) whereby  $z(t)$  represents the filtered data.

$$s_l^2 = \frac{1}{4} \sum_{i=-2}^2 (y_{t+i} - z_{t+i})^2 \quad [ 6.98 ]$$

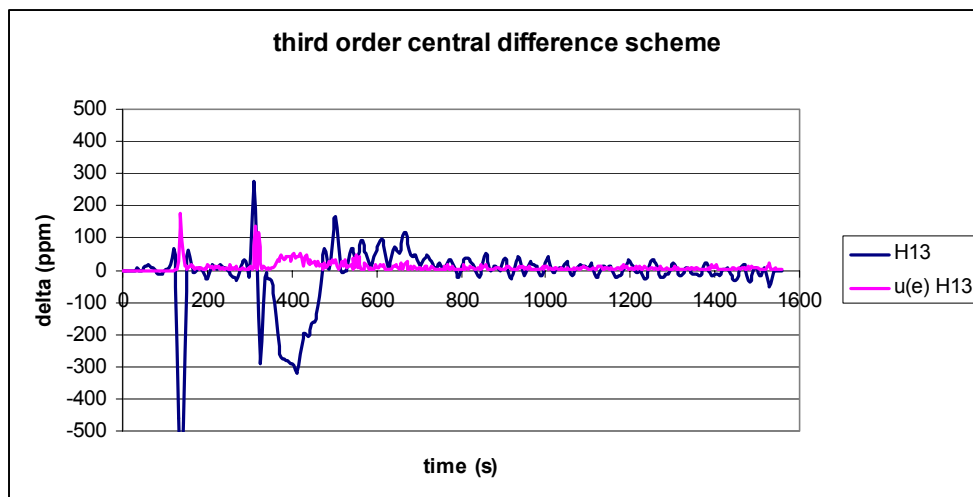


Figure 53. Transient error and standard uncertainty estimate on filtered data

**c) Use fixed values**

The bias may either be estimated as discussed in a) or b), or may be estimated based on a worst case scenario. In this last case, the bias estimate cannot be used to ‘correct’ the data.

The worst case scenario is taken as the steep rise in heat release for a heptane pool fire (SBI heptane calibration; Ghent University; SBI RR2). The thus obtained maximum transient error estimates, and the corresponding ‘standard error’ estimates – assuming a triangular distribution with width equal to the maximum error – are summarised in Table 16.

component	maximum transient error	standard uncertainty estimate
X_O <sub>2</sub>	1260 ppm	514 ppm
X_CO <sub>2</sub>	642 ppm	262 ppm
T <sub>ms</sub>	2.8 K	1.2 K

Table 16. transient error estimate based on heptane pool fire calibration

#### 6.4.2.2 Estimate error and increase uncertainty interval (uncorrected bias)

Instead of correcting the data for the estimated bias, one may prefer to leave the measured data uncorrected and to increase the uncertainty interval.

The bias may be estimated by any of the three methods as discussed in 6.4.2.1.

The uncertainty interval will be widened according to the method as described in section 6.2.7.

#### 6.4.2.3 Reduce bandwidth and neglect any remaining bias

A third option is to consider inherent to a test instrument a bias related to transient phenomena and to further ignore the uncertainty related to it. In order to do so, it is of primary importance that all laboratories have the same BW for their test facility. Section 5.4 gives guidance on how to reach this.

In this dissertation either the uncertainty interval is increased (6.4.2.2) based on a fixed uncertainty estimate (6.4.2.1.c; worst case) or the BW will be reduced neglecting any further remaining bias (6.4.2.3). The latter is the preferred option since it minimises the uncertainty estimate.

### 6.4.3 Aliasing error

One of the fundamental rules of discretisation of signals is that the sampling frequency is at least twice the maximum frequency existing in the signal. If this rule is not respected, the reconstruction of the original analogue signal becomes impossible and spurious information is added to the digitised signal. This spurious information does not exist in the analogue part and is created by the sampling procedure. This effect is called aliasing.

Reconsidering the oscillation of  $f_k = 0.371 \text{ Hz}$  on the signal of the oxygen analyser (see Figure 20), and sampling with a frequency of  $f_s = 1/3 \text{ Hz}$ , an apparent frequency  $f_0$  will be measured whereby

$$f_0 = f_k - f_s \tag{ 6.99 }$$

In this specific case  $f_0 = 0.0377 \text{ Hz}$  ( $T_0 = 26.5 \text{ s}$ ).

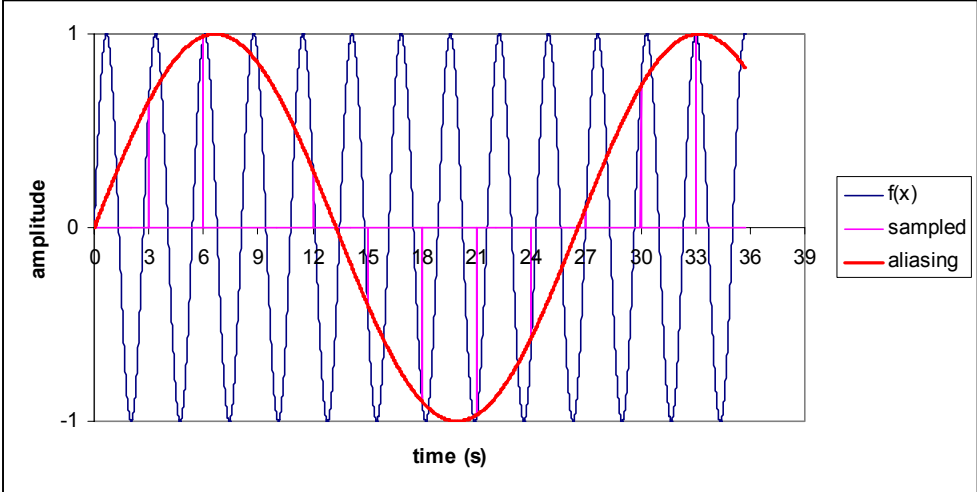


Figure 54. Example of aliasing effect

In general, all sines with frequency  $f_k = f_0 + kf_s$  ( $k = 0, 1, 2, \dots$ ) have the same value at the sampling intervals  $t = nT_s$ .

As a general rule, it is therefore recommended to use an analogue low pass filter to remove all higher frequencies that are of no interest and to set the sampling rate equal to 10 times the bandwidth of the signal to be sampled.

It will further be assumed that all measurement data are free from aliasing.

#### 6.4.4 Uncertainty on data synchronicity

There is also an uncertainty associated with the scan rate and time shifting of the data. In practice, the data acquisition system often incorporates a multiplexing switching module that senses one data channel after the other. For high accuracy measurements, typical integration times, i.e. time required to do the actual measurement, is 1 PLC (Power Line Cycle = 20 ms @ 50 Hz). Adding to this the switching and stabilisation time, the time elapsed between two consecutive measurement channels can easily reach 50 to 100 ms. This is dependent on other factors like the measurement range, whether the display is turned on or off, etc. In the SBI, the strict minimum of channels to be measured is nine, which makes that the time between the sensing of the first and the last channel can easily reach half a second.

Another reason why data may not be synchronised is because of delay times. In general, there is a delay time of several seconds (approximately nine seconds in the lab) in-between a change in heat release rate and the actual change in the measured gas concentration. Shifting of the data with  $n$ -times ( $n = 0, 1, 2, \dots$ ) the sampling interval  $n \cdot \Delta t$  only allows to partially eliminate the delay time.

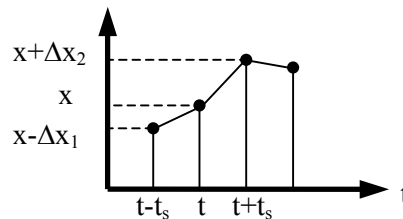


Figure 55. sampled signal at regular intervals

Assuming that the data signal in-between consecutive measurements of a same channel varies linearly and assuming that the non-synchronicity is somewhere in the interval  $\pm t_s/2$ , a rectangular distribution applies with a width  $\Delta x/2$ . The associated standard uncertainty becomes

$$u(\Delta t) = \frac{\Delta x}{2\sqrt{3}} \quad [ 6.100 ]$$

In order to keep symmetry in the uncertainty interval, the variation  $\Delta x$  is set equal to the maximum variation forward ( $\Delta x_2$ ) or backwards ( $\Delta x_1$ ) in time  $\Delta x = \text{MAX}[\Delta x_1, \Delta x_2]$ .

Asynchrony introduces a phase shift which is more important for the higher frequencies. In case of sampling 10 times faster than the highest frequency of interest, the maximum phase shift reduces to  $(2 \cdot \pi / 10) / 2 = 18$  degrees for the highest frequency and drops fast for slower processes.

This, once again, demonstrates clearly the necessity to cutoff all frequencies above the highest frequency of interest  $f_c$  and to sample 10 times faster.

Reducing the sampling interval  $t_s$  reduces the variation  $\Delta x$  and thus the uncertainty.

By way of example, the values used for classification *Figra* and *THR600s* are calculated from 30 different data sets, each representing a test on a same sample. For this occasion, a test was run on a MDF board (product P2, fourth sample, SBI RR2) with the data acquisition running at 10 samples a second (10 Hz). Then the data set was reduced to 30 different data sets by taking every 30th data point starting with element  $i$  ( $i = 1 \dots 30$ ). In this way, it is as if we have thirty different data sets at a scanrate of 1/3 Hz (as required by the standard) from a same test. Ideally all thirty data sets should produce the same result, which clearly they don't.

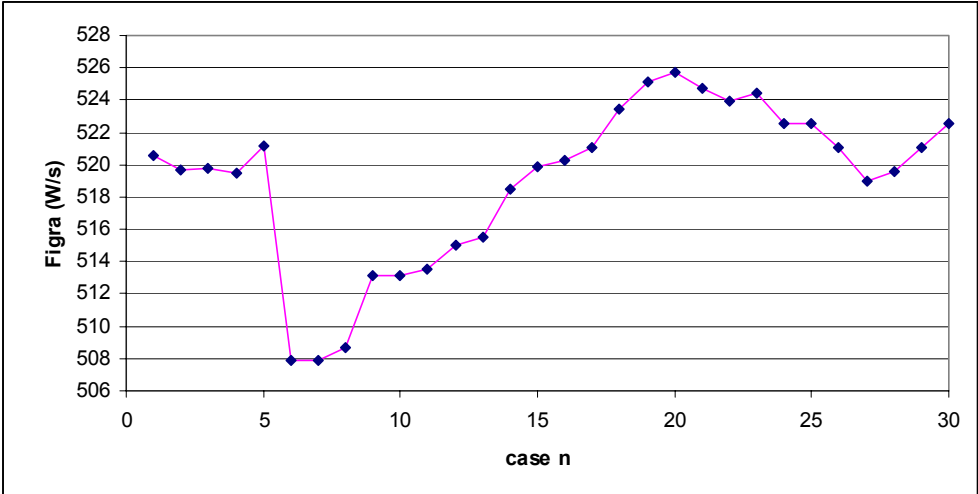


Figure 56. Slow scan rate (1/3 Hz) results in a spread of possible classification results (*FIGRA*)

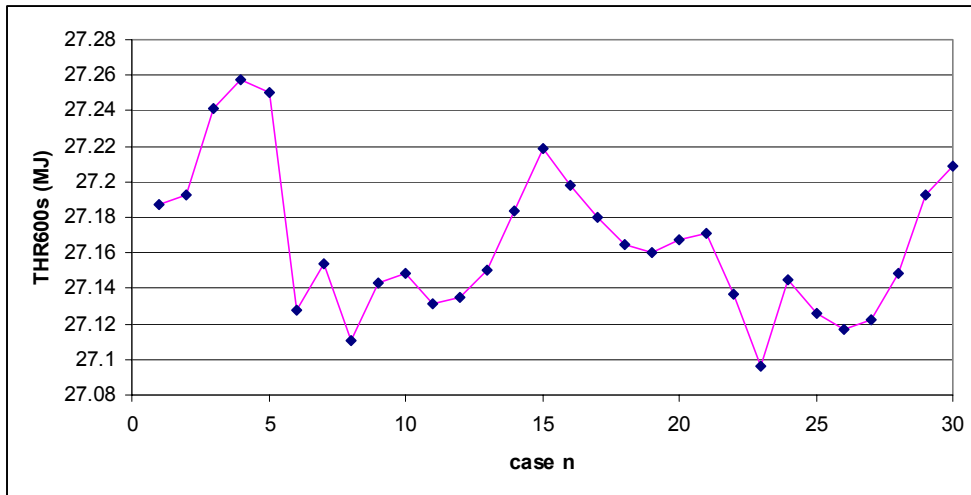


Figure 57. Slow scan rate (1/3 Hz) results in a spread of possible classification results (THR<sub>600s</sub>)

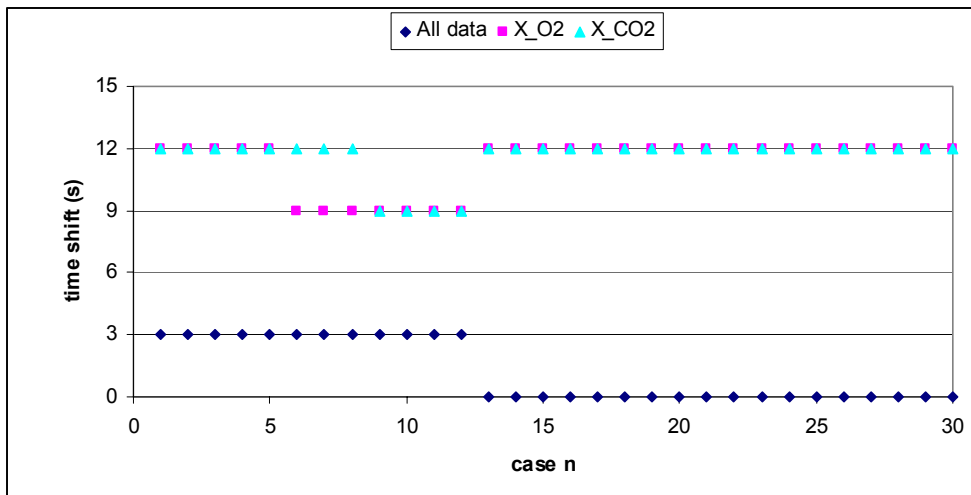


Figure 58. Slow scan rate (1/3 Hz) results in important discontinuities in time shifting

### 6.4.5 Uncertainty on the component E and E'

It has been established by Thornton<sup>[59]</sup> that most organic liquids and gases release a more or less constant net amount of heat per unit mass of oxygen consumed for complete combustion. In 1980 Hugget<sup>[49]</sup> rediscovered this study and showed that this is also true for most plastics and solid materials used in buildings. He concluded that the heat release from fires involving conventional organic fuels is  $E=13.1$  kJ per gram of oxygen consumed, and this with an accuracy of  $\pm 5\%$  or better. He also concluded that incomplete combustion and variation in fuel have only a minor effect on this result.

For the uncertainty analysis distinction is made between the case where the chemical composition of the fuel is known, and the case where it is not known on beforehand what is being burnt.

#### a. Fuel composition is known

For calibration purposes of the test instrument often pure substances are used such as methane, propane, heptane and pmma. The E-factors of those substances can be found in the literature<sup>[26][49][30][39]</sup> to four significant digits.

MJ/kg O <sub>2</sub>	Reference				Annex B.7	
	[26]	[49]	[30]	[39]		u(x)
Propane	12.78	.	12.80	12.9	12.774	0.004*
n-heptane	12.68	.	.	12.7	12.684	0.013*
methane	12.51	12.54	12.54	12.5	12.536**	0.005**
PMMA	12.97		12.98	13.1		
Propene	13.38	.	.	.		
n-butane	12.77	12.78	12.80	12.7		
iso-butane	12.62	.	.	.		
ethane	12.75	12.75	11.21	12.7		
CO	17.69	.	17.69	.		
PE	12.63	12.65	12.65	12.8		
PP	12.62	12.66	12.66	12.7		
PS	12.93	12.97	12.97	12.7		
PVC	12.00	12.84	12.84	11.7		
PC	13.14	13.12	13.12	13.1		

\* apparent standard uncertainty based on a 95% confidence interval by means of a small sample t-test (value divided by 2)

\*\* derived from NIST-JANAF<sup>[20]</sup> values

Table 17. Heats of combustion per unit mass of oxygen found in the literature.

Although the values are given to four significant digits, except for reference [39], there is some spread on the reported values. Furthermore, no tolerance is given on the reported values.

Since the number of references is so low and since some of the data may come out of a same primary source, no reliable 'standard error of mean' can be calculated. Therefore a different approach has been followed and heats of combustion are calculated out of heats of formation.

The heat of combustion, whether expressed in heat release per unit mass of fuel or in unit mass of oxygen consumption, is more precisely defined as the enthalpy of combustion. In a constant-pressure process, the heat added to – or eliminated from – a system is equal to the change in its enthalpy

$$Q = H_2 - H_1 = \Delta H \quad [ 6.101 ]$$

whereby Q is the heat added to the system and ΔH is the change in enthalpy.

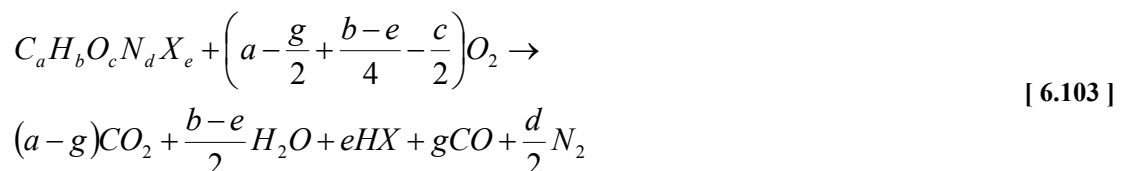
The heat of combustion ΔH<sub>c</sub> can be computed out of the heats of formation ΔH<sub>f</sub><sup>0</sup> of both the initial products and the reactants.

$$\Delta H_c = - \sum_{\text{products}} n \Delta H_f^0 + \sum_{\text{reactants}} n \Delta H_f^0 \quad [ 6.102 ]$$

n is the number of moles of a particular product or reactant species.

The heat of formation of any chemical species is defined as the heat which is required to be added in order to form that species out of its constituent elements, with the elements being in their standard state. By convention, the standard state is defined to be at a temperature of 298.15K and a pressure of 1 atm.

Now for a fairly general expression for combustion of a fuel in oxygen



The above expression remains unchanged for combustion in air, except that an identical number of nitrogen molecules should be added to both sides. The letter X stands for any of the halogen atoms like F, Cl, Br, etc.

Since both oxygen and nitrogen are 'constituent' elements in their ground state (gas at 298K) their heat of formation is zero by definition and the heat of combustion can be written as



$$\Delta H_c = -(a - g)\Delta H_f^0|_{CO_2} - \frac{b - e}{2}\Delta H_f^0|_{H_2O} - e\Delta H_f^0|_{HX} - g\Delta H_f^0|_{CO} + \Delta H_f^0|_{C_dH_bO_cN_dX_e} \quad [ 6.104 ]$$

Division by the amount of moles of oxygen consumed, results in the heat of combustion per unit mass of oxygen as given in Table 17. The table shows, besides some literature values, the computed values for methane, propane and n-heptane together with an estimate on the standard uncertainty. Calculation details can be found in annex B.7.

If the lower, or net, heat of combustion is computed, the heat of formation of H<sub>2</sub>O in the gas phase should be taken. For the computation of the upper, or gross, heat of combustion, the formula requires the use of the heat of formation of H<sub>2</sub>O in the liquid phase.

According to Babrauskas<sup>[27]</sup>, who gives a good overview of the fundamentals of combustion theory, the relationship between upper and lower heat of combustion can be written as

$$\Delta H_c^l = \Delta H_c^u - 0.2183[\%H] \quad \text{MJ/kg} \quad [ 6.105 ]$$

where [%H] is the percent of hydrogen, by mass, in the fuel.

Indeed, knowing the heat of formation of H<sub>2</sub>O in the gas phase  $\Delta H_f^0(g) = -241.826 \pm 0.042$  kJ/mol and in the liquid phase  $\Delta H_f^0(l) = -285.830 \pm 0.042$  kJ/mol<sup>[20]</sup> and knowing the molecular weight of the Hydrogen atom =  $1.00794 \pm 0.00007$  kg/kmol<sup>[24][85]</sup> the above correction coefficient is found. Out of an uncertainty analysis (annex B.12) we find a corresponding standard uncertainty in the order of 0.1%.

$$(0.2183 \pm 0.0003)[\%H] \quad [ 6.106 ]$$

In practice, it proves to be very difficult and expensive to obtain pure substances. Therefore the SBI standard prescribes the use of commercial grade propane having a purity of 95% and a high quality heptane with a purity better than 99%. This however introduces an additional uncertainty on the heat release.

For propane an estimate of the standard uncertainty has been made in Annex B.6 based on a ‘typical’ composition of commercial grade propane (on the Belgian market), which also may contain propene, n- and iso- butane, ethane and ethene. The result is summarised in Table 18.

Although a purity of better than 99% is prescribed for the n-heptane, different sub qualities are available on the market. In a product catalogue of a typical chemical components supplier<sup>[74][81]</sup> 6 different commercially available qualities were found. That the chemical nature of the remaining fraction may differ a lot from quality to quality was demonstrated in the second SBI round robin. Two laboratories, including Ghent University, demonstrated that changing suppliers could potentially double the amount of smoke measured when burning the heptane in a pool fire. This indicates that the variation in composition of this 1% may be substantial.

Assuming that the unknown fraction has an E-factor which is identical to the pure substance with an uncertainty of 10% (which is conservative), an overall uncertainty of 0.1% is obtained due to this unknown fraction. The apparent standard uncertainty on the E-value (annex B.7) is 0.04% which brings the global standard uncertainty to  $\sqrt{(0.1)^2 + (0.04)^2} = 0.11\%$ .

Making the same assumption on the unknown fraction for methane with a purity of 99.5% (uncertainty 0.05%), and combining this with the standard uncertainty on the heat of combustion per unit mass of oxygen consumption, E, the global standard uncertainty is estimated at  $\sqrt{(0.05)^2 + (0.02)^2} = 0.054\%$ .

In the SBI standard<sup>[2]</sup> E', defined as ‘the net heat of combustion *per unit volume* of oxygen consumed at 298K’, is used instead of E (*per unit mass*). The oxygen density at standard conditions (273,15K; 101325Pa) is taken to be  $(1.429 \pm 0.0005)\text{kg/m}^3$  which results in a standard uncertainty of 0.2% assuming a rectangular distribution. E' now becomes

$$E' = E\rho_{O_2} \frac{273.15}{298.15} \cong (1.3092 \pm 0.0026)E \quad [\text{MJ/kg}] \quad [6.107]$$

Substance	Purity (%) SBI standard	E (MJ/kg O <sub>2</sub> )	Estimated st. unc. E (%)	E' (MJ/m <sup>3</sup> O <sub>2</sub> ) (at 298K)	Est. st. unc. E' (MJ/m <sup>3</sup> O <sub>2</sub> )	Estimated st. unc. E' (%)	E' (MJ/m <sup>3</sup> O <sub>2</sub> ) SBI standard
Propane <sup>[2]</sup>	≥ 95	12.774	0.2	16.72	0.047	0.28	16.8
n-Heptane <sup>[2]</sup>	≥ 99	12.684	0.11	16.61	0.038	0.23	16.5
Methane <sup>[4]</sup>	≥ 99.5	12.536	0.054	16.41	0.034	0.21	-

Table 18. Estimated uncertainties for fuels

b. Fuel is unknown

In most practical cases the E-factor will be unknown since the chemical nature of the product under test is (partially) unknown. In the heating and power industries the theoretical air requirement is determined from an empirical guide. The heat of combustion per unit mass of oxygen consumed is estimated at 13.4 MJ/kg<sup>[39][36]</sup>. Tewarson<sup>[39]</sup> finds a value of 12.8 MJ/kg  $\pm$  7% as an average of the mean value of different generic groups of fuels.

In this dissertation, the uncertainty will be estimated based on Hugget's conclusions, i.e. 13.1 MJ/kg with an accuracy of  $\pm$ 5% or better. Assuming a normal distribution and a 95% confidence interval, the uncertainty on E becomes 2.55% and the standard uncertainty on E' becomes 2.56%.

E' becomes

$$E' = E\rho_{O_2} \frac{273.15}{298.15} = 17.15 \pm 0.44 \quad [\text{MJ/kg}] \quad [ 6.108 ]$$

In the SBI standard<sup>[2]</sup> E' is set by definition to 17.2 MJ/m<sup>3</sup> which is within the standard uncertainty found above.

#### 6.4.6 Uncertainty on the component $X_{O_2}^A$

The oxygen concentration is by far the most critical measurand when calculating the Heat Release Rate using the oxygen depletion technique. Unfortunately, manufacturers of paramagnetic oxygen analysers typically report accuracies in the range 0.5-1.0%<sup>[66]</sup> of its full scale deflection which is an order of magnitude higher than what is required by the standards<sup>[2][4][6]</sup>. Enright<sup>[66]</sup> proposes to use the noise and drift over a 30 minute period instead but this only gives an estimate of the standard uncertainty for an analyser working around its calibration point.

In 'reaction to fire' tests like the SBI<sup>[2]</sup> and the cone calorimeter<sup>[4]</sup> however the working range is between 17Vol% and 21Vol%. In the Room Corner<sup>[6]</sup> test this range is even expanded to 0 - 21 Vol%.

The overall uncertainty associated with the oxygen concentration is very much related to the gas analyser used, the gas preparation and the test and calibration procedure.

A gas analysis rack has been custom designed around fire applications by the author in collaboration with the companies Siemens Belgium and Siemens Germany. Details on the gas analysis rack can be found in 3.2.

The calibration procedure associated with this specific gas analysis rack consists of two steps and is as follows:

1. *Every morning*, calibration gas is fed into the instrument. The calibration gas is typically composed of O<sub>2</sub> (17Vol%), CO<sub>2</sub> (3.5Vol%), CO (0.4Vol%) and the balance by Nitrogen. The given concentrations represent limit values that under normal burning conditions will not be surpassed. Oxygen in the downward sense, carbon dioxide and carbon monoxide in the upward sense. Note that for Room Corner Testing, where the fire is often ventilation controlled, other values apply. When the analyser reaches steady state, the output signal (C1) is recorded. This is done for all analysers present (O<sub>2</sub> , CO<sub>2</sub> , CO, ...). In the SBI only O<sub>2</sub> and CO<sub>2</sub> concentrations are measured.
2. *Prior to every test*, when the sample gas is still composed of ambient air, the output signals (C2) of the analysers are recorded. Those values correspond to the following gas concentrations O<sub>2</sub> (20.95Vol%), CO<sub>2</sub> (0.04Vol%), CO (0.00Vol%). This is true because practically all water is removed from the gas sample prior to the analysis and these concentrations apply for dry air. Details can be found in Annex B.1.  
By calibrating for C2 prior to every single test, the uncertainty related to C2 can be minimised to a strict minimum.

Siemens claim that, because of the measurement principle, the uncertainty on the linearity of the oxygen analyser is negligible. The output of the carbon dioxide/monoxide analysers is linearised by the manufacturer. This makes that any measured new output signal relates to a certain gas concentration which can be found by means of linear interpolation between points C1 and C2. Details on the combined standard uncertainty calculation are given in B.8.

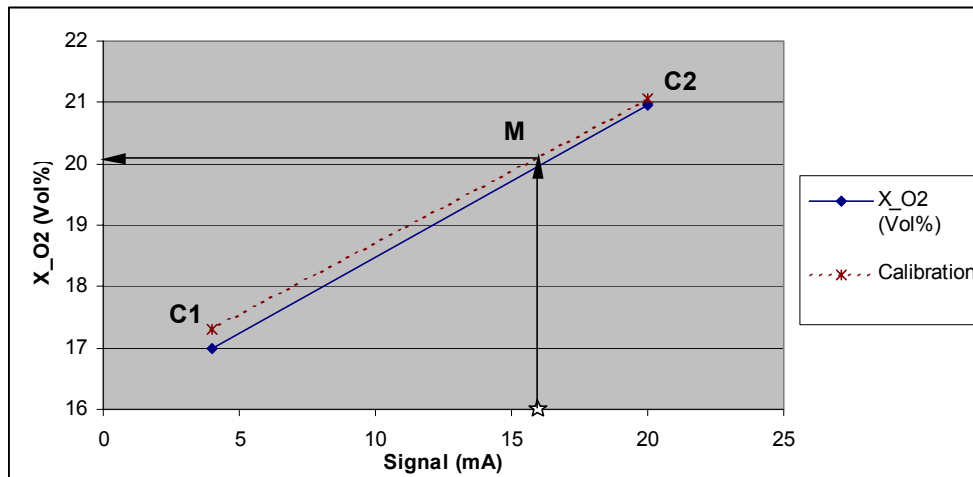


Figure 59. Calibration principle gas analyser

The uncertainty on any measured signal is composed of<sup>[76]</sup> the uncertainty related to:

- i Ambient air temperature: < 0.5% on Measuring Range per 10K; Since the analyser is built-in in a temperature controlled 19" housing the temperature variation over:
  - half an hour is estimated to lie within  $\pm 2\text{K}$ ;
  - one working day is estimated to lie within  $\pm 5\text{K}$ .
- ii Pressure measuring gas: < 0.2% on Measuring Range per 1% pressure variation; This sensitivity is mainly related to the counter pressure experienced by the analyser at the outlet. Since outlet pressure is barometric pressure the variance of pressure over
  - half an hour is estimated at 100 Pa;
  - one working day is estimated to lie within 1 000 Pa.
- iii Power supply: < 0.1% on Measuring Range with rated voltage  $\pm 10\%$
- iv Non-linearity: Linear by measurement principle
- v Measurement noise: obtained out of a root-mean-square deviation around the linear trend line over a period of 30 minutes; the maximum value allowed by the SBI standard for the sum of noise and drift is 100 ppm (parts per million). The value obtained out of SBI RR2<sup>[70]</sup> is 27 ppm. This value will be used for calibration point C1 and C2. For the measurement point M, an estimate based on the local variance (see 5.3.1) will be used.
- vi Signal drift: defined as the absolute difference between the readings at 0 min and at 30 min of this linear trend line; although the drift is partly due to the above influences, it will be considered as independent for the purpose of this dissertation. In this way we want to

include all other effects not covered by the here listed items (minor changes in desiccant, ...). The distribution is assumed to be rectangular and the width for:

- one test period will be taken as the measured drift over that same period;
- one working day will be taken as the value found out of a 'Noise & Drift'-calibration. The value obtained out of SBI RR2<sup>[70]</sup> is 37 ppm.

- vii Data Acquisition system: the standard uncertainty is estimated to be 0.028mA (PLC; §6.4.1); this corresponds to a standard uncertainty of 70 ppm when working in a 17-21Vol% and a 4-20mA range. Since the theory requires relative oxygen concentration rather than absolute values and since the uncertainty is mainly due to ambient temperature variations of the DAQ system (at 25°C the standard uncertainty reduces to 12 ppm), it is assumed that the uncertainty related to the DAQ system is included in the uncertainty related to the signal drift.

The specifications given in the manual are conservative statements. Out of contacts with the technical department of Siemens Karlsruhe who developed the analysers we learned that “100% of the analysers have to fulfil the specifications. If verifications, in-house or by the client, would result in a violation of the limits then the instrument goes to maintenance and is replaced if necessary”. Although Siemens says the batch of instruments is too small to report any coverage factor officially, a Gaussian distribution with a coverage factor of 3 is suggested.

An additional source of uncertainty for calibration point C1 is related to:

- viii Calibration gas:  $\pm 0.02$  Vol% ABS

Any deviation in zero point corresponding to paramagnetic/diamagnetic deviation of residual gas (Annex B.15) is neglected and the corresponding uncertainty introduced is attributed to the E factor, i.e. the heat release per unit mass of oxygen consumed as discussed in 6.4.5.

Since the oxygen depletion technique requires changes in oxygen concentration rather than absolute oxygen concentrations, calibration point C2 – which is determined prior to every test – can be used as a reference point. This makes that the uncertainties related to items i) to iv) and vi) disappear.

The global uncertainty on the oxygen concentration is composed of two parts. On the one hand there is the uncertainty related to the calibration (dashed line is used instead of the true solid line in Figure 59). On the other hand there is the uncertainty related to the measurement itself. Table 19 summarises the estimated uncertainties on both calibration points and on the measurement. Details can be found in Annex B.9. It can be seen that the uncertainty increases with oxygen depletion.

Uncertainty related to	$u(X)$	see
Signal C1 (cal. gas 1)	$u(x_1)$	§B.9 and $x_1$ in §B.7
Signal C2 (cal. gas 2 $\equiv$ air)	$u(x_2)$	§B.9 and $x_2$ in §B.7
Calibration gas 1 (O <sub>2</sub> , CO <sub>2</sub> , N <sub>2</sub> mixture)	$u(y_1)$	§B.9 and $y_1$ in §B.7
Calibration gas 2 (dried ambient air)	$u(y_2)$	§B.9 and $y_2$ in §B.7
measurement	$u(x)$	§B.9 and $x$ in §B.7
Global uncertainty	$u(y)$	formula 10.1 in §B.7

Table 19. Estimated uncertainty on oxygen concentration

Please note that in most modern oxygen analysers a barometric pressure compensation is integrated in the instrument to correct for pressure fluctuations. Throughout this dissertation it will be assumed that oxygen analysers have barometric pressure compensation as in the Ghent equipment.

#### 6.4.7 Uncertainty on the component $X_{CO_2}^A$

The carbon dioxide concentration in the combustion gases is measured by means of an infrared analyser. Compared to the oxygen concentration measurement, the sensitivity coefficient for carbon dioxide is much lower. Uncertainty on CO<sub>2</sub> will therefore influence the Heat Release Rate less than uncertainty on O<sub>2</sub>.

The uncertainty on any measured signal is composed of<sup>[76]</sup> the uncertainty related to:

- i Ambient air temperature: < 1% on Measuring Range per 10K; Since the analyser is built-in in a temperature controlled 19" housing the temperature variation over:
  - half an hour is estimated to lie within  $\pm 2K$ ;
  - one working day is estimated to lie within  $\pm 5K$ .
- ii Pressure measuring gas: < 0.15% on Measuring Range per 1% pressure variation; This sensitivity is mainly related to the counter pressure experienced by the analyser at the outlet. Since outlet pressure is barometric pressure the variance of pressure over:
  - half an hour is estimated to 100 Pa;
  - one working day is estimated to lie within 1 000 Pa.
- iii Power supply: < 0.1% on Measuring Range with rated voltage  $\pm 10\%$

- iv Non-linearity: < 0.5% of full-scale value
- v Measurement noise: obtained out of a root-mean-square deviation around the linear trend line over a period of 30 minutes; the maximum value allowed by the SBI standard for the sum of noise and drift is 100 ppm (parts per million). The value obtained out of SBI RR2<sup>[70]</sup> is 39 ppm. This value will be used for calibration point C1 and C2. For the measurement point M, an estimate based on the local variance (see 5.3.1) will be used.
- vi Signal drift: defined as the absolute difference between the readings at 0 min and at 30 min of this linear trend line; although the drift is partly due to the above influences, it will be considered as independent for the purpose of this dissertation. In this way we want to include all other effects not covered by the here listed items (minor changes in desiccant, ...). The distribution is assumed to be rectangular and the width for:
  - one test period will be taken as the measured drift over that same period;
  - one working day will be taken as the value found out of a ‘Noise & Drift’-calibration. The value obtained out of SBI RR2<sup>[70]</sup> is 36 ppm.
- vii Data Acquisition system: the standard uncertainty is estimated to be 0.028mA (PLC; §6.4.1); this corresponds to a standard uncertainty of 70 ppm when working in a 0-4Vol% and a 4-20mA range. Since the uncertainty is mainly due to ambient temperature variations of the DAQ system (at 25°C the standard uncertainty reduces to 12 ppm), it is assumed that the uncertainty related to the DAQ system is included in the uncertainty related to the signal drift.

An additional source of uncertainty for calibration point C1 (Figure 59) is related to:

- viii Calibration gas:  $\pm 0.5$  Vol% REL

The global uncertainty on the carbon dioxide concentration is – as for the oxygen concentration – composed of two parts. On the one hand there is the uncertainty related to the calibration (dashed line is used instead of the true solid line in Figure 59). On the other hand there is the uncertainty related to the measurement itself. Table 20 summarises the estimated uncertainties on both calibration points and on the measurement. Details can be found in Annex B.10. It can be seen that the uncertainty increases with CO<sub>2</sub> production.



Uncertainty related to	$u(X)$	see
Signal C1 (cal. gas 1)	$u(x_1)$	§B.10 and $x_1$ in §B.7
Signal C2 (cal. gas 2 $\equiv$ air)	$u(x_2)$	§B.10 and $x_2$ in §B.7
Calibration gas 1 (O <sub>2</sub> , CO <sub>2</sub> , N <sub>2</sub> mixture)	$u(y_1)$	§B.10 and $y_1$ in §B.7
Calibration gas 2 (dried ambient air)	$u(y_2)$	§B.10 and $y_2$ in §B.7
measurement	$u(x)$	§B.10 and $x$ in §B.7
Global uncertainty	$u(y)$	formula 10.1 in §B.7

Table 20. Estimated uncertainty on carbon dioxide concentration

### 6.4.8 Uncertainty on the component $\phi$

The relative humidity  $\phi$  together with the barometric pressure and the room temperature are used to calculate the humidity in ambient air  $X_{H20}^0$ . The SBI<sup>[2]</sup> standard prescribes the use of a relative humidity sensor ‘having an accuracy of  $\pm 5\%$  within the range 20% to 80%’.

The Hygrometer used in the Ghent laboratory (Annex B.11) has a bias not more than 2.1% in the range 20% to 80% with a standard deviation not more than 0.25%. In other words, the ‘trueness’ of the instrument is to within 2.1% and the standard deviation on the precision is not more than 0.25%.

Assuming a rectangular distribution with width 2.1%, the standard uncertainty related to trueness becomes 1.21%. Combining this with the uncertainty on the measurement and the uncertainty of the data acquisition system (DAQ), the overall standard uncertainty is estimated to be 1.25% as shown in the table.

Quantity $X_i$	estimate $x_i$ (range)	‘uncertainty’	probability distribution	standard uncertainty $u(x_i)$	sensitivity coefficient $c_i$	uncertainty contribution $u_i(y)$
$\phi_{\text{bias}}$	20-80%	2.1 %	rectangular	1.21 %	1.0	1.21 %
$\phi_{\text{st.dev.}}$	20-80%	0.25 %	normal	0.25 %	1.0	0.25 %
$\phi_{\text{DAQ}}$	20-80%	0.028 mA	normal	0.18 %	1.0	0.18 %
$\phi$	20-80%					1.25 %

Table 21. Estimated uncertainty contribution of the hygrometer

In this dissertation, relative humidity  $\phi$  is only used for determining the water vapour concentration in ambient air. The sensitivity coefficient at a relative humidity concentration of 50% is three times lower than the sensitivity coefficient of the room temperature. The standard uncertainty is estimated to be 1.25%.

#### 6.4.9 Uncertainty on the component $p_{atm}$

The barometric pressure together with the relative humidity  $\varphi$  and the room temperature are used to calculate the humidity in ambient air  $X_{H2O}^0$ . The SBI<sup>[2]</sup> standard prescribes the use of a barometric pressure sensor ‘having an accuracy of  $\pm 200$  Pa’.

Comparing the sensitivity coefficients of the barometric pressure measurement with the humidity measurement (6.3.6;  $\varphi=50\%$ ,  $p=101\,325$ Pa) a variation of 1% on  $\varphi$  causes an equal variation on the heat release as a variation of 2 000 Pa (20 mbar) on  $p_{atm}$ .

The uncertainty on  $p_{atm}$  is therefore considered to be negligible.

For completeness the standard deviation is estimated to be 0.01% ABS.

Quantity $X_i$	estimate $x_i$	‘uncertainty’	probability distribution	standard uncertainty $u(x_i)$	sensitivity coefficient $c_i$	uncertainty contribution $u_i(y)$
$p_a$	101 325 Pa	100 Pa	normal	100 Pa	1.0	100 Pa
$p_a$	101 325 Pa					100 Pa

Table 22. Estimated uncertainty on barometric pressure

Please note that in most modern oxygen analysers a barometric pressure compensation is integrated in the instrument to correct for pressure fluctuations. Throughout this dissertation it will be assumed that oxygen analysers have barometric pressure compensation.

If no barometric pressure compensation were installed, the error made is in the order of 200 ppm for every 100 Pa ( $\cong 1$  mbar) pressure variation for the oxygen analyser.

In this dissertation, the barometric pressure is only used for determining the water vapour concentration in ambient air. The sensitivity coefficient is low compared to the sensitivity coefficients of the relative humidity  $\varphi$  and room temperature. The uncertainty on  $p_{atm}$  is therefore considered to be negligible.

#### 6.4.10 Uncertainty on the component $T_{\text{room}}$

The room temperature together with the relative humidity  $\varphi$  and the barometric pressure are used to calculate the humidity in ambient air  $X_{H20}^0$ . The SBI<sup>[2]</sup> standard prescribes the use of a K-type thermocouple in accordance with EN 60584-1 with a diameter of  $(2 \pm 1)$  mm.

The sensitivity coefficients of the temperature measurement is a factor 3 higher than the sensitivity coefficient for the humidity measurement (6.3.6;  $\varphi=50\%$ ,  $T=298\text{K}$ ). This means that to reduce the uncertainty on the heat release associated with  $T_{\text{room}}$  to the same level as  $\varphi$ , temperature should be measured with a standard uncertainty of 1.24 K, i.e. 1.25% from 298K divided by 3.

✓ Tolerance on a new thermocouple  $t_t$ :

The quality system maintained in the Ghent University fire laboratory prescribes the use of Class 2 thermocouples according to IEC 60584-2<sup>[11]</sup>. The tolerance allowed on new Class 2 thermocouples according to this standard is:

- $\pm 2.5^\circ\text{C}$  in the range  $-40^\circ\text{C}$  to  $333^\circ\text{C}$
- $\pm 0.0075 t$  ( $t$  in  $^\circ\text{C}$ ) in the range  $333^\circ\text{C}$  to  $1200^\circ$

✓ Effect of ageing  $t_a$ :

Since K-type thermocouples are subject to calibration changes on temperature cycling to  $500^\circ\text{C}$  or above (like in fire resistance tests), and since no temperatures above  $400^\circ\text{C}$  are to be expected in the SBI, ageing effects will be considered to be negligible.

✓ Effect of data acquisition and extension wires  $t_{\text{DAQ}}$ :

The uncertainty related to the data acquisition, extension wires and connectors is estimated (6.4.1) to be 1.0 K.

✓ Radiation error  $t_r$ :

Since the thermocouple is supposed to measure the ambient room temperature the radiation error is considered to be negligible.

However, care should be taken that the thermocouple does not see hot surfaces like furnaces, heaters, etc. nor that it is exposed to direct sunlight. (add remark in SBI standard)

✓ Velocity error  $t_v$ :

The air velocities at the height of the probe are estimated to be smaller than 1 m/s. No velocity error needs therefore to be introduced.

✓ Conduction error  $t_c$ :

Negligible.

✓ Transient error  $t_r$ :

Negligible.

Quantity $X_i$	estimate $x_i$	'uncertainty'	probability distribution	standard uncertainty $u(x_i)$	sensitivity coefficient $c_i$	uncertainty contribution $u_i(y)$
$t_t$	0 °C	2.5 °C	rectangular	1.44 °C	1.0	1.44 °C
$t_a$	0 °C	0 °C	-	0 °C	1.0	0 °C
$t_{DAQ}$	0 °C	1.0 °C	normal	1.0 °C	1.0	1.0 °C
$t_r$	0 °C	0 °C	-	0 °C	1.0	0 °C
$t_v$	0 °C	0 °C	-	0 °C	1.0	0 °C
$t_c$	0 °C	0 °C	-	0 °C	1.0	0 °C
$t_r$	0 °C	0 °C	-	0 °C	1.0	0 °C
T	0 °C					1.8 °C

Table 23. Room temperature measurement by means of thermocouple

The use of class 1 thermocouples:

- $\pm 1.5^\circ\text{C}$  in the range  $-40^\circ\text{C}$  to  $375^\circ\text{C}$
- $\pm 0.004 t$  ( $t$  in  $^\circ\text{C}$ ) in the range  $375^\circ\text{C}$  to  $1000^\circ\text{C}$

would reduce the uncertainty contribution to  $1.3^\circ\text{C}$ .

A probably better alternative is to measure the room temperature by means of a 4-wire RTD (Resistive Temperature Detector; Pt-100).

Quantity $X_i$	estimate $x_i$	'uncertainty'	probability distribution	standard uncertainty $u(x_i)$	sensitivity coefficient $c_i$	uncertainty contribution $u_i(y)$
$t_t$	0 °C	$< 0.1^\circ\text{C}$	rectangular	$< 0.06^\circ\text{C}$	1.0	$< 0.06^\circ\text{C}$
$t_{DAQ}$	0 °C	0.3 °C	rectangular	0.17 °C	1.0	0.17 °C
T	0 °C					$< 0.18^\circ\text{C}$

Table 24. Room temperature measurement by means of a 4-wire RTD

In this dissertation, the room temperature is only used for determining the water vapour concentration in ambient air. The sensitivity coefficient is three times higher than the sensitivity coefficient on the relative humidity (concentration of 50%). The standard uncertainty is estimated to be 1.8°C. The standard uncertainty on the room temperature could be reduced with a factor 10 by using a 4-wire RTD (Pt-100) instead of a thermocouple.

### 6.4.11 Uncertainty on the component $\alpha$

The expansion factor  $\alpha$  is defined as the ratio of the number of moles of combustion products to the number of moles of dry air fully depleted of its oxygen. It is related to  $\beta$  by

$$\alpha = 1 + 0.2095(\beta - 1) \quad [ 6.109 ]$$

where  $\beta$  is defined as the ratio of the moles of combustion products formed to the moles of oxygen consumed. As an example the expansion factor  $\alpha$  of propane is calculated as



$$\alpha = 1 + 0.2095\left(\frac{3+4}{5} - 1\right) = 1.0838 \quad [ 6.111 ]$$

If the fuel composition and the reaction chemistry is known,  $\beta$  and  $\alpha$  are known.

It is assumed that the nitrogen contained in the fuel is released as molecular nitrogen. (Temperatures in building fires are usually not high enough to produce noticeable amounts of nitrogen oxides)

As the composition of the fuel is usually not known, some average value has to be used for  $\alpha$ . Complete combustion of pure carbon (no H<sub>2</sub>O formation) results in  $\alpha = 1$ , while complete combustion of hydrogen (no CO<sub>2</sub> formation) results in  $\alpha = 1.21$ . A recommended value in the literature<sup>[33]</sup> is  $\alpha = 1.105$ , which is correct for methane. This is also the value that has been adopted in most fire test standards.

Quantity $X_i$	estimate $x_i$	'uncertainty'	probability distribution	standard uncertainty $u(x_i)$	sensitivity coefficient $c_i$	uncertainty contribution $u_i(y)$
$\alpha$	1.105	0.105	rectangular	0.061	1.0	0.061
$\alpha$	1.105					0.061

Table 25. Uncertainty on the expansion factor

Assuming a rectangular distribution from  $\alpha = 1$  to 1.21, the standard deviation on  $\alpha$  is equal to 5.5%.

### 6.4.12 Uncertainty on the component c

The component c is given by the following equation and is – by the standard – defined to be 22.4

$$c = \sqrt{\frac{2T_{298}}{\rho_{298}}} = 22.4 \quad [ 6.112 ]$$

with corresponding uncertainty estimate ( $T_{298} = 298.15\text{K}$ ):

$$u(c) = \sqrt{\left(\frac{c \cdot u(\rho)}{2\rho}\right)^2} = \frac{c \cdot u(\rho)}{2\rho} \quad [ 6.113 ]$$

This introduces an error due to the fact that it is assumed that the gas flowing in the exhaust duct has a density equal to dry air. The molecular weight of air is however significantly affected by the presence of water vapour. Jones<sup>[34]</sup> gives an extensive development and comes to the following equation for density of air as a function of temperature (K), pressure (Pa) and relative humidity ( $\phi$ )

$$\rho_{air} = \left(\frac{0.0034847}{T}\right)(p - 0.003796 p_s \phi) \quad [ 6.114 ]$$

where the saturation pressure is related to temperature by

$$p_s = (1.7526E + 11)e^{\left(\frac{-5315.56}{T}\right)} \quad [ 6.115 ]$$

Since the ambient temperature, the barometric pressure and the relative humidity are used in the calculation of the depletion factor  $\phi$  they are readily available to correct for the effect of moisture content on the c-factor through the air density.

Table 26 shows the effect of barometric pressure and relative humidity on the ‘constant’ c. The variation in barometric pressure at sea level is taken as  $\pm 3\ 000\text{Pa}$ , while the range in relative humidity is chosen to lie between 20 and 80%. For those laboratories that lie substantially above sea-level, the mean barometric pressure, in general, will lie below the standard value of 101 325Pa at sea-level.



T (K)	$\phi$ (%)	$P_{atm}$ (Pa)	$P_s$ (Pa)	$\rho_{air}$ (kg/m <sup>3</sup> )	c (m <sup>2</sup> s <sup>-1</sup> N <sup>-1/2</sup> K <sup>1/2</sup> )	error (%)
at sea level						
298.15	20	98'325	3'169	1.146	22.807	1.82%
298.15	20	104'325	3'169	1.217	22.140	-1.16%
298.15	80	98'325	3'169	1.138	22.891	2.19%
298.15	80	104'325	3'169	1.208	22.217	-0.82%
at 100m above sea level						
298.15	20	97'200	3'169	1.133	22.939	2.41%
298.15	20	103'132	3'169	1.203	22.268	-0.59%
298.15	80	97'209	3'169	1.125	23.024	2.78%
298.15	80	103'140	3'169	1.194	22.345	-0.24%

Table 26. variation of c-factor with barometric pressure and relative humidity

Note that:

- The mean level of Ghent is 8m above sea-level.
- The minimum/maximum barometric pressure in Gruitrode (Belgium) for the year 2004 is 984hPa/1036hPa.
- Outside air is often saturated ( $\phi=100\%$ ) but is often heated ( $\phi$  drops) before it enters the test instrument.

So the tabulated values are believed to represent limit cases in the determination of the variation on the c-factor. The distribution of the c-factor will assumed to be triangular with limit values -1.2%/2.2% around the actual used value of 22.4.

The thus obtained standard deviation is -0.5%/+0.9%.

Quantity $X_i$	estimate $x_i$	'uncertainty'	probability distribution	standard uncertainty $u(x_i)^*$	bias	sensitivity coefficient $c_i$	uncertainty contribution $u_i(y)^*$
c	22.4	-1.2%/2.2%	triangular	$\pm 0.7\%$	0.5%	1.0	$\pm 0.16$
c	22.4				0.5%		$\pm 0.16$

\* see 6.2.4 for calculation of bias and standard uncertainty

Table 27. Uncertainty contribution if c is taken constant

Correcting for the bias this becomes:

Quantity $X_i$	estimate $x_i$	'uncertainty'	probability distribution	standard uncertainty $u(x_i)^*$	sensitivity coefficient $c_i$	uncertainty contribution $u_i(y)^*$
c	22.51	$\pm 1.7\%$	triangular	$\pm 0.7\%$	1.0	$\pm 0.16$
c	22.51					$\pm 0.16$

\* see 6.2.4 for calculation of bias and standard uncertainty

Table 28. Uncertainty contribution if c is taken constant (corrected for bias)

If the c-factor is calculated out of the above formulas, the uncertainty contribution reduces, but still can not be neglected, as can be seen from Table 29.

Quantity $X_i$	estimate $x_i$	'uncertainty'	probability distribution	standard uncertainty $u(x_i)$	sensitivity coefficient $c_i$	uncertainty contribution $u_i(y)$
T	293 K	$\pm 1.8$ K	normal	$\pm 1.8$ K	$-4.41^{E-03}$	$\pm 0.0079$
$\varphi$	50 %	$\pm 1.23\%$	normal	$\pm 1.23\%$	$-1.046^{E-04}$	$\pm 0.000129$
p	101 325 Pa	$\pm 100$ Pa	normal	$\pm 100$ Pa	$1.19^{E-05}$	$\pm 0.00119$
$\rho_{air}$	1.200 kg/m <sup>3</sup>			$\pm 0.008$ kg/m <sup>3</sup>	-9.284	$\pm 0.074$
c	22.282					$\pm 0.074$

Sensitivity coefficients calculated around the estimate values

Table 29. Uncertainty contribution if c is calculated ( $T_{room}$  via thermocouple)

Note from Table 30 that the uncertainty would even reduce further if a 4-wire RTD (Resistive Temperature Detector; Pt-100) would be used to measure the room temperature as explained in 6.4.10.

Quantity $X_i$	estimate $x_i$	'uncertainty'	probability distribution	standard uncertainty $u(x_i)$	sensitivity coefficient $c_i$	uncertainty contribution $u_i(y)$
T	293 K	$\pm 0.18$ K	normal	$\pm 0.18$ K	$-4.41^{E-03}$	$\pm 0.000794$
$\varphi$	50 %	$\pm 1.23\%$	normal	$\pm 1.23\%$	$-1.046^{E-04}$	$\pm 0.000129$
p	101 325 Pa	$\pm 100$ Pa	normal	$\pm 100$ Pa	$1.19^{E-05}$	$\pm 0.00119$
$\rho_{air}$	1.200 kg/m <sup>3</sup>			$\pm 0.00144$	-9.284	$\pm 0.013$
c	22.282					$\pm 0.013$

Sensitivity coefficients calculated around the estimate values

Table 30. Uncertainty contribution if c is calculated ( $T_{room}$  via RTD)

In summary:

The 'constant'  $c$  does vary with barometric pressure and relative humidity and introduces a standard uncertainty of  $\pm 0.7\%$  at the Ghent premises. This uncertainty can be reduced by a factor 10 by actually calculating the  $c$ -factor and by measuring the room temperature with a four-wire RTD instead of with a thermocouple. This operation requires no additional measurements.

### 6.4.13 Uncertainty on the component A

The cross sectional area of the exhaust duct is governed by the roundness and the diameter. Out of a discussion with the supplier we learned that the roundness is within  $\pm 1$  mm around the nominal diameter of 315 mm as confirmed by measurements.

Also soot deposit may change the cross sectional area of the duct. The assumption made is that a soot layer of between 0 and 1mm is formed on the duct wall. For ease of calculation we will widen this range to 0 – 1.15 mm as will become clear later.

In addition, due to the nature of the testing, the duct wall temperature will increase over the test, resulting in a higher cross sectional area. The steel used for the inner duct is Stainless Steel 304 (18/8 steel) which has a linear expansion coefficient of 1.7mm per meter and per 100°C temperature rise.

Figure 60 shows the measured wall temperature in three test cases:

- when burning a particle board (continued heat release);
- when running a heptane calibration;
- when running a step calibration.

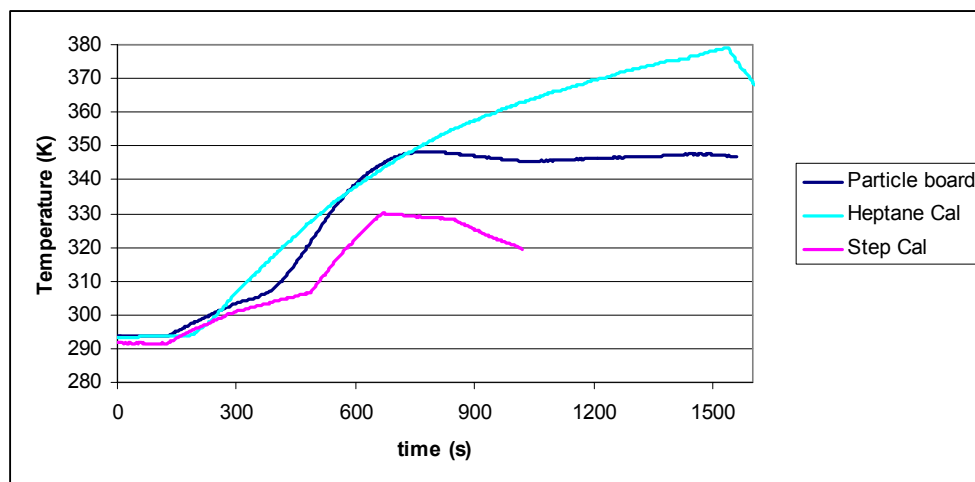


Figure 60. Measured duct wall temperatures in three particular tests

Assuming:

- the maximum temperature rise to be of the order of 85°C over a test (case heptane calibration);
- a triangular distribution,

the standard uncertainty related to the cross sectional area A is estimated in Table 32.

Quantity $X_i$	estimate $x_i$	'uncertainty'	probability distribution	standard uncertainty $u(x_i)^*$ (m)	bias (mm)	sensitivity coefficient $c_i$	uncertainty contribution $u_i(y)^*$
$D_{\text{radius}}$	0.315 m	$\pm 1.0^{E-03}$ m	rectangular	$\pm 0.577^{E-03}$	0	0.495	$\pm 0.286^{E-03}$
$D_{\text{soot}}$	0.315 m	$-2.3^{E-03}$ m	rectangular (one sided)	$\pm 0.664^{E-03}$	-1.15	0.495	$\pm 0.329^{E-03}$
$D_{\text{temperature}}$	0.315 m	$+0.455^{E-03}$ m	triangular (one sided)	$+0.107^{E-03}$	0.15	0.495	$+0.053^{E-03}$
A (m <sup>2</sup> )	$77.93^{E-03}$						$\pm 0.44^{E-03}$

\* see 6.2.4 for calculation of bias and standard uncertainty

Table 31. Standard uncertainty and bias related to the cross section area

Although the temperature effect has only a minor effect, the effect may become important in full scale tests like the room corner test where the temperature rise may attain several hundred degrees Celcius.

In order to remove the bias, the diameter estimate will be reduced with 1 mm (-1.15 + 0.15).

Quantity $X_i$	estimate $x_i$	'uncertainty'	probability distribution	standard uncertainty $u(x_i)^*$	sensitivity coefficient $c_i$	uncertainty contribution $u_i(y)^*$
$D_{\text{radius}}$	0.314 m	$\pm 1.0^{E-03}$ m	rectangular	$\pm 0.577^{E-03}$ m	0.495	$\pm 0.286^{E-03}$
$D_{\text{soot}}$	0.314 m	$\pm 1.15^{E-03}$ m	rectangular	$\pm 0.664^{E-03}$ m	0.495	$\pm 0.329^{E-03}$
$D_{\text{temperature}}$	0.314 m	$\pm 0.228^{E-03}$ m	triangular (asymm.)	$\pm 0.107^{E-03}$ m	0.495	$\pm 0.053^{E-03}$
A (m <sup>2</sup> )	$77.44^{E-03}$					$\pm 0.44^{E-03}$

Table 32. Standard uncertainty related to the cross section area

#### 6.4.14 Uncertainty on the component $q_{\text{gas}}$

$q_{\text{gas}}$  represents the ‘theoretical’ heat release rate as obtained out of: 1) a mass flow measurement of propane gas that feeds the burner and 2) the lower heat of combustion of propane gas.

$$\dot{q}_{\text{gas}}(t) = \Delta h_{c,\text{eff}} \dot{m}_{\text{gas}}(t) \quad [ 6.116 ]$$

The value of  $q_{\text{gas}}$  when the burner is running at a 30 kW level is used to calibrate the test instrument ( $k_t$ -factor, see 6.4.15).

The lower heat of combustion of commercial grade propane and its standard uncertainty are estimated at  $(46\,340 \pm 50)$  kJ/kg (see B.6).

The global uncertainty related to the mass flow measurement originally was thought to be  $\pm 0.5\%$  of the measurement value plus  $\pm 0.1\%$  of the full scale, which corresponds to a standard uncertainty of 0.26 kW for the burner running at 30 kW (full scale corresponds to approximately 105 kW). Those values apply for a special polynomial calibration of the test instrument.

However, out of contacts with the mass flow controller supplier, we learned that these values only apply when calibrating under actual conditions. This means with the same gas, at same temperature and pressure conditions.

Due to the explosive character of propane gas, a reference gas (nitrogen) is used instead for calibration and the tight uncertainty limits no longer hold.

The manufacturer stated that this is common practice for all mass flow controllers commercially available on the market.

They further suggested to use the somewhat conservative estimate of:  $\pm 1\%$  of the measurement value plus  $\pm 0.2\%$  of the full scale (or  $\pm 1\%$  of the full scale, whichever is the lowest). The resulting estimated standard uncertainty is 0.51 kW for the burner running at 30 kW (1.7%). This is higher than what the standard requires (1%).

For the standard mass flow controllers (without polynomial calibration) they recommend to use the estimate of  $\pm 1\%$  of the full scale (estimated standard uncertainty of 1.05 kW or 3.5%).

A better solution would be to introduce an extra mass flow controller with a range of 0 to 30 or 31 kW (say 0 to 20 nl/min). The standard uncertainty would then reduce to approximately 1%. This would

however only slightly improve the uncertainty on the  $k_{t,qgas}$  factor (2.9% instead of 3.2%; see next section).

## **6.4.15 Uncertainty on the component $k_t$**

### **6.4.15.1 Introduction**

The velocity profile correction factor  $k_t$  accounts for the fact that the velocity measured by means of a bi-directional probe on the axis of the exhaust duct is a factor  $k_t$  higher than the mean velocity in the duct. The  $k_t$  factor used in the standard is defined as the average of three independent calibrations being the ‘step calibration’ ( $k_{t,qgas}$ ), the ‘heptane calibration’ ( $k_{t,qheptane}$ ) and the ‘velocity profile measurement’ ( $k_{t,v}$ ).

$k_t$  is directly proportional to the volume flow and therefore to the heat release rate and its derived parameters FIGRA and THR600, and to the smoke production rate and its derived parameters SMOGRA and TSP600.

In medium to large scale heat release testing equipment, the  $k_t$  factor is used to correct for all measurement errors, and this at the moment of calibration. One way to ‘calibrate’ the test equipment is to burn a combustible with a well known heat of combustion and to fit the  $k_t$  factor until the measured heat release corresponds to the theoretic value. In the SBI the  $k_t$  factor is the mean value of three calibrations, two of which are based on the burning of a known combustible ( $k_{t,qgas}$  &  $k_{t,qheptane}$ ).

In those heat release tests, the  $k_t$  factor is considered to be constant which it clearly isn’t as discussed in [58], which forms an integral part of this work (see 4.4), and [52].

First the uncertainty related to  $k_t$  and its measurement and calculation procedure is estimated by determining the uncertainty on the three composing  $k_t$  factors.

Next, the intrinsic variation on  $k_t$  is estimated as described in [58].

### **6.4.15.2 Uncertainty on the component $k_{t,v}$**

The velocity profile correction factor obtained out of a direct measurement of the velocities in some discrete points results in  $k_{t,v}$ . The measurements are taken at 90° intervals on 5 different radii ( $v_n$ ;  $n=1...5$ ) and at the centre position making use of a pitot tube or a hot wire anemometer. The profile factor  $k_{t,v}$  is then:

$$k_{t,v} = \frac{1}{5} \sum_{n=1}^5 \frac{v_n}{v_c} \quad [ 6.117 ]$$

Taking the partial derivative to the different components  $x_i$  results in the corresponding sensitivity coefficients  $c_i$ :

$$c_1 \equiv \frac{\partial k_{t,v}}{\partial v_n} = \frac{1}{5v_c} = \frac{k_{t,v}}{\sum v_n} \quad [ 6.118 ]$$

$$c_2 \equiv \frac{\partial k_{t,v}}{\partial v_c} = -\frac{k_{t,v}}{v_c} \quad [ 6.119 ]$$

and to the combined standard uncertainty

$$u(k_{t,v}) = k_{t,v} \sqrt{\sum_i \left( \frac{u(v_i)}{\sum_n v_n} \right)^2 + \left( \frac{u(v_c)}{v_c} \right)^2} \quad [ 6.120 ]$$

The estimated uncertainty (see §6.2.2) on the velocity components for a 95% confidence interval and 3 degrees of freedom (4 measurement positions;  $t_{0,025} = 3.18$ ) is:

Quantity $X_i$	estimate $x_i$	standard deviation $s$	probability distribution	95% confidence interval	sensitivity coefficient $c_i$	uncertainty contribution $u_i(y)$ [95%]
$v_1$	7.00	1.132	t (d.f.=3)	1.799	0.0198 $k_{t,v}$	0.0355 $k_{t,v}$
$v_2$	9.39	0.412	t (d.f.=3)	0.655	0.0198 $k_{t,v}$	0.0129 $k_{t,v}$
$v_3$	10.62	0.531	t (d.f.=3)	0.845	0.0198 $k_{t,v}$	0.0167 $k_{t,v}$
$v_4$	11.25	0.180	t (d.f.=3)	0.287	0.0198 $k_{t,v}$	0.0057 $k_{t,v}$
$v_5$	12.37	0.223	t (d.f.=3)	0.355	0.0198 $k_{t,v}$	0.0070 $k_{t,v}$
$v_c$	12.39	0.636	t (d.f.=3)	1.011	-0.0807 $k_{t,v}$	-0.0816 $k_{t,v}$
$k_{t,v}$	$k_{t,v} = 0.817$					0.092 $k_{t,v}$

Table 33. Standard uncertainty related to  $k_{t,v}$



which finally results in an uncertainty of 9.2% for a 95% confidence interval.

The uncertainty related to the position of the measurement head (estimated accurate to within 0.5 mm) for the outer radius where the velocity gradient is highest, is estimated at 1.2 % based on the theoretical velocity profile as proposed by Schlichting<sup>[32]</sup> at a Reynolds number of around 160 000. This makes that this uncertainty, in comparison with the values in Table 33, may be neglected.

The apparent standard deviation, defined as the uncertainty for a 95% interval divided by 1.96, will thus be set to 4.7 %. (This is much larger than the value of 1.044% reported by SP<sup>[69]</sup> for their Room Corner<sup>[6]</sup> duct.)

Note that the largest variations occur close to the wall where the velocity gradient is highest. More important however, in view of a lower standard uncertainty, is the careful measurement of the velocity component on the central axis of the duct since its sensitivity coefficient is a factor 4 higher.

The standard uncertainty could further be reduced by measuring for example on 2 or 4 additional lines from wall to centre thus increasing – besides the number of samples – the degrees of freedom in the t-distribution to 5 respectively 7 and so reducing the value of the critical point  $t_{0.025}$  ( $t_{0.025}$  (d.f. = 5) = 2.57;  $t_{0.025}$  (d.f. = 7) = 2.36).

Using the last N calibrations instead of just the recent one – in fact taking the mean of N measurements considered to be independent – could further reduce the standard uncertainty for the population mean by a factor  $\sqrt{N}$ .

#### 6.4.15.3 Uncertainty on the component $k_{t,qgas}$

The component  $k_{t,qgas}$  follows out of a so called ‘Step Calibration’ which consists of burning a known combustible, in this case propane, with a well known heat of combustion and to fit the  $k_t$  factor until the measured heat release rate,  $Q_{step}$ , corresponds to the theoretic value,  $q_{gas}$ .

$$k_{t,qgas} = k_t \frac{q_{gas}}{Q_{step}} \quad [ 6.121 ]$$

whereby  $k_t$  is the flow profile factor used for the calculation of  $Q_{step}$ . Both the nominator and denominator on the right hand side of the equation contain  $k_t$ , so  $k_t$  drops out and thus the uncertainty on  $k_t$  can be set to zero.

The uncertainty on Q (6.3.4) then reduces to 0.82 kW (for the 30 kW level). This is also because the fuel is known namely ‘commercial grade propane’.

The combined standard uncertainty on  $k_{t,qgas}$  is estimated at 3.2%:

$$u(k_{t,qgas}) = k_{t,qgas} \sqrt{\left(\frac{u(q_{gas})}{q_{gas}}\right)^2 + \left(\frac{u(Q_{step})}{Q_{step}}\right)^2} \cong 0.032k_{t,qgas} \quad [ 6.122 ]$$

This value is obtained neglecting the bias associated with: the ‘c’-component, the cross section of the duct ‘A’ and the differential pressure probe ‘k<sub>p</sub>’. Increasing the uncertainty for this uncorrected bias results in

$$k_{t,qgas} = 0.791 \begin{matrix} + 2.4\% \\ - 6.6\% \end{matrix} \quad [ 6.123 ]$$

The above values are based on the second SBI round robin step calibration of the Ghent University laboratory ( $k_{t,qgas} = 0.791$ ). Complete combustion is assumed.

Using the last N calibrations instead of just the recent one – in fact taking the mean of N measurements considered to be independent – could further reduce the standard uncertainty for the population mean by a factor  $\sqrt{N}$ .

#### 6.4.15.4 Uncertainty on the component $k_{t,qheptane}$

The component  $k_{t,heptane}$  follows out of a so called ‘Heptane Calibration’ which consists of burning a given quantity of a known combustible, in this case heptane, with a well known heat of combustion and to fit the  $k_t$  factor until the measured total heat release,  $Q_{heptane}$ , corresponds to the theoretic value,  $Q_{heptane}$ .

$$k_{t,heptane} = k_t \frac{q_{heptane}}{Q_{heptane}} = k_t \frac{\Delta h_{c,heptane} m_{heptane}}{Q_{heptane}} \quad [ 6.124 ]$$

whereby  $k_t$  is the flow profile factor used for the calculation of  $Q_{heptane}$ . Both the nominator and denominator on the right hand side of the equation contain  $k_t$ , so  $k_t$  drops out and thus the uncertainty on  $k_t$  can be set to zero.

The uncertainty on  $Q_{\text{heptane}}$  (6.3.4) then reduces to 643 kJ. This is also because the fuel is known namely ‘99% pure heptane’.

$$Q_{\text{heptane}} = \sum_{i=180s}^{\text{end}} \dot{Q}_{\text{heptane}}^i T_s \quad [ 6.125 ]$$

$$u(Q_{\text{heptane}}) = \sqrt{\sum_{i=180s}^{\text{end}} [u(\dot{Q}_{\text{heptane}}^i T_s)]^2} \cong 643 \text{kJ} \quad [ 6.126 ]$$

The combined standard uncertainty on  $k_{t,\text{heptane}}$  is estimated out of

$$u(k_{t,\text{heptane}}) = k_{t,\text{heptane}} \sqrt{\left(\frac{u(\Delta h_{c,\text{heptane}})}{\Delta h_{c,\text{heptane}}}\right)^2 + \left(\frac{u(m_{\text{heptane}})}{m_{\text{heptane}}}\right)^2 + \left(\frac{u(Q_{\text{heptane}})}{Q_{\text{heptane}}}\right)^2} = 0.0053 k_{t,\text{heptane}} \quad [ 6.127 ]$$

whereby  $\Delta h_{c,\text{heptane}} = (44\,550 \pm 50)$  kJ/kg and  $m_{\text{heptane}} = (2.840 \pm 0.001)$ kg.

The above uncertainty estimate is obtained by neglecting the bias associated with: the ‘c’-component, the cross section of the duct ‘A’ and the differential pressure probe ‘ $k_p$ ’. Increasing the uncertainty for this uncorrected bias results in

$$k_{t,\text{heptane}} = 0.839 \begin{matrix} +0.55\% \\ -0.61\% \end{matrix} \quad [ 6.128 ]$$

The above values are based on the second SBI round robin heptane calibration of the Ghent University laboratory ( $k_{t,\text{heptane}} = 0.839$ ). Complete combustion is assumed. Out of the statistical analysis of the second SBI round robin data there are some indications that this may not be true (Table 5 in [56]). This needs further analysis.

Using the last  $N$  calibrations instead of just the recent one – in fact taking the mean of  $N$  measurements considered to be independent – could further reduce the standard uncertainty for the population mean by a factor  $\sqrt{N}$ .

Since  $k_t$  is calculated as the average of three values  $k_{t,v}$ ,  $k_{t,qgas}$  and  $k_{t,qheptane}$  which are independent measurements, the standard uncertainty on  $k_t$  reduces to

$$u(k_t) = \frac{1}{3} \sqrt{u^2(k_{t,v}) + u^2(k_{t,qgas}) + u^2(k_{t,qheptane})} \cong 0.015 \quad [ 6.129 ]$$

This finally results in  $k_t = (0.815 \pm 0.015)$  or thus a standard uncertainty of 1.8%.

Increasing the uncertainty for the uncorrected bias results in:

$$k_t = 0.815 \begin{array}{l} +1.8\% \\ -2.7\% \end{array} \quad [ 6.130 ]$$

This is the uncertainty on  $k_t$  related to both the natural variation and to the method by which it is obtained. This value should be used in the calculations. By using the last N calibrations of the individual  $k_{t,x}$  calibrations instead of only the recent one, the standard uncertainty for mean value (out of N calibrations) could further reduce by a factor  $\sqrt{N}$ .

The evolution in time of the different  $k_{t,x}$  calibration values can also be used as a warning signal for a major revision of the test instrument.

#### 6.4.15.5 Uncertainty on $k_t$ ; alternative method

In the paper of section 4.4, the intrinsic variation of  $k_t$  is estimated. The conclusion there is that for the SBI test equipment running at constant mass flow rate (extraction), the standard uncertainty on the mass flow rate related to temperature effects is estimated to 0.6%. This method not only includes the variation of  $k_t$  with Reynolds number, but also the opposite effect of variation in density profile which otherwise would not be included in the uncertainty analysis.

This means that there is still some room left for improvement of the measurement procedure & equipment (1.8%/-2.7% versus 0.6%).

### 6.4.16 Uncertainty on the component $k_p$

In the paper ‘Critical considerations on the use of a bi-directional probe in heat release measurements’ [56], which forms an integral part of this work (see chapter 4), it is shown that the pressure probe currently used in the SBI is Reynolds dependant. Since the pressure probe factor  $k_p$  is considered to be constant, this introduces an additional uncertainty on  $k_p$ .

In order to estimate the uncertainty related to the Reynolds dependence of the pressure probe, we assume:

- a constant mass flow. Table 4 of that same paper reveals that the maximum error is  $-0\%/+7\%$  (combustion gases at 600K);
- a triangular distribution.

The standard uncertainty now becomes

Quantity $X_i$	estimate $x_i$	‘uncertainty’	probability distribution	standard uncertainty $u(x_i)^*$ (m)	bias	sensitivity coefficient $c_i$	uncertainty contribution $u_i(y)^*$
$k_{p,Reynolds}$	1.080	-0%/+7%	triangular (one sided)	$\pm 1.65$	2.33 (%)	1	$\pm 0.018$
$k_{p,calibration}$	1.080	-0.011/0.009	normal	$\pm 0.01$	-	1	$\pm 0.01$
$k_p$	1.080						$\pm 0.021$

\* see 6.2.4 for calculation of bias and standard uncertainty

Table 34. Uncertainty contribution if  $c$  is taken constant

or, removing the bias,

Quantity $X_i$	estimate $x_i$	‘uncertainty’	probability distribution	standard uncertainty $u(x_i)$	sensitivity coefficient $c_i$	uncertainty contribution $u_i(y)$
$k_{p,Reynolds}$	1.105	-0%/+7%	triangular (asymm.)	$\pm 1.65$	1	$\pm 0.018$
$k_{p,calibration}$	1.105	-0.011/0.009	normal	$\pm 0.01$	1	$\pm 0.01$
$k_p$	1.105					$\pm 0.021$

Table 35. Uncertainty contribution if  $c$  is taken constant (corrected for bias)

An alternative and probably better solution would be to move away from the actual probe design, which includes a steel supporting rod that heavily disturbs the flow around the pressure chambers, and to introduce either the design of McCaffrey & Heskestad[51] or the design of Sette[57].

Quantity $X_i$	estimate $x_i$	'uncertainty'	probability distribution	standard uncertainty $u(x_i)$	sensitivity coefficient $c_i$	uncertainty contribution $u_i(y)$
$k_{p,McCaffrey \& H.}$	1.046					-0.011/+0.009
$k_{p,Sette}$	1.224					$\pm 0.008$

Table 36. Uncertainty contribution of alternative probes

After correcting for the bias (2.33%), the uncertainty contribution of the SBI pressure probe actually lies around 2% but can easily be reduced to less than 1% by introducing any of two existing design alternatives.

#### 6.4.17 Uncertainty on the component $\Delta p$

The volume flow through the exhaust duct is measured by means of a bi-directional velocity pressure probe. The probe is basically a device that relates the velocity of the exhaust gases to a differential pressure.

The expected velocity range at the height of the probe in the SBI lies between 5 and 16 m/s ( $T=288\dots 600$  K;  $V_{298}=0.4\dots 0.7$  m<sup>3</sup>/s;  $k_t=0.8\dots 0.9$ ). This corresponds to differential pressures roughly between 20 and 150 Pa.

The pressure transducer used to measure the differential pressure over the probe has a range from 0 to 250 Pa with the following specifications:

- a linearity of  $\pm 0.5\%$  FS (Full Span)
- an hysteresis of 0.1% FS
- no zero drift because of automatic zero set function
- a temperature effect on the span value of 0.03%/K in the range +10°C-50°C
- the transducer was calibrated at 20°C

Assuming:

- a rectangular distribution
- the instrument is operating between +10°C and +30°C

- the effect causing non-linearity, hysteresis and the temperature effect are independent the one from the other

the standard deviation is estimated to be 0.38% (0.95 Pa).

Quantity $X_i$	estimate $x_i$	'uncertainty'	probability distribution	standard uncertainty $u(x_i)$	sensitivity coefficient $c_i$	uncertainty contribution $u_i(y)$
$\Delta p_{\text{linearity}}$	$\Delta p$	0.5% FS	rectangular	0.29% FS	1.0	0.29% FS
$\Delta p_{\text{hysteresis}}$	$\Delta p$	0.1% FS	rectangular	0.058% FS	1.0	0.058% FS
$\Delta p_{\text{temperature}}$	$\Delta p$	0.3% FS	rectangular	0.17% FS	1.0	0.17% FS
$\Delta p_{\text{DAQ}}$	$\Delta p$	0.3% FS	rectangular	0.17% FS	1.0	0.17% FS
$\Delta p$	$\Delta p$					0.95 Pa

\*FS: Full Span (250 Pa)

Table 37. Uncertainty contribution of the differential pressure meter

#### 6.4.18 Uncertainty on the component $T_{ms}$

The combustion gas temperature at the height of the measuring section (ms) is measured by means of three K-type, sheathed and insulated, thermocouples having an outside diameter of 0.5mm. The position of the tips is at a radius of  $(87 \pm 5)$ mm from the axis and with  $120^\circ$  mutual angular distance.

✓ Tolerance on a new thermocouple  $t_t$ :

The quality system maintained in the Ghent University fire laboratory prescribes the use of Class 2 thermocouples according to IEC 60584-2<sup>[11]</sup>. The tolerance allowed on new Class 2 thermocouples according to this standard is:

- $\pm 2.5^\circ\text{C}$  in the range  $-40^\circ\text{C}$  to  $333^\circ\text{C}$
- $\pm 0.0075 t$  (t in  $^\circ\text{C}$ ) in the range  $333^\circ\text{C}$  to  $1200^\circ\text{C}$

✓ Effect of ageing  $t_a$ :

Due to ageing effects an additional uncertainty should be taken into account. Based on ageing effects of K-type sheathed thermocouples after 50 hours of use inside a furnace for fire resistance tests<sup>[12]</sup> a variance of  $\pm 2^\circ\text{C}$  can be expected for temperature measurements around  $120^\circ\text{C}$ . Since K-type thermocouples are subject to calibration changes on temperature cycling to  $500^\circ\text{C}$  or above (like in fire resistance tests), and since no temperatures above  $400^\circ\text{C}$  are to be expected in the SBI, it is reasonable to say that ageing effects will be limited to  $\pm 2^\circ\text{C}$  around the nominal value.

✓ Effect of data acquisition and extension wires  $t_{DAQ}$ :

The uncertainty related to the data acquisition, extension wires and connectors is estimated (6.4.1) to be 1.0 K.

✓ Radiation error  $t_r$ :

Another important effect is the radiation error. Due to the thermal inertia of the duct system, the thermocouple will initially see a 'cold' surface when gas temperatures start to rise. This results in an underestimation of the real gas temperature. Further on in the test when temperatures decay, the thermocouple sees a 'hot' duct surface and will overestimate the gas temperature. This effect is non-linear and is judged to have a standard uncertainty of  $\pm 2.2^\circ\text{C}$  (annex B.5).

✓ Velocity error  $t_v$ :

The error related to the velocity has its origin in the fact that not all of the kinetic energy of the fluid is recovered when a gas is brought to rest near a thermocouple. Ideally the gas should be brought to rest



adiabatically. The recovery factor is  $\alpha = 0.68 \pm 0.07^{[25]}$  for wires normal to the flow. The error associated with the velocity is given by

$$(1 - \alpha) \frac{v^2}{2c_p} \quad [ 6.131 ]$$

whereby  $v$  is the mean velocity,  $c_p$  is the specific heat of the thermocouple material and  $\alpha$  is the recovery factor.

Initially the velocity at the height of the thermocouples in the SBI is around 8 m/s. This value can increase to approximately 16 m/s when the gas temperature rises to 300°C and keeping the mass flow constant.

Assuming that:

- $\alpha = 0.68$
- $v = 16$  m/s
- $c_p = 500$  J/kg.K

the overestimation of the temperature is 0.08 K

✓ Conduction error  $t_c$ :

The thermocouples are inserted into the exhaust duct perpendicular to the flow over a length of about 7 cm. Conduction errors can therefore be neglected.

✓ Transient error  $t_\tau$ :

The transient error associated with the response time  $\tau$  of the thermocouple is given by

$$\tau \frac{dT}{dt} \quad [ 6.132 ]$$

$\tau$  is estimated theoretically to be approximately  $\tau = 1.15$  s (annex B.2) for flow gases around room temperature. For higher temperatures the time constant decreases slightly resulting in a reduced error. For a heptane calibration according to the SBI standard the maximum initial temperature rise is of the order of 2.5 °C/s which results in a maximum underestimation of about 2.84 °C. This calibration can be seen as the maximum temperature rise of the smoke gases at the height of the measuring section.

Quantity $X_i$	estimate $x_i$	'uncertainty'	probability distribution	standard uncertainty $u(x_i)$	sensitivity coefficient $c_i$	uncertainty contribution $u_i(y)$
$t_t$	0 °C	2.5 °C	rectangular	1.44 °C	1.0	1.44 °C
$t_a$	0 °C	2.0 °C	rectangular	1.15 °C	1.0	1.15 °C
$t_{DAQ}$	0 °C	1.0 °C	normal	1.0 °C	1.0	1.0 °C
$t_r$	0 °C	2.2 °C	normal	2.2 °C	1.0	2.2 °C
$t_v$	0.04 °C	0.04 °C	rectangular	0.023 °C	1.0	0.023 °C
$t_c$	0.0 °C	0.0 °C	-	0.0 °C	1.0	0.0 °C
$t_\tau$	0 °C	2.84 °C	triangular	1.16 °C	1.0	1.16 °C
T	0 °C					3.2 °C

Table 38. Uncertainty contribution of the temperature measurement

If type 1 thermocouples would be used, the uncertainty contribution would slightly reduce to 3.0 °C. If however, in addition, the thermocouple would be shielded, the uncertainty contribution drops to 2.1°C.

If transient errors are neglected, as discussed in paragraph 6.4.2.3, the component  $t_\tau$  drops out.

## 6.5. Conclusions

In this chapter a theoretic uncertainty estimate of the values used in the SBI for classification – FIGRA and  $THR_{600s}$  – and of the MARHE value have been derived along the lines of the ISO Guide to the Expression of Uncertainty in Measurements (GUM).

It is the first study that does not limit itself to the estimation of the uncertainty of the heat release rate, but also treats the derived parameters FIGRA and  $THR_{600s}$ .

Different from previous attempts to estimate uncertainty in fire testing, asymmetric distributions are used where necessary, correlations between the oxygen, carbon dioxide, differential pressure and exhaust gas temperature are taken into account and a method to deal with uncorrected bias has been introduced.

Furthermore this dissertation estimates for the first time the uncertainty related to transient phenomena and to asynchronous data.

Next the uncertainty is estimated on all measurands and for all calculation steps whereby some of the uncertainties are for example heat release rate dependent. This makes that it is often not possible to assign a fixed uncertainty to a specific measurand. Assigning a fixed number would often require overestimation of the uncertainty.

The uncertainty will therefore be calculated in function of time for some real test data in the next chapter.

It should be noted that the determination of the uncertainty has been worked out for the Ghent University test rig wherever a general approach for all laboratories was not possible.

## 7 Evaluation and results of the Analytical Model

### 7.1. Introduction

Chapter 7 brings together all the information of the previous chapters into one analytical uncertainty estimation model and includes the cascade of all uncertainties. Since several uncertainties are function of for example the heat release rate, the uncertainty estimate is function of time. In this chapter the analytical model is applied to some real test data.

After checking the model that it corresponds with the formulas presented in chapter 6, the results of the model are first compared with the results of SBI RR2. A round robin is another, independent way to come to an uncertainty estimate on the values used for classification.

Next the model is used to evaluate the changes suggested in chapters 5 and 6 in relation to uncertainty reduction.

### 7.2. Comparing the model with the SBI RR2 results

One way to check the ability of the model to estimate the uncertainty interval is to compare its results with the results that followed out of SBI RR2<sup>[70]</sup>. In this round robin, the Ghent laboratory formed part of a first group of ten labs – nine of which reported in due time – who had to test three samples three times.

The results of the estimated repeatability limits  $r$  on the values used for classification i.e. FIGRA and  $\text{THR}_{600s}$  – obtained by means of a round robin exercise and by means of the analytical model – are compared. The repeatability limit is defined as *the value less than or equal to which the absolute difference between two test results obtained under repeatability conditions may be expected to be with a probability of 95%.*<sup>[15]</sup>

$$r = \sqrt{2}U \quad [7.1]$$

The relative repeatability limit,  $r/m$ , is further defined as

$$\frac{r}{m} = \frac{\sqrt{2}U}{m} \quad [7.2]$$

whereby  $m$  represents the measured value,  $U$  represents the expanded uncertainty for a 95% confidence interval ( $1.96 \cdot u$  for a normal distribution) and whereby the factor  $\sqrt{2}$  arises from the fact that  $r$  refers to the difference between two single test results.

### 7.2.1 Repeatability limit estimated by means of round robin

A first way to estimate the repeatability limit of a given test instrument is to perform a statistical analysis in accordance with ISO 5725. In SBI RR2 a first group of nine laboratories tested three products (P1 – P3) three times which resulted in the repeatability limits on the values FIGRA and THR<sub>600s</sub> as shown in Table 39.

	<b>P1: Faced glass wool</b>		<b>P2: MDF board</b>		<b>P3: Plastisol coated steel</b>	
	Figra (W/s)	THR <sub>600s</sub> (MJ)	Figra (W/s)	THR <sub>600s</sub> (MJ)	Figra (W/s)	THR <sub>600s</sub> (MJ)
<b>SBI RR2 test results of 9 laboratories</b>						
<b>m</b> (mean value)	17	1.0	455	25	257	1.8
<b>r</b>	9	0.2	31	1	41	0.3
<b>r/m</b>	<b>52 %</b>	<b>22 %</b>	<b>7 %</b>	<b>4 %</b>	<b>16 %</b>	<b>17 %</b>

Table 39. Repeatability limits for products P1-P3 by means of round robin

Note that, for every product, 27 (9 x 3) tests have been done to obtain the estimate on the relative repeatability limit.

In addition, it must be stressed that the so found repeatability limits are a sort of mean value for this group of nine laboratories and also includes variance related to non-technical issues like e.g. operator, etc. Individual laboratories may have higher or lower repeatability limits than the group mean which makes that the comparison of the results with the ones found by the analytical model requires the necessary prudence.

### 7.2.2 Repeatability limit estimated by means of small sample t-test

A second approach consists of using the SBI RR2 test results of the Ghent laboratory only, and to estimate the repeatability limits out of a small sample t-test as follows. The sample standard deviation 's' is multiplied with a t-distribution coefficient  $t_{0,025}$  with two degrees of freedom ( $n = 3$  samples;  $t_{0,025} = 4.3$ ), instead of with the normal distribution coefficient  $z_{0,025} = 1.96$ , to obtain an expanded

uncertainty  $U$  with a 95% confidence interval. By widening the uncertainty interval, a 95% confidence interval can still be maintained although it is based on a limited number of observations.

$$U = t_{0.025} \frac{s}{\sqrt{n}}$$

The expanded uncertainty then combines with formula 7.2 to obtain the relative repeatability limit  $r/m$ . The results are summarised in Table 40.

	<b>P1: Faced glass wool</b>		<b>P2: MDF board</b>		<b>P3: Plastisol coated steel</b>	
	Figra (W/s)	THR <sub>600s</sub> (MJ)	Figra (W/s)	THR <sub>600s</sub> (MJ)	Figra (W/s)	THR <sub>600s</sub> (MJ)
<b>SBI RR2 test results of the Ghent laboratory (t-test)</b>						
Sample 1	27.38	1.347	490.28	25.166	276.76	1.923
Sample 2	19.73	1.064	490.13	24.937	240.33	1.782
Sample 3	18.33	1.216	502.27	24.811	204.84	1.8
mean m	21.81	1.209	494.23	24.971	240.64	1.835
s	4.87	0.142	6.97	0.180	35.96	0.0767
r	12.09	0.352	17.29	0.4468	89.28	0.1905
<b>r/m</b>	<b>55.44%</b>	<b>29.08%</b>	<b>3.50%</b>	<b>1.79%</b>	<b>37.10%</b>	<b>10.38%</b>

Table 40. Repeatability limits for products P1-P3 by means of small sample t-test

### 7.2.3 Repeatability limit estimated by means of the analytical model

Finally, the third approach makes use of the analytical model. The model allows to calculate the repeatability limit on all three individual samples of the SBI RR2 test results of the Ghent laboratory.

In order to be able to compare the results with the previous two cases, the uncertainty related to transient phenomena is neglected and no bias corrections are done. This because all laboratories have similar instrumentation and no correction for bias and/or transient phenomena is done.

Though the instrumentation is similar, it is not identical and the response times of measuring devices may still differ a lot from laboratory to laboratory. This makes that we expect that the repeatability limit resulting from the round robin will be higher than the one calculated by means of the analytical model.

Table 41 shows the estimated relative repeatability limits  $r/m$  for all three individual samples on the three products tested. Two cases are given. One where the running average on the Heat Release Rate

reduces the uncertainty on the same, and one where we assume that the running average leaves the uncertainty on HRR unchanged as explained in section 6.3.2.

	<b>P1: Faced glass wool</b>		<b>P2: MDF board</b>		<b>P3: Platisol coated steel</b>	
	Figra (W/s)	THR <sub>600s</sub> (MJ)	Figra (W/s)	THR <sub>600s</sub> (MJ)	Figra (W/s)	THR <sub>600s</sub> (MJ)
<b>Analytical model (assumption: running average on HRR reduces uncertainty)</b>						
<b>r/m (Sample 1)</b>	<b>36.8 %</b>	<b>14.3 %</b>	<b>5.5 %</b>	<b>1.4 %</b>	<b>12.6 %</b>	<b>12.2 %</b>
<b>r/m (Sample 2)</b>	<b>79.6 %</b>	<b>34.4 %</b>	<b>5.9 %</b>	<b>1.7 %</b>	<b>12 %</b>	<b>10 %</b>
<b>r/m (Sample 3)</b>	<b>33 %</b>	<b>14.8 %</b>	<b>5.5 %</b>	<b>1.4 %</b>	<b>16.5 %</b>	<b>13.3 %</b>
<b>Analytical model (assumption: running average on HRR does not reduce uncertainty)</b>						
r/m (Sample 1)	120.3 %	15.1 %	17.4 %	1.6 %	48.6 %	13 %
r/m (Sample 2)	259.2 %	35.4 %	18.1 %	1.7 %	39.2 %	10 %
r/m (Sample 3)	108.9 %	15.8 %	16.3 %	1.4 %	51.6 %	13.3

Table 41. Repeatability limits for products P1-P3 by means of analytical model

The relative repeatability limits r/m of the model are in line with the values that follow out of the statistical analysis of the results of the nine labs. And this for materials that produce both low heat release rates – like product 1 – and materials with higher heat release rates – like product 2.

In general, the repeatability limits estimated out of the analytical model are somewhat lower than the ones found out of the round robin. This can reasonably be attributed to neglecting – for reasons of comparison of the different methods as explained above – all transient phenomena and to the qualitative test data of the Ghent fire laboratory. The Ghent fire laboratory has always played a leading role on the international fire scene especially in heat release rate related test equipment.

The assumption that the measurements to obtain the heat release rate results are uncorrelated, as discussed in section 6.3.2 (30 s averaging results in a reduction of the uncertainty by a factor  $\sqrt{N}$  whereby N is the number of samples used for averaging;  $r = 0$ ), produces far more realistic results than the assumption that the measurements are highly correlated (uncertainty does not reduce;  $r = 1$ ). The hypotheses that all measurements can be treated as independent therefore seems to hold.

All measurements will further be treated as being independent the one from the others.

These first results suggest that the analytical model can be used to estimate the uncertainty interval for routine testing. This offers huge advantages over the actual approach where uncertainty estimates are

based on round robin results. Since the latter have a very large range, the results can only be applied to *similar* products and even then, one may argue what the *real* confidence interval is. As an example both the range and the average repeatability limits of SBI RR2 are given below<sup>[70]</sup>.

	<b>FIGRA<sub>0,2MJ</sub></b>	<b>FIGRA<sub>0,4MJ</sub></b>	<b>THR<sub>600s</sub></b>
Number of products	9	9	9
Range r /m	7 - 70 %	7 - 93 %	4 – 35 %
Average r /m	32 %	38 %	23 %
Number of products *	5	4	2
Range r /m *	7 – 29 %	7 – 35 %	4 – 27 %
Average r /m *	16 %	20 %	16 %
*: products with very low mean values –which are less relevant for classification – excluded			

Table 42. repeatability limits as of SBI RR2



### **7.3. Using the model to improve the test method**

Besides the estimation of the uncertainty interval, the model presented provides an understanding of the contributors, that cause the uncertainty of the measurement process and their relative magnitude. This is a major strength of the GUM method which allows us to efficiently improve the test method. A round robin exercise is not able to do that.

A limitation of the method is that it is based on assumed distributions. The estimate of the measuring uncertainty cannot be any better than these assumptions. Fortunately, the error committed when assuming the wrong distribution, generally changes the effect of the contributor no more than 15 - 20 % and it is possible to always err on the safe side, by always choosing the most conservative of the two considered distributions, when in doubt. As we see, it is only the largest contributor for which it is critical to assume the correct distribution, since a 15 - 20 % change in the influence of any other contributor would be negligible.

This section discusses a detailed uncertainty analysis under different assumptions. To help the discussion, all calculations will be based on the test results of a *fourth sample* of product P2 (MDF). The sample was supplied as a spare in the round robin exercise and was tested – for the occasion of the present study – with the data acquisition running at 10 samples a second (10 Hz) and an integration time of 1 PLC (20 ms). Several Keithley multimeters have been used in parallel for this test.

For the first three cases discussed below, the data set was reduced afterwards to have sampled data every three seconds. This was done by simply taking every n-th point ( $n = 30$ ).

#### **7.3.1 Case 1: SBI according to EN 13823**

In a first case 1, the values used for classification together with the associated combined global uncertainty are calculated when running the equipment in accordance with the SBI standard. Different from section 7.2, the uncertainty related to transient phenomena and related to uncorrected bias are included. A – worst case – fixed uncertainty interval is used for transient phenomena as discussed in 6.4.2.1.c.

top level (relevant for HRR)	sub-level (relevant for $X_i$ )	contribution to $u(X_i)$	contribution to $u(\text{HRR}_{30\text{kW}})$
Quantity $X_i$	Quantity $x_j$	$c(x_j).u(x_j)/X_i$ (%)	$c(X_i).u(X_i)/\text{HRR}$ (%)
$V_{D298}$			<b>7.20479</b>
	c	1.97998	
	A	1.73538	
	$k_t$	2.57009	
	$k_p$	6.12593	
	$\Delta p$	0.75892	
	$T_{ms}$	0.518	
$\phi$			<b>22.5903</b>
	$X_{O_2}$	21.98039	
	$X_{CO_2}$	2.43105	
	$X_{O_2}^\circ$	4.7441	
	$X_{CO_2}^\circ$	0.53061	
E			2.55814
$X_{O_2}^{D^\circ}$			0.12155
	$X_{O_2}^\circ$	0.0537	
	H	0.03003	
	p_bar	0.00092	
	$T_{room}$	0.10483	
$\alpha$			0.08607
standard uncertainty on HRR (excluding cross correlations)			<b>23.86279</b>
standard uncertainty on HRR (including cross correlations)			<b>26.32742</b>

Table 43. Uncertainty analysis at HRR = 30kW (case 1)

Table 43 represents an uncertainty analysis on the Heat Release Rate at the 30 kW level. The 30 kW level corresponds to the contribution of the burner and is, especially for materials that end up in class A2 or B, the most important level.

Column 1 represent those quantities  $X_i$  that compose the heat release rate Formula 2.1. The second column represents those quantities  $x_i$  that compose the quantities  $X_i$ . Columns 3 and 4 represent the contribution of the different components to the combined standard uncertainty on the heat release rate.

The last two rows of the table summarise the standard uncertainty on the heat release rate: 1) without taking into account cross correlations or 2) taking cross correlations into account as discussed in 6.2.5.2.

$k = 2$ (95%)	$m$	$U+(m)$	$U-(m)$	$U+/m$	$U-/m$	$r/m$
FIGRA (W/s)	520.6	43.7	54.8	8.4 %	10.5 %	<b>14.8 %</b>
THR600s (MJ)	27.19	0.69	0.82	2.5 %	3 %	<b>4.2 %</b>
MARHE (kW)	49.72	1.54	1.85	3.1 %	3.7 %	<b>5.2 %</b>

Table 44. Uncertainty analysis on values used for classification and the MARHE value  
( $k = 2$ ) (case 1)

Table 44 summarises the mean value  $m$  of the values used for classification and the MARHE value, together with the expanded (upper  $U+$  and lower limit  $U-$ ) uncertainty for a 95% confidence interval and the relative expanded uncertainty  $U/m$ . The last column gives the estimated repeatability limit  $r/m$ .

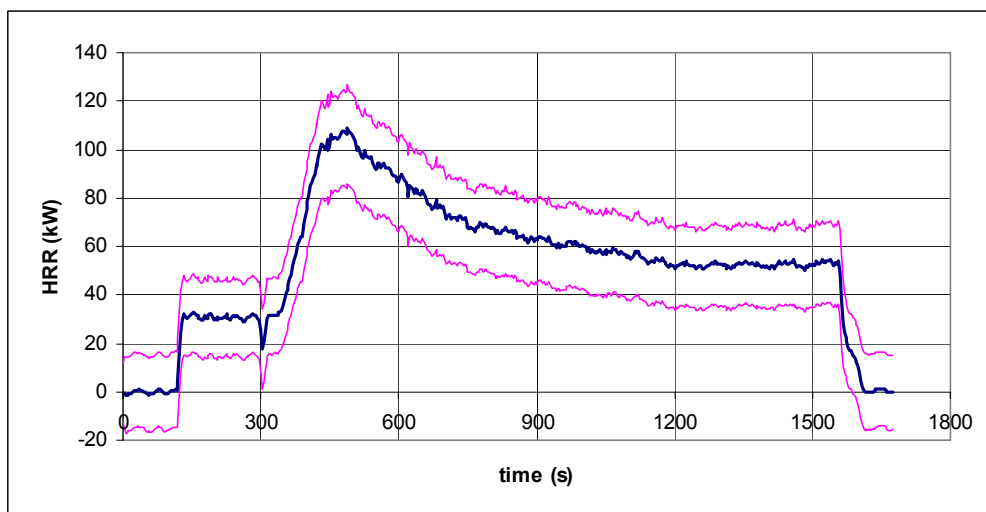


Figure 61. HRR curve with 95% confidence interval ( $k = 2$ ) (case 1)

Figure 61 shows the heat release rate curve together with its 95% confidence interval.

As expected, the standard uncertainty on the depletion factor and more specific the oxygen concentration, is huge because the uncertainty related to the transient error is based on the steep heat release rate rise of a heptane pool fire. For the majority of products tested in the SBI, the resulting uncertainty interval is far too conservative. Taking appropriate measures, as discussed in case 3, reduces this uncertainty to substantially lower levels.

Besides the depletion factor  $\phi$ , the uncertainty contribution of the flow rate  $V_{D298}$  is also substantial. Case 2 focuses on how to reduce this contribution.

### 7.3.2 Case 2: Eliminating systematic errors and introducing obvious improvements

In chapter 6, some measures have been proposed to eliminate some known bias and to reduce the standard uncertainty on some components. Case 2 quantifies, for this particular MDF-test, the effect when introducing the proposed changes (Table 45).

Action	see section	bias correction	u(x) old	u(x) new
The use of a 'four wire RTD' <sup>(*)</sup> instead of a thermocouple to measure ambient temperature	6.4.10	-	1.8 (°C)	0.18 (°C)
Calculate 'c' instead of assuming it constant	6.4.12	variable	0.16 (..)	0.013 (..)
Remove bias from the cross sectional area 'A'	6.4.13	-0.49 <sup>E-3</sup> m <sup>2</sup>		
Use of alternative pressure probe	6.4.16	0.025 (-)	0.021 (-)	0.008 (-)
Use of shielded type 1 thermocouples	6.4.18	-	3.3 (°C)	2.1 (°C)
*Note that the four wire RTD also helps to reduce the uncertainty on the 'c' factor as explained in 6.4.12				
*RTD: Resistive Temperature Detector				

Table 45. Procedure and apparatus measures taken to improve accuracy

Besides the actual heat release rate test, these measures will also improve the  $k_{t,qgas}$  and  $k_{t,qheptane}$  and resulting  $k_t$  value since these components are based on heat release rate test data. The effect on  $k_t$  has been simulated for this case.

top level (relevant for HRR)	sub-level (relevant for $X_i$ )	contribution to $u(X_i)$	contribution to $u(\text{HRR}_{30\text{kW}})$
Quantity $X_i$	Quantity $x_j$	$c(x_j).u(x_j)/X_i$ (%)	$c(X_i).u(X_i)/\text{HRR}$ (%)
$V_{D298}$			<b>2.94487</b>
	c	0.71429	
	A	0.5682	
	$k_t$	1.75234	
	$k_p$	0.74074	
	$\Delta p$	0.75892	
	$T_{ms}$	0.32964	
$\phi$			<b>22.5903</b>
	$X_{O_2}$	21.98039	
	$X_{CO_2}$	2.43105	
	$X_{O_2}^\circ$	4.7441	
	$X_{CO_2}^\circ$	0.53061	
E			2.55814
$X_{O_2}^{D^\circ}$			0.06241
	$X_{O_2}^\circ$	0.0537	
	H	0.03003	
	p_bar	0.00092	
	$T_{room}$	0.01048	
$\alpha$			0.08607
standard uncertainty on HRR (excluding cross correlations)			<b>22.86066</b>
standard uncertainty on HRR (including cross correlations)			<b>25.58986</b>

Table 46. Uncertainty analysis at HRR = 30kW (case 2)

The uncertainty contribution at the 30 kW level for the volume flow rate drops from 7.2% down to 3%. The most spectacular result is obtained by replacing the actual *bi-directional probe* (with the steel supporting rod) by the hemi-spherical probe (see 4.3). The uncertainty contribution drops from about 6% to below 1%.

As a result, the second highest contributor to the uncertainty, the  $k_t$  factor, also drops substantially (from 2.6% to 1.75%).  $u(k_t)$  would further improve by: 1) increasing the number of measurement positions in obtaining the velocity profile correction factor  $k_{t,v}$  (§6.4.15.2) and 2) by using the last N calibrations instead of just the most recent one in calculating  $k_{t,v}$ ,  $k_{t,qgas}$  and  $k_{t,qheptane}$  (see 6.4.15).

Next the uncertainties on the *factor c and cross sectional area A* drop from around 2% to values well below 1%. The original uncertainty – that basically can be attributed to uncorrected bias – related to the factor c strongly depends on ambient condition and is therefore variable. It can exceed the 2%.

The uncertainty on the cross sectional area A is, different from what was found by Axelsson et al<sup>[62]</sup>, not negligible and this because of a bias error. After correcting for this bias, the uncertainty reduces to an almost negligible level.

The use of *shielded thermocouples* to measure the exhaust gas temperatures is of no real use to reduce the uncertainty.

The use of a *four wire RTD* to measure the incoming air temperature is of no real use to reduce the uncertainty on  $X^{D^{\circ}}_{O_2}$  but it is also used to substantially reduce the uncertainty on the factor ‘c’ as explained in 6.4.12. It is therefore recommended to replace the K-type thermocouple by a four wire RTD to measure the ambient air temperature.

k = 2 (95%)	m	U+(m)	U-(m)	U+/m	U-/m	r/m
FIGRA (W/s)	520.6	44	44	8.5 %	8.5 %	<b>12 %</b>
THR600s (MJ)	27.19	0.69	0.69	2.5 %	2.5 %	<b>3.5 %</b>
MARHE (kW)	49.72	1.55	1.55	3.1 %	3.1 %	<b>4.4 %</b>

Table 47. Uncertainty analysis on values used for classification and the MARHE value

(k = 2) (case 2)

The repeatability limit *r/m* on the values used for classification and MARHE reduces to between 15 % and 20 %.

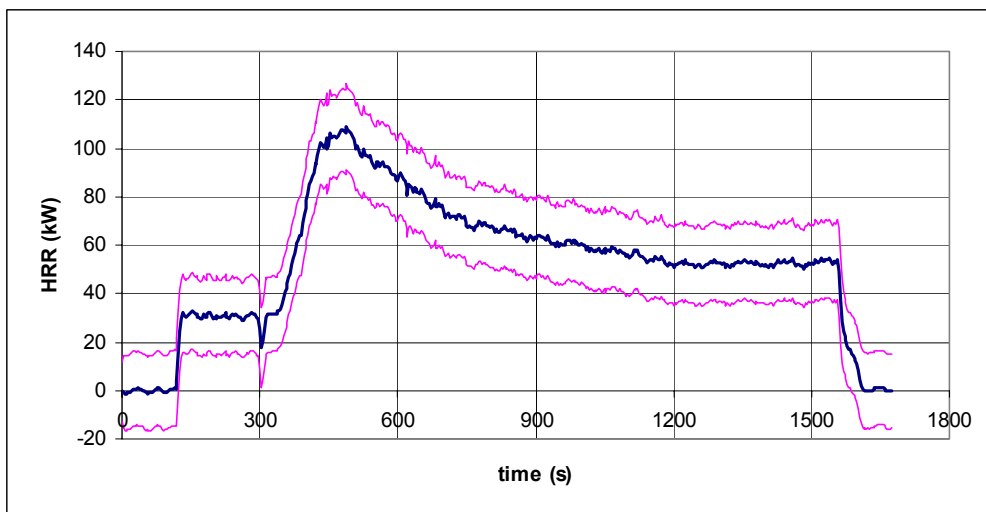


Figure 62. HRR curve with 95% confidence interval (k = 2) (case 2)

### 7.3.3 Case 3: Introduction of first level changes in the data acquisition

The assumption of a fixed uncertainty interval related to transient phenomena proves to be too conservative as demonstrated in case 1. Although these results would improve by more accurately estimating the transient error based on inverse techniques (see 6.4.2.1.b), a better solution is to modify the way measurement data are gathered and handled. In chapter 5 two alternative methods, called *first level* and *second level* changes, are proposed and are discussed in cases 3 and 4 respectively.

By introducing first level changes in the data acquisition the bandwidth reduces to 1/30 Hz and, as discussed in §5.4.1, we can further neglect any transient error. This results in a spectacular improvement of the uncertainty on the depletion factor  $\phi$ .

top level (relevant for HRR)	sub-level (relevant for $X_i$ )	contribution to $u(X_i)$	contribution to $u(\text{HRR}_{30\text{kW}})$
Quantity $X_i$	Quantity $x_j$	$c(x_j) \cdot u(x_j) / X_i$ (%)	$c(X_i) \cdot u(X_i) / \text{HRR}$ (%)
$V_{D298}$			<b>7.20495</b>
	c	1.97994	
	A	1.73538	
	$k_t$	2.57009	
	$k_p$	6.12593	
	$\Delta p$	0.76068	
	$T_{ms}$	0.51818	
$\phi$			<b>1.67323</b>
	$X_{O_2}$	1.46261	
	$X_{CO_2}$	0.7404	
	$X_{O_2}^\circ$	0.30752	
	$X_{CO_2}^\circ$	0.16127	
E			<b>2.55814</b>
$X_{O_2}^{D^\circ}$			0.10914
	$X_{O_2}^\circ$	0.00348	
	H	0.03003	
	$p_{bar}$	0.00092	
	$T_{room}$	0.10486	
$\alpha$			0.08595
standard uncertainty on HRR (excluding cross correlations)			<b>7.82789</b>
standard uncertainty on HRR (including cross correlations)			<b>7.97193</b>

Table 48. Uncertainty analysis at HRR = 30kW (case 3)

The uncertainty contribution at the 30 kW level for the depletion factor  $\phi$  drops below 2% and the uncertainty estimate is governed by the flow rate and more specific the bi-directional probe as discussed in the previous case.

$k = 2$ (95%)	m	U+(m)	U-(m)	U+/m	U-/m	r/m
FIGRA (W/s)	521.9	19.5	38.3	3.7 %	7.3 %	<b>10.3 %</b>
THR600s (MJ)	27.2	0.24	0.5	0.9 %	1.8 %	<b>2.5 %</b>
MARHE (kW)	49.77	0.56	1.17	1.1 %	2.4 %	<b>3.4 %</b>

Table 49. Uncertainty analysis on values used for classification and the MARHE value  
( $k = 2$ ) (case 3)

The repeatability limit  $r/m$  on the values used for classification and MARHE drops by approximately 30%

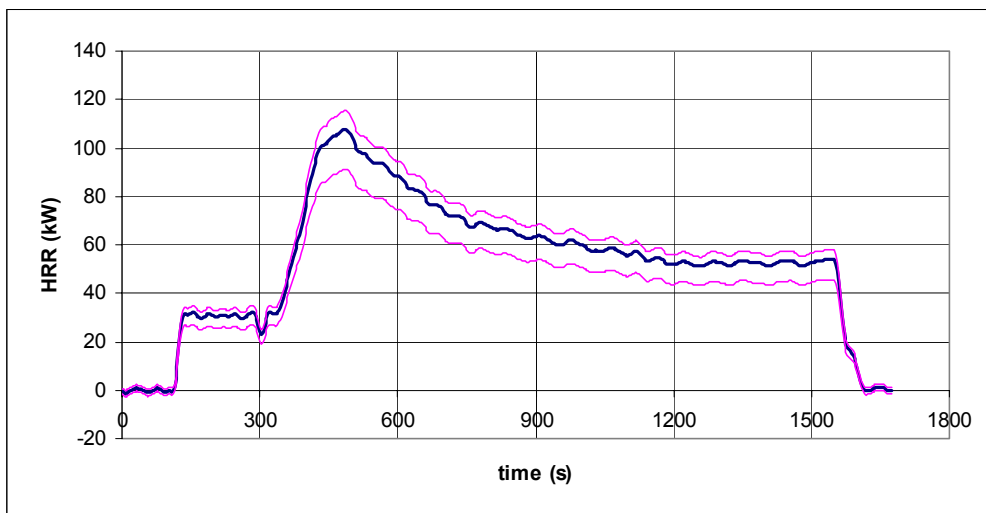


Figure 63. HRR curve with 95% confidence interval ( $k = 2$ ) (case 3)

The asymmetry in the 95% confidence interval is mainly due to the bias on the bi-directional probe (due to the steel supporting rod).



### 7.3.4 Case 4: Introduction of second level changes in the data acquisition

By introducing second level changes in the data acquisition the bandwidth reduces to 1/10 Hz and, as discussed in §5.4.2, we can further neglect any transient error.

For convenience, the data has been sampled at a scan rate of  $t_s = 3$  s after treating the data as set out in §5.4.2. For future use, we however recommend to re-sample the data at a scan rate of  $t_s = 1$  s in order not too loose relevant information though still keeping the data file within acceptable limits.

top level (relevant for HRR)	sub-level (relevant for $X_i$ )	contribution to $u(X_i)$	contribution to $u(\text{HRR}_{30\text{kW}})$
Quantity $X_i$	Quantity $x_j$	$c(x_j).u(x_j)/X_i$ (%)	$c(X_i).u(X_i)/\text{HRR}$ (%)
$V_{D298}$			7.20525
	c	1.97998	
	A	1.73538	
	$k_t$	2.57009	
	$k_p$	6.12593	
	$\Delta p$	0.76359	
	$T_{ms}$	0.5179	
$\phi$			1.66269
	$X_{O_2}$	1.45348	
	$X_{CO_2}$	0.73567	
	$X_{O_2}^\circ$	0.30545	
	$X_{CO_2}^\circ$	0.16023	
E			2.55814
$X_{O_2}^{D^\circ}$			0.10913
	$X_{O_2}^\circ$	0.00348	
	H	0.03003	
	$p_{bar}$	0.00092	
	$T_{room}$	0.10486	
$\alpha$			0.08648
standard uncertainty on HRR (excluding cross correlations)			7.82591
standard uncertainty on HRR (including cross correlations)			7.96855

Table 50. Uncertainty analysis at HRR = 30kW (case 4)

$k = 2$ (95%)	m	U+(m)	U-(m)	U+/m	U-/m	r/m
FIGRA (W/s)	517.4	18.4	36.4	3.6 %	7 %	<b>9.9 %</b>
THR600s (MJ)	27.14	0.24	0.5	0.9 %	1.8 %	<b>2.5 %</b>
MARHE (kW)	49.48	0.56	1.17	1.1 %	2.4 %	<b>3.4 %</b>

Table 51. Uncertainty analysis on values used for classification and the MARHE value  
( $k = 2$ ) (case 4)

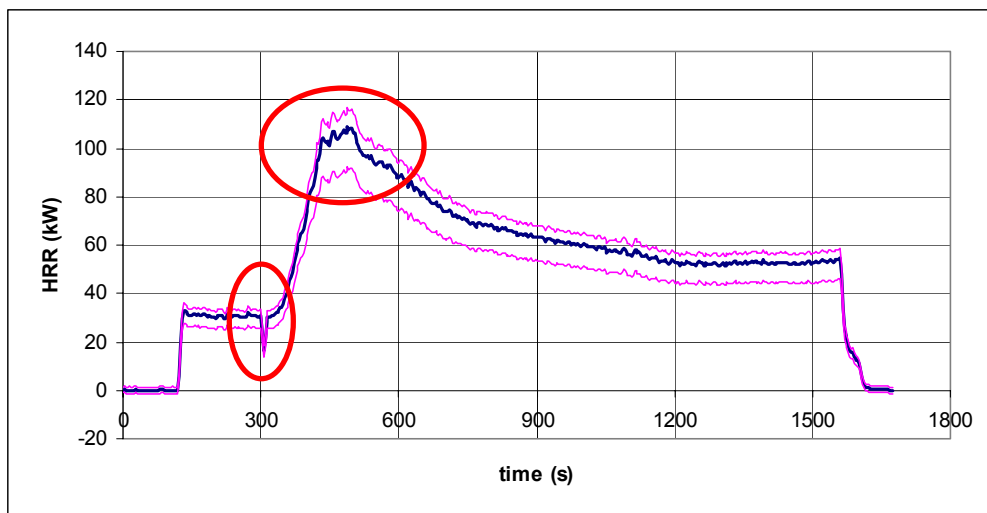


Figure 64. HRR curve with 95% confidence interval ( $k = 2$ ) (case 4)

The uncertainty estimate on the values used for classification when introducing second level changes to the data acquisition system is similar to when introducing first level changes (case 3).

The improvement does not lie in an improved confidence interval but rather in more qualitative measurement:

1. Due to the increased BW more detail is left in the data as can be seen by way of example on the heat release rate curve. In case 3 ( $BW = 1/30$  Hz) there is a monotonous increase in heat release to the peak value while in case 4 ( $BW = 1/10$  Hz) some fluctuations are observed around the peak. Also the switching between the burners around 300 s is more accurately represented by case 4.
2. Second level changes guarantee data free of aliasing while for first level changes this can not be guaranteed. Aliasing introduces, as explained in §6.4.3, phantom data; things are seen that are not there!
3. Second level changes allow for more accurate synchronisation of data. There is no need – as for first level changes – to resample the data from  $f_s = 1/3$  Hz up to  $f_s = 10$  Hz. Resampling also requires an assumption on the data behaviour in-between consecutive measurement points (linear, quadratic, ...)

Level two changes result, pure from a measurement point of view, in both a better repeatability and reproducibility. Since the data contains more information (larger BW), it includes more variation and

small differences in burning behaviour between different samples may (or may not) result in slightly higher repeatability and reproducibility limits in a round robin exercise.

### 7.3.5 Case 5: Combining case 2 and 3

As a result of the present work, the proposal is to introduce so called *first level* or *second level* changes to the SBI test method. First level changes require minor modification to only the calculation procedures while second level changes require substantial changes to both the calculation procedures and the data acquisition. Second level changes are the preferred option but require the political willingness to introduce them.

Case 5 represents the results for the MDF sample when introducing obvious changes as discussed under case 2 and, in addition, first level changes.

Case 6 is identical but introducing second level changes instead of first level changes.

top level (relevant for HRR)	sub-level (relevant for $X_i$ )	contribution to $u(X_i)$	contribution to $u(\text{HRR}_{30\text{kW}})$
Quantity $X_i$	Quantity $x_j$	$c(x_j).u(x_j)/X_i$ (%)	$c(X_i).u(X_i)/\text{HRR}$ (%)
$V_{D298}$			<b>2.94527</b>
	c	0.71429	
	A	0.5682	
	$k_t$	1.75234	
	$k_p$	0.74074	
	$\Delta p$	0.76068	
	$T_{ms}$	0.32975	
$\phi$			<b>1.67323</b>
	$X_{O_2}$	1.46261	
	$X_{CO_2}$	0.7404	
	$X_{O_2}^\circ$	0.30752	
	$X_{CO_2}^\circ$	0.16127	
E			<b>2.55814</b>
$X_{O_2}^{D^\circ}$			0.03202
	$X_{O_2}^\circ$	0.00348	
	H	0.03003	
	p_bar	0.00092	
	$T_{room}$	0.01049	
$\alpha$			0.08595
standard uncertainty on HRR (excluding cross correlations)			<b>3.80702</b>
standard uncertainty on HRR (including cross correlations)			<b>4.22578</b>

Table 52. Uncertainty analysis at HRR = 30kW (case 5)

k = 2 (95%)	m	U+(m)	U-(m)	U+/m	U-/m	r/m
FIGRA (W/s)	521.9	19	19	3.6 %	3.6 %	<b>5.1 %</b>
THR600s (MJ)	27.2	0.23	0.23	0.9 %	0.9 %	<b>1.3 %</b>
MARHE (kW)	49.77	0.54	0.54	1.1 %	1.1 %	<b>1.6 %</b>

Table 53. Uncertainty analysis on values used for classification and the MARHE value  
(k = 2) (case 5)

The repeatability limit r/m for Figra is estimated around 5% while for THR<sub>600s</sub> and MARHE it is estimated smaller than 2%.

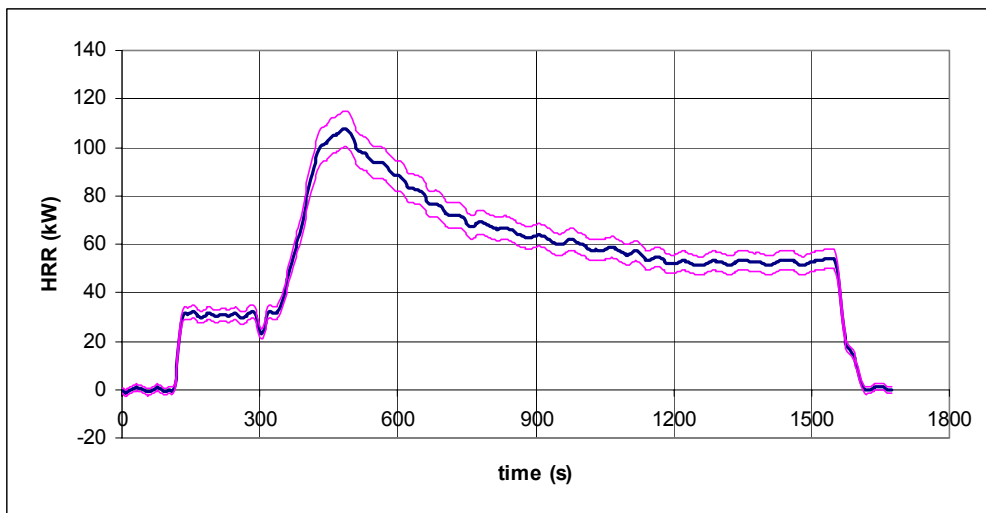


Figure 65. HRR curve with 95% confidence interval (k = 2) (case 5)

Comparing these results with the case where transient phenomena are neglected just like that and where uncertainties related to known biases are disregarded (Table 54, Table 55 & Figure 66), there apparently is no major improvement of the repeatability limit.

It must be said however that for case 5 the bias has been removed from the results, the synchronisation procedure has been improved and that dynamic aspects have been taken into account.

This makes that case 5 will have more reproducible results than is now the case.

top level (relevant for HRR)	sub-level (relevant for $X_i$ )	contribution to $u(X_i)$	contribution to $u(\text{HRR}_{30\text{kW}})$
Quantity $X_i$	Quantity $x_j$	$c(x_j).u(x_j)/X_i$ (%)	$c(X_i).u(X_i)/\text{HRR}$ (%)
$V_{D298}$			3.47275
	c	0.71429	
	A	0.5646	
	$k_t$	1.75234	
	$k_p$	1.94444	
	$\Delta p$	0.75892	
	$T_{ms}$	0.518	
$\phi$			1.84217
	$X_{O_2}$	1.64274	
	$X_{CO_2}$	0.75344	
	$X_{O_2}^\circ$	0.32433	
	$X_{CO_2}^\circ$	0.16363	
E			2.55814
$X_{O_2}^{D^\circ}$			0.10911
	$X_{O_2}^\circ$	0.00367	
	H	0.03003	
	$p_{bar}$	0.00092	
	$T_{room}$	0.10483	
$\alpha$			0.08607
standard uncertainty on HRR (excluding cross correlations)			4.36429
standard uncertainty on HRR (including cross correlations)			4.74209

Table 54. Uncertainty analysis at HRR = 30kW

(neglecting transient phenomena without first taking appropriate measures)

$k = 2$ (95%)	m	U+(m)	U-(m)	U+/m	U-/m	r/m
FIGRA (W/s)	520.6	21.8	21.8	4.2 %	4.2 %	5.9 %
THR600s (MJ)	27.19	0.27	0.27	1 %	1 %	1.4 %
MARHE (kW)	49.72	0.63	0.63	1.3 %	1.3 %	1.8 %

Table 55. Uncertainty analysis on values used for classification and the MARHE value

( $k = 2$ ) (neglecting transient phenomena without first taking appropriate measures)

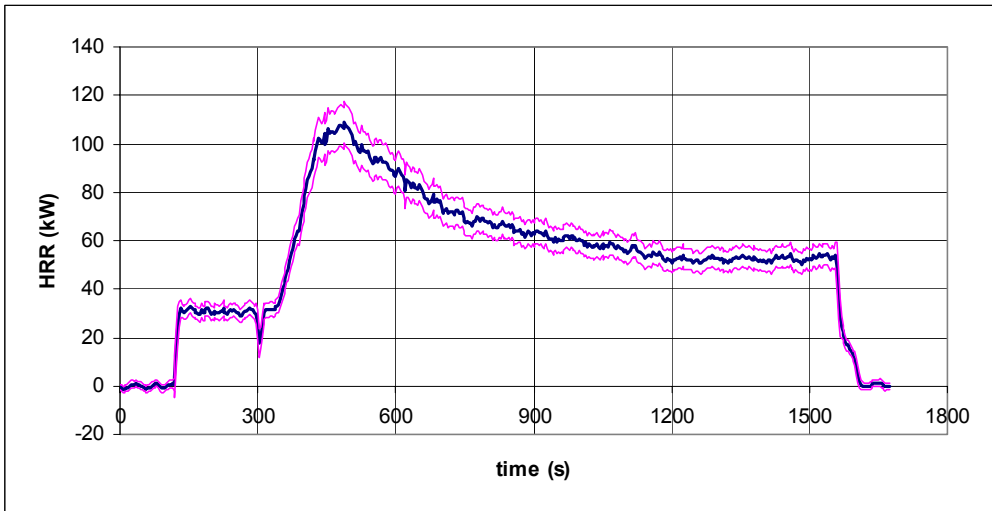


Figure 66. HRR curve with 95% confidence interval ( $k = 2$ )  
(neglecting transient phenomena without first taking appropriate measures)

### 7.3.6 Case 6: Combining case 2 and 4

Finally case 6 represents the optimised SBI test method including both the *obvious changes* as discussed in chapter 6 and the *second level changes* as discussed in chapter 5.

top level (relevant for HRR)	sub-level (relevant for $X_i$ )	contribution to $u(X_i)$	contribution to $u(\text{HRR}_{30\text{kW}})$
Quantity $X_i$	Quantity $x_j$	$c(x_j).u(x_j)/X_i$ (%)	$c(X_i).u(X_i)/\text{HRR}$ (%)
$V_{D298}$			3.47372
	c	0.71429	
	A	0.5646	
	$k_t$	1.75234	
	$k_p$	1.94444	
	$\Delta p$	0.76359	
	$T_{ms}$	0.5179	
$\phi$			1.66269
	$X_{O_2}$	1.45348	
	$X_{CO_2}$	0.73567	
	$X_{O_2}^\circ$	0.30545	
	$X_{CO_2}^\circ$	0.16023	
E			2.55814
$X_{O_2}^{D^\circ}$			0.10913
	$X_{O_2}^\circ$	0.00348	
	H	0.03003	
	p_bar	0.00092	
	$T_{room}$	0.10486	
$\alpha$			0.08648
standard uncertainty on HRR (excluding cross correlations)			<b>4.22624</b>
standard uncertainty on HRR (including cross correlations)			<b>4.48484</b>

Table 56. Uncertainty analysis at HRR = 30kW (case 6)

k = 2 (95%)	m	U+(m)	U-(m)	U+/m	U-/m	r/m
FIGRA (W/s)	517.4	19.7	19.7	3.8 %	3.8 %	5.4 %
THR600s (MJ)	27.14	0.26	0.26	1 %	1 %	1.4 %
MARHE (kW)	49.48	0.6	0.6	1.2 %	1.2 %	1.7 %

Table 57. Uncertainty analysis on values used for classification and the MARHE value

(k = 2) (case 6)



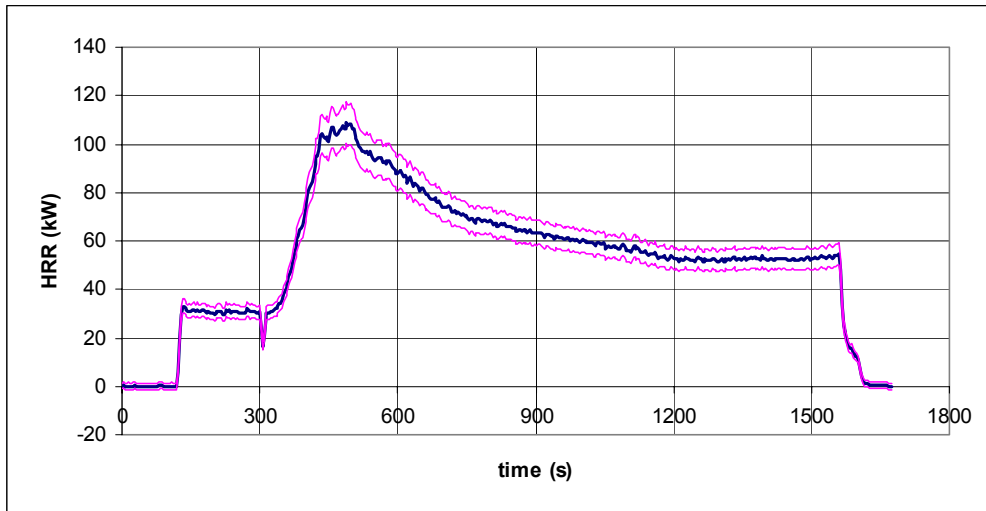


Figure 67. HRR curve with 95% confidence interval ( $k = 2$ ) (case 6)

Comparing cases 6 and 1, the standard uncertainty on the heat release rate at the 30 kW level drops from 26 % down to 4.5 %. The repeatability limit on the values used for classification reduces roughly with a factor 3.

It is also interesting to compare Figure 67 with Figure 61. Figure 67 contains more variation though less noise as can be seen well for the heat release values above 100 kW. There is also a spectacular improvement in the estimated 95 % confidence interval.

## 7.4. Conclusions

Chapter 7 discusses the results of a computer model based on the formulas presented in chapter 6. Comparison of the model with SBI RR2 results makes it likely that the model can be used confidently to estimate the repeatability limits on the values used for classification i.e. FIGRA and  $THR_{600s}$ .

Next it is shown that transient errors can drown out the uncertainty analysis and that they should at least be considered in the analysis. Reducing the bandwidth of the system to either 1/30 Hz or 1/10 Hz are two valid options to control transient phenomena. The first option is the cheapest and easiest one but dampens out variations with a periodicity below 30 s. The second option requires some new investments in data acquisition equipment and in software modifications but gives an unseen variance for events with a periodicity as low as 10 s, still eliminating disturbing noise. In addition it guarantees the complete elimination of spurious data on the results known as *aliasing*.

The changes as proposed in chapter 6 to remove *bias* and to improve the standard uncertainty on some individual components have a big impact on the global uncertainty estimate. The *bi-directional probe* ( $k_p$ ) as used in the SBI is the most critical factor for uncertainty but can easily be reduced to almost negligible levels. The proposals for change to the *factor c* and the *cross sectional area A* have both a positive effect on the uncertainty and are therefore recommended for inclusion in the reviewed SBI standard. The use of *four wire RTD* (Resistive Temperature Detector) to measure ambient temperature substantially reduces the uncertainty on the factor c and is therefore recommended.

The use of *shielded thermocouples* in the exhaust duct has a marginal effect on the overall uncertainty and can therefore be omitted.

## 8 Conclusions

### 8.1. Introduction

The SBI test method has been developed as a result of the implementation of the *Construction Products Directive* (CPD) 89/106/CE in Europe and is used now to assess the reaction to fire performance of construction products, excluding floorings, in the European Union.

The development of the SBI test method was ordered by the European Commission and carried out under direct guidance of the Fire Regulators Group. A consortium of nine fire testing laboratories was formed with the task to develop the method. The aim was to develop a test method that produces results representative for the behaviour of building products when exposed to typically one single burning object, e.g. a litter basket on fire, placed in the corner of a room.

The SBI test method was developed under high pressure of time because holding up the introduction of the free market for construction products in Europe. After acceptance of the design and prototypes a large interlaboratory round robin project was held. The results of the round robin demonstrated that the SBI test method is able to measure the required characteristics in a repeatable and reproducible way to an acceptable level, however under the condition of some further improvements.

In addition EN ISO 17025:1999<sup>[9]</sup>, - which sets out the general requirements for the competence of testing and calibration laboratories - makes the estimation, measurement and reporting of uncertainty of test results mandatory.

These two factors, the demand for technical improvements and the requirement for reporting uncertainty, are the immediate cause for this dissertation.

Few authors have published on the subject even in the larger framework of fire tests based on the oxygen depletion technique. The weak points in the work done so far are that:

- not all relevant phenomena are taken into account,
- the rough estimates made on uncertainties on the different components are sometimes very arbitrary,
- dynamic effects of the apparatus have not or insufficiently been taking into account,
- covariances between the different measurands have been neglected,
- uncertainties related to synchronisation are neglected.

So far, to the authors knowledge, only Axelsson et al. published an uncertainty analysis on the individual measurands of the intermediate scale SBI test. They however did not estimate the uncertainty on the values used for classification i.e. FIGRA and  $THR_{600s}$ . Other relevant publications are from the hand of Bryant et al. and Enright et al. who focus on the large scale respectively small scale test facilities.

This dissertation makes a significant contribution in developing a method of calculating experimental uncertainty in HRR measurements in general and to the SBI in particular. It brings into practice the general outlines of the ISO Guide to the Expression of Uncertainty in Measurement (GUM)<sup>[13]</sup>. The work faces items like dynamic effects, covariances, etc. avoided in previous approaches. It also brings to the attention phenomena like variation of the velocity and density profile due to thermal inertia of the duct system, the Reynolds dependence of the SBI pressure probe and the angular dependence of all probes currently used in intermediate to large scale fire tests.

After participating in the development of the SBI and in the first round robin exercise on the same test, the author has started the work on the present document.

### ***Evaluation of SBI pressure probe***

First a detailed study on the estimation of the different uncertainty components is made that goes far beyond any existing study in the field. From this dissertation it became clear that the pressure probe currently used in the SBI test is Reynolds dependent and the ‘probe constant’ is higher than stated in the standard. As a consequence, calibration of the equipment leads to underestimation of heat release and smoke production for products with reduced heat release rate and overestimation for products with a higher heat release rate. This is due to the modification of the pressure probe, introducing a supporting rod.

It is therefore strongly recommended to either include the Reynolds number in the heat release formulas or to omit the steel supporting rod and to stick to the original design of McCaffrey & Heskestad.

### ***Evaluation of the McCaffrey & Heskestad probe***

The original McCaffrey & Heskestad probe has a probe factor which is constant for Reynolds numbers above 2 500. This corresponds to the range that can practically be expected in the ISO Room Corner test, the SBI test and similar devices. If one wants to measure heat release in post flashover scenarios, the probe factor should be calculated as a function of Reynolds number.

The main disadvantage of the McCaffrey & Heskestad probe however is that angular distortions of the probe axis with respect to the exhaust duct axis introduce an error in the order of 2 to 4% (2% by 3°; 4% by 5°). Guide vanes upstream the pressure probe should help to reduce any angular distortion of the flow. Angular distortions result in an overestimation of the Heat Release Rate.

When installing a pressure probe in the exhaust duct, the operator should take readings of the pressure difference at different angles of attack ( $\theta$ ) in a range of 10° centred around the estimated zero angle ( $\theta = 0$ ). The minimum pressure difference will then indicate the exact zero ( $\theta = 0$ ) position.

Wind tunnel measurements indicated a lower probe constant – than the 1.08 currently used – for the McCaffrey & Heskestad probe. The  $k_p$ -factor is estimated to be 1.046 for an aspect ratio  $L/D = 2$ , with a standard uncertainty of +0.009 and -0.011. Modifying the aspect ratio  $L/D$  requires a new calibration.

#### ***Development of a hemispherical pressure probe***

Heat release measurements would benefit from an optimised pressure probe design limiting the sensitivity to angular variations but without compromising on the benefits of the actual probes. As a result of these findings, further research has been undertaken which has resulted in a newly developed, hemispherical pressure probe design that combines a low angular sensitivity with Reynolds independency over a wide range.

The probe factor is estimated at  $1.224 \pm 0.008$  for Reynolds numbers in the range 5 000 to 60 000. This corresponds to a pressure gain with respect to a Pitot-static tube of approximately 50%. The probe is insensitive to angular variations over a range that exceeds  $\pm 20^\circ$ . Furthermore it is expected that it will behave at least equally as good in smoky environments as the bi-directional probe. First experiments seem promising.

The design is straightforward, its limited size make that only a small hole needs to be drilled to install it and the head losses related to drag of the probe are negligible. Furthermore, no accurate alignment is needed when installing or servicing the probe.

The use of the hemispherical probe is not limited to closed conduits nor to fire applications.

#### ***Introduction of 'bluff-body blockage' in fire testing***

When bluff bodies are placed in a flow, they modify the streamlines of the undisturbed flow. In closed conduits, the disturbance is however much higher than one would – at first view – expect comparing the cross sectional areas of both the object and the conduit.

The probe factor  $k_p$  should therefore be corrected for ‘bluff-body blockage’ when used in ducts with reduced diameter. The correction factor to be applied is given in sections 4.2 and 4.3.

#### ***Effect of thermal inertia of the duct on the heat release rate***

The thermal time constant of the SBI duct system lies in the order of 220 s. So for all burning phenomena with a time constant in the same order of magnitude or smaller, transient thermal effects add to the overall uncertainty. The sharper the temperature rise or fall and the higher the magnitude, the larger the error. The maximum underestimation of the calculated mass flow rate for sudden, high heat releases is estimated to 1.4% for the SBI test equipment running at constant mass flow rate. Based on this value, the standard uncertainty related to temperature effects in the SBI is estimated to 0.6%. When running at constant volume flow rate, the standard uncertainty reduces to 0.3% for the specific case of the SBI.

Since all values used for classification in the SBI are based on the first part of the test, i.e. the heating phase, the uncertainty may be considered as a one sided distribution when calculating the global uncertainty on these values.

So, in summary, transient thermal effects tend to underestimate the mass flow rate through the duct system.

Knowing the velocity profile in the duct at anyone time, is of no use to correctly measure the mass flow rate if one does not know the density distribution in the measuring section over time. The derived velocity profile correction factor may as well be taken as a constant based on calibrations.

It is better to measure the velocity in multiple points by installing several *thermocouple – pressure probe pairs* as for example applied in the NIST 3 Megawatt Facility<sup>[64]</sup>. Bluff-body blockage will however become more important and should certainly be corrected for.

#### ***Uncertainty analysis including on the values used for classification***

In chapter 6 an uncertainty estimate of the values used in the SBI for classification – FIGRA and  $THR_{600s}$ , – and of the MARHE value have been derived along the lines of the ISO Guide to the Expression of Uncertainty in Measurements (GUM).

It is the first dissertation that does not limit itself to the estimation of the uncertainty of the heat release rate, but also treats the derived parameters FIGRA and  $THR_{600s}$ .

#### ***Inclusion of transient phenomena, bias correction, correlations etc.***

Different to previous attempts to estimate uncertainty in fire testing, asymmetric distributions are used where necessary, correlations between the oxygen and carbon dioxide concentration, differential

pressure and exhaust gas temperature are taken into account and a method to deal with uncorrected bias has been introduced.

Furthermore this dissertation estimates for the first time the uncertainty related to the transient character of the measurement and to asynchronous data.

### ***Detailed study on the estimation of the different uncertainty components***

A detailed study on the estimation of the different uncertainty components is made that goes far beyond any existing study in the field. This includes amongst others an estimation on the heat of combustion  $E$  for pure substances like propane and heptane, a heat release dependent uncertainty on both the oxygen and carbon dioxide concentration, an uncertainty estimate on the cross section of the exhaust duct and an estimate for the velocity pressure probe  $k_p$  and the velocity profile correction factor  $k_t$ .

### ***Introduction of the 'bandwidth' concept in fire testing***

In chapter 5, the concept of bandwidth (BW) – well known in electronics engineering and process control – has been introduced. The BW is the frequency below which an input signal is transferred without substantial distortion in amplitude and/or phase-shift. If a signal is passed through a filter whose BW is less than that of the signal, the result is a smearing or broadening of the input waveform.

Peak heat release rate values, which are often used in fire regulations, are meaningless if not accompanied with the BW of the test instrumentation. The consequence for the European classification system is that test results for products that did not go to flashover in the Room Corner test end up with a high uncertainty interval because based on peak heat release rate divided by the time to reach this peak. The large scale Room Corner test is considered, within the European classification system, the reference scenario for behaviour of products in 'real' fires. The criteria for the classification system in the SBI and other intermediate scale tests have been based on how well they correlate with the results of the Room Corner test.

The BW of the different measuring devices, mass flow controller and data acquisition system of the Ghent premises have been identified together with the behaviour of the built in adjustable filters in some of the measuring devices.

### ***How to deal with bandwidth in fire testing***

Due to differences in BW between instrumentation and in-between laboratories, measurement results can vary substantially. In order to overcome a lack of reproducibility between labs three possible levels of changes to the standard have been proposed. A first level only requires some minor changes to the software calculation procedures and results in an approximate BW of 1/30 Hz. A second level

involves substantial changes to both the calculation procedures and the data acquisition system and results in an approximate BW of 1/10 Hz. This is our preferred option because it: guarantees the complete elimination of any possible aliasing effect, is able to capture events with a periodicity down to 10 s, allows for a better smoothing and synchronisation of the data with a resulting better repeatability and reproducibility.

A third level requires the introduction of inverse filters and potentially allows to recover some BW up to 1 Hz. Since the periodicity of events of interest in the SBI test method is in the order of 10 s or higher the proposal is not to follow this route for intermediate and large scale heat release rate test equipment. The technique may be of interest in small scale tests like the Cone Calorimeter. It needs to be stressed however that this method is very sensitive to noise and that it requires a complete redesign and optimisation of the gas analysis train.

#### ***Introduction of an alternative synchronisation method***

Also an alternative automatic synchronisation method based on the maximisation of a correlation coefficient has been proposed. Contrary to the actual method, which is based on the synchronisation of times when signals surpass a certain limit value after a stepwise burner change, the method does take differences in dynamic behaviour of the different components into account.

#### ***Introduction of Henderson moving average filters in fire testing***

Flat running average filters are popular for smoothing data over time. Although they are easy to understand and implement, they not only dampen out the higher frequencies but they also disturb the lower frequencies which are of interest in these tests. This results in a high local bias and a poor local variance. The concept of weighted, Henderson, moving average filters is introduced. Henderson filters are often used as trend filters in economics. The Henderson filters can reproduce polynomials up to degree three which enables them to adequately capture trend turning points and points of inflection.

#### ***Development of a computer model for uncertainty estimation***

A computer model based on the formulas presented in chapter 6 has been developed. Comparison of the model with SBI RR2 results show that it is likely that the model can be used confidently to estimate the repeatability limits on the values used for classification FIGRA and THR<sub>600s</sub>.

#### ***Proposed changes to the data acquisition system***

Next it is shown that transient errors can drown out the uncertainty analysis and that they should at least be considered in the analysis. Reducing the bandwidth of the system to either 1/30 Hz or 1/10 Hz are two valid options to control transient phenomena. The first option is the cheapest and easiest one but dampens out variations with a periodicity below 30 s. The second option requires some new investments in data acquisition equipment and in software modifications but captures events with a



periodicity as low as 10 s, still eliminating disturbing noise. In addition it guarantees the complete elimination of spurious data on the results known as *aliasing*.

### ***Other changes proposed to the test***

The changes as proposed in chapter 6 to remove *bias* and to improve the standard uncertainty on some individual components has a big impact on the global uncertainty estimate. The *bi-directional probe* ( $k_p$ ) as used in the SBI is the most critical factor but can easily be reduced to almost negligible levels. The proposals for change to the *factor c* and the *cross sectional area A* have both a positive effect on the uncertainty and are therefore recommended for inclusion when reviewing the SBI standard. The uncertainty on the *factor c* can be kept low if a *four wire RTD* (Resistive Temperature Detector) is used to measure ambient air temperature instead of a K-type thermocouple. It is therefore recommended to use this four wire RTD. The use of *shielded thermocouples* in the exhaust duct has a marginal effect on the overall uncertainty and can therefore be omitted.

### ***Fulfilling all requirements of EN ISO 17025***

The work has resulted in a full and reliable experimental uncertainty analysis of HRR and its derivatives of the Ghent SBI fire test equipment in line with EN ISO 17025. Smoke production rate has not been considered.

### ***Other contributions***

The present dissertation is a continuation of the work done in developing the SBI test and improving other heat release rate based test instrumentation. On the way to achieving the goal of examining the uncertainty related to SBI fire tests, other contributions are made. The most tangible of these contributions – while not always a unique contribution to the body of knowledge – are:

- the final design and production of workshop drawings of the SBI-test which have been overtaken in the SBI standard;
- design and production of the burner control system of the SBI;
- the production of the first twelve SBI's for distribution all over Europe;
- automation of the calibration procedures and test sequences in the SBI test equipment;
- design of a universal gas analysis system optimised for use with the SBI, the Room Corner test, the Cone Calorimeter test, and similar. In other words, for all small-, intermediate- or large-scale fire test equipment that make use of the oxygen depletion technique;
- design and production of the third generation Cone Calorimeter test equipment;
- design and production of the heat release rate and smoke release rate add on for the electric cables fire test

**In terms of contributions to the body of knowledge, a significant contribution is made in developing methods of calculating experimental uncertainty in Heat Release Rate measurement.**

**The contributions made in this work are of interest and direct relevance to those working in the field of fire testing, fire engineering, quality control and accreditation.**

**The contribution in developing a new velocity pressure probe is of interest and direct relevance to those working with flows or measuring velocities, and is not at all limited to fire applications.**

## 8.2. Recommended changes specific to the SBI standard

### *Modify data acquisition and/or treatment of data*

In this work some advice is given on how to reduce the uncertainty interval for the SBI test method.

The main challenge is to account for transient phenomena which, so far, have not been included in previous studies. If fully taken into account by increasing the uncertainty interval, transient phenomena completely overshadow the uncertainty analysis.

Therefore a method has been worked out that basically consists of equally reducing the bandwidth of all instrumentation in all laboratories and to neglect (consider inherent to the test method) any remaining transient error.

Three options have been elaborated that respectively reduce the bandwidth to 1/30 Hz, 1/10 Hz or 1 Hz or, in other words, that dampen out events with a periodicity below respectively  $t_s = 30$  s, 10 s or 1 s. Only the first two are of practical use in the SBI and the second is the preferred option.

In a nutshell the method consists of increasing the data acquisition scan rate to 10 Hz, to introduce an analogue anti-aliasing filter with a cutoff frequency of 1 Hz, to equate the response times of the dynamic measurands and to apply a Henderson 111-term moving average filter on the raw data.

The currently used flat moving average filter on the heat release data prior to calculation Figra is no longer used.

The effect of this measure is difficult to quantify since dependent on the heat release rate, but reduces the uncertainty contribution of the depletion factor on the heat release rate at the 30 kW level from over 22 % (conservative estimate) to well below 2 %.

### *Remove systematic errors and introduce some obvious changes*

Eliminating the above discussed dominating transient factor, the flow measurement becomes predominant. In order of appearance, the following measures are proposed to reduce the uncertainty interval.

1. Replace the SBI pressure probe by the *hemispherical* pressure probe:
  - a. Eliminates bias due to Reynolds dependence of existing probe.
  - b. Eliminates bias due to potential misalignment of the probe.
  - c. Increases the signal to noise ratio.

Uncertainty contribution reduces from 6 % to less than 1 % at the 30 kW level.

2. Calculate the *c factor* instead of assuming it constant at 22.4:

- a. Eliminates a variable bias which is function on relative humidity, ambient temperature and barometric pressure.
  - b. Reduces the standard uncertainty on the c factor by more than a factor 10.  
Uncertainty contribution reduces from typically 2 % (variable) to 0.7 % at the 30 kW level.
3. Remove the bias from the *cross sectional area A*:
- a. Takes into account the effect of soot and corrosion on the exhaust duct wall.  
Uncertainty contribution reduces from 1.7 % (variable) to 0.6 % at the 30 kW level.

Combining all the above changes will result in slightly different results of the values used for classification – FIGRA and  $THR_{600s}$  – that however better approach the true values. In addition the standard uncertainty on the heat release rate at the 30 kW level reduces from 26 % to 4.5 %.

***Reduce standard uncertainty on  $k_{t,v}$***

By measuring on 2 or 4 additional lines from wall to centre on the occasion of a velocity profile calibration, the standard uncertainty can further be reduced. Besides the increased number of samples, the degrees of freedom in the t-distribution used to calculate the uncertainty increases from 3 to 5 respectively 7 which reduces the multiplication factor  $t_{0.025}$  from 3.18 to 2.57 or 2.36 respectively.

***Reduce standard uncertainty on  $k_{t,v}$ ,  $k_{t,gas}$  and  $k_{t,qheptane}$***

Using the last N calibrations instead of just the most recent one, could further reduce the standard uncertainty on the mean value of these components by a factor  $\sqrt{N}$ .

***Keep track of  $k_{t,v}$ ,  $k_{t,gas}$  and  $k_{t,qheptane}$***

The evolution in time of the different  $k_{t,x}$  calibration values can be used as a warning signal for when to do a major revision of the test instrument.

### **8.3. General recommendations to all Heat Release Rate based test facilities**

#### ***Enforce a fixed bandwidth in every test standard***

In order to obtain reproducible dynamic fire data like heat release rate and smoke production rate worldwide, the bandwidth of the instrumentation used should be harmonised. This can be achieved easily by specifying a fixed bandwidth for every test standard.

The proposal is to set the bandwidth for all heat release rate based test methods to 1/10 Hz making use of the aforementioned *second level changes*. In those applications where a larger bandwidth is required, both the bandwidth and the method used to attain it should be specified.

#### ***Replace the McCaffrey & Heskestad probe***

The original *McCaffrey & Heskestad probe* is sensitive to angular variations and realises only a limited differential pressure gain of about 10 % over a classic pitot-static tube.

The *hemispherical probe* is like the *McCaffrey & Heskestad probe* Reynolds independent over a wide range, but combines this with an insensitivity to angular distortions in a range of  $\pm 20^\circ$ . In addition, the probe realises a differential pressure gain of about 50 % over a classic pitot-static tube thus increasing the signal to noise ratio of this measurement.

#### ***Account for bluff-body blockage***

When using pressure probes in closed conduits, the probe factors shall be corrected for *bluff-body blockage*.

## **8.4. Main contribution of this work to the measuring technique**

### **8.4.1 Added value to fire science**

#### *Uncertainty model*

An uncertainty model has been developed and validated for the SBI test method. The model can easily be applied for other heat release rate test equipment based on oxygen depletion technique. Several assumed uncertainties have been investigated in more depth and hush up items like transient errors, synchronisation errors, asymmetric distributions etc. have been discussed.

#### *Introduction of the bandwidth concept in fire testing*

The effect of instrumentation dynamics, whose existence is identified by several authors, has for the first time been demonstrated, in a more fundamental way. The tools presented allow fire laboratories to harmonise their instrumentation, resulting in better reproducibility. A multiplier effect of this will be that this allows modellers to improve their models since the uncertainty on their input data reduces.

#### *Introduction of a new velocity pressure probe*

A new tool to measure flow in the harsh conditions of a fire is available. It eliminates some drawbacks of existing pressure probe designs.

### **8.4.2 Added value to industry**

#### *Increased confidence in test results*

Although the concept of uncertainty may be related to a "doubt", in the real sense the knowledge of uncertainty implies increased confidence in the validity of results. The present work offers a tool for test institutes to include an uncertainty analysis for every individual test conducted.

In addition, the proposed changes to the standard will help to reduce both the repeatability and reproducibility limits on test results.

This gives the manufacturer increased confidence in the classification result obtained wherever the product has been tested. This is extremely important in relation to the manufacturer's responsibility when CE marking his product.

The risk that a product is classified in a too low class or in a too high class is reduced by narrowing the uncertainty interval. This is of benefit to both the manufacturer and the end user.

### *New tool to measure flow velocities*

A new tool has been developed that can be used to measure flow velocities in all applications where fluids are transported through pipes, chimneys, tunnels, etc. and in applications where motion of objects relative to fluids need to be measured.

The probe has a high degree of simplicity such that it is easy to produce, install and maintain. It can also be made in a wide variety of materials such that it can also be used in extreme physical and chemical conditions.

Furthermore its size can be kept small such that the probe produces low head losses.

### **8.4.3 Added value to legislative and regulative bodies**

Narrowing the uncertainty interval increases the reliability of test and classification results. This indirectly contributes to a better fire safety.

## **8.5. Further research**

### ***The influence of chemical desiccants on HRR measurements***

Chemical desiccants are used as a second step to remove practically all water vapour from the sampled gas prior to presenting the gas to the analysers. Absorption of carbon dioxide, saturation, regeneration etc. all need to be investigated in dept and recommendations should be given on what product to use, how to use it and when to replace it.

A good understanding of the product and guidelines on how to use it will contribute to the stability of the measurement and to the reduction of the uncertainty interval.

### ***Uncertainty analysis on the SPR and the light transmission in specific***

If the uncertainty on the light transmission is known, the findings of the present work can be used to calculate the uncertainty interval on the Smoke Production Rate and its derived parameters like SMOGRA and TSP<sub>600s</sub>. The derived parameters form the basis for the sub-classification on smoke i.e. s1, s2 or s3.



## References

- [1] \*\*\*\*\* STANDARDS & DIRECTIVES\*\*\*\*\*
- [2] European Standard - Reaction to fire tests for building products - Building products excluding floorings exposed to the thermal attack by a single burning item. EN 13823:2002. CEN Central Secretariat, Brussels 2002
- [3] European and International Standard – Fire classification of construction products and building elements – Part 1: Classification using test data from reaction to fire tests. EN 13501-1:2002; CEN Central Secretariat, Brussels (2002)
- [4] International Standard – Reaction-to-fire tests – Heat release, smoke production and mass loss rate – Part 1 : Heat release rate (cone calorimeter method) ; ISO 5660-1:2002
- [5] EGOLF/R4; Accreditation of Fire Test Laboratories – Interpretation of the European Standard EN ISO/IEC 17025:1999 when applied to Fire Test Laboratories; EGOLF / R4:2001
- [6] International Standard – Fire tests – Full-scale room test for surface products; ISO 9705:1993; International Organisation for Standardisation, Geneva, 1993
- [7] European Standard – Common test methods for cables under fire conditions – Heat release and smoke production measurement on cables during flame spread test – Part 1: Apparatus; prEN 50399-1; CENELEC project 15315
- [8] European Standard - Railway applications - Fire protection on railway vehicles; prEN 45545; CENELEC project 12281
- [9] European and International Standard – General requirements for the competence of testing and calibration laboratories. EN ISO/IEC 17025:2000.; CEN Central Secretariat, Brussels (2000) and International Organisation for Standardisation, Geneva (1999)
- [10] European Standard – General criteria for the operation of testing laboratories; EN 45001:1989; CEN Central Secretariat, Brussels 1989
- [11] International Standard – Thermocouples – Part 2: Tolerances; IEC 60584-2; International Electrotechnical Commission, Geneva, 1982
- [12] European Standard – Fire resistance tests - Part 1: General requirements; EN 1363-1:1999; CEN Central Secretariat, Brussels 1999
- [13] GUM, Guide to the expression of uncertainty in measurement; BIPM/IEC/IFCC/ISO/IUPAC/OIML; ISBN 92-67-10188-9
- [14] International Standard – Quality assurance requirements for measuring equipment – Part 1: Metrological confirmation system for measuring equipment. ISO 10012-1:1992; International Organisation for Standardisation, Geneva (1992)
- [15] International Standard – Accuracy (trueness and precision) of measurement methods and results – ISO 5725 Parts 1 to 6; International Organisation for Standardisation, Geneva, 1996-1998

- [16] European and International Standard – General requirements for the competence of testing and calibration laboratories. EN ISO/IEC 17025:2000.; CEN Central Secretariat, Brussels (2000) and International Organisation for Standardisation, Geneva (1999)
- [17] Thermocouples, International Reference Tables. Temperatures according to IPTS-68
- [18] Aardolieproducten - Brandstoffen (klasse F) - Vloeibaar gemaakt petroleumgas – Specificaties; NBN T 52-706:2004
- [19] JANAF Thermochemical Tables, 2<sup>nd</sup> Edn. NSRDS-NBS 37, National Bureau of Standards, Washington, DC, 1971
- [20] Chase M.W., NIST-JANAF Thermochemical Tables, 4<sup>th</sup> Edn., American Institute of Physics, Woodbury, New York, 1998
- [21] The Construction Products Directive; Council Directive 89/106/EEC of 21 December 1988 on the approximation of laws, regulations and administrative provisions of the Member States relating to construction products; European Commission, Enterprise, 1989
- [22]
- [23] \*\*\*\*\* BOOKS \*\*\*\*\*
- [24] Atomic Weights of the Elements 1997; IUPAC Compendium of Chemical Terminology; Pure Appl. Chem., Vol. 71, No. 8, pp. 1593-1607, 1999.
- [25] Arts T., et al. ; Measurement Techniques in Fluid Dynamics – An Introduction ; von Karman Institute for Fluid Dynamics ; Sint-Genesius-Rode, Belgium, 1994
- [26] Babrauskas V.; Heat of combustion and potential heat; Heat release in fires; Babrauskas V., Grayson S.J., Eds; pp. 207-223, Elsevier Science Publishers Ltd, London, UK, 1992
- [27] Babrauskas V.; Ignition Handbook; Fire Science Publishers, Fire Science and Technology Inc., Issaquah, 2003
- [28] Boyce W.E. and DiPrima R.C; Elementary Differential Equations and Boundary Value Problems, Fourth Edition; John Wiley & Sons, Singapore, 1986
- [29] Brigham E.O. (1988); The Fast Fourier Transform and its applications; Prentice-Hall International, London
- [30] Drysdale D.D.; Thermochemistry; SFPE Handbook of Fire Protection Engineering; DiNenno, et al.; Eds. The National Fire Protection Association, USA 1995
- [31] Fox R.W. and McDonald A.T.; Introduction to fluid mechanics; John Wiley & Sons, New York 1985
- [32] Holman J.P.; Heat Transfer; McGraw-Hill Book Company, Singapore 1989
- [33] Janssens M., Parker W.J.; Oxygen Consumption Calorimetry; Heat release in fires; Babrauskas V., Grayson S.J., Eds; pp. 31-59, Elsevier Science Publishers Ltd, London, UK, 1992
- [34] Jones F.E.; Techniques and Topics in Flow Measurements; CRC Press, Boca Raton, FL, 1995

- [35] Keithley Instruments, Inc. (2001); Data Acquisition and Control Handbook, A Guide to Hardware and Software for Computer-Based Measurement and Control; Keithley Instruments, Inc.; Cleveland, Ohio, USA
- [36] Macrae J.C.; An Introduction to the Study of Fuel; Elsevier Publishing Company, London, 1966
- [37] Özisik M.N.; Finite Difference Methods in Heat Transfer; CRC Press, Boca Raton, Florida, 1994
- [38] Schoukens J. and Pintelon R. (1991); Identification of Linear Systems – A practical guideline to accurate modelling; Pergamon Press Oxford
- [39] Tewarson A.; Generation of heat and chemical compounds in fires; SFPE Handbook of Fire Protection Engineering; DiNenno, et al.; Eds. The National Fire Protection Association, USA 1995
- [40] Vandebril A.; Demystificatie van de Operationele Versterker; Kluwer technische boeken B.B., Deventer, 1980
- [41] Wonnacott T.H. and Wonnacott R.J.; Introductory Statistics for Business and Economics; fourth edition; John Wiley & Sons, Inc., Singapore, 1990
- [42] Zhu Y.C. and A.C.P.M. Backx (1993); Identification of Multivariable Industrial Processes: for Simulation, Diagnosis and Control; Springer-Verlag London
- [43]
- [44] \*\*\*\*\* PAPERS \*\*\*\*\*
- [45] Dagum E.B. and Luati A.; Relationship between Local and Global Nonparametric Estimators Measures of Fitting and Smoothing; Studies in Nonlinear Dynamics & Econometrics, vol. 8, n. 2; The Berkeley Electronic Press, 2004
- [46] Dagum E.B. and Luati A.; Global and Local Statistical Properties of Fixed-Length Nonparametric Smoothers; Statistical Methods and Applications, vol. 11, n. 3, pp.313-333
- [47] Enright P., and Fleischmann C.; Uncertainty of Heat Release Rate Calculation of the ISO 5660-1 Cone Calorimeter Standard Test Method; Fire Technology, Vol. 35, 1999, pp. 153-169
- [48] Henderson R.; Note on Graduation by Adjusted Average; Transaction of the Actuarial Society of America, 17, pp. 43-48, 1916
- [49] Huggett C.; Estimation of Heat release rate by Means of Oxygen Consumption Measurements; Fire and Materials, Vol. 4, N°. 2, p. 61-65, 1980
- [50] Janssens M.; Variability in Oxygen Consumption Calorimetry Tests; Thermal Measurements: The Foundation of Fire Standards, ASTM STP 1427, ASTM International, West Conshohocken, PA, 2002
- [51] McCaffrey B.J. and Heskestad, G.; A Robust Bidirectional Low-Velocity Probe for Flame and Fire Application; Combustion and Flame 26, 125-127 (1976)

- [52] Merci B., Theuns E., Sette B., Vandeveld P.; Numerical Investigation of the Influence of Gas Heating and Cooling on the Velocity Profile Correction Factor in the SBI-Configuration; Fire and Materials; Under review
- [53] Messerschmidt B. and Van Hees P.; Influence of Delay Times and Response Times on Heat Release Measurements; Fire and Materials 24 (2), pp 121-130, 2000
- [54] Parker W. J. (1982); Calculation of the heat release rate by oxygen consumption for various applications; U.S. Department of Commerce, Washington DC
- [55] Phillips S.D., Eberhardt K.R. and Parry B.; Guidelines for Expressing the Uncertainty of Measurement Results Containing Uncorrected Bias; Journal of Research of the National Institute of Standards and Technology, Vol. 102, Number 5, 1997
- [56] Sette B.J.G.; Critical considerations on the use of a bi-directional probe in heat release measurements; Fire and Materials; In press
- [57] Sette B.J.G.; Development of a new Robust Velocity Pressure Probe for Heat Release Applications; Fire and Materials; In press
- [58] Sette, B., Theuns E., Merci B., Temperature effects on the mass flow rate in the SBI and similar Heat Release Rate Test Equipment, Fire and Materials, Under review
- [59] Thornton W.; The Relation of Oxygen to the Heat of Combustion of Organic Compounds; Philosophical Magazine and Journal of Science, Vol. 33, No. 196, 1917
- [60]
- [61] \*\*\*\*\* REPORTS \*\*\*\*\*
- [62] An Introductory Course on Time Series Analysis – Electronic Delivery; Australian Bureau of Statistics; January 2005
- [63] Axelsson J., Andersson P., Lönnemark A. and Van Hees P.; Uncertainty in Measuring Heat and Smoke Release Rates in the Room/Corner Test and the SBI; SP Report 2001:04; Swedish National Testing and Research Institute, Borås, Sweden, 2001
- [64] Bryant R.A. et al; The NIST 3 Megawatt Quantitative Heat Release Rate Facility – Description and Procedures, NISTIR 7052; National Institute of Standards and Technology, Washington, September 2004
- [65] Dahlberg M.; Error Analysis for Heat Release Rate Measurements with the SP Industry Calorimeter; SP Report 1994:29; Swedish National Testing and Research Institute, Borås, Sweden, 1994
- [66] Enright T.; Heat Release and the Combustion Behaviour of Upholstered Furniture; Fire Engineering Research Report 99/17; ISSN 1173-5996; University of Canterbury, Christchurch, New Zealand, 1999
- [67] Plastics; A material of choice in building and construction, APME, figures of 1995
- [68] Official Laboratories Group; Development of the Single Burning Item Test – Results of the SBI Round Robin tests – Regulators Group document RG N115 (1997)

- [69] Sundström B., P. Van Hees and P. Thureson; Result and Analysis from Fire Tests of Building Products in ISO 9705, the Room/Corner Test, SP Report 2001:04, Borås (2001)
- [70] Project for the European Commission: Enterprise Directorate-General; "SBI (Single Burning Item) Second Round Robin"; Call Identifier ENTR/2002/CP11; Applicant: EGOLF
- [71]
- [72] \*\*\*\*\* CATALOGUES \*\*\*\*\*
- [73] KEITHLEY Instruments, Inc. ; Model 2000 Multimeter – User's Manual; Document Number: 2000-900-01 Rev. D; Cleveland, Ohio, U.S.A., 1995
- [74] MERCK KGaA; Chemical Reagents; Darmstadt, 1999/2000
- [75] SIEMENS AG; SIMATIC Komponenten für Totally Integrated Automation; Katalog ST 70 - 1999, Nürnberg, 1999
- [76] SIEMENS AG; Oxymat 6, Ultramat 6 - Analysatoren für IR-absorbierende Gase und Sauerstoff; C79000-G5200-C143-03, Karlsruhe, 1998
- [77]
- [78] \*\*\*\*\* WEBSITES \*\*\*\*\*
- [79] <http://users.pandora.be/peterulenaers/WEERGRAFIEKEN.HTM>; December 2004
- [80] <http://webbook.nist.gov/chemistry/>; February 2005
- [81] <http://www.chemdat.de/>; August 2004
- [82] [http://www.devosenergie.be/nl/tf\\_propaangas.aspx](http://www.devosenergie.be/nl/tf_propaangas.aspx); August 2004
- [83] [http://www.kauffman-gaz.com/cadre\\_neerlandais.htm](http://www.kauffman-gaz.com/cadre_neerlandais.htm); August 2004
- [84] Weisstein E.W.; "Triangular Distribution." From MathWorld--A Wolfram Web Resource. <http://mathworld.wolfram.com/TriangularDistribution.html>; February 2005
- [85] <http://www.webelements.com/webelements/scholar/properties/definitions/atomic-weight.html>; February 2005



**ANNEXEN A en B**  
**ANNEXES A and B**





## **A Annex**

### **A.1. Article 1**

*Sette B.J.G.; Critical considerations on the use of a bi-directional probe in heat release measurements; Fire and Materials<sup>[56]</sup>*

Out for review: 5 October 2004

Accepted for publication: 21 December 2004



# **Critical considerations on the use of a bi-directional probe in heat release measurements**

*Bart J.G. Sette*

*Ghent University, Department of Flow, Heat and Combustion Mechanics*

*Ottergemsesteenweg 711, B-9000 Gent, Belgium*

*E-mail: Bart.Sette@UGent.be ; Tel.: +32 9 243 77 50; Fax: +32 9 243 77 51*

## **Abstract**

*In various medium to large scale fire test equipment, like the ISO Room Corner (RC) test and more recently the Single Burning Item (SBI) test, the mass flow measurement of the combustion gases plays a key role in the determination of the heat release rate and smoke production rate.*

*To date a bi-directional low-velocity pressure probe is used to calculate this flow based on a differential pressure measurement on the axis of the exhaust duct. The objectives of this paper are to evaluate this bi-directional probe - and the modified SBI version - when used for measuring flows in exhaust ducts.*

*Recommendations are given on the future use of pressure probes measuring exhaust gas mass flows.*

*Key words: flow velocity, volume flow, pressure probe, heat release rate, smoke production rate*

## Nomenclature

$\mu$	dynamic viscosity [Pa.s]	D	characteristic diameter probe [m]
$\nu$	kinematic viscosity [m <sup>2</sup> /s]	HRR	Heat Release Rate [kW]
$\theta$	angle of attack [°]	L	length of the probe [m]
$\rho$	density of air [kg/m <sup>3</sup> ]	p	pressure [Pa]
$k_p$	probe constant [-]	$\Delta p$	differential pressure [Pa]
$k_t$	velocity profile correction factor [-]	Re	reynolds number [-]
A	surface area [m <sup>2</sup> ]	S	frontal area of the probe [m <sup>2</sup> ]
$C_t$	closed test section area [m <sup>2</sup> ]	T	temperature [K]
$C_D$	drag coefficient [-]	u(x)	standard uncertainty on x
$C_{DC}$	corrected drag coefficient [-]	v	velocity [m/s]
$C_{DU}$	uncorrected drag coefficient [-]	X O <sub>2</sub>	concentration of oxygen [%mol]
RC	Room Corner test		
SBI	Single Burning Item test		
SBI RR2	Second SBI round robin[12]		

## Introduction

Since there is a clear tendency to classify products according to their fire behaviour based on dynamic fire data like Heat Release Rate (HRR) and Smoke Production Rate (SPR), accuracy and uncertainty on the used test methods become even more important.

Several authors have tried to quantify uncertainty associated with the calculation of HRR and SPR [1][2][3]. However, out of a review of all major round robins, Janssens[4] found that the results suggest that the uncertainty is much greater than the theoretically found values, in particular for intermediate and large-scale tests.

A key element in the determination of dynamic fire data is the accurate measurement of the mass flow of the combustion gases. Except for the small scale tests like the Cone Calorimeter, to date nearly all intermediate to large scale test equipment use a bi-directional low-velocity probe[5] for this purpose. The bi-directional probe was originally designed for measuring the low velocity of (buoyancy-driven) fire induced flows associated with small to medium size fires. It has been ‘copy-pasted’ into various international standards and is considered to be the state of the art for measuring mass flows in combustion gases. Recently the SBI standard[8], which is used to assess the fire behaviour of building materials for the European market, prescribes a slightly modified design.

The present paper quantifies the impact of modifying the original design on the probe constant  $k_p$  and estimates the standard uncertainty associated with the use of the original probe. Recommendations are given on the calibration and future use of pressure probes measuring exhaust gas mass flows.

## **Design**

The original design, Fig.1.a., has been adopted in most standards that make reference to this bi-directional probe. An exception to this is the SBI standard[8], where the dimensions have been modified for practical reasons, Fig. 1.b/1.c.

In addition to this, a steel rod has been welded on the opposite side of the ‘support tubes’ where the pressure measurement is taken, Fig. 1.c. The argument for introducing this rod was that it allowed to accurately position the axis of the tube in line with the axis of the duct while it was felt that the support tubes could easily twist resulting in an angular distortion of the probe axis.

For the purpose of this study the characteristic diameter of design 1.a was chosen 16mm.

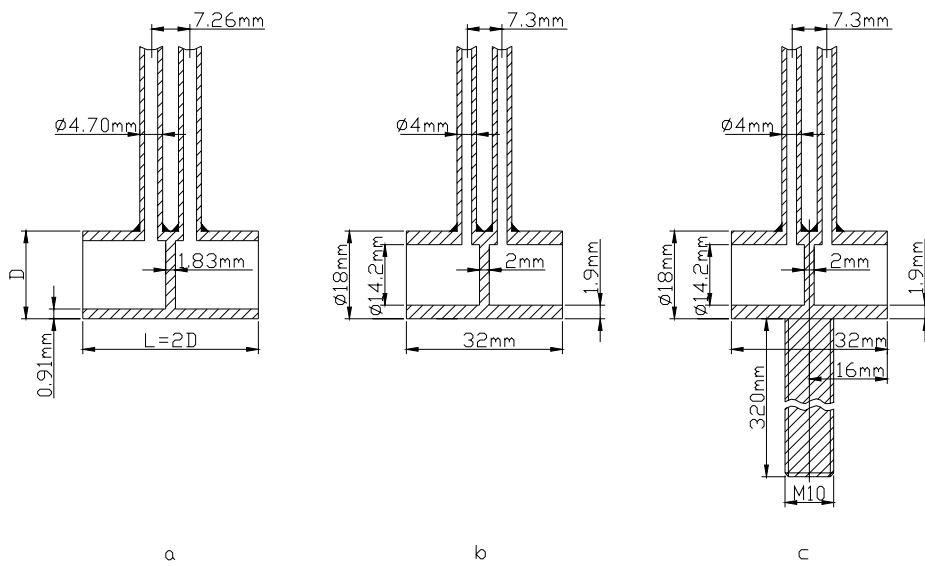


**Fig. 1: Different pressure probe designs**

## Measurements

The research focuses on two items. First of all, the probe constant is determined experimentally as a function of Reynolds number. The influence of the steel supporting rod in the design of Fig. 1.c is demonstrated and the effect of decreasing the aspect ratio  $L/D$  with respect to the original design is investigated.

Secondly, the effect of angular distortion of the probe axis with respect to the incoming flow is quantified.

## Instrumentation

### Wind tunnel

All measurements have been done in two wind tunnels at the Engineering Faculty of Ghent University.

*Wind tunnel 1* is a low speed, open circuit wind tunnel of the suction type. It incorporates an air inlet, fitted with honeycomb and meshes, a contraction and a test section of 500 mm height by 600 mm width. Velocity can range from 0.3 m/s to 4.3 m/s. The turbulence level varies from 1.3% for the highest velocities to 2% for velocities around 1 m/s and increases significantly for velocities below 0.9 m/s. Wind tunnel 1 is calibrated by means of Laser Doppler Anemometry.

*Wind tunnel 2* is a low speed, closed circuit wind tunnel. Looking downstream the test section, it incorporates a diffuser, two contra rotating axial fan blades, a diffuser, a honeycomb followed by a

settling chamber, a contraction and a test section of 446 mm height by 180 mm width. Maximum flow speed is 40 m/s. Wind tunnel 2 is calibrated by means of a pitot-static tube with an outside diameter of 4mm. Because of viscosity effects on the Probe, measurements start to be ‘incorrect’ for Reynolds numbers below 200 (‘Barker Effect’) which corresponds to velocities below 0.8 m/s ( $T=298K$ ;  $\nu=1.56E-05$ ). This effect, together with the expected high turbulence intensity for smaller velocities and the availability of wind tunnel 1, make that the minimum flow speed for the experiment is set at 3m/s.

### **Pressure transducers**

All differential pressure measurements made in wind tunnel 1 use a highly sensitive transducer with a range from 0 to 20 Pa (Table 1). The measurements in wind tunnel 2 are done with two pressure transducers ranging from 0 to 250Pa and to 1250Pa. The pressure transducers are zeroed prior to the first measurement of the day.

Type	Range (Pa)	$u(\Delta p)$ (Pa)	Used in
Druck LPX9481	0 – 20	0.0116	Windtunnel 1
Halstrup P92	0 – 250	0.85	Windtunnel 2
MKS Baratron	0 – 1250	7.2	Windtunnel 2

**Table 1: Pressure transducers used**

### **Data acquisition**

All data taken are based on the mean value of 300 consecutive measurement samples taken at a scanrate of 10Hz. The data acquisition system used is a Keithley 2700/7702 Multimeter based on the Integrating A/D principle. The integration process works as a low pass filter with, for the integration time set to 20ms (one power line cycle), a cut-off frequency (-3dB) of 22Hz.

### **Test conditions**

All measurements are taken with air at room temperature. Air densities are calculated as a function of temperature, pressure and relative humidity.

All instrumentation is switched on at least one hour prior to taking the first measurements.

## Uncertainty Analysis

### *Definitions*

#### **Probe constant $k_p$**

A pressure probe is basically a device that relates the velocity of a fluidum - in which it is positioned - with a differential pressure. As an example, the pitot-static pressure probe captures the difference between the incoming total pressure and the static pressure i.e. the dynamic pressure which is equal to  $\Delta p = \frac{1}{2} \rho v^2$ . If a pressure probe measures a differential pressure different from the dynamic pressure, a probe constant  $k_p$  needs to be introduced. The probe constant  $k_p$  is defined as

$$k_p = \frac{\sqrt{\frac{2\Delta p}{\rho}}}{v} \quad [-] \quad (1)$$

#### **Reynolds number**

The Reynolds number is a dimensionless number which is a measure of the ratio of inertia forces to viscous forces and is defined as

$$Re = \frac{\rho \cdot v \cdot D}{\mu} = \frac{v \cdot D}{\nu} \quad [-] \quad (2)$$

The factor D is a ‘characteristic length’ of the probe which is – for the present study – defined as the probes outside diameter.

In table 2, Reynolds numbers are given that realistically can be expected in the SBI- and RC-test on the axis of the exhaust tube and related to the probes diameter. In the SBI, a gas temperature at the height of the measuring section of approximately 600K is considered to be the maximum allowed temperature above which the test is interrupted. For the Room Corner test, the limit is set arbitrarily – for the purpose of this study – to 900K. The assumption is that the room has gone to flashover for values above this number.



	RC			SBI			
		constant volume	constant mass		constant volume		constant mass
T (K)	290	900	900	290	400*	600*	600
$\nu$ (m <sup>2</sup> /s)	14.8.10 <sup>-6</sup>	103.10 <sup>-6</sup>	103.10 <sup>-6</sup>	14.8.10 <sup>-6</sup>	26.4.10 <sup>-6</sup>	52.7.10 <sup>-6</sup>	52.7.10 <sup>-6</sup>
D (m)	16.10 <sup>-3</sup>	16.10 <sup>-3</sup>	16.10 <sup>-3</sup>	18.10 <sup>-3</sup>	18.10 <sup>-3</sup>	18.10 <sup>-3</sup>	18.10 <sup>-3</sup>
$v$ (m/s)	20	20	60	9	9	9	18
Re (-)	21 600	3 100	9 300	11 000	6 100*	3 100*	6 200

**Table 2: Expected Reynolds numbers related to the probe outside diameter**

\*: In the SBI the volume flow normalised to 298K ( $V_{298}$ ) is imposed to lie between 0.5 m<sup>3</sup>/s and 0.65 m<sup>3</sup>/s which makes that 'constant volume' can only be maintained to temperatures of approximately 400K

This implies that the Reynolds number varies between 3 000 and 22 000 for the Room Corner test and between 6 000 and 11 000 for the SBI test.

### ***Combined uncertainty for Windtunnel 1***

Windtunnel 1 is calibrated by means of Laser Doppler Anemometry to find a relationship between the frequency of the frequency controller and the velocity  $v$  in the wind tunnel test section. In this case, the probe constant  $k_p$  is calculated from equation (1).

The partial derivative to the different components results in the corresponding sensitivity coefficients:

$$\frac{\partial k_p}{\partial v} = -\frac{k_p}{v}$$

$$\frac{\partial k_p}{\partial \Delta p} = \frac{k_p}{2\Delta p}$$

$$\frac{\partial k_p}{\partial \rho} = -\frac{k_p}{2\rho}$$

and the combined standard uncertainty

$$u(k_p) = \sqrt{\sum_i \left( \frac{\partial k_p}{\partial x_i} u(x_i) \right)^2} = k_p \sqrt{\left( \frac{u(v)}{v} \right)^2 + \frac{1}{4} \left( \frac{u(\Delta p)}{\Delta p} \right)^2 + \frac{1}{4} \left( \frac{u(\rho)}{\rho} \right)^2}$$

### ***Combined uncertainty for Windtunnel 2***

Windtunnel 2 is calibrated by means of a pitot-static tube to find a relationship between the frequency of the frequency controller and the velocity  $v$  in the wind tunnel test section. In this case the probe constant  $k_p$  is derived from

$$k_p = k_{p0} \frac{v_1}{v_2} \sqrt{\frac{\rho_1 \Delta p_2}{\rho_2 \Delta p_1}} = k_{p0} \tilde{v} \sqrt{\tilde{\rho} \frac{\Delta p_2}{\Delta p_1}} \quad [-]$$

where  $\tilde{v}$  and  $\tilde{\rho}$  represent the velocity and density change with respect to the reference values  $v_2$  and  $\rho_2$  respectively. Both values are close to one. Index 2 refers to the reference measurement with the pitot-static tube, while index 1 stands for the measurement of the probe that needs to be calibrated.

The partial derivative to the different components results in the corresponding sensitivity coefficients:

$$\begin{aligned} \frac{\partial k_p}{\partial k_{p0}} &= \frac{k_p}{k_{p0}} \\ \frac{\partial k_p}{\partial \tilde{v}} &= \frac{k_p}{\tilde{v}} \\ \frac{\partial k_p}{\partial \tilde{\rho}} &= -\frac{k_p}{2\tilde{\rho}} \\ \frac{\partial k_p}{\partial \Delta p} &= \frac{k_p}{2\Delta p} \\ \frac{\partial k_p}{\partial \Delta p_0} &= -\frac{k_p}{2\Delta p_0} \end{aligned}$$

and the combined standard uncertainty

$$u(k_p) = k_p \sqrt{\left(\frac{u(k_{p0})}{k_{p0}}\right)^2 + \left(\frac{u(\tilde{v})}{\tilde{v}}\right)^2 + \frac{1}{4}\left(\frac{u(\tilde{\rho})}{\tilde{\rho}}\right)^2 + \frac{1}{4}\left(\frac{u(\Delta p)}{\Delta p}\right)^2 + \frac{1}{4}\left(\frac{u(\Delta p_0)}{\Delta p_0}\right)^2}$$

### ***Uncertainty on the different components***

#### **Uncertainty on the velocity $v$**

In the range from 0.3 m/s to 4.5 m/s the velocity distribution is assumed to be Gaussian. The measured standard uncertainty ( $N=300$ ) is limited to 0.05 m/s. Since 300 consecutive measurements are taken at

10Hz, the standard uncertainty on the mean velocity reduces with a factor  $\sqrt{300}$  to 0.0029 m/s.

The reproducibility on the mean velocity for a given set frequency is estimated (N=4) to be 0.4%. The uncertainty on the velocity in the range from 0.3 m/s to 4.5 m/s is therefore estimated to be  $u(v)=\text{SQRT}[(0.004*v)^2 + (0.0029)^2]$  (m/s).

In the range from 4.5 m/s to 40 m/s the measured standard uncertainty is limited to 0.5 % on the measured value. Since 300 consecutive measurements are taken at 10Hz, the standard uncertainty on the mean velocity reduces to 0.029 %.

The reproducibility on the mean velocity for a given set frequency is estimated (N=10) to be 1.14% (k=1) at a velocity of 5 m/s (resonance interval) and 0.34% at a velocity of 13 m/s (outside resonance interval). It is assumed that the uncertainty for velocities below 6 m/s is 1.14% [ $u(v)=0.0114v$ ] and for velocities above 6 m/s is 0.4% [ $u(v)=0.004v$ ]. The uncertainty on the velocity change is  $u(\tilde{v}) = \sqrt{2}u(v)$ .

#### **Uncertainty on the density $\rho$**

All measurements have been taken with a room temperature variation within 0.5°C, a relative humidity variation within 3% and a barometric pressure variation within 200Pa with respect to the calibration conditions. This variation includes the uncertainty related to the different measurands. Out of a parameter variation and assuming a rectangular distribution within those limits, the standard uncertainty on the density equals  $u(\rho)=5.7\text{E-}03$  kg/m<sup>3</sup>.

#### **Uncertainty on the differential pressure $\Delta p$**

In wind tunnel 1, all measurements have been taken with a highly sensitive differential pressure transducer ranging from 0 to 20Pa. In wind tunnel 2, the measurements have been split up over two different pressure transducers at a value of around 250Pa. Table 1 shows the standard uncertainty associated with the different models.

#### **Uncertainty on the probe constant of the pitot-static tube $k_{p0}$**

The probe constant of the pitot-static tube used is  $1 \pm 0.5\%$ . Assuming a rectangular distribution the standard uncertainty on the constant is estimated at  $u(k_{p0})=0.0029$ .

## Results and Discussion

### Corrections

Air densities used in the calculations do take into account the ambient temperature, ambient pressure and relative humidity.

Since both wind tunnels have a closed test section, all measurements are corrected for blockage effects due to the probe and its supporting tubes. This bluff-body blockage correction takes into account that any bluff body placed in a stream modifies this stream. In closed test sections this results in a drag increase with test model area. The normalised incremental drag change due to blockage,  $(C_{DU} - C_{DC})/C_{DC}$ , as a function of the drag in the test/measuring section, given by the blockage parameter  $C_{DU}(S/2C_t)$ , is given by[11]

$$\frac{C_{DU} - C_{DC}}{C_{DC}} = 2.53C_{DU} \left( \frac{S}{2C_t} \right) \quad [3]$$

If friction forces are neglected, the drag coefficient is defined as

$$C_D = \frac{\int \Delta p dA}{\frac{1}{2} \rho v^2 A} \quad [4]$$

Maskell[7], who first explored the physics of the interaction of boundaries, assumed that the pressure distribution is invariant in the presence of the constraining test section wall. This would mean that the differential pressure over the probe changes proportionally with the variance in  $C_D$  and that formula (3) can be used to calculate the correction on  $\Delta p$ .

It needs to be pointed out that when using pressure probes in enclosed spaces like ducting, a same correction factor needs to be applied, especially in the SBI where the cross section of the probe facing the flow is important. Table 3 displays the increase in drag, and thus  $\Delta p$ , for frequently used duct diameters (formula 3). Thus the probe factor  $k_p$  should be adjusted with the square root of one plus the corresponding value in table 3:  $k_p^{corrected} = k_p^{probe} \sqrt{1 + \Delta C_D}$

	Probe 1.a	Probe 1.b	Probe 1.c
Estimated $C_{DU}$	1.12	1.12	1.12
$\Delta C_D$ (%) ( $\phi=0.315m$ )	1.64	1.54	4.24
$\Delta C_D$ (%) ( $\phi=0.4m$ )	1.24	1.15	3.30

**Table 3: Drag increase in closed test/measurement sections**

### ***Probe factor $k_p$ as a function of $Re$***

Figure 2 displays the  $k_p$  probe factor as function of the Reynolds number with a 95% confidence interval. For high Reynolds numbers ( $Re > 2\,500$ ) the probe factor for the original McCaffrey and Heskestad[5] probe (Fig. 1.a) is calculated to be  $k_p = 1.046$  ( $N=64$ ;  $Re = 2\,500 \dots 18\,500$ ). The standard error on this mean value (t-test) is 0.001 while the standard deviation is 0.007. Assuming an uncertainty of 0.011 (95% confidence) on the measurements and a maximum error of 1% due to misalignment of the probe, the standard uncertainty is found to be

$$k_p = 1.046_{-0.011}^{+0.009}$$

From[5][6] it is not quite clear whether McCaffrey & Heskestad corrected for bluff-body blockage. If not, they overestimated  $k_p$  with 1.25% ([6]: test section  $\phi=12^\circ$ ; probe  $D=7/8''$ ; support tubes  $\phi=0.286D$ ).

Changing the aspect ratio  $L/D$  slightly (Fig. 1.b),  $k_p$  tends to lower a bit to a value of  $k_p = 1.044$ .

These differences are so small that no real conclusions can be drawn from these numbers. However, the drag coefficient for cylinders initially drops and later increases when  $L/D$  increases. So modifying the aspect ratio requires a new calibration.

It must be said however that although the probes were aligned experimentally (looking for minimum  $\Delta p$ ) for yaw and pitch angle, small misalignments may have resulted in a higher  $k_p$  value. This implies that the reported values should be seen as maximum values since  $k_p$  increases initially with angular distortions as will be discussed later. The corresponding error made is estimated to be maximum 1%.

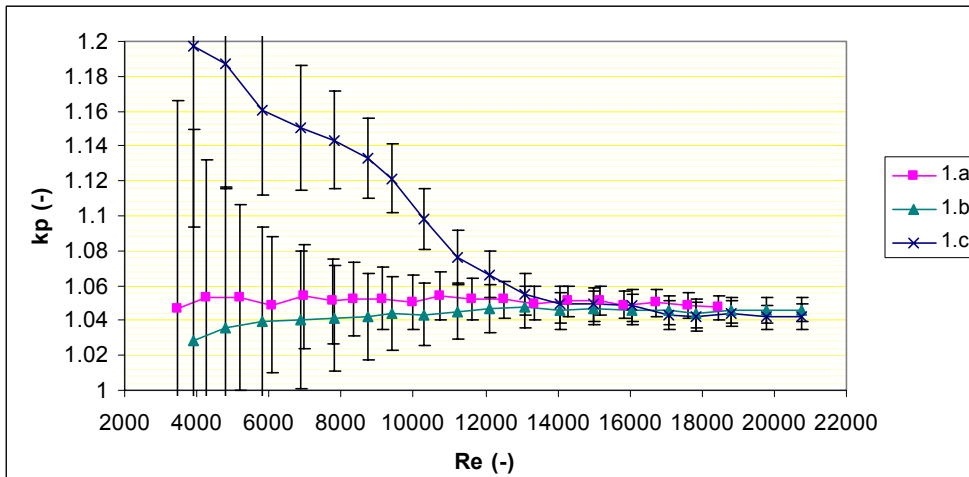


**Figure 2:  $k_p$  probe factor as function of Re (95% confidence interval)**

The probe constant of probe 1.b drops for values below  $Re = 5\ 000$  to a minimum of  $k_p = 1.015$  for  $Re = 3\ 000$ , as can be seen on figures 2 and 3. This makes this modified version less suited for mass flow measurements in fire testing, unless the mass flow through the ductwork is kept constant thus keeping  $Re > 5\ 000$  (see Table 2).

The effect of the probe factors being independent to Reynolds number variations in such a wide interval, is obtained due to the sharp edges of the probes. The sharp edges make that the flow separation point is fixed on this edge irrespective of the Reynolds number ( $Re \gg 1\ 000$ )[9]. This in contrast with streamlined bodies like cylinders.

On the SBI-probe body, a cylindrical positioning rod has been welded. This makes that – at the height of this rod – the flow no longer detaches at a fixed point and thus becomes Reynolds dependent. This means that, when the density and viscosity change because of a change in temperature of the combustion gases, or because air is partially replaced by combustion gases having other physical properties, the Reynolds number will change and correspondingly the probe constant. The example in Table 4 quantifies this effect:

T (K)	290	400*	600*	325**	380***	400	600
v (m/s)	9	9	9	10.1	11.8	12.4	18.6
v (m <sup>2</sup> /s)	14,8.10 <sup>-6</sup>	26,4.10 <sup>-6</sup>	52,7.10 <sup>-6</sup>	18.4.10 <sup>-6</sup>	24.2.10 <sup>-6</sup>	26,4.10 <sup>-6</sup>	52,7.10 <sup>-6</sup>
D (m)	18.10 <sup>-3</sup>	18.10 <sup>-3</sup>	18.10 <sup>-3</sup>	18.10 <sup>-3</sup>	18.10 <sup>-3</sup>	18.10 <sup>-3</sup>	18.10 <sup>-3</sup>
Re (-)	11 000	6 100	3 100	9 900	8 800	8 500	6 400
k <sub>p</sub> (-)	1.081	1.158	1.207	1.108	1.132	1.136	1.155
error (%)	+0.1	+7.2*	+11.8*	+2.6	+4.8	+5.2	+7.0
k <sub>p_ref</sub> = 1.08							

**Table 4: Effect of temperature (through v) on the SBI-probe constant**

\*: In the SBI the volume flow normalised to 298K ( $V_{298}$ ) is imposed to lie between 0.5 m<sup>3</sup>/s and 0.65 m<sup>3</sup>/s which makes that ‘constant volume’ can only be maintained to temperatures of approximately 400K

\*\*: typical values for SBI step calibration

\*\*\*: typical values for SBI heptane calibration

The pressure probe used in the SBI (Fig. 1.c) test equipment has a probe constant which is clearly different from the value of 1.08 put forward by the standard. At typical initial working conditions (T=290K;  $V_{298}=0.6\text{m}^3/\text{s}$ ;  $k_t=0,87$ ), the Reynolds number lies around 11 000 and the corresponding probe constant is 1.081. So the theoretical and the experimental values match to within the measurement uncertainty. As soon as temperature starts to rise however, the Reynolds number lowers and the probe factor rises. For the SBI, the lower limit for Re is estimated at 6 000 with a corresponding  $k_p = 1.159$ . This corresponds with an error of 7.3% compared to the value of 1.08 put forward by the standard.

In reality the error on the HRR will be less or will even be compensated by the ‘velocity profile’ correction factor  $k_t$  which will overcompensate when doing calibrations based on burning a known combustible.

$$\text{HRR}(t) \sim \frac{k_t}{k_p} \quad [5]$$

One way to ‘calibrate’ the test equipment is to burn a combustible with a well known heat of combustion and to fit the  $k_t$  factor until the measured heat release corresponds to the theoretic value. In the SBI the  $k_t$  factor is the mean value of three calibrations, two of which are based on the burning of a known combustible.

The first is a step calibration where propane is burned at different heat release levels. The mean temperature during a typical calibration (steps 2,3 and 5) is 325 K (constant mass; SBI RR2 data). At this temperature, the  $k_p$  factor is underestimated with approximately 2.6% (Table 4). To compensate (formula 5), the  $k_{t,\text{step}}$  factor is underestimated with the same 2.6%.

The second calibration consists of a heptane pool fire. A typical mean temperature there (while burning) was found to be 380 K (constant mass; SBI RR2 data) resulting in an underestimation of  $k_p$  – and thus  $k_{t,\text{hept}}$  – with approximately 4.8% (Table 4). These temperatures are only rough estimates that may vary from laboratory to laboratory, but they clearly demonstrate that the  $k_p$  value put forward by the standard is a too low number when combustion is taking place.

The  $k_t$  factor that follows out of the calibrations will thus be underestimated by 2.5%  $[(2.6+4.8+0)/3]$ .

This also seems to be confirmed by the results of SBI RR2[12]. Table 5 shows the mean values of the  $k_t$ -factors found by means of a step calibration, a heptane calibration and a hot wire anemometer calibration. The results are based on measurements in 28 different laboratories. No uncertainty data on those measurements is available. Both the  $k_{t,\text{step}}$  and  $k_{t,\text{hept}}$  are lower than  $k_{t,v}$  found out of the direct measurement of the velocity profile.

The observation that  $k_{t,\text{hept}}$  is higher than  $k_{t,\text{step}}$  can reasonably be attributed to other effects like incomplete combustion (pool fire). Incomplete combustion results in an overestimation of the  $k_t$  value.



N=28	$k_{t,step}$ step calibration	$k_{t,hept}$ heptane calibration	$k_{t,v}$ hot wire anemometer	$k_t$ mean (step; hept.;anem.)
Mean	0.858	0.865	0.875	0.866
Deviation from $k_{t,v}$ (%)	-2.03	-1.15	0.00	-1.07
Std. Error of Mean	0.0081	0.0083	0.0064	0.0064
Std. Deviation	0.0428	0.0442	0.0341	0.0340

**Table 5: velocity profile correction factors reported in the SBI round robin II project**

The use of probe 1.c in the SBI can also partially explain why the heat release in step 5 of the step calibration is found to be systematically higher than in steps 2 and 3, although the same 30kW are burnt. In step 4 of this calibration the burner heat output is increased to 93kW which makes that, due to the heating of the system,  $k_p$  in step 5 is higher than in steps 2 and 3. As  $k_p$  is underestimated, the HRR will appear high. Although the HRR curve of a step calibration with probe 1.b seems to better follow the expected values, a large number of tests would be required to statistically prove any improvement.

For pressure probe 1.a and 1.b, the measurements have been extended to the range  $Re = 340 - 19000/66000$  respectively. The results are displayed in figure 3 together with the  $k_p$  factor proposed by McCaffrey & Heskestad[5] for design 1.a.

The results for probe 1.a (1.b) suggest that:

- ✓  $k_p$  is fairly constant for  $Re > 3\ 000$  (5 000)
- ✓  $k_p$  starts to rise for  $Re < 2\ 500$  (2 000)
- ✓  $k_p$  drops slightly for in-between values

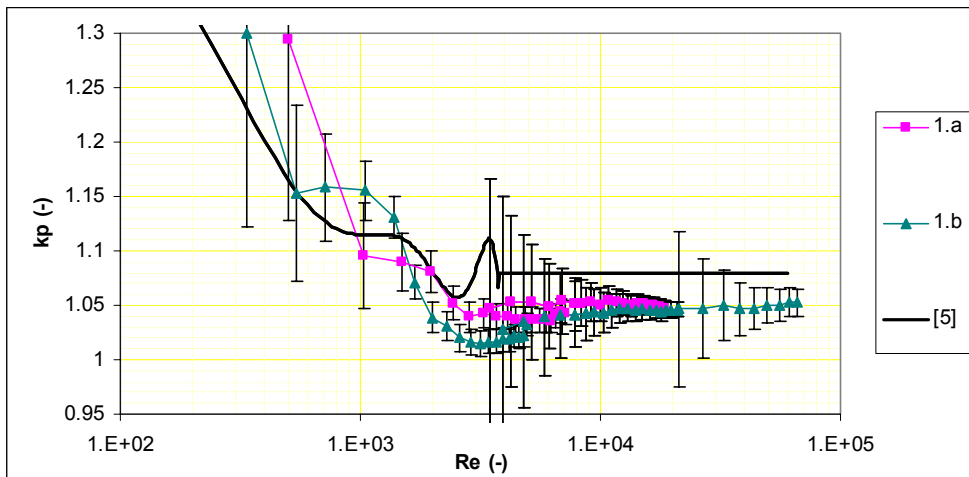


**Figure 3:  $k_p$  probe factor as function of Re (95% conf. interval)**

The flow gases introduce a drag force onto the pressure probe which is mainly caused by the pressure distribution over the probe. The drag caused by friction reduces considerably for Reynolds numbers above 1 000 ( $\pm 5\%$  at  $Re=1\ 000$ )[9] and can be neglected for even higher Reynolds numbers. When friction forces can be neglected, the drag coefficient reduces to formula 4.

For all objects with sharp edges, the drag coefficient is essentially independent of Reynolds number for Reynolds numbers well above 1 000. This is true because the sharp edges make that the flow separation points are fixed by the geometry of the object irrespective of the flow velocity. The flow profile over the object is invariable.

### ***Compressibility of air***

One of the assumptions made to calculate the velocity out of the differential pressure is that the combustion gases are incompressible. This relation holds for Mach numbers below 0.3 (error  $< 1\%$ )[9] which corresponds to velocities around 100 m/s in air at ambient temperature and to Reynolds numbers for the probes under discussion of approximately 100 000.

### ***Thermal expansion of the probe***

Thermal expansion of the probe has no direct effect on the probe constant. Through the Re-number however, it could have a limited contribution if  $k_p$  were function of temperature - and thus Reynolds.

For every 100K temperature rise, the probe diameter - and so will the Re-number - increases with 0,1 to 0,2% depending on the type of steel used. These variations can be disregarded since their influence on  $k_p$  - if any - is negligible.

***Influence of combustion gas chemistry on  $k_p$***

The effect of air partially being replaced by combustion gases has a negligible effect on the Re-number under 'normal' heat release test fire conditions ( $X_{O_2} > 17\text{Vol}\%$ ).

In the assumption of having complete combustion of propane gas,  $O_2$  will partially be replaced by the combustion products  $CO_2$  and  $H_2O$ . The kinematic viscosity - which is used in the Re-equation - for  $CO_2$  and  $H_2O$  is different from the one for  $O_2$ . Assuming the hypothetical case of stoichiometric combustion (all  $O_2$  consumed; 3 to 4MW of heat release for every  $m^3/s$  - referenced to 298K - of combustion gases extracted) the kinematic viscosity of the combustion gases is approximately 5% higher than the kinematic viscosity of clean air at the same temperature (Calculated making use of [10]).

This variation is temperature dependent but remains in the order of 5% in the expected temperature range of the exhaust gases (part of the heat is 'lost' to the environment before arriving in the measuring section).

The above results in a reduction of the Re-number which - even in the hypothetical case of stoichiometric combustion - leads to a reduction in the order of 5%. In the SBI test equipment such conditions are never reached, so that the minor variation on Re-number has no influence on  $k_p$ . In the Room Corner test and similar test equipment, it is important to stick to the original probe design 1.a - without the positioning rod - and to keep the working point above  $Re=2\ 500$ . In this case,  $k_p$  remains constant and combustion gases have no influence on  $k_p$ .

### Angular sensitivity

Under optimal circumstances, the axis of the bi-directional probe should be inline with the incoming flow ( $\theta = 0$ ; pitch and yaw angle equal to zero). Due to improper alignment and/or a radial velocity component on the incoming flow, the angle of attack ( $\theta$ ) can be different from zero.

Figure 4 displays the amplification factor as a function of the angle of attack ( $\theta$ ) in the range from  $-15^\circ$  to  $+15^\circ$ . The mean velocity is set to approximately 8.5 m/s ( $Re = 10\,000$ ). Values of the amplification factor above one mean that the pressure difference over the probe increases with respect to the situation where the axis of the probe is in line with the incoming flow.

$$\text{Amplification Factor} = \frac{k_p(\theta)}{k_p(\theta = 0)}$$

Slight variations of the angle of attack ( $\theta$ ) lead to an increase of the probe constant (2% by  $3^\circ$ ; 4% by  $5^\circ$ ) for probes 1.a and 1.b. The working point ( $\theta = 0$ ) represents a sharp minimum and can be used to align the probes.

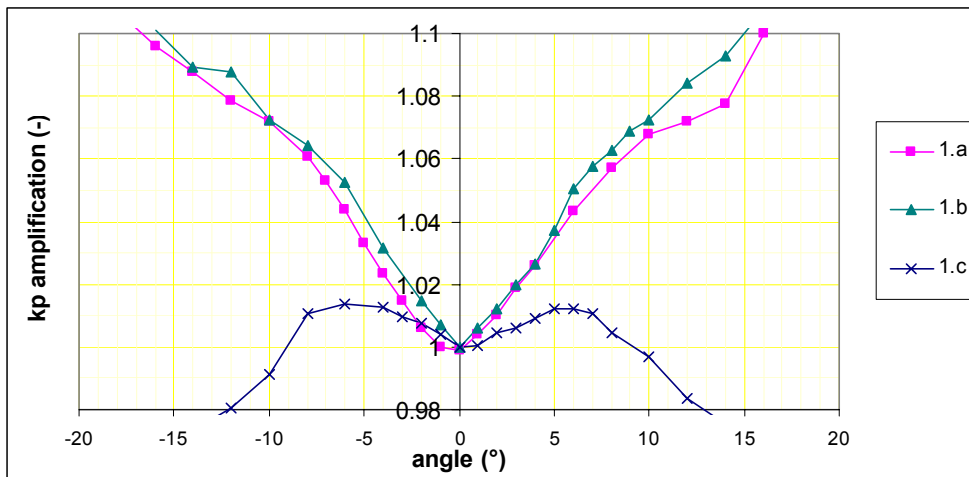


Figure 4: Angular sensitivity ( $Re \approx 10\,000$ )

The SBI-probe on the other hand is less sensitive to the attack angle (1% by  $3^\circ$ ;  $<1.5\%$  in the range from  $-10^\circ$  to  $10^\circ$ ).

Figure 5 shows that only for Reynolds numbers well below values that can be expected in the SBI and RC test the angular sensitivity seems to lower.

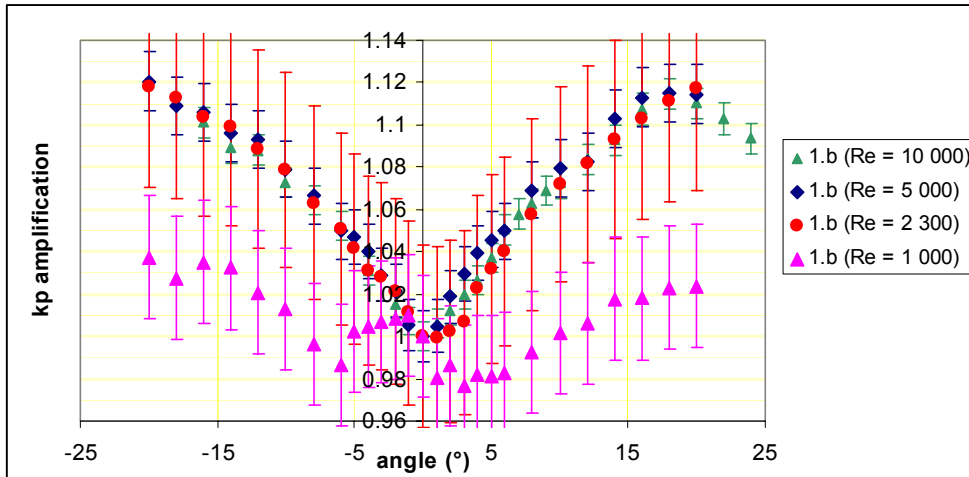


Figure 5: Angular sensitivity as a function of Re (probe 1.b; coverage factor k=1)

## Conclusions

The pressure probe currently used in the SBI test is Reynolds dependent and the ‘probe constant’ is higher than stated in the standard. As a consequence, calibration of the equipment leads to underestimation of heat release and smoke production – which are both proportional to the measured mass flow – for products with reduced heat release rate and overestimation for products with a higher heat release rate. Based on theoretical considerations and the information reported in this contribution, taking into account the influence of exhaust gas temperatures measured in the SBI, an underestimation of roughly 1% is predicted for the burner with dummy specimen, and an overestimation of about 6% at the maximum HRR capacity allowed by the standard in the SBI test. These numbers are for test instruments running at constant mass flow rate and will be higher when running the equipment at constant volume flow rate. They also explain part of the ‘average relative standard deviation’ for the classification parameters in the SBI. The reported values[8] for the total heat release in the first ten minutes of the test, THR600s, are 11% and 21% for repeatability and reproducibility respectively.

It is therefore strongly recommended to calibrate the SBI probe and introduce the probe value in the heat release formulas as a function of the Reynolds number. The Reynolds number can be calculated based on the properties of air at the same temperature as the exhaust gases.

An alternative and probably better solution would be to remove the steel rod and to stick to the design of fig. 1a or 1b.

The SBI pressure probe has a lower sensitivity to angular variations with respect to the flow. In the range from  $-3^\circ$  to  $3^\circ$  the influence to the probe constant is limited to 1%. In the range from  $-10^\circ$  to  $10^\circ$  to 1.5%.

The original McCaffrey & Heskestad probe has a probe factor which is constant for Reynolds numbers above 2 500. This corresponds to the range that can practically be expected in the ISO Room Corner test, the SBI test and similar devices. If one wants to measure heat release in post flashover scenarios, the probe factor should be calculated as a function of Reynolds number.

Angular distortions introduce an error in the order of 2 to 4% (2% by  $3^\circ$ ; 4% by  $5^\circ$ ).

Guide vanes upstream the pressure probe should help to reduce any angular distortion of the flow. Angular distortions result in an overestimation of the Heat Release Rate.

When installing a pressure probe in the exhaust duct, the operator should take readings of the pressure difference at different angles of attack ( $\theta$ ) in a range of  $10^\circ$  centred around the estimated zero angle ( $\theta = 0$ ). The minimum pressure difference will then indicate the exact zero ( $\theta = 0$ ) position.

Any flow conditioner upstream should be designed such to eliminate any radial or rotary velocity component. Especially when applying probe design 1.a or 1.b which are more sensitive for angular misalignments than design 1.c.

A lower probe constant was found for the McCaffrey & Heskestad probe. The  $k_p$ -factor is estimated to be 1.046 with a standard uncertainty of +0.009 and -0.011. Modifying the aspect ratio L/D requires a new calibration.

The  $k_p$ -factor should be corrected for ‘bluff-body blockage’ if used in ducts with reduced diameter. The corrected  $k_p$ -factors for probe designs 1.a and 1.b are tabulated below for two frequently used duct diameters.

	Probe 1.a	Probe 1.b
$k_p$ (open air)	1.046	1.044
$k_p$ ( $\phi_{\text{duct}}=0.315\text{m}$ )	1.055	1.052
$k_p$ ( $\phi_{\text{duct}}=0.4\text{m}$ )	1.052	1.050

**Table 6: Probe factor  $k_p$  corrected for bluff-body blockage**

Heat release measurements would benefit from an optimised pressure probe design limiting the sensitivity to angular variations but without compromising on the benefits of the actual probes. As a result of these findings, further research has been undertaken which has resulted in a new pressure probe design that combines the best of both worlds: a low angular sensitivity and Reynolds independency over a wide range. The results will soon become available.

## Reference List

- [1] Dahlberg M.; Error Analysis for Heat Release Rate Measurements with the SP Industry Calorimeter; SP Report 1994:29; Swedish National Testing and Research Institute, Borås, Sweden, 1994
- [2] Axelsson J., Andersson P., Lönnemark A. and Van Hees P.; Uncertainty in Measuring Heat and Smoke Release Rates in the Room/Corner Test and the SBI; SP Report 2001:04; Swedish National Testing and Research Institute, Borås, Sweden, 2001
- [3] Enright P., and Fleischmann C.; Uncertainty of Heat Release Rate Calculation of the ISO 5660-1 Cone Calorimeter Standard Test Method; Fire Technology, Vol. 35, 1999, pp. 153-169
- [4] Janssens M.; Variability in Oxygen Consumption Calorimetry Tests; Thermal Measurements: The Foundation of Fire Standards, ASTM STP 1427, ASTM International, West Conshohocken, PA, 2002
- [5] McCaffrey B.J. and Heskestad, G.; A Robust Bidirectional Low-Velocity Probe for Flame and Fire Application; Combustion and Flame 26, 125-127 (1976)
- [6] Heskestad, G.; Bidirectional Flow Tube for Fire Induced Vent Flows, Appendix K in Croce, P.A. and Emmons, H.W.; The Large-Scale Bed-Room Fire Tests; July 11, 1973; Factory Mutual Research; FMRC S/N 21011.4, July 1974
- [7] Maskell E.C.; A Theory of the Blockage Effects on Bluff Bodies and Stalled Wings in a Closed Wind Tunnel; ARC R&M No. 3400, HMSO, London, 1965
- [8] European Standard - Reaction to fire tests for building products - Building products excluding floorings exposed to the thermal attack by a single burning item. EN 13823:2002. CEN Central Secretariat, Brussels 2002
- [9] Fox R.W. and McDonald A.T.; Introduction to fluid mechanics; John Wiley & Sons, New York 1985
- [10] GASEQ Software Version 0.76; A Chemical Equilibrium Program for Windows; <http://www.gaseq.co.uk>; March 2003



- [11] Cooper K.; Bluff-Body Blockage Corrections in Closed- an Open-Test-Section Wind Tunnels; Chapter 6 of the handbook edited by Ewald B.F.R.; Wind Tunnel Wall Correction; AGARD-AG-336, 1998
- [12] Project for the European Commission: Enterprise Directorate-General; “SBI (Single Burning Item) Second Round Robin”; Call Identifier ENTR/2002/CP11; Applicant: EGOLF



## **A.2. Article 2**

*Sette B.J.G.; Development of a new Robust Velocity Pressure Probe for Heat Release Applications; Fire and Materials<sup>[57]</sup>*

Out for review: 1 February 2005

Accepted for publication: 30 March 2005



# Development of a Velocity Pressure Probe

*Bart J.G. Sette*

*Ghent University, Department of Flow, Heat and Combustion Mechanics, Ghent, Belgium*

*Correspondence address:*

*Ottergemsesteenweg 711, B-9000 Ghent, Belgium*

*E-mail: Bart.Sette@UGent.be ; Tel.: +32 9 243 77 50; Fax: +32 9 243 77 51*

## **Abstract**

*In intermediate and large scale fire test applications, a bi-directional low-velocity pressure probe is used to obtain the volume flow. The probe was presented by McCaffrey and Heskestad in 1976 and has found its way to several international standards including the Room Corner test and the Single Burning Item test (SBI). The probe is considered 'state of the art' for measuring flow rate in fire test applications.*

*The main disadvantage however is that the probe factor changes with pitch and/or yaw angle variations. The modified SBI pressure probe is less sensitive to angular variations but then again is Reynolds dependent.*

*A new pressure probe design has been developed that combines a low angular sensitivity with a Reynolds independency over a wide range. Although the probe has been developed for intermediate and large scale fire test applications, its use is not limited thereto.*

*Key words: velocity, flow velocity, pressure probe, volume flow rate, mass flow rate*

## Nomenclature

$\mu$	dynamic viscosity [Pa.s]	$p$	pressure [Pa]
$\nu$	kinematic viscosity [m <sup>2</sup> /s]	$p_{\text{tot}}$	total pressure [Pa]
$\theta$	angle of attack [°]	$p_{\text{stat}}$	static pressure [Pa]
$\rho$	density [kg/m <sup>3</sup> ]	Re	Reynolds number [-]
A	probe surface area [m <sup>2</sup> ]	S	frontal area of the probe [m <sup>2</sup> ]
$C_D$	drag coefficient [-]	T	temperature [K]
D	characteristic diameter probe [m]	$v$	velocity [m/s]
$k_p$	probe constant [-]		
M	Mach number [-]		
$\Delta p$	differential pressure [Pa]		

## Introduction

In various medium to large scale fire test equipment, like the ISO Room Corner (RC) test<sup>[6]</sup> and more recently the Single Burning Item (SBI) test<sup>[3]</sup>, the mass flow rate measurement of the combustion gases plays a key role in the determination of the heat release rate and smoke production rate.

To date a bi-directional low-velocity pressure probe is used to calculate this flow rate based on a differential pressure measurement on the axis of the exhaust duct. The bi-directional probe, first introduced by McCaffrey & Heskestad<sup>[7]</sup> in 1976, was originally designed for measuring the low velocity of (buoyancy-driven) fire induced flows associated with small to medium size fires. It has been ‘copy-pasted’ into various international standards and is considered to be the state of the art for measuring flow in combustion gases in fire tests. Recently the SBI standard, which is used to assess the fire behaviour of building materials for the European market, prescribes a slightly modified design.

One major drawback of the bi-directional probe however is that its probe factor changes with pitch and/or yaw angle variations. Previous research<sup>[9]</sup> revealed that such angular deviations introduce an

error in the order of 2 to 4% (2% by 3°; 4% by 5°). Due to improper alignment of the probe angular deviations can never be excluded.

The modified SBI pressure probe is less sensitive to angular variations (1% by 3°; <1.5% in the range from -10° to 10°) but is Reynolds dependent on the contrary. This means that when velocity, density or viscosity change because of a change in extraction rate, a change in temperature of the combustion gases, or because air is partially replaced by combustion gases having other physical properties, the Reynolds number will change and correspondingly the probe constant. The expected maximum variation in the SBI of the probe constant when running the equipment at constant mass flow is approximately 7%.

A conclusion<sup>[9]</sup> out of the above observations is that intermediate and large scale fire tests would benefit from an optimised pressure probe design, limiting the angular sensitivity without compromising on the benefits of the actual probes. Further research, as summarised in this contribution, has resulted in a new pressure probe design that combines a low angular sensitivity with Reynolds independency over a wide range.

The assumption of incompressible flow will be maintained throughout this study.

## **Requirements**

When first developing the present probe the goal was to develop a probe suited for measuring the flow rate of combustion gases in closed conduits of circular cross-section. A review of the most common intermediate and large scale fire tests learned that velocities between 5 m/s and 10 to 20 m/s are to be expected. This means that differential pressures between 15 Pa and 59 to 236 Pa ( $T=298K$ ,  $p=101325Pa$ ,  $\rho=1,18kg/m^3$ ) would be obtained using a pitot-static tube. When combustion gas

temperatures rise to say 600K those values further reduce with a factor 2 if constant volume flow rate is maintained. 600K is considered to be the maximum allowed temperature in the SBI.

Those pressure differences are so low that any positive gain would be beneficial in reducing the measurement uncertainty.

A second, even more important design parameter is the insensitivity to angular distortions in a range of at least  $\pm 5^\circ$  and preferably more. Angular distortions lead to a bias on the measurement results and should be avoided at any time. This however is not always possible certainly not for small deviations from the probes zero position.

A third point of attention is the ability to work in 'contaminated' environments (smoke, dust, soot, ...). One of the reasons why a pitot-static tube is not used in fire applications is because its pressure ports can easily get obstructed by particles transported by the medium. Especially the positive total pressure port which points upstream is sensitive to blockage.

Furthermore the design of the probe should preferably be straightforward and it should be easy to maintain and manufacture.

## **Short review of single point velocity pressure probes**

This section gives a brief overview of velocity pressure probes that sense for the velocity in a single discrete point except for one probe, discussed at the end of this section, that senses in multiple discrete points. The list is non exhaustive and only highlights the main characteristics. Specific designs that sometimes involve only minor changes, can result in different characteristics. It is therefore difficult to compare, e.g. in a table, the characteristics of the different groups of probes.



An alternative method to single point velocity measurements for determination of the volume flow in closed conduits are orifice plates, nozzles and Venturi meters. Those instruments fall out of scope of the present paper.

*Pitot-static tubes and shielded (Kiel) probes*

The most commonly used Pitot-static tubes are the National Physical Laboratory (NPL) standard hemispherical-nose and ellipsoidal nose tubes. For engineering purposes, the probe factor of those instruments can be set to 1 with an error tolerance of less than 0.5% on velocity in the range from 6 m/s up to 60 m/s<sup>[8]</sup>. For the ellipsoidal-nose instrument, this range can be enlarged down to 1 m/s. These speed ranges relate to air at ordinary temperatures and pressures.

The effect of yaw angle variations on the differential pressure reading is about 0.5% at 5° and about 1% at 10° for the ellipsoidal nose, and about 1% at 5° and 3% at 10° for the hemispherical nose<sup>[8]</sup>



**Figure 1: Example of a Pitot-static tube (a) and a Kiel-probe (b)**

However, Pitot-static tubes can be designed such that they are not very sensitive to angles of attack. Gracey<sup>[5]</sup> investigated a large number of pressure probes. He found that for simple, non shielded tubes, the usable angular range (differential pressure variations of less than 1%) was found to depend on the external shape of the nose section, the size of the impact opening (relative to the tube diameter), and the shape of the internal chamber behind the impact opening. He concluded that the best combination of these design features is a tube having a cylindrical nose shape, an impact opening equal to the tube diameter, and a 30° conical chamber. The usable range in this case is about ±28° at a Mach number of

0.26. He further concluded that for most of the unshielded tubes the usable range increases with Mach number, whereas for shielded tubes it decreases with Mach number.

Extreme values of angular insensitivity are obtained with shielded probes. The insensitivity range of a shielded tube having a conical entry is about  $\pm 41^\circ$  ( $M = 0.26$ ). Changing the shape of the entry of the shield to a highly curved section increases this range to about  $\pm 63^\circ$  ( $M = 0.26$ ). This design requires venting of the throat through the wall of the shield.

The main disadvantage of Pitot-static tubes is however that the pressure ports can easily get obstructed by particles transported by the medium, resulting in erroneous readings. Especially the positive total pressure port, which points upstream, is sensitive to blockage. The Pitot tubes therefore are not suited for measurements in contaminated environments, such as smoke, dust, soot, etc. Their main application is in laboratories and aeronautics.

#### *Type "S" or Reverse Pitot-Static probe*

The type "S" (Stauscheibe) or Reverse Pitot-Static probe consists (Fig. 2) of two stainless steel tubes with impact holes oriented at  $180^\circ$  angles to one another. One hole faces upstream for the measurement of total pressure; the other is aligned in a downstream direction for static pressure measurement. The difference between these two pressures approximately equals 150% of the velocity pressure of the fluid. "S" probes are designed for easy entry into small holes in stack or flow passage walls, and due to their relatively large impact (sensing) holes, are especially effective in the presence of high concentrations of clogging particulate matter. The "S" probe however is sensitive to angular variations, which are even different for pitch and yaw angle variations, and is Reynolds dependent<sup>[8]</sup>.

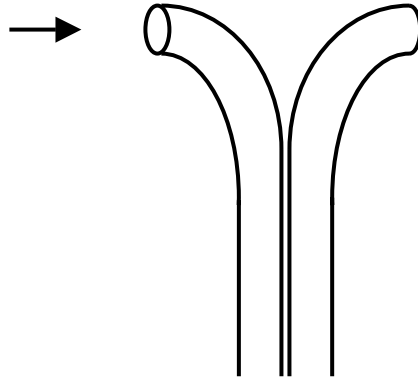


**Figure 2: Schematic of a type "S" probe**

*Venturi probes*

Venturi Probes are used to amplify the measured velocity pressure in a flowing fluid. The flow is accelerated in the venturi passages, as in a flow nozzle, so that the dynamic pressure increases and the static pressure reading is lower than that obtained with a Pitot-static probe (Fig. 3). According to the particular design, values of up to 8 times the velocity head are obtained. Even higher factors, up to 14, have been obtained with double-venturi probes. Disadvantages here are the relatively high probe diameter compared to a Pitot, the dependence on Reynolds number and the sensitivity to angular variations.

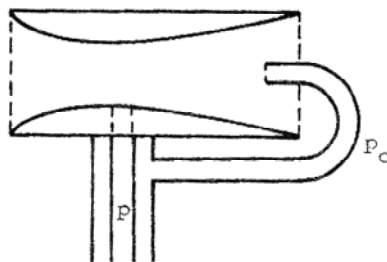


**Figure 3: Schematic of a Venturi probe**

*Incidence insensitive static pressure probes*

For low speed flows ( $M \ll 1$ ) incidence insensitive probes have been developed that are based on measuring the static pressure in the cavity downstream a blunt body with sharp edges (Figure 4<sup>[10]</sup>). Two examples thereof are illustrated by the probes shown in Figure 4. The sharp edges make that the

separation point is fixed independent of Reynolds number. The reading of the probe may be different from the real static pressure and a calibration is needed. The angular insensitivity is in the order of  $\pm 20^\circ$ .

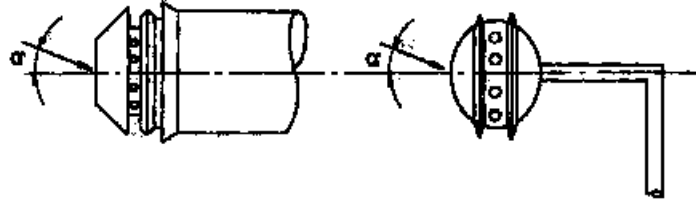


**Figure 4: Incidence insensitive static pressure probes**

#### *Averaging pitots for measuring flow rate in pipes*

Besides flanges, nozzles and to a lesser extent venturis, averaging Pitots are often used in industry to measure flow rates in conduits. It is in effect a multi-port averaging Pitot. A front view of a multi-port averaging Pitot system is shown in Figure 5. The flow element operates by sensing an impact pressure and a reference pressure through multiple sensing ports, at specific locations across a pipe, connected to dual averaging plenums. The resultant difference is a differential pressure signal. Sensing ports are located on both the up and downstream sides of the flow element. The number of ports is proportional to the pipe diameter. Several designs are available (Annubar<sup>®</sup>, Torbar<sup>®</sup>, etc.), each claiming superior hydrodynamic flow characteristics. In the specific design shown in Figure 5, the square shape establishes a fixed separation point of the fluid from the sensor. The fixed separation point reduces changes in the low pressure and makes the probe Reynolds independent in a wide practical range. A disadvantage of this design may be that the probe traverses the duct causing an important obstruction for the flow with a corresponding pressure loss. Furthermore it may be necessary to introduce corrections to account for the bluff-body blockage effect<sup>[1]</sup>. The axial alignment usually is also critical.

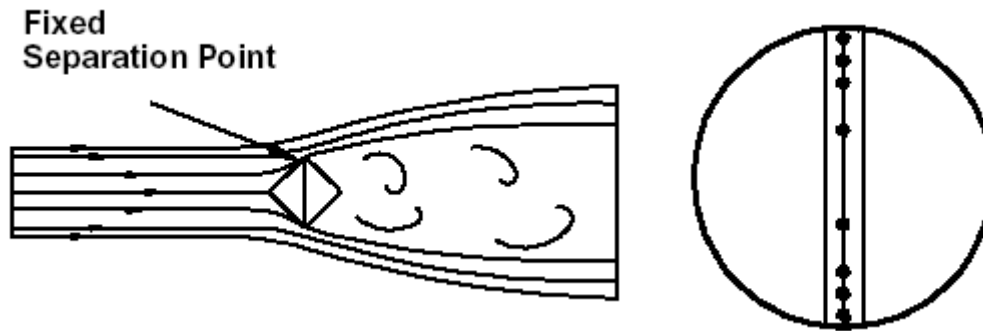


Figure 5: a. Flow around an averaging pitot; b. averaging pitot traversing a pipe<sup>[2]</sup>

## Design alternatives

In the search for an optimised velocity pressure probe, two alternative roads are followed.

### *Venturi type*

A first idea to increase the pressure gain of the probe is to introduce a venturi like design to boost up the differential pressure. This design – which already exists – would be adapted to cope with problems like soot deposit etc.

Major concerns here are the pressure losses over the venturi which, if they become too high, will result in a small velocity gain. Other concerns are that soot and other deposits might disturb the good functioning of the probe.

It is expected that the angular insensitivity will be better than for the bi-directional probe since the velocity in the throat – where the static pressure is taken – will remain constant for small angular variations. This is not true for the bi-directional probe where small angular variations lead to important changes in the turbulent wake behind the probe where the lower pressure is measured.

### *Drag type*

A second idea to obtain a pressure gain over the probe is to play with the shape of the probe and to find an appropriate location for the pressure ports.

The main idea here is that the drag coefficient – and thus the pressure difference – of objects can be increased by selecting an appropriate shape as can be seen from table 1.





The drag coefficient can be made independent of Reynolds number ( $Re > 1\,000$ ) by introducing sharp edges. The sharp edges make that the flow separation points are fixed by the geometry of the object irrespective of the flow velocity. The flow profile over the object is invariable. This in contrast with streamlined bodies like cylinders who are strongly Reynolds dependent.

For Reynolds numbers below 1 000 friction forces become important relative to forces associated with the pressure distribution over the object. For Reynolds numbers well above 1 000 friction forces can be neglected and the drag coefficient relates to the pressure distribution by the equation

$$C_D = \frac{\oint p dA}{\frac{1}{2} \rho v^2 A}$$

Major concerns here are the angular insensitivity and the location of the pressure ports. The angular insensitivity requires rotational symmetry so that the study can be limited to those objects having cylindrical, conical or sphere like shapes. Since the purpose of this study is to increase the differential pressure over the object, only those shapes with a drag coefficient above one have been considered.

Some examples of drag coefficients ( $C_D$ ) are given in table 1.

Object	Diagram	$C_D$ ( $Re > 1000$ )
Disk		1.17
Hollow semi-cylinder opposite stream		1.20
Hollow Hemisphere opposite stream		1.42
Solid Hemisphere flow normal to flat side		1.17

**Table 1: Drag coefficient data for selected objects ( $Re > 1000$ )<sup>[4]</sup>**

Note that increasing the drag may also be realised by introducing vents in the side wall of the probe.

# Experiments

## Probes tested

A venturi based pressure probe is made composed of an upper cylindrical recess to measure the total head, this in analogy with the bi-directional probe, and a venturi. The constraints to the outer dimensions are governed by the limitation that it should be possible to introduce the probe into the conduit through a cylinder with inner diameter 50mm.

The convergent part has an angle of around 21° in order to efficiently speed up the flow over a short distance. In a first prototype A15\_D8, the convergence angle is only about 15° in order to have the throat section centrally in the probe. This has later been optimised in prototypes D10, D8 and D6 where the convergence is 21.2° and the diameter of the throat section is 10mm, 8mm or 6mm respectively. Downstream the throat, a diffuser with a reduced angle of 4.4° is installed<sup>[4]</sup>. This angle needs to be small in order for the flow not to detach and to recover in this way a maximum amount of kinetic energy. Indeed the flow has to oppose a rising pressure gradient.

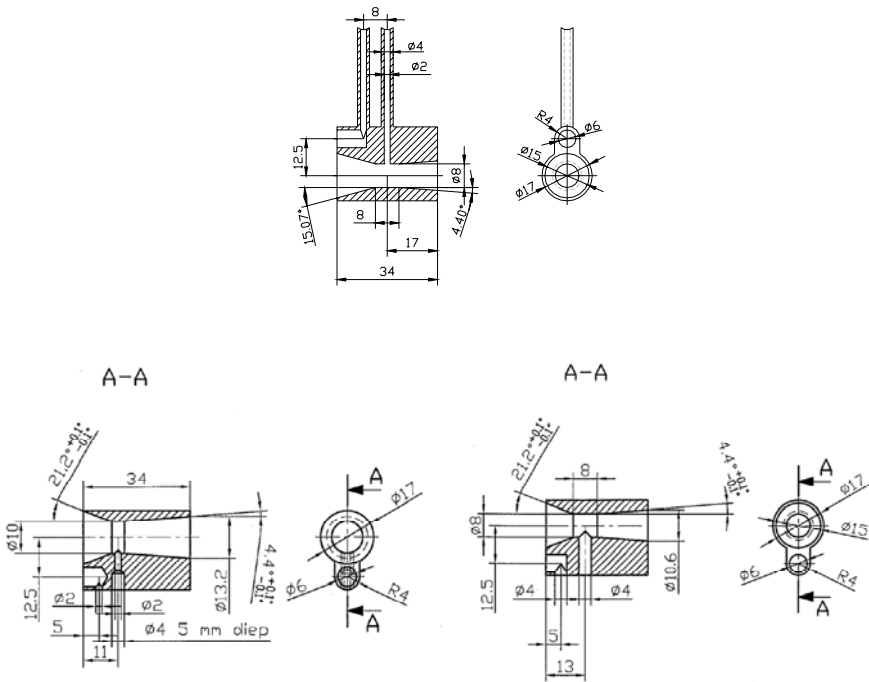


Figure 6: Venturi probes; Prototypes A15\_D8 (top), D10 (left) and D8 (right)

Besides the venturi based probes, several probes based on the pressure drag have been fabricated that have 1) a rotational symmetry; 2) a drag coefficient above one; 3) sharp edges for the flow to detach at a fixed point and 4) a simple and robust design.

A selection of 4 of those probes, together with the bi-directional probe<sup>[7]</sup>, are presented below.

Probe	Section view	Frontal view
Bi-dir (Bi-directional probe)		
HSphere_Sphere (Hemispherical probe; shell)		
Hsphere_Con (conical shape inside)		
Disc (sharp edge)		
Cone (α = 18°)		

**Table 2: Overview of probes tested**

The hemispherical probe (shell) tested has an outer diameter of 22.6 mm and a shell thickness of 1 mm which is reduced down to 0.5 mm at the circular border facing the flow.

All positive pressure measurements are taken centrally through the back part (right hand side) of the instrument except for the bi-directional probe. All lower pressure measurements are taken at the back of the probes just underneath or above the higher pressure conduit.

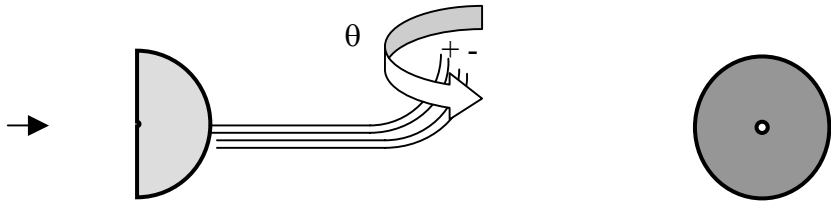


**Figure 7: Location of pressure ports on the prototypes tested; sectional and frontal view**

**In a first experiment** the angle of incidence  $\theta$  of the probe is varied from  $-90^\circ$  to  $+90^\circ$  at an air speed of about 4.1 m/s (Figure 8; only part of the data is shown). The experiment is done in windtunnel 1 as described in [9].



The experiment has been repeated in a range from  $-20^\circ$  to  $+20^\circ$  for the Bi-directional probe, the hemisphere probe and the Venturi probe at a velocity of 8.2 m/s with similar, even more stable results.

**In a second experiment** the probes are calibrated as function of the Reynolds number in a velocity range from 1 to 40 m/s. The uncertainty on the velocities below 0.9 m/s (down to 0.3 m/s) are so high that they have been excluded from the report.

### *Instrumentation and uncertainty analysis*

A detailed description of the instrumentation used and the uncertainty analysis conducted is given in [9].

## **Results and discussion**

All probes have been evaluated against five major criteria being 1) angular sensitivity; 2) pressure gain; 3) Reynolds independence; 4) expected behaviour in ‘dirty’ media and 5) design complexity.

The results are summarised in table 3.

### *Angular sensitivity*

Figures 8 till 11 show the test results for flow angle dependency for several probes tested, as described in the previous section. The figures display the ratio of the probe factor at an incidence angle  $\theta$  to the probe factor at neutral position  $\theta = 0$ , i.e.  $k_p(\theta)/k_p(\theta=0)$  ( $M \ll 1$ ).

Figure 8 shows the results for the Venturi type probes at an air velocity of 8.2 m/s. Comparing the results of the probes A15\_D8 and D8, which are basically the same except for the convergent part which is  $15.1^\circ$  respectively  $21.2^\circ$ , the results suggest that less convergence results in better angular insensitivity. For probe A15\_D8 the angular insensitivity, defined as the maximum angular deviation ( $\pm$ ) within which the error remains limited to 1%, is  $4^\circ$  to  $5^\circ$ .

The results for probes D8 and D6 are not really better than the results obtained with the Bi-directional probe.

The somewhat strange results of probe D10 can partly be attributed to the fast changing probe factor for Reynolds numbers around 10 000 (Fig. 12).

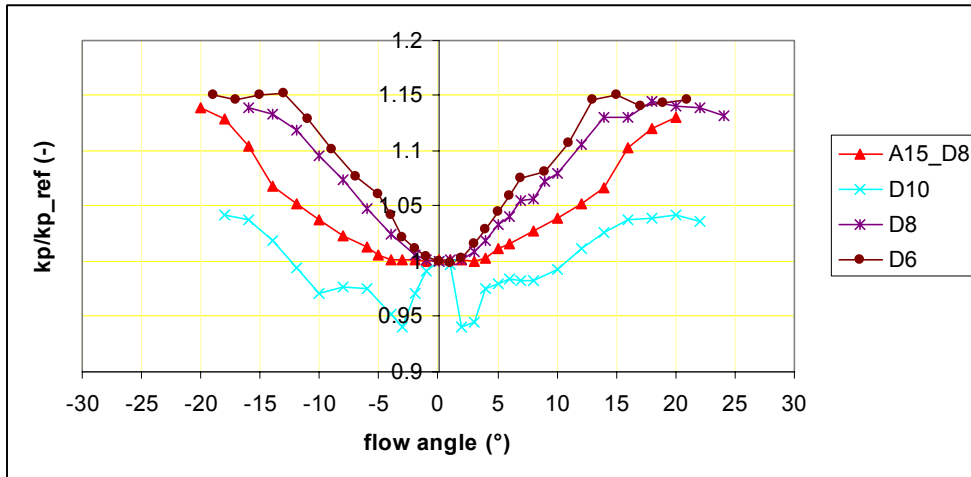


**Figure 8: Angular sensitivity of the Venturi based probes**

For the drag based probes two measurement series at velocities of about 4.1 m/s and 8.2 m/s are taken (Fig. 9, 10 & 11). The measured standard deviation at 4.1 m/s is 0.05 m/s and the turbulence intensity is 1.3%. The selection of the air speed is based on the lowest expected Reynolds numbers when running fire tests according to the SBI standard. The results at a velocity of 8.2 m/s show more stable results as shown in Figure 9 for a hemispherical probe.

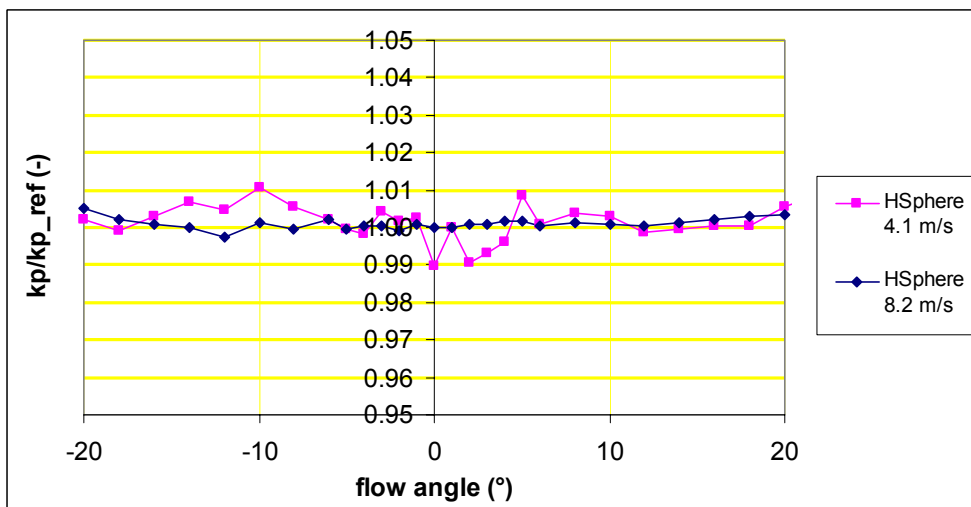


**Figure 9: Influence of air speed on stability of results**

Figure 10 shows that the probe factor as measured for the Bi-directional probe, increases with roughly 1% per degree initially. This is a high number so much the more because small angular variations due to misalignment or due to flow effects can often not be excluded.

For the hemisphere shell (Fig. 9) the error is limited to approximately 1% in the range  $-20^\circ$  to  $+20^\circ$ . Furthermore, in the range from  $-45^\circ$  to  $45^\circ$  the error remains limited to 5%. Outside that range, the differential pressure drops fast and the exact location of the low-pressure port becomes predominant.

The disc and the conical probe show errors in the order of 2% and 4% respectively in the  $\pm 20^\circ$  range. This indicates that the drag force over a disc object changes little for limited angular variations.

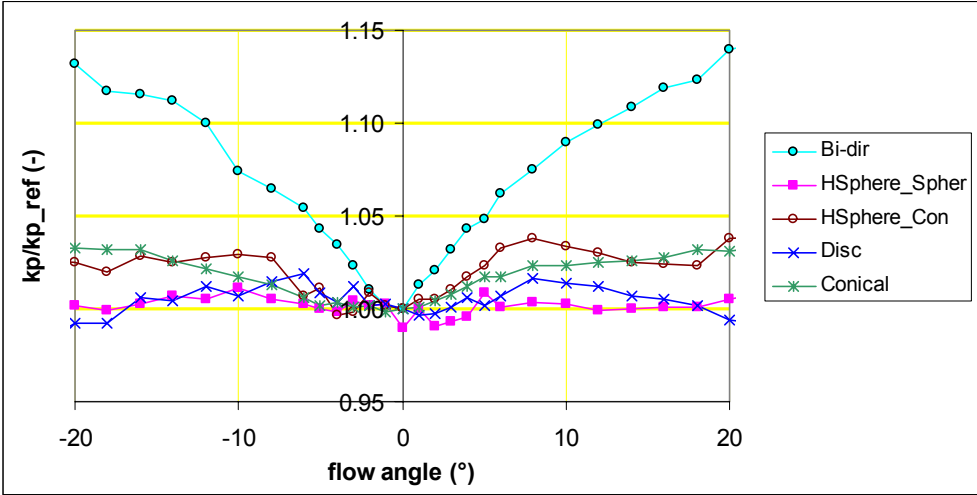


**Figure 10: Angular sensitivity of drag based probes (v = 4.1 m/s)**

The effect of modifying the inlet geometry is demonstrated by comparing two hemispherical probes with either a spherical inlet thus defining a hemispherical shell probe or a hemisphere with a conical inlet. Figure 11 shows that although the error remains limited to 5% in a range between  $+25^\circ$  and  $-25^\circ$ , there is a clear negative influence modifying the inlet from hemispherical to conical. It is expected, for a hemispherical probe, that any deviation from the hemispherical shape for the inlet port has a negative effect on the angular insensitivity. However, different inlet port shapes may still give considerable better results than obtained with a bi-directional probe.

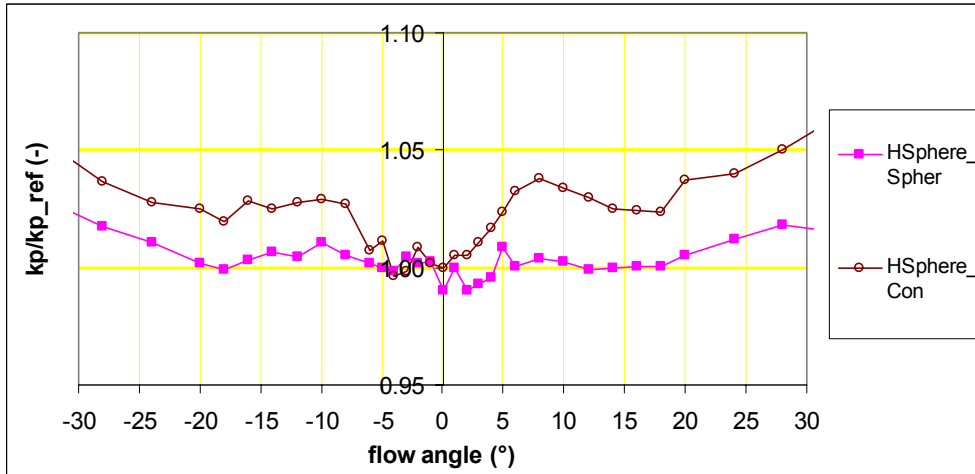


**Figure 11: Angular sensitivities for conical and spherical inlets**

*Differential pressure gain and Reynolds dependence*

The probe factor is a number that needs to be introduced if the differential pressure measured over the probe is different from the dynamic pressure ( $p_{\text{dyn}} = \rho v^2 / 2$ ). It is defined as

$$k_p = \frac{\sqrt{\frac{2\Delta p}{\rho}}}{v} \quad [-]$$

Practically speaking the probe factor for a NPL Pitot-static tube is equal to 1. Figures 12 and 13 display the probe constant as a function of the Reynolds number related to the outside diameter of the probes. The Reynolds number is defined as

$$\text{Re} = \frac{\rho \cdot v \cdot D}{\mu} = \frac{v \cdot D}{\nu} \quad [-]$$

and is a measure of the ratio of inertia forces to viscous forces.

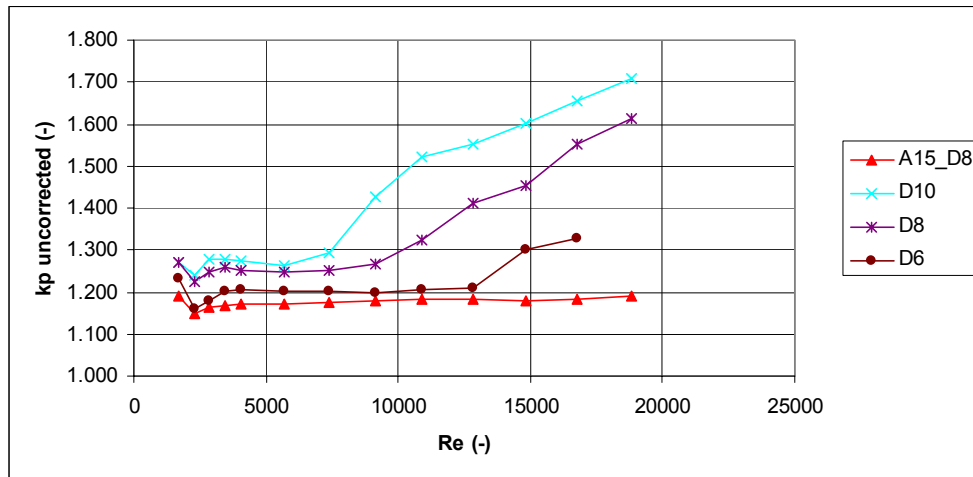


**Figure 12: Uncorrected (for bluff body blockage) probe factor for the Venturi type probes**

Figure 12 reveals that the venturi probes only start to boost up the pressure for higher Reynolds numbers. Below a critical Reynolds number, which is probe dependent, the probe factors are fairly constant. With respect to pressure gain and Reynolds independence, probe A15\_D8 and especially probe D6 could be used in the SBI. When running the SBI test equipment within the specifications of the standard, the expected Reynolds numbers with respect to the probe outside diameter (17mm) roughly remain between  $Re = 5\ 000$  and  $11\ 000$ .

Probe D6 is to be preferred since it has a slightly higher pressure gain and, based on these first results, is more stable in the envisaged range. However, probe D6 is very sensitive to small angular variations (Figure 8).

The probe factors as displayed in Figure 12 have not been corrected for bluff body blockage. The results presented are therefore overestimated by a factor in the order of 1%.

The results for the drag based probes show that the hemisphere shell has a constant probe factor as high as 1.22 to 1.23 for Reynolds numbers above 5 000. This corresponds to a differential pressure gain of around 50% with respect to a Pitot-static tube. The probe can be used at lower Reynolds numbers but then requires calibration. The results obtained so far suggest that the probe factor first decreases to 1.20 for  $Re = 2\ 000$  after which it begins to rise to high numbers (1.43 at  $Re = 420$ ; the

95% confidence interval is however in the order of 20% in this point). This is when friction forces become more important and when their effect on the drag can no longer be neglected.

Based on the statistical analysis of the measurements in the interval  $Re = 4\,900$  to  $60\,000$  the probe factor is calculated to be  $k_p = 1.224$  ( $N = 29$ ). The standard error of the mean value (t-test) is  $0.008$  while the standard deviation is  $0.0043$ . For the test instrumentation used, the uncertainty (95% confidence) on the individual measurements remains below  $0.013$  for Reynolds values between  $4\,900$  and  $7\,000$  and between  $20\,000$  and  $60\,000$ . Assuming that this uncertainty is also valid in the remaining points (in reality it is higher), the standard uncertainty is estimated to be  $k_p = 1.224 \pm 0.008$ . This assumption is not so unrealistic since the measurements consist out of three data sets, each with different instrumentation. When the uncertainty of one data set reaches its highest level, it matches closely the next data set which has, at that point, its lowest uncertainty.

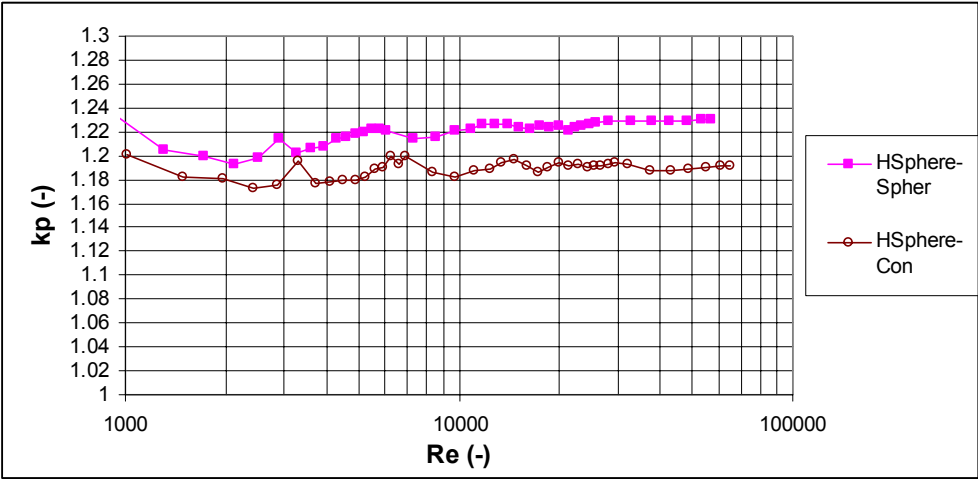


**Figure 13: Probe factor for Hemispherical probes with conical and hemispherical recess**

Changing the inner shape of the probe from hemispherical to conical (HSphere Con) reduces the probe factor with approximately 3% to  $1.195$  which makes that the differential pressure over the probe reduces with some 6%. A similar slight reduction in the probe factor is observed for Reynolds numbers below  $2\,000$  to  $3\,000$ .

A Reynolds dependence is not favourable for a pressure probe since it requires corrections to be introduced.

*Expected behaviour in 'dirty' media*

The behaviour of the probes in “dirty media” plays an important role as e.g. small particles, transported by the combustion gases, can block the pressure ports, which results in erroneous measurements. In aviation for example, planes have crashed because the pilot had a wrong picture of the plane’s speed due to blockage of one of the pressure ports.

The position of the pressure ports plays an important role in this respect. If the high pressure port is placed perpendicular to the main stream flow, particles do not tend to block the pressure port.

Therefore the total pressure port is positioned such that it is not in the main stream flow, but preferably as much as possible, makes an angle with the main stream flow.

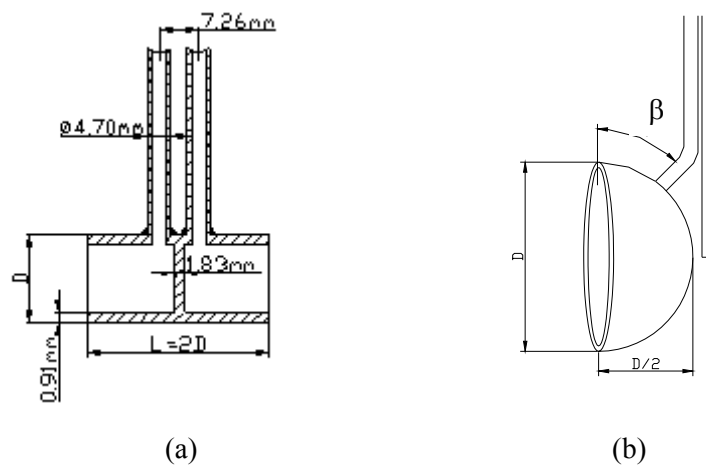


**Figure 14: a. bi-directional probe; b. Hemisphere shell**

The pressure port thus is, with respect to blockage, positioned preferably substantially perpendicular to the main stream flow (Figure 14.b: angle ‘β’ approaching zero). In this way, and when the probe axis is placed horizontally, deposits drop out even more easily from the hemispherical cup – without ever blocking the pressure port – than in the case of the bi-directional probe.

It is expected that the pressure inside the hemisphere cup equals the total head and is almost constant within the cup so that the high pressure sensing port can have any desired location on the hemisphere shell. Ower and Pankhurst<sup>[8]</sup> write in relation to Pitot-static tubes that “there is abundant experimental evidence to confirm that the pressure indicated by a properly aligned open-ended tube facing the current is accurately equal to the local total head – except for viscosity effects at very low Reynolds numbers – and that the shape of the tube may be varied within wide limits without sensibly affecting the observed pressure.”

The low pressure sensing port typically is positioned at the back or the side portion of the hemisphere shell such that it has a sensing port in the wake of the body. The actual position of the lower pressure port in the wake of the body is less important. Turning the probe with respect to the incoming flow will however influence this wake. Because of symmetry reasons, the lower pressure port preferably lies on the axis of symmetry of the probe.

Eventually the lower pressure could, in analogy with the bi-directional probe, be taken from a small cylinder welded on the back side of the hemisphere (Fig. 15). This may change the probe factor slightly.

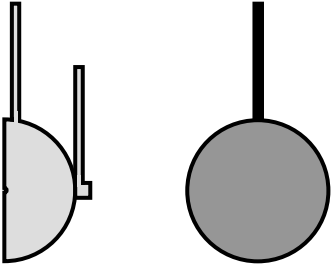


**Figure 15: Possible pressure port position on the hemisphere**

In the form shown in figure 14.b the body is mounted with a hollow tube that connects the inner hollow hemisphere with a (positive) pressure port. This tube supports and positions the device in the flow. The second hollow tube shown measures the pressure in the downstream wake of the device. In the form shown, it is connected loose from the device



The total head pressure opening of the Venturi type probes has an inner diameter of 8mm which is approximately a factor 2 smaller than for the bi-directional probe and a factor 4 when expressed in surface area. This makes that, with respect to the bi-directional probe, the Venturi probe is less favourable. Experience will have to demonstrate whether this is really a drawback or not. As for the bi-directional probe the higher pressure port is placed perpendicular to the flow. When the probes are placed horizontally, gravity will help to keep the pressure ports free.

The expectation is that the lower pressure port in the throat section will remain free due to the local acceleration of the flow. For probe D6 where the throat section reduces down to 6mm, this may no longer be true when the throat itself gets obstructed.

It is our believe that, with respect to 'dirty' media, the hemispherical probe will behave at least equally as good as the bi-directional probe. Both the hemispherical probe and the Venturi probe A15\_D8 have been tested successfully in the SBI. They both passed without any problem a propane burner (step) calibration and a heptane pool fire calibration.

#### *Design complexity and practical use*

In relation to the bi-directional probe, the hemispherical probe is straightforward to manufacture while the Venturi probe requires specialty tools.

The angular insensitivity of the Hemispherical probe makes it easy to install since accurate positioning is no longer crucial. The Venturi probe A15\_D8 requires accurate positioning. The local minimum in differential pressure for a well aligned probe can be used to do a proper alignment.

## Conclusions

In view of the sensitivity of the bi-directional probe to angular variations, two new velocity pressure probes have been developed. The bi-directional probe is used in most intermediate and large scale heat release rate tests and is considered state of the art.

A first design accelerates the flow in a Venturi throat section to obtain a reduced static pressure measurement thus increasing the differential pressure. The differential pressure gain of the preferred Venturi design, A15\_D8, is in the order of 37% with respect to a Pitot-static probe. With this probe, an angular insensitivity of about  $\pm 5\%$  has been achieved. The probe factor remains almost constant in the range  $Re = 4\ 000$  to at least  $19\ 000$ . Furthermore, the probe is suited to be used in smoky environments and the first tests, that include a heptane pool fire, look promising.

A second design consists of a bluff body with sharp edges. The bluff body generates a high pressure drag while the sharp edges make the flow separate from the body at a fixed zone, thus making the flow profile over the object invariable of the flow velocity. This results, for the proposed hemispherical shell, in a steady probe factor that is estimated at  $1.224 \pm 0.008$  for Reynolds numbers in the range  $5\ 000$  to  $60\ 000$ . This corresponds to a pressure gain with respect to a Pitot-static tube of approximately 50%. The Reynolds numbers are related to the outside probe diameter. The probe is insensitive to angular variations over a range that exceeds  $\pm 20^\circ$ . Furthermore it is expected that it will behave at least equally as good in smoky environments as the bi-directional probe.

The design is straightforward, its limited size make that only a small hole needs to be drilled to install it and the head losses related to drag of the probe are negligible. Furthermore, no accurate alignment is needed when installing or servicing the probe.

Table 3 summarises the findings of the experiments. The differential pressure gain given is with respect to a pitot-static tube. The angular insensitivity is expressed as the limiting angle in which interval the error on the square root of the differential pressure remains limited to 1% respectively 2%.

Probe	Angular insensitivity 1%/2% ( $\pm$ °)	Re insensitivity (Re > 5 000)	approximate $\Delta p$ gain (%)	Head losses	Size	Manufacturing	'dirty' media
Bi-dir	1 / 2	++	11	++	+	0	++
HSphere_Sphere	23 / 30	++	50	++	++	++	++
Hsphere_Con	4 / 6	++	43	++	++	0	++
Venturi D6	1 / 3	+	44	++	+	-	0
Venturi A15_D8	5 / 6	++	37	++	+	-	+

**Table 3: Summary table of experiments**

Based on the findings as presented in this paper and which have been summarised in Table 3, it is recommended to replace the bi-directional probe in all heat release rate test equipment by the hemispherical probe. This would lead to higher differential pressure signals, thus reducing the uncertainty. The main improvement however would be that small misalignments of the probe would have no noticeable effect on the results.

As a general remark for all probes discussed in this paper, the measurements should be corrected for bluff body blockage<sup>[1][9]</sup> if used in closed conduits. Table 4 displays the increase in drag, and thus  $\Delta p$ , for frequently used duct diameters. Thus the probe factor  $k_p$  should be adjusted with the square root of one plus the corresponding value in Table 4:  $k_p^{corrected} = k_p^{probe} \sqrt{1 + \Delta C_D}$ . For a hemispherical probe with outside diameter of  $\phi=22.6$  mm introduced in a duct with inner diameter  $\phi=315$  mm and with a 4mm diameter support tube lying in the same cross section as the probe, the corrected probe factor becomes  $k_p^{corrected} = 1.224 \sqrt{1 + 0.0227} = 1.238$ .

	Without support tube in same plane			With support tube $\phi=4\text{mm}$ in same plane		
$\phi$ probe (mm)	22.6	20	15	22.6	20	15
Estimated $C_{DU}$	1.42	1.42	1.42	1.42	1.42	1.42
$\Delta C_D$ (%) ( $\phi=0.250\text{m}$ )	1.47	1.15	0.65	3.13	2.83	2.37
$\Delta C_D$ (%) ( $\phi=0.315\text{m}$ )	0.92	0.72	0.41	2.27	2.08	1.79
$\Delta C_D$ (%) ( $\phi=0.4\text{m}$ )	0.57	0.45	0.25	1.65	1.54	1.35
$\Delta C_D$ (%) ( $\phi=0.5\text{m}$ )	0.37	0.29	0.16	1.24	1.17	1.05
$\Delta C_D$ (%) ( $\phi=1.0\text{m}$ )	0.09	0.07	0.04	0.54	0.52	0.49

**Table 4: Drag increase of the hemisphere probe in closed test/measurement sections**

The use of the hemispherical probe is not limited to closed conduits nor to fire applications.

## Reference List

- [1] Cooper K.; Bluff-Body Blockage Corrections in Closed- an Open-Test-Section Wind Tunnels; Chapter 6 of the handbook edited by Ewald B.F.R.; Wind Tunnel Wall Correction; AGARD-AG-336, 1998
- [2] Dieterich Standard, a subsidiary of Rosemount Inc.; Product data sheet: “Diamond II+Annubar® Primary Flow Element”; 00813-0100-4760, DS-4009
- [3] European Standard - Reaction to fire tests for building products - Building products excluding floorings exposed to the thermal attack by a single burning item. EN 13823:2002. CEN Central Secretariat, Brussels 2002
- [4] Fox R.W. and McDonald A.T.; Introduction to fluid mechanics; John Wiley & Sons, New York 1985
- [5] Gracey W.; Wind tunnel investigation of a number of total pressure tubes at high angles of attack – subsonic, transonic and supersonic speeds; NACA TR 1303, 1957

- [6] International Standard – Fire tests – Full-scale room test for surface products; ISO 9705:1993; International Organisation for Standardisation, Geneva, 1993
- [7] McCaffrey B.J. and Heskestad, G.; A Robust Bidirectional Low-Velocity Probe for Flame and Fire Application; Combustion and Flame 26, 125-127 (1976)
- [8] Ower E. and Pankhurst R.C.; The Measurement of Air Flow; Pergamon Press Ltd., Oxford, 1966
- [9] Sette B.J.G.; Critical considerations on the use of a bi-directional probe in heat release measurements; Fire and Materials; Accepted for publication December 2004
- [10] Van den Braembussche R.A.; Measurement Techniques in Fluid Dynamics, An Introduction; von Karman Institute for Fluid Dynamics, 1994



### **A.3. Article 3**

*Sette, B., Theuns E., Merci B., Temperature effects on the mass flow rate in the SBI and similar Heat Release Rate Test Equipment, Fire and Materials<sup>[58]</sup>*

Out for review: 7 December 2004





# Temperature effects on the mass flow rate in the SBI and similar Heat Release Rate Test Equipment

*Bart J.G. Sette<sup>1</sup>, Erwin Theuns<sup>1,2</sup>, Bart Merci<sup>1,3</sup>*

*<sup>1</sup>Ghent University, Department of Flow, Heat and Combustion Mechanics, Ghent, Belgium*

*<sup>2</sup>Stockman Engineering, Ghent, Belgium*

*<sup>3</sup>Postdoctoral Researcher of the Fund of Scientific Research – Flanders (Belgium) (FWO-Vlaanderen)*

*Correspondence address:*

*Ottergemsesteenweg 711, B-9000 Ghent, Belgium*

*E-mail: Bart.Sette@UGent.be ; Tel.: +32 9 243 77 50; Fax: +32 9 243 77 51*

## **Abstract**

*In various medium to large scale fire test equipment like the ISO Room Corner test (RC) and more recently the Single Burning Item test (SBI) the mass flow rate measurement of the combustion gases plays a key role in the determination of the heat release rate and smoke production rate.*

*With the knowledge of the velocity profile and the temperature of the flow, the mass flow rate is obtained by measuring the velocity on the axis of the duct. This is done by means of a bi-directional probe based on the pitot principle.*

*However, due to the variation of the mean temperature and the temperature gradient in any cross section of the duct, introduced by ever changing combustion gas temperatures, the velocity nor the density profile are constant in time. This paper examines the resulting uncertainty on the mass flow rate.*

*Key words: fire tests, mass flow rate, heat release rate, velocity profile, uncertainty*

## Nomenclature

$\delta$	deviation [%]	HRR	Heat Release Rate [kW]
$\mu$	dynamic viscosity [Pa.s]	$\dot{m}$	mass flow rate [kg/s]
$\nu$	kinematic viscosity [m <sup>2</sup> /s]	Nu	Nusselt number [-]
$\rho$	density [kg/m <sup>3</sup> ]	p	pressure [Pa]
$\bar{\rho}$	mean $\rho$ over a cross section [kg/m <sup>3</sup> ]	$\Delta p$	differential pressure [Pa]
$\tau$	time constant [s]	Pr	Prandtl number [-]
$\tau_{\text{duct}}$	time constant of the duct [s]	r	radius (cylindrical coordinates)
$k_p$	probe constant [-]	R	radius of the duct [m]
$k_t$	velocity profile correction factor [-]	Re	Reynolds number [-]
A	surface area [m <sup>2</sup> ]	T	temperature [K]
c	heat capacity [J/kg.K]	u(x)	standard uncertainty on x
D	characteristic probe diameter [m]	v	velocity [m/s]
h	convectivity [W/m <sup>2</sup> .K]	$\bar{v}$	mean v over a cross section [m/s]
RC	Room Corner test		
SBI	Single Burning Item test		
SBI RR2	Second SBI round robin[4]		

## Introduction

The research for the present paper started as a result of the observation of an apparent hysteresis effect in the Single Burning Item test (SBI)[1] between the heating mode, when the fire is still growing, and the cooling mode, when the Heat Release Rate (HRR) diminishes.

In a ‘step calibration’ according to the SBI standard, a first burner is ignited after two minutes and remains burning for three minutes at a level of 30kW. After this five minutes period, the propane supply is switched from the first burner to the main burner, which after another period of three minutes is switched temporarily to approximately 93kW (see Table 1).

Step number	Time [min]	Burner	HRR [kW]
I	0 to 2	-	0
II	2 to 5	auxiliary	30
III	5 to 8	main	30
IV	8 to 11	main	92.7
V	11 to 14	main	30
VI	14 to 17	-	0

**Table 1: Sequence SBI step calibration**

One can clearly observe that the measured HRR in step V, when the burner comes back to 30kW, is systematically higher than the HRR measured in steps II and III. (Figure 1; Table 2).

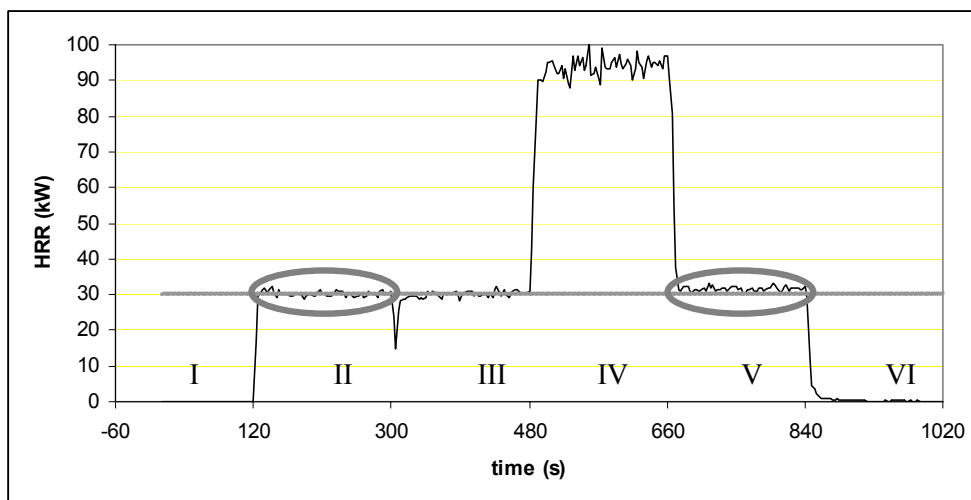


**Figure 1: Step calibration SBI; example**

Table 2 shows the mean HRR values for steps II till VI of this ‘step calibration’, based on the data of 30 laboratories who participated in the second SBI round robin program (SBI RR2) [4].

Besides the mean value, the ‘standard error of mean’ and the ‘standard deviation’ are given. The standard error of mean is a measure for the variability of the population mean. As an example, there is a 95% probability that the mean value for step II lies in the interval  $(29.84 \pm \sigma * 0.09)$  whereby the

factor  $\sigma$  is the coverage factor which is approximately 2 for a 95% confidence interval. The standard deviation on the other hand expresses the probability that any new sample taken lies within the given interval. In the case for step II, the chance that any new value lies within  $(29.84 \pm 2 * 0.52)$  is 95%.

N=30	Step II	Step III	Step IV	Step V	Step VI
Mean (kW)	29.85	29.89	92.29	30.55	0.54
Deviation from Step II (%)	0.00	0.13	-	2.35	-
Std. Error of Mean (kW)	0.10	0.10	0.52	0.10	0.14
Std. Deviation (kW)	0.54	0.54	2.81	0.54	0.77

**Table 2: Mean HRR values found in the ‘step calibration’ of the SBI RR2**

Note that for the statistical analysis of tables 2 and 3:

- two outliers have been excluded from the calculations for step III and one for step IV.
- all distributions can be considered to be normal (Kolmogorov-Smirnov test).

## Factors possibly causing the deviation

Table 2 confirms in a statistical way the observation of a systematic deviation in step V. The HRR measured in step V is, on average, 2.35% higher than in step II.

A first possible explanation is shown in table 2 by means of step VI. Apparently there is a net drift on the equipment. This drift amounts 1.8% of the burner heat output at 30kW and finds its cause in a drift on the oxygen analyser (see table 3).

N=30	Drift O <sub>2</sub>	Drift CO <sub>2</sub>
Mean (ppm)	-36	10
Std. Error of Mean (ppm)	13	7
Std. Deviation (ppm)	69	39

**Table 3: Drift on gas analysers in the ‘step calibration’ of the SBI RR2**

Although the standard allows for a drift of 200ppm on both the oxygen and carbon dioxide analyser, the above shows that even a small drift has a substantial effect on the HRR.

Table 2 further suggests that besides the drift on the gas analysers, other effect(s) may play.

The propane mass flow rate to the burners is controlled by means of a mass flow rate controller. The repeatability of the instruments, used in at least 2/3 of the labs participating in SBI RR2, is better than 0.2% of the reading. No information was available on the remaining instruments but the repeatability is expected to be of the same order.

Another element that can explain this deviation in the HRR in step V is the way the mass flow rate is obtained.

## Mass flow rate

The technique for measuring mass flow rate currently used in intermediate to large scale calorimeter tests consists of measuring the velocity on the axis of the duct and to multiply this with a correction factor  $k_t$  to obtain the mean velocity. This mean velocity is then multiplied with the mean density and the surface area to obtain the mass flow rate.

$$\dot{m}(t) = \bar{\rho} k_t v_{axis}(t) A \quad [1]$$

$k_t$  is the velocity profile correction factor and is defined as

$$k_t(t) = \frac{\int v(t) dA}{v_{axis}(t) A} \quad [2]$$

Since the distribution of the velocity is not known,  $k_t$  is approximated and taken as a constant over time. If we knew the velocity distribution, the mass flow rate could be approximated by

$$\dot{m}(t) = \bar{\rho} \int_A v(t) dA \quad [3]$$

which is only correct when the density is uniform over the measuring section. Ideally we would want to measure

$$\dot{m}(t) = \int_A \rho(t) v(t) dA \quad [4]$$

Assuming a good mixing of the combustion gases prior to reaching the measurement section, the only possible cause for having a non uniform density distribution is a temperature effect. The initially cool, horizontally placed duct wall absorbs energy and cools down the combustion gases nearby while later

on in the test, it may partially give back the energy to the fluid resulting in higher gas temperatures close to the wall. This cooling and heating process of the flow also introduces two contra rotating swirls that are symmetrical to a vertical plane through the duct axis. These swirls introduce a velocity component perpendicular to the axis of the duct. The process is governed by natural convection perpendicular to the flow direction.

The velocity on the axis is measured by means of a bi-directional probe. In [5] it is demonstrated that the bi-directional pressure probe used in the SBI introduces an error on the HRR. The probe factor ( $k_p$ ), which is assumed to be constant over the working range, increases with decreasing Reynolds number. In other words, when combustion gases get hotter, the probe 'constant' increases resulting in an overestimation of HRR and SPR. Based on the expected temperature differences of combustion gases between step V and steps II and III (figure 4), the related error is estimated to lie between 0.5 and 1%.

Additional errors may be introduced by approximating formula 4 by formula 1. This is done since the velocity and density distribution over the measuring section are not known at anyone time in the test. Actually the following approximations are made:

- ✓ The density over the test section is constant; The density is obtained from a temperature measurement at one (or more) positions;
- ✓ The velocity profile correction factor  $k_t$  is constant over time; It is thus independent of temperature and, more general, Reynolds number; It follows out of one (or more) calibrations.
- ✓ The combustion gases have the same properties as air.

The last assumption cannot cause the deviation in step V since the burner heat output is the same for steps II,III and V.

In order to quantify the error made assuming a uniform density distribution and a constant velocity profile over time, a simplified CFD model of a straight piece of duct is made where the incoming air

follows a heating-cooling cycle. The same model also allows to quantify the error in the hypothetical case that the exact velocity profile ( $k_t$ ) is known at any time. Details of the model used can be found in [6]. Before discussing the model, the time constant of the duct system is estimated.

### Time constant duct system

The order of magnitude of the time constant of the duct system is estimated out of the empirical relationship for turbulent flow in the entrance region of smooth tubes as recommended by Nusselt[8]

$$Nu = 0.036 Re^{0.8} Pr^{\frac{1}{3}} \left(\frac{D}{L}\right)^{0.055} \quad \text{for } 10 < L/D < 400$$

where D represents the inner duct diameter and L is the distance from the entrance.

It must be said that errors in the order of  $\pm 25\%$  are not uncommon so that the derived time constant should be read as an order of magnitude rather than as an absolute number.

The duct inner diameter is 0.315m, the distance from the entrance is 6m and the physical properties of the stainless steel, which is 2mm thick, are  $\rho = 7800 \text{ kg/m}^3$  and  $c=440 \text{ J/kg.K}$ .

Furthermore it is assumed that the fluid has the same properties as air and that the velocity in the duct changes with temperature to obtain constant mass flow rate at the height of the measurement section.

The initial mean velocity at room temperature is 7.7m/s which, in the set-up of the SBI, corresponds with a volume flow rate of  $0.6 \text{ m}^3/\text{s}$  as required by the standard[1].

T(K)	v(m/s)	Re(-)	Pr(-)	Nu(-)	h(W/m <sup>2</sup> .K)	$\tau_{\text{duct}}$ (s)
300	7.7	152 500	0.707	382	31.9	225
350	9.0	135 500	0.700	347	33.0	217
400	10.3	123 000	0.690	319	34.3	209

**Table 4: Estimate of the time constant of the SBI duct system**

The time constant  $\tau_{\text{duct}}$  is derived out of the convection coefficient assuming that the heat transfer between the fluid and the duct wall is governed by convective heat transfer only.

$$\tau_{duct} = \frac{\rho c V}{h A}$$

V/A is the ‘volume to surface area’ ratio of the inner duct. So roughly speaking, the time constant of the duct lies around 220s. It is now legitimate to state that ‘if transient thermal effects play a role on  $k_t$  and  $\dot{m}$ , they can only be eliminated by maintaining the same burning conditions for at least two times  $\tau_{duct}$ ’.

If the transient effects are confirmed, they introduce an additional uncertainty on  $k_t$  and  $\dot{m}$ . Furthermore, calibration procedures like the step calibration should then be revised to increase the settling time – which is now set to one minute – to something like ten minutes.

Note that the hood and collector, which are located just in front of the ductwork, have an even greater time constant.

### **Effect of transient heating phenomena on the mass flow rate**

To investigate the influence of the thermal inertia of the duct wall on the mass flow rate, a straight piece of insulated duct with a diameter of 0.315 m and a length of 7 m is modelled whereby the measurement section is defined to lie at a distance of 6 m from the inlet. This corresponds to the actual situation in the SBI if one omits the bends and guide vanes.

The boundary conditions for the flow are either constant volume flow rate or constant mass flow rate at the inlet. The temperature of the gas at the inlet rises linearly from 300 K to either 400 K or 600 K in either 30 s or 300 s, and then falls back linearly to 300K in the same time period.

Test cycle	I	II	III	IV
$\Delta T_{max}$	100K	300K	100K	300K
$\Delta t$	300s	300s	30s	30s
Initial temperature $T^{\circ}=300K$				

**Table 5. Overview of the different numerical test cases.**



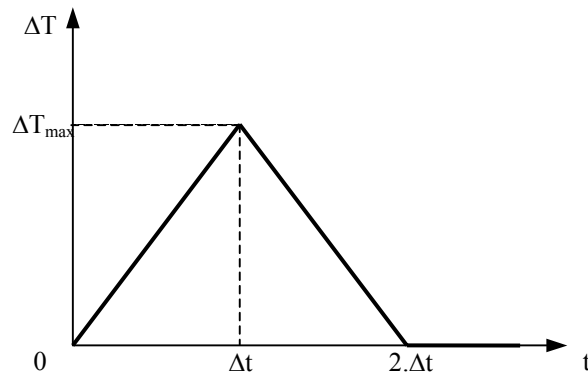


Figure 2: Variation of the fluid temperature at the inlet.

**Expected behaviour**

*Density effects*

A first expectation is that in the heating phase, i.e. the first part of the simulation, the temperature close to the duct wall will be lower than on the axis. In other words, the measured temperature – which is taken at a distance from the wall – is higher than the mean temperature. This implies that the *air density* is *underestimated* as will be the mass flow rate. Figure 3 clearly shows this for test cycle II (table 5).

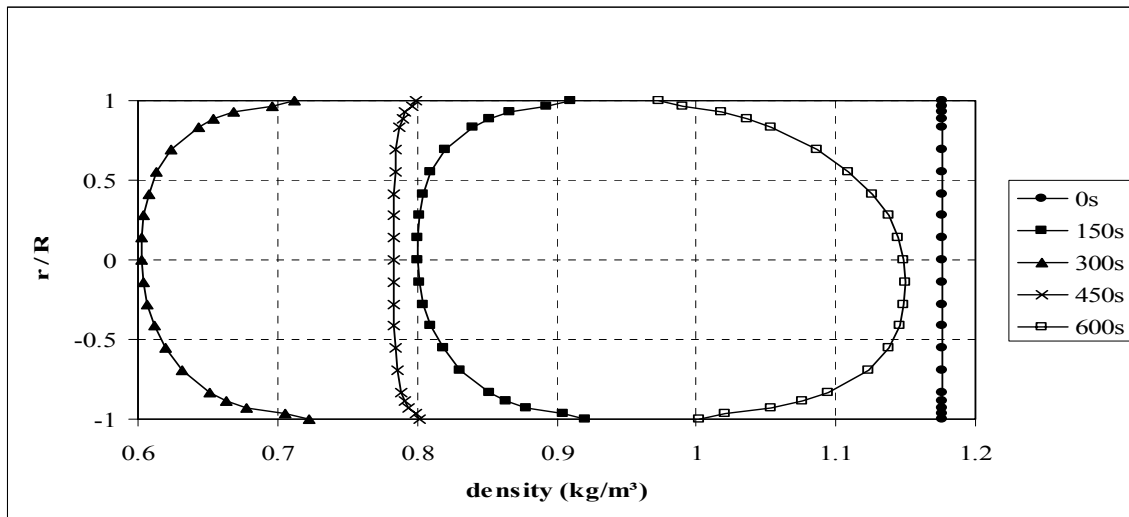


Figure 3. Evolution in time of density in the measurement section for test cycle II.

### *Effects on the velocity profile*

It is known that the velocity profile is function of the Reynolds number and thus of temperature and velocity. For low Reynolds numbers the flow becomes laminar ( $Re < 2300$  in piping) and the velocity profile has a parabolic shape (low  $k_t$ ). For higher Reynolds numbers the boundary layer thickness becomes smaller and the velocity profile flattens (high  $k_t$ ).

So even in 'steady state', the gas temperature and the flow velocity will have an influence on  $k_t$  through the Reynolds number.  $k_t$  will decrease when temperature rises. Since  $k_t$  is assumed to be constant, this implies that  $k_t$  is *overestimated* as will be the mass flow rate.

If mass flow rate is kept constant the effect will be less pronounced since the velocity ( $v$ ) increase will partially cancel out the effect of temperature, through the kinematic viscosity  $\nu$  increase, on Reynolds number.

$$Re = \frac{vD}{\nu}$$

In a transition period from a cool duct system at the start of the test to a certain heat release level, the flow close to the duct axis will follow the temperature changes quite fast while the flow close to the duct wall will lag behind. This makes that the  $k_t$  factor will lag behind the value we would expect in steady state.

In order to have a first feeling of the impact of temperature on the  $k_t$  factor an empirical formula, which gives the velocity profile as a function of Reynolds number, will be used. From a large number of experimental results for flow in pipes, various authors have proposed universal velocity profiles. A classic result is that of Schlichting[8]:

$$\frac{v(r)}{v_{axis}} = \left( \frac{R-r}{R} \right)^{1/n} \quad \text{with} \quad n = 3 Re^{0.08}$$

This profile is in excellent agreement with experimental results for values of  $Re$  ranging from  $10^3$  to about  $10^6$  and thus covers the range of  $5 \cdot 10^4$  to  $5 \cdot 10^5$  which is to be expected in the SBI and RC. This exponential law however is not correct close to the wall nor on the axis of the pipe but gives an

acceptable global profile. Furthermore, it is only valid in steady state since for transient phenomena there is no one-to-one correspondence between the velocity profile shape and the instantaneous Reynolds number as shown in [6].

Integrating this formula over the circular section results in an estimate of the  $k_t$  factor as a function of Reynolds.

$$k_t = \frac{\int_0^{2\pi} \int_0^R \left( \frac{R-r}{R} \right)^{1/n} r \cdot dr d\theta}{1 \cdot \pi R^2}$$

which results in

$$k_t = \frac{2n^2}{(1+n)(1+2n)}$$

For typical working conditions in the SBI and the RC test table 6 gives an estimate – under the limitations described above – of the  $k_t$  factor at different temperatures.

	SBI			RC			
T (K)	290	400	600	290	600	900	900
v (m/s)	7.7	10.6	15.9	20	41.4	62.1	20
v (m <sup>2</sup> /s)	14.8.10 <sup>-6</sup>	26.4.10 <sup>-6</sup>	52.7.10 <sup>-6</sup>	14.8.10 <sup>-6</sup>	52.7.10 <sup>-6</sup>	102.9.10 <sup>-6</sup>	102.9.10 <sup>-6</sup>
D (m)	315.10 <sup>-3</sup>	315.10 <sup>-3</sup>	315.10 <sup>-3</sup>	400.10 <sup>-3</sup>	400.10 <sup>-3</sup>	400.10 <sup>-3</sup>	400.10 <sup>-3</sup>
Re (-)	164 000	126 500	95 000	540 500	314 000	241 500	78 000
$k_t$ (-)	0.834	0.831	0.827	0.847	0.841	0.838	0.825
$\delta$ (%)	0.0	-0.36	-0.84	0.0	-0.7	-1.1	-2.6
ref. T=290K							

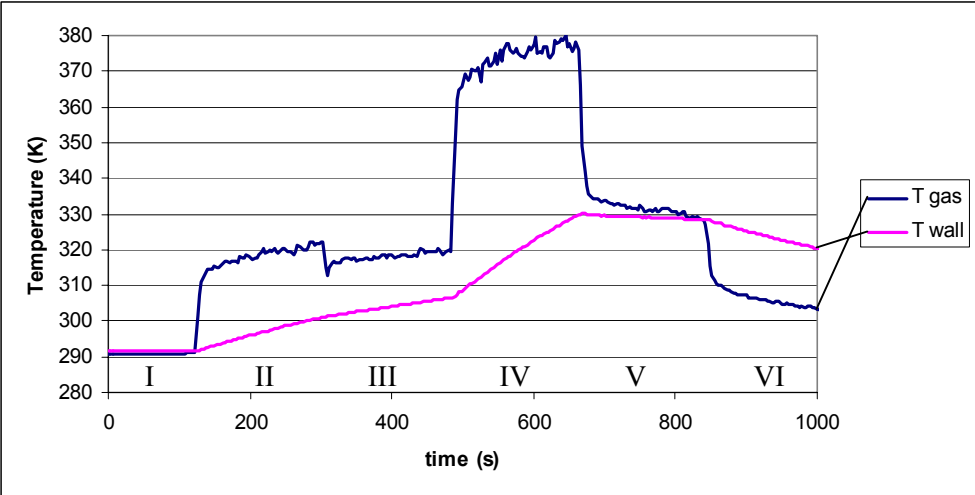
**Table 6: Estimate of the  $k_t$ -factor at different gas temperatures**

Table 6 suggests that the approximation that  $k_t$  is constant can lead to an error in the order of 1% if mass flow rate is kept constant over the test and to about 3% in the RC (at T = 900 K) if volume flow rate is constant.

So in order to keep the error on the  $k_t$  factor low, it is recommended to run the equipment with constant mass flow rate rather than with constant volume flow rate. However, the  $k_t$  factor is not the only factor influenced by temperature. In view of a correct mass flow rate measurement, it will be demonstrated later that the changing  $k_t$  factor helps to reduce the error on the mass flow rate, because the error has opposite sign to the error introduced by the density measurement by means of a thermocouple.

The table further reveals another cause – be it small – of the deviation in HRR in step V. As can be seen in figure 4, the measured gas temperature for step V is higher than for steps II and III. This results in an overestimation of  $k_t$  and thus the HRR. The thermal inertia of the duct system will add to this. Indeed, the previously discussed lagging behind of the  $k_t$  factor upon thermal changes makes that the  $k_t$  factor in step II will be somewhere in between the  $k_t$  factors of steps I and II if we would have a uniform temperature, equal to the gas temperature, over the cross section.

In step V, there is hardly any temperature gradient over the test section so that the time lagging does not play.



**Figure 4: Gas and wall temperature in the measurement section (SBI; step calibration)**

The above described effects result in an overestimation of HRR. A rough estimate, based on results of figure 8 which will be discussed later, suggests that the deviation would be in the order of 0.2% for step V compared to step II. The assumption is that the deviation is based on a temperature difference

of between 12°C ( $\Delta$  step V – II) and 40°C ( $\Delta$  step V – I). From figure 8 we learn that the corresponding errors roughly lie between 0.1% and 0.2%.

So the thermal inertia of the duct system has only a negligible effect on the deviation in HRR in step V of the SBI ‘Step Calibration’.

### ***Error on calculated mass flow rate***

In the numerical simulation, several options and approximations made in calculating the mass flow rate can be evaluated. The reported error is always referred to the real mass flow rate as calculated by means of formula 4. The different cases considered are:

1. ‘SBI’, where the mass flow rate is approximated by formula 1 with  $k_t$  taken constant, and whereby the density is calculated based on the mean temperature of three thermocouples positioned at 120° intervals on a radius of 87mm (as in SBI [1]).
2. ‘T on axis’, where the mass flow rate is approximated by formula 1 with  $k_t$  taken constant, and whereby the density is calculated based on the temperature measured on the axis of the duct (as in RC [2]).
3. ‘Real  $k_t$ ’, where the mass flow rate is approximated by formula 3 with the velocity profile known, and whereby the density is calculated based on the mean temperature of three thermocouples positioned at 120° intervals on a radius of 87mm.
4. ‘Real  $k_t$  + T on axis’, where the mass flow rate is approximated by formula 3 with the velocity profile known, and whereby the density is calculated based on the temperature measured on the axis of the duct.

Figure 5 shows the error for the four different cases for test cycle I. This figure clearly shows that it is useless knowing the ‘true’  $k_t$  value over time when no information is available on the temperature and density gradient over the measurement section.

Furthermore it shows that it is better to measure the temperature of the flow gases away from the centre since the so found value better represents the mean temperature.

It is also interesting to see that for a temperature variation that can be considered as a limit case for the majority of samples tested in the SBI, the error on the mass flow rate – as a result of an ever changing temperature gradient over the measurement section – remains limited to 0.5%.

Figure 6 further shows that two major errors with opposite sign help to cancel out the error in case of the SBI. On the one hand the velocity profile correction factor ( $k_t$ ) is overestimated in the first part of the test, but on the other the temperature of the flow gases ( $T_{ms}$ ) is also overestimated.

$$\dot{m}(t) = cA \frac{k_t}{k_p} \sqrt{\frac{\Delta p(t)}{T_{ms}(t)}}$$

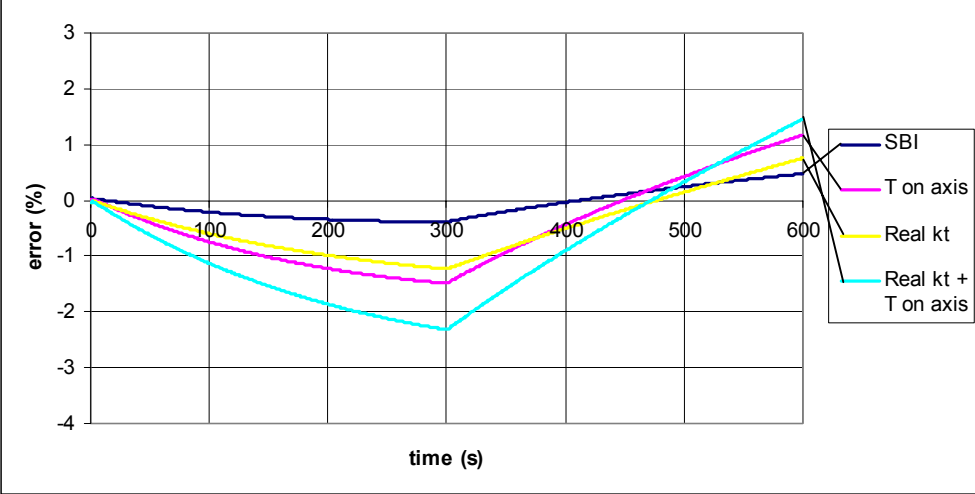


**Figure 5: Error on mass flow rate; constant mass; test cycle I**

Running the equipment with constant volume flow rate, increases the error on the  $k_t$  factor but further reduces the error on the mass flow rate in the first part of the test as can be seen from comparison of figures 6 and 8.

In order to better compare the different results, the x-axis represents the time either in seconds or in tens of seconds.

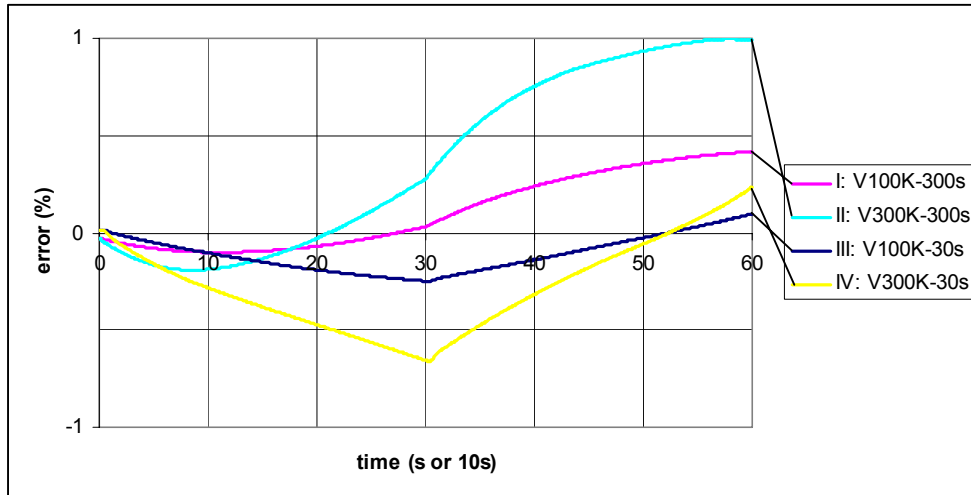


**Figure 6: Error on mass flow rate; constant volume; SBI**

Figure 7 shows the error made when calculating the mass flow rate in the hypothetical case that the flow profile correction factor  $k_t$  is known at any instance. In this case, the error can entirely be attributed to the way the gas density is approximated. All four cycles I till IV are considered (table 4).

This graph clearly demonstrates the inertia of the duct system. For fast events ( $\tau \ll \tau_{\text{duct}}$ ), there is a high temperature gradient over the measurement cross section with a resulting large error on the estimate of the mean density. For slower events however ( $\tau \approx \tau_{\text{duct}}$ ), the duct better follows the flow temperatures and the error reduces. In the limit case of very slow heating ( $\tau \gg \tau_{\text{duct}}$ ), the duct wall follows even better the flow temperature and will depend on the outer boundary conditions. The error further reduces.

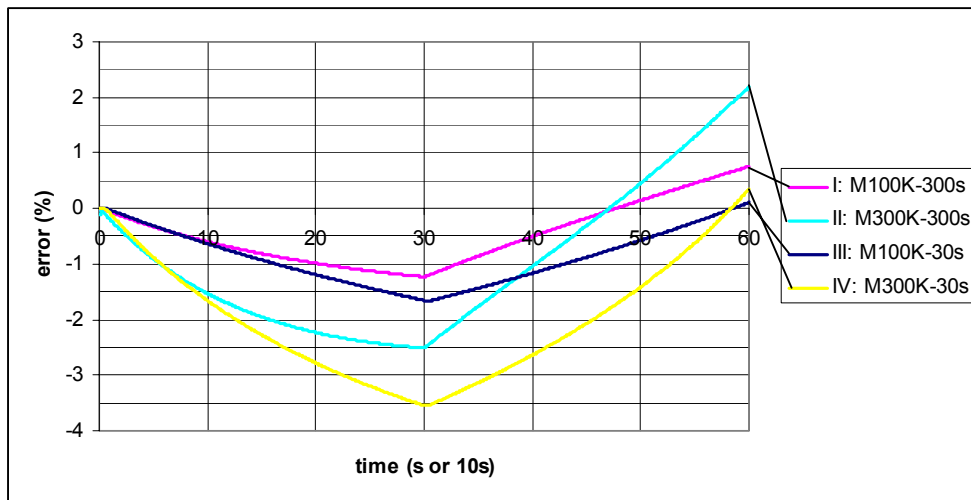


**Figure 7: Error on mass flow rate; constant mass;  $k_t$  known**

### ***Uncertainty related to temperature effects***

In order to estimate the uncertainty related to these temperature effects, figures 6 and 8 consider the same four cases as figure 7, but with the mass flow rate calculated as in the SBI test i.e. the density is calculated based on the mean temperature of three thermocouples positioned at  $120^\circ$  intervals on a radius of 87mm, and the  $k_t$  factor is taken constant.

Test cycle IV can be considered as a limit case in the SBI. In the SBI, a gas temperature at the height of the measuring section of approximately 600K is considered to be the maximum allowed temperature above which the test is interrupted. Note that this does not have to happen necessarily at the start of the test when the equipment is at room temperature. It may happen later in the test when, for example, the flames reach the core of a sandwich panel with a highly flammable product.

The corresponding maximum error is 1.4% for constant mass flow rate and 0.7% for constant volume flow rate. Assuming a triangular distribution, with 1.4% respectively 0.7% being the limit case, the standard uncertainty related to temperature effects in the SBI is estimated to be 0.6% ( $1.4/\text{SQRT}(6)$ ) for constant mass flow rate and 0.3% for constant volume flow rate [3]. This is only true for the actual thermocouple position. For temperature measurements on the axis of the duct like in the RC, the standard uncertainty increases to 2.0% and 1.8% respectively.

Another observation is that the mass flow rate, and thus the HRR, is underestimated in the first part of the test, while only in the last stage of the test, there is a possible overestimation.



This together with the knowledge that the classification parameters like FIGRA, SMOGRA, THR600s and TSP600s in the SBI are based on the first part of the test (heating phase), makes that the uncertainty may be considered as a one sided distribution when calculating the global uncertainty on these classification parameters.

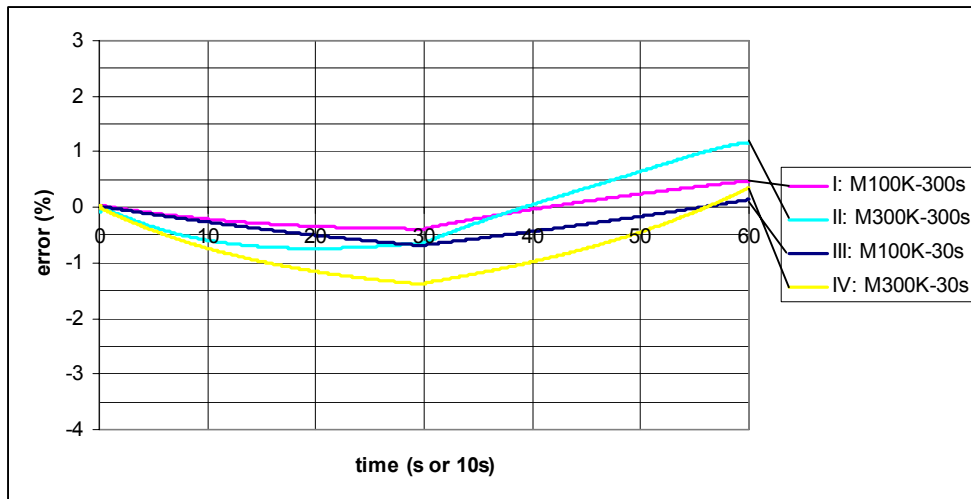


**Figure 8: Error on mass flow rate; constant mass; SBI**

Figure 8 also shows that when the combustion gas temperature drops below the duct wall temperature, the error on the mass flow rate reverses and becomes positive. In other words, the HRR and SPR are overestimated when this happens.

## Conclusions

The observation of a deviation in the heat release rate of a ‘step calibration’ according to the SBI standard, has statistically been proved. The main cause is a drift on the gas analysers and, more specific, the oxygen analyser. The effect of thermal inertia of the duct on the heat release rate, through the mass flow rate, is negligible for this specific calibration.

The thermal time constant of the SBI duct system lies in the order of 220s. So for all burning phenomena with a time constant in the same order of magnitude or smaller, transient thermal effects

add to the overall uncertainty. The sharper the temperature rise or fall and the higher the magnitude, the larger the error. The maximum underestimation of the calculated mass flow rate for sudden, high heat releases is estimated to 1.4% for the SBI test equipment running at constant mass flow rate. Based on this value, the standard uncertainty related to temperature effects in the SBI is estimated to 0.6%. When running at constant volume flow rate, the standard uncertainty reduces to 0.3% for the specific case of the SBI.

Since all classification parameters in the SBI are based on the first part of the test, i.e. the heating phase, the uncertainty may be considered as a one sided distribution when calculating the global uncertainty on these classification parameters.

So, in summary, transient thermal effects tend to underestimate the mass flow rate through the duct system.

The numerical model suggests that the position of the thermocouples is of primary importance. The position of the thermocouples for measuring the combustion gas temperature lies preferably closer to the duct wall than to the axis. This in order to better follow the mean gas temperature. The optimal position for a qualitative mass flow rate measurement, which will still overestimate the temperature in the heating phase of the test, is this that helps to compensate the error made assuming the *velocity profile correction factor* is a constant.

Knowing the velocity profile in the duct at anyone time, is of no use to correctly measure the mass flow rate if one does not know the density distribution in the measuring section over time. The derived velocity profile correction factor may as well be taken as a constant based on calibrations.

## Reference List

- [1] European Standard - Reaction to fire tests for building products - Building products excluding floorings exposed to the thermal attack by a single burning item. EN 13823:2002. CEN Central Secretariat, Brussels 2002
- [2] ISO Room Corner; International Standard – Fire tests – Full-scale room test for surface products; ISO 9705:1993; International Organisation for Standardisation, Geneva, 1993
- [3] GUM, Guide to the expression of uncertainty in measurement; BIPM/IEC/IFCC/ISO/IUPAC/OIML; ISBN 92-67-10188-9
- [4] Project for the European Commission: Enterprise Directorate-General; “SBI (Single Burning Item) Second Round Robin”; Call Identifier ENTR/2002/CP11; Applicant: EGOLF
- [5] Sette B.J.G.; Critical considerations on the use of a bi-directional probe in heat release measurements; Fire and Materials; Under review
- [6] Merci B., Theuns E., Sette B., Vandeveld P.; Numerical Investigation of the Influence of Gas Heating and Cooling on the Velocity Profile Correction Factor in the SBI-Configuration; Fire and Materials; Under review
- [7] Fox R.W. and McDonald A.T.; Introduction to fluid mechanics; John Wiley & Sons, New York 1985
- [8] Holman J.P.; Heat Transfer; McGraw-Hill Book Company, Singapore 1989



#### **A.4. Article 4**

*Merci B., Theuns E., Sette B., Vandeveldel P.; Numerical Investigation of the Influence of Gas Heating and Cooling on the Velocity Profile Correction Factor in the SBI-Configuration; Fire and Materials<sup>[52]</sup>*

Out for review: 7 December 2004



# Numerical Investigation of the Influence of Gas Heating and Cooling on the Velocity Profile Correction Factor in the SBI-Configuration

Bart Merci<sup>1,2</sup>, Erwin Theuns<sup>1,3</sup>, Bart Sette<sup>1</sup> and Paul Vandeveldel<sup>1</sup>

<sup>1</sup>Ghent University, Department of Flow, Heat and Combustion Mechanics, Ghent, Belgium

<sup>2</sup>Postdoctoral Researcher of the Fund of Scientific Research – Flanders (Belgium) (FWO-Vlaanderen)

<sup>3</sup>Stockman Engineering, Ghent, Belgium

Correspondence address:

Bart Merci  
Ghent University  
Department of Flow, Heat and Combustion Mechanics  
Sint-Pietersnieuwstraat 41  
B-9000 Ghent  
Belgium  
Tel.: +32 9 264 33 14; Fax: +32 9 264 35 86  
E-mail: [Bart.Merci@UGent.be](mailto:Bart.Merci@UGent.be)

## Abstract

The possible flow measurement error due to heating or cooling of exhaust gases in the Single-Burning-Item (SBI) test is estimated from numerical experiments. It is illustrated that there is no one-to-one correspondence between the velocity profile shape and the instantaneous Reynolds number, due to the time-dependent temperature and density profile evolution in the exhaust gas pipe. A non-ambiguous relation is found between the velocity profile shape and an ‘effective’ Reynolds number, based on the turbulent viscosity. The maximum variation of the velocity profile correction factor, relating the mean velocity to the velocity on the pipe axis, is found to be in the order of 2% for limiting circumstances for the SBI test. The primary effect is caused by instantaneous Reynolds number variations. The effect of heating or cooling of the flow by the hot or cold pipe is noticeable, too. The statements are proved to be valid independent of the computational grid, the turbulence model and the time steps taken to obtain the numerical solutions.

## 1. Introduction

The ‘Single-Burning-Item’-test (SBI) is a well-defined standardized 20-minute test procedure for the classification of building products with respect to their behavior in fire conditions [1]. The two basic quantities on which this classification is based, are the FIGRA (fire growth rate) and the SMOGRA (smoke growth rate). These indices rely on the determination of the heat-release and smoke-production-rate. The knowledge of the flow rate is important for the accurate determination of these quantities.

During the SBI-test, the exhaust gases are removed from the test room at a constant extraction rate (between 0.5 and 0.65m<sup>3</sup>/s at atmospheric pressure and 298K). Here, a constant normalized flow rate of 0.6Nm<sup>3</sup>/s is imposed. This corresponds to a constant exhaust gas mass flow rate equal to  $\dot{m} = 0.71\text{kg/s}$ . In the SBI-test, this extraction rate is determined from velocity measurements on the axis of the pipe that collects the exhaust gases on the one hand and from temperature measurements on three off-axis positions in the same pipe section. An assumption must be made then with respect to the shape of the velocity profile in order to relate the flow rate to the velocity on the pipe axis. This relation is expressed through the factor  $k_t$ , defined as:

$$k_t = \frac{U_b}{U_{cl}} \quad , \quad (1)$$

with  $U_{cl}$  the velocity on the centerline and  $U_b$  the bulk (or average) velocity:

$$U_b = \frac{\int_0^R U(r) 2\pi r dr}{\pi R^2} \quad , \quad (2)$$

with  $R$  the inner pipe radius. The flow rate is then computed from the mean density (obtained from the three measurement points), the cross-sectional pipe area, the bulk velocity and the factor  $k_t$ . [Note that in the SBI procedure,  $k_t$  is determined from three independent  $k_t$  measurements [1]; in this paper, we only focus on what is called  $k_{t,v}$  in this reference].

In the SBI-test the factor  $k_{t,v}$  is determined by velocity measurements with a pitot tube or hot wire anemometer. The velocity in the exhaust duct is measured at 5 radial distances ( $r/R = 0.278; 0.566; 0.695; 0.847$  and  $0.962$ ), with four measurement points for each radial distance. The mean of these velocities is divided by the centerline velocity to give the factor  $k_{t,v,SBI}$ . This determination of the factor  $k_{t,v}$  is an approximation for the factor given in eq. (1). Clearly, it is very important to obtain accurate values for  $k_{t,v}$  for the determination of the flow rate. In the SBI test procedure, it is determined once and then kept constant during the complete test.



It is typical in the SBI-test for the exhaust gases to heat up during the test due to the fire. In a later stage, particularly for fastly burning products, the exhaust gases may cool down again. During the test, the exhaust gas collection pipe heats up and cools down, too. In this paper, we perform a numerical study on the effect of this heating and cooling on the  $k_{t,v}$ -factor in order to estimate the possible variation of  $k_{t,v}$  during the SBI-test, with constant exhaust gas mass flow rate. We point out that, under the considered circumstances, there is no longer a one-to-one relationship between  $k_{t,v}$  and the instantaneous Reynolds number value of the flow in the pipe. When an ‘effective’ Reynolds number is defined, based on the turbulent viscosity, an unambiguous relation is recovered. All numerical results are checked with respect to their accuracy, in order to eliminate numerical error sources. In [2], the authors estimate the standard uncertainty in relation to mass flow rate measurements in the SBI test procedure.

## 2. Description of Numerical Simulations

### a. Description of the numerical experiments

The turbulent flow in a horizontal pipe is considered. The constant mass flow rate matches the exhaust gas extraction rate of the SBI-test. Air is chosen as fluid. The ideal gas law is applied. The molecular kinematic viscosity varies with temperature. For the basic simulations, the standard  $k$ - $\varepsilon$  turbulence model [2] is applied, with modifications to account for buoyancy:

$$\begin{cases} \frac{\partial(\rho k)}{\partial t} + \nabla \cdot (\rho k \bar{v}) = P_k + G_k - \rho \varepsilon + \nabla \cdot \left( \frac{\mu_t}{\sigma_k} \nabla k \right) \\ \frac{\partial(\rho \varepsilon)}{\partial t} + \nabla \cdot (\rho \varepsilon \bar{v}) = c_{\varepsilon 1} P_k \frac{\varepsilon}{k} + G_\varepsilon - c_{\varepsilon 2} \rho \varepsilon \frac{\varepsilon}{k} + \nabla \cdot \left( \frac{\mu_t}{\sigma_\varepsilon} \nabla \varepsilon \right) \end{cases} \quad (3)$$

The source term  $P_k$  is the production rate of turbulent kinetic energy of the turbulent stresses:

$$P_k = -\overline{v'_i v'_j} \frac{\partial \bar{v}_i}{\partial x_j} = \mu_t S_{ij} \frac{\partial \bar{v}_i}{\partial x_j}, \text{ with application of the summation convention, the strain rate}$$

$$\text{tensor component } S_{ij} = \frac{1}{2} \left( \frac{\partial \bar{v}_i}{\partial x_j} + \frac{\partial \bar{v}_j}{\partial x_i} \right) - \frac{1}{3} \delta_{ij} \frac{\partial \bar{v}_k}{\partial x_k}, \delta_{ij} \text{ the Kronecker delta and } \mu_t = \rho c_\mu \frac{k^2}{\varepsilon} \text{ the}$$

turbulent viscosity. The buoyancy source terms  $G_k$  and  $G_\varepsilon$  are defined as:

$$G_k = \beta g_i \frac{\mu_t}{\rho Pr_t} \frac{\partial \rho}{\partial x_i}, \quad G_\varepsilon = c_{\varepsilon 1} \tanh \left| \frac{v}{u} \right| G_k \frac{\varepsilon}{k} \quad (4),$$

with  $v$  the velocity component parallel to the gravity vector and  $u$  the velocity magnitude. As such,  $G_\varepsilon$  equals zero for horizontal flows.

Standard wall functions are used to deal with the near-wall treatment. The values of the model constants are given in table 1.

Model constant	$c_\mu$	$c_{\varepsilon 1}$	$c_{\varepsilon 2}$	$\sigma_k$	$\sigma_\varepsilon$
Value	0.09	1.44	1.92	1.0	1.3

Table 1. Model constants of the standard k- $\varepsilon$  model.

In order to illustrate that the statements made in this paper do not depend on the turbulence model, one set of calculations is made with the ‘realizable’ k- $\varepsilon$  model of [3]. In this model, the transport equation for the turbulent kinetic energy  $k$  is the same as in (2), but the equation for the turbulent dissipation rate now becomes:

$$\frac{\partial(\rho\varepsilon)}{\partial t} + \nabla \cdot (\rho\varepsilon\bar{v}) = C_1 S \rho \varepsilon + G_\varepsilon - C_2 \rho \varepsilon \frac{\varepsilon}{k} + \nabla \cdot \left( \frac{\mu_t}{\sigma_\varepsilon} \nabla \varepsilon \right). \quad (5)$$

The strain rate  $S$  is defined as  $S = \left( 2S_{ij}S_{ij} \right)^{1/2}$  (with the summation convention and  $S_{ij}$  as above). The model parameters are:  $C_1 = \max \left( 0.43; \frac{Sk/\varepsilon}{5 + Sk/\varepsilon} \right)$ ,  $C_2 = 1.9$  and  $\sigma_\varepsilon = 1.2$ .

The energy equation is solved, too, in order to account for the turbulent convective heat transfer in the pipe. Again, standard wall functions are applied and the turbulent Prandtl number is set to  $\sigma_h = 0.9$ , with application of the linear gradient diffusion hypothesis for the turbulent heat transfer.

Four different cases have been studied. A temperature variation in time is imposed at the inlet of the pipe, schematically represented in figure 1. The initial temperature is 300K. The four cases differ in the maximum temperature difference and in the time interval length. An overview is summarized in table 2. The four cases represent different possible reactions of products in the SBI: some products burn very fast, while others burn more slowly, some materials have a high HRR and thus high gas temperatures in the exhaust system and vice versa.

Case	I	II	III	IV
$\Delta T_{\max}$	100K	300K	100K	300K
$\Delta t$	300s	300s	30s	30s

Table 2. Overview of the different numerical test cases (initial temperature: 300K).

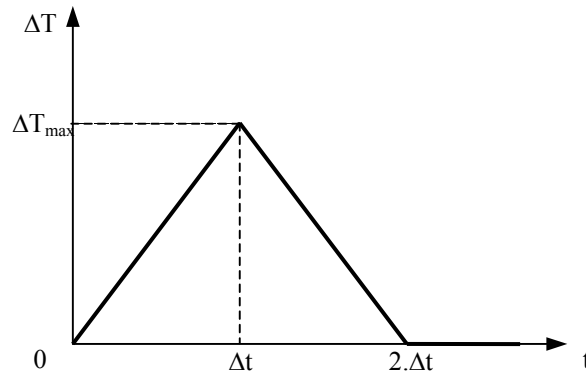


Figure 1. Variation of the fluid temperature at the pipe inlet.

Spatial accuracy is of second order: second-order upwinding for the convective terms and standard central discretization for the pressure term. Coupling between pressure and velocity is through the SIMPLE method. The implicit first order backward Euler scheme is applied to perform the time-accurate simulation, with a constant time step  $\delta t = 1s$  or  $0.1s$ .

#### b. Simulation domain and boundary conditions

The flow in the pipe is in principle symmetric. Therefore, the solution domain contains only half the cross-section surface. The length of the pipe is 7m. The inner diameter is 0.315m. The ‘measurement’ section, where  $k_{t,v}$  is determined from the velocity profiles and where the density measurement points are positioned, is at a distance of 6m from the inlet section. The flow simulation domain contains 14000 cells: 20 cells in the radial direction (with smaller cells at the wall and stretching toward the axis), 20 cells in the tangential direction and 35 cells in the axial direction. The solid pipe material is modeled as stainless steel (2mm) and insulation material (40mm) and contains 10 cells in the radial section. The conduction coefficients vary linearly with temperature between  $k_{\text{steel}} = 14W/(m.K)$  for  $T = 0^\circ C$  and  $k_{\text{steel}} = 20W/(m.K)$  for  $T = 350^\circ C$ ; and between  $k_{\text{insulation}} = 0.0375W/(m.K)$  for  $T = 0^\circ C$  and  $k_{\text{insulation}} = 0.097W/(m.K)$  for  $T = 350^\circ C$ .

At the inlet of the domain, a uniform velocity is imposed. Turbulent kinetic energy and dissipation rate are estimated from a separately computed fully developed turbulent flow. The

temperature is varied as described above (fig. 1 and table 2) but remains uniform over the inlet cross-section. The density varies accordingly. Obviously, the inlet velocity is adjusted so that the inlet mass flow rate is constant. Pressure at the inlet is extrapolated from the flow field. At the outlet of the pipe, constant (atmospheric) pressure is imposed while all other quantities are determined from the flow field by setting the axial derivatives equal to zero. In the pipe, heat is conducted towards the outer diameter (0.4m). There, adiabatic boundary conditions are imposed. This is justified because temperature variations are very small anyway, so that there is hardly any effect when natural convection is accounted for.

**c. Numerical accuracy**

It is of utmost importance to eliminate numerical errors when numerical experiments are performed. Therefore, test case I has been performed on a refined grid (but keeping the size of the cells at the pipe wall constant in order not to disturb the performance of the wall functions) and with smaller time steps ( $\delta t = 0.1s$ ). In section 3.c the accuracy of the results is further discussed.

**3. Discussion of the Results**

**a. Slow heating and cooling**

In this section, results are presented for cases I and II of table 2. Figure 2 shows density curves over the measurement section at different times. From this figure, the physical processes can be understood.

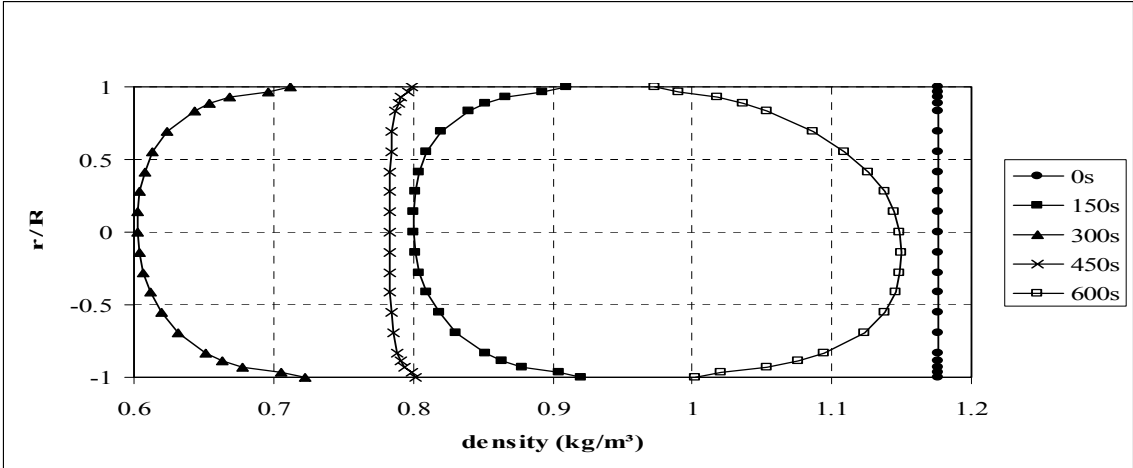
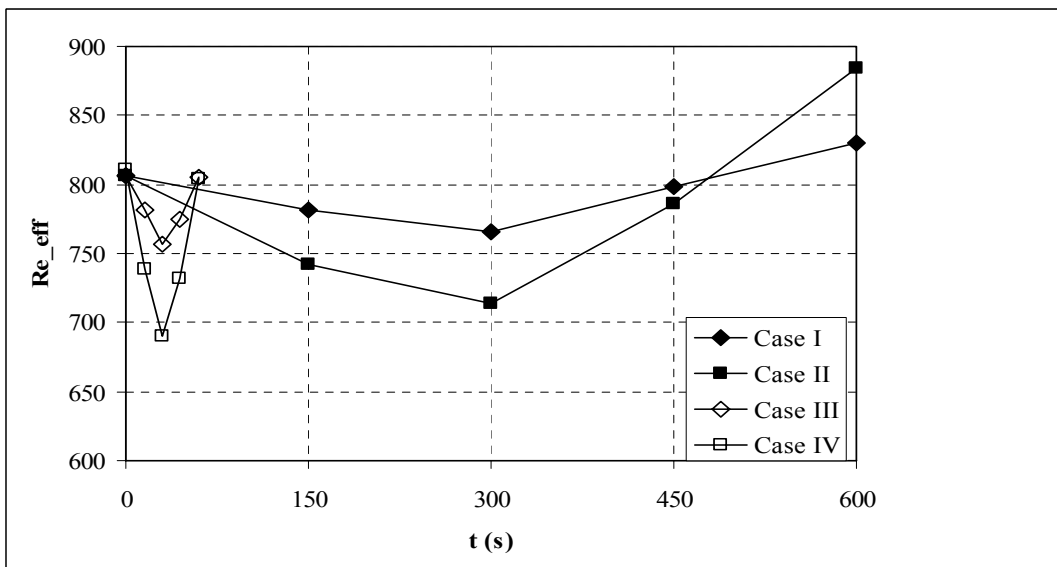
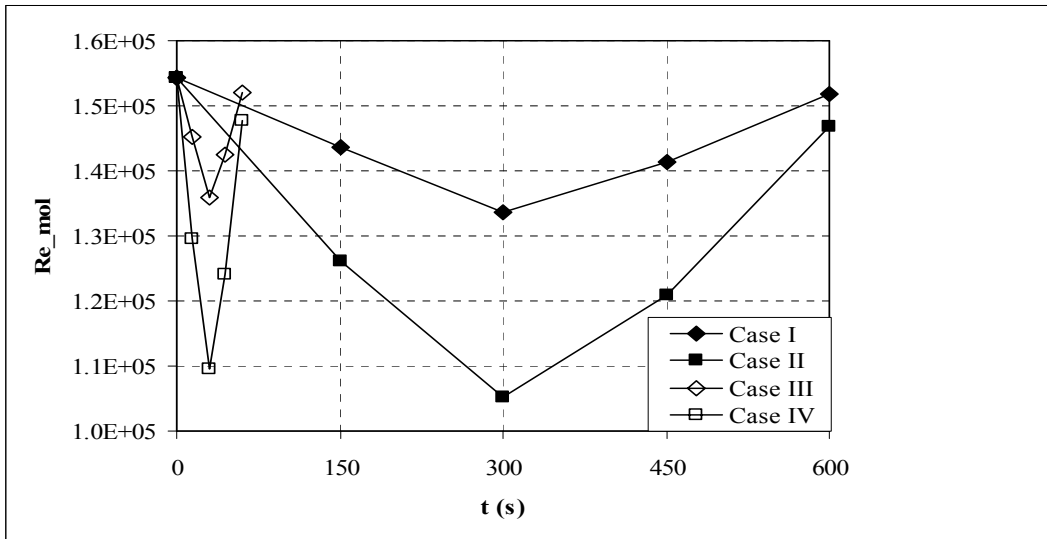


Figure 2. Evolution in time of density in the measurement section for case II.



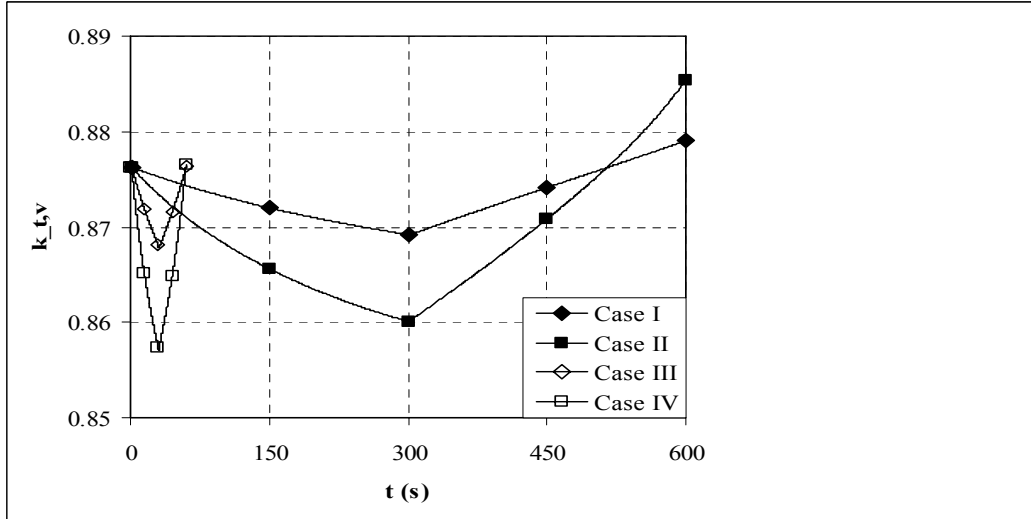


Figure 3. Evolution of the instantaneous Reynolds number (6), the ‘effective’ Reynolds number (7) and  $k_{t,v}$  (2) in the measurement section.

The primary effect of the fluid heating up and cooling down is a variation of the Reynolds number:

$$Re = \frac{U_b D}{\nu} = \frac{\rho U_b D}{\mu} \quad , \quad (6)$$

with  $\nu$  the kinematic viscosity and  $U_b$  from (2). All (averaged) values, including the material properties, are obtained from an integration as in equation (2). The effect on the Reynolds number is seen in figure 3. An increase in temperature causes an increase of the molecular dynamic viscosity  $\mu$  and thus, for constant mass flow rate ( $\rho U_b$  is constant) a decreasing Reynolds number value. In other words, the increase of  $U_b$  is less pronounced than the increase of the kinematic viscosity  $\nu$  when the temperature increases. Obviously, the Reynolds number influences the value of  $k_{t,v}$ . It is well known that only for sufficiently large Reynolds number the shape of the velocity profile becomes independent of the exact Reynolds number value. However, the typical Reynolds number here is in the order of  $Re = 150000$ , which is not sufficiently large for Reynolds number independence of  $k_{t,v}$ . The lower the Reynolds number, the more the velocity profile tends towards the parabolic laminar profile, which has a lower  $k_{t,v}$ -factor than the flatter high-Reynolds number turbulent velocity profiles. Consequently, the value of  $k_{t,v}$  becomes smaller as the Reynolds number decreases. This is indeed confirmed in fig. 3. Similarly, the Reynolds number increases again during the cooling down period, with opposite effects on  $k_{t,v}$ . This clearly illustrates that the primary

effect of temperature variations on the  $k_{t,v}$ -factor is through the variation of the instantaneous Reynolds number.

However, if this were the only significant effect, the  $k_{t,v}$ -factor at the end of the numerical experiment, where the inlet temperature equals the initial temperature, should be practically the same. Figure 3 shows that this is not the case. One obvious reason at first sight is the fact that the temperature in the measurement section is not yet the same as the initial temperature (see figure 2). Indeed, it is higher due to the heat exchange from the pipe to the fluid. However, this cannot be the reason, since the higher temperature results in a lower Reynolds number (fig. 3), so that the  $k_{t,v}$ -factor should be lower at the end of the numerical experiment, while the observation is the opposite. This is explained now.

First of all, we define an ‘effective’ Reynolds number:

$$Re_{\text{eff}} = \frac{\rho U_b D}{\mu_{\text{eff}}} \quad , \quad (7)$$

with  $\mu_{\text{eff}} = \mu + \mu_t$  the sum of the molecular and the turbulent viscosity. The correlation between the evolution of  $Re_{\text{eff}}$  and the  $k_{t,v}$ -factor in figure 3 is striking. This is not surprising, since the turbulent viscosity is two orders of magnitude larger than the molecular viscosity, so that it is the turbulent viscosity that determines the velocity profile shape. Of course, this is always true, but normally there is a one-to-one relationship between the ‘effective’ Reynolds number (7) and the classical Reynolds number (6). Here, this is no longer true, due to the heating up and cooling down.

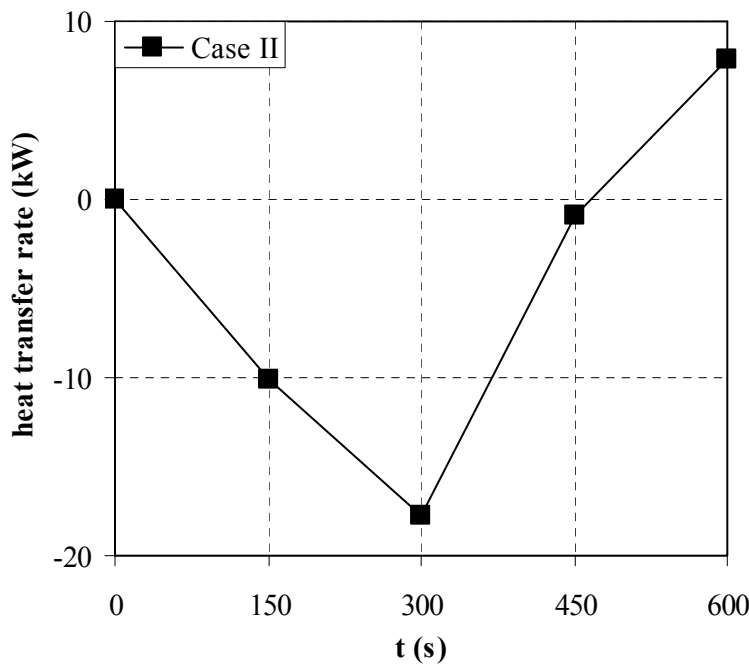


Figure 4. Evolution in time of heat transfer rate from the pipe to the fluid for case II.

In figure 4, we see that during the heating period ( $t < 300\text{s}$ ), heat is transferred from the fluid to the pipe (negative values denote transfer to the pipe wall). Only during the last part of the cooling down period ( $t > 460\text{s}$ ), heat is transferred back from the pipe to the fluid. In general, less heat per time unit is interchanged between the fluid and the pipe during the cooling down period ( $t > 300\text{s}$ ) than during the heating period. As a consequence, the average fluid temperature is lower during the heating period than at the ‘symmetrical’ time during the cooling down period. By ‘symmetrical’ time we mean symmetrical with respect to the time, corresponding to the peak temperature in fig. 1 (e.g. here  $t = 150\text{s}$  and  $t = 450\text{s}$  are ‘symmetrical’ times). Since the turbulence is hardly influenced by the buoyancy for the flows under study (see later), the kinematic turbulent viscosity  $\nu_t$  is hardly affected by the heating and cooling of the fluid at symmetrical times (not shown). Due to the differences in density, however, the turbulent viscosity  $\mu_t$  is affected: it is lower during the cooling down period, due to the higher average temperature (and thus lower average density). As a result, the effective Reynolds number (7) is higher and there is no unambiguous relation between the instantaneous Reynolds number (6) and the effective Reynolds number (7). This secondary, but most certainly non-negligible, effect also explains why the  $k_{t,v}$ -value at the end of the numerical experiment is not equal to the value at the beginning.

For obvious reasons, the above findings remain true for smaller temperature variations (case I), but the effects are less pronounced. Interesting to note is that the evolution of the instantaneous molecular Reynolds number is such that the end values for cases I and II are almost equal, the end value of case II being slightly lower due to the higher average fluid temperature. The curves of the ‘effective’ Reynolds number cross each other, as do the curves for the  $k_{t,v}$ -factor. The reason is the same: a higher average temperature and thus a lower density and turbulent viscosity  $\mu_t$  (the kinematic turbulent viscosities  $\nu_t$  are practically the same for both cases). This is again a clear illustration of the direct unambiguous relation between  $k_{t,v}$  and  $Re_{\text{eff}}$ , while the one-to-one relation with the molecular Reynolds number is lost.

#### **b. Rapid heating and cooling**

The time period of heating and cooling is relatively short now. As a consequence, the pipe wall temperature does not rise as strongly as in the previous cases. As a result, it is seen in fig. 5 that, due to convective heat exchange with a solid at a lower temperature, the fluid density near the pipe wall is higher than for cases I and II (fig. 3). Consequently, for case IV the



‘effective’ Reynolds number becomes smaller than for case II (fig. 3). The instantaneous molecular Reynolds number on the other hand does not vary as strongly as in case IV, because mean fluid temperature variations are smaller now than for case II. The reason for this is again that the fluid exchanges heat with a solid on lower temperature than for case II, so that the average fluid temperature is lower (and thus the variation in temperature or density is smaller). Since the variation in  $k_{t,v}$  is somewhat larger than for case II, as is the case for the effective Reynolds number, this once again illustrates the direct link between  $k_{t,v}$  and  $Re_{eff}$ . Furthermore, heat is transferred from the pipe to the fluid during a relatively shorter time period than in case II. As a result, the pipe temperature remains lower for case IV and the density profiles at ‘symmetrical’ times are closer to each other than for case II (fig. 2). As a consequence, the evolution of  $Re_{eff}$  is more ‘symmetrical’ than for case II. This is again reflected in a more ‘symmetrical’ evolution of  $k_{t,v}$ : the end values for cases III and IV are practically equal to the initial values.

The differences between cases III and IV are completely in line with the observations made for cases I and II, for exactly the same reasons. The intersection of the curves for  $Re_{eff}$  and  $k_{t,v}$  is hardly visible, because there is almost perfectly symmetrical behavior, as has just been explained.

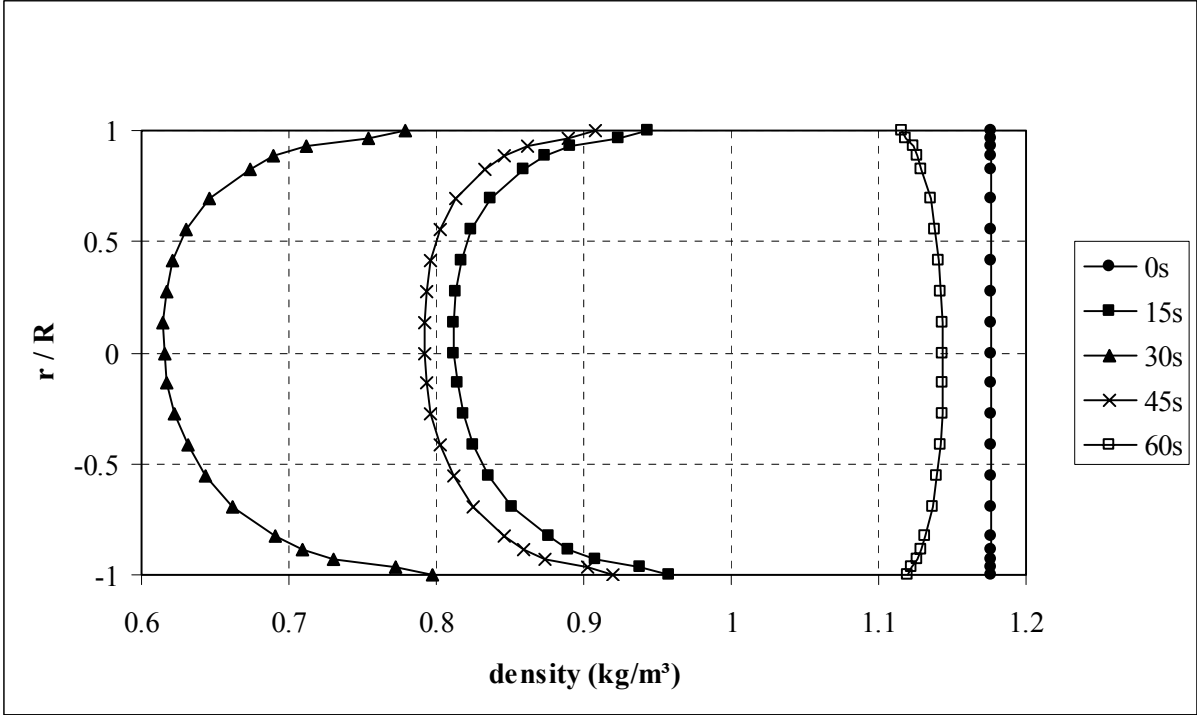


Figure 5. Evolution in time of density in the measurement section for case IV.

To conclude this discussion, table 3 provides an overview of the variations in  $k_{t,v}$  for the different cases. As explained above and observed in fig. 3, the largest variation (compared to

the initial value) occurs for case IV (rapid heating and cooling with the larger  $\Delta T$ ). It is in the order of 2%.

Case	$k_{t,v,init}$	$k_{t,v,min}$	$k_{t,v,max}$	$(k_{t,v,init}-k_{t,v,min})/k_{t,v,init}$	$(k_{t,v,max}-k_{t,v,init})/k_{t,v,init}$
I	0.877	0.869	0.879	0.009	0.002
II	0.877	0.860	0.886	0.019	0.010
III	0.877	0.868	0.877	0.009	0.000
IV	0.877	0.857	0.877	<b>0.023</b>	0.000

Table 3. Maximum variation of  $k_{t,v}$  for the different cases.

### c. Buoyancy

The effect of buoyancy is expected to be small. This is easily seen when the Froude number is determined:

$$Fr = \frac{U_b^2}{gD}. \quad (8)$$

For a typical bulk velocity in the order of 8m/s or more, this number is much larger than 1, so that buoyancy effects must be negligible. This has been confirmed numerically, as is illustrated in figure 6. Two curves for the evolution of  $k_{t,v}$  are given for case I: one curve with the real gravitational field and one where gravity has artificially been turned off. Clearly, the differences between the curves are negligible, so that it is confirmed that buoyancy does not affect the evolution of  $k_{t,v}$ .

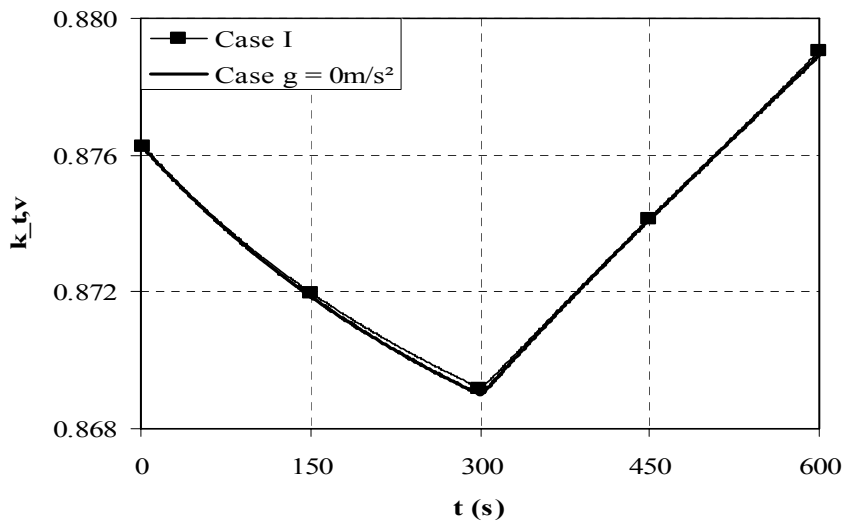


Figure 6. Influence of buoyancy on  $k_{t,v}$  for case I.

#### d. Inner pipe wall at constant temperature

Some observations in sections 3.a and 3.b have been explained through differences in heat transfer to and from the pipe. In order to confirm these statements, a numerical experiment has been performed in which the pipe inner wall temperature is kept constant at its initial value ( $\Delta T = 0$ ) for case II.

Two statements must be verified. Firstly, the evolution of  $k_{t,v}$  must be perfectly symmetrical, because the rate and direction of heat transfer from fluid to pipe is perfectly symmetrical. Secondly, the minimum  $k_{t,v}$  (at 300s) value must be lower than for the original case II, due to a globally higher density (and thus higher turbulent viscosity  $\mu_t$  and lower  $Re_{eff}$ ).

Both statements are confirmed in figure 7.

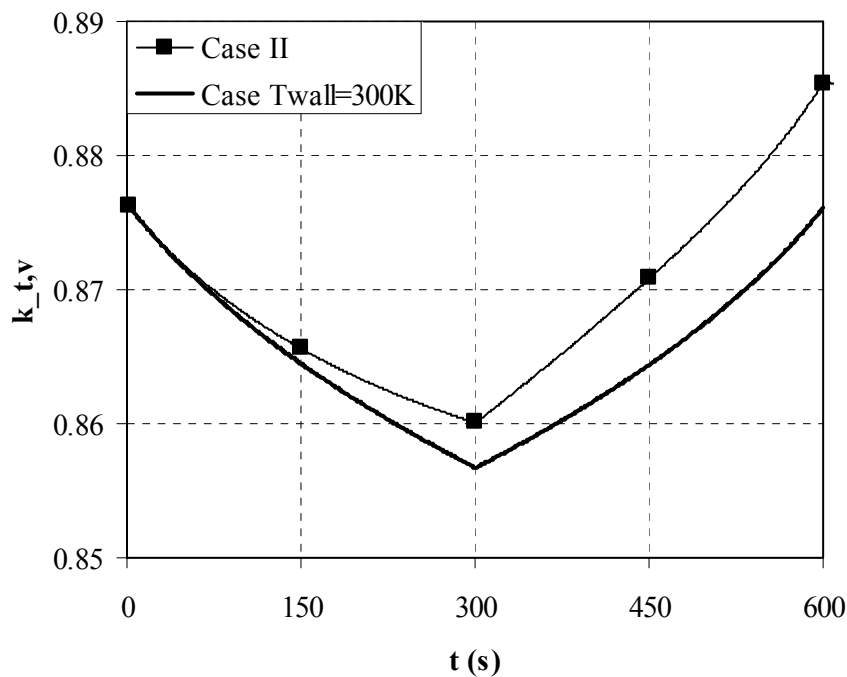


Figure 7. Evolution of  $k_{t,v}$  for case II with constant pipe inner wall temperature.

#### e. Approximate determination of $k_{t,v}$ as described in the SBI standard [1]

In the above results,  $k_{t,v}$  has been determined as the ratio of the bulk velocity (2) to the centerline velocity. As mentioned in the introduction, in [1] the bulk velocity is not determined from a rigorous integration as in (2), but from an averaged velocity, obtained from measurements at five different radial positions (with four measurement points for each radial position). Consequently, some deviation may occur from (2), especially when the velocity profile is not perfectly symmetrical. This is the case, due to buoyancy, but the amount of asymmetry is small (not shown). In order to give an impression on the deviations between  $k_{t,v}$  as determined from (1) and (2) and  $k_{t,v,SBI}$  as determined from [1], figure 8 shows the evolution of both quantities for cases I and II. Clearly, the differences are very small and, more importantly, the trends observed in the evolutions of  $k_{t,v}$  and  $k_{t,v,SBI}$  are the same.

In order to avoid misunderstandings, it is stressed once more that in the SBI standard, the  $k_t$ -value is kept constant throughout the test. What is labeled as the ‘SBI-method’ here, only refers to the approximation of expression (2) as described in [1]. This approximation is then used in the numerical experiments, rather than the exact integration (2).

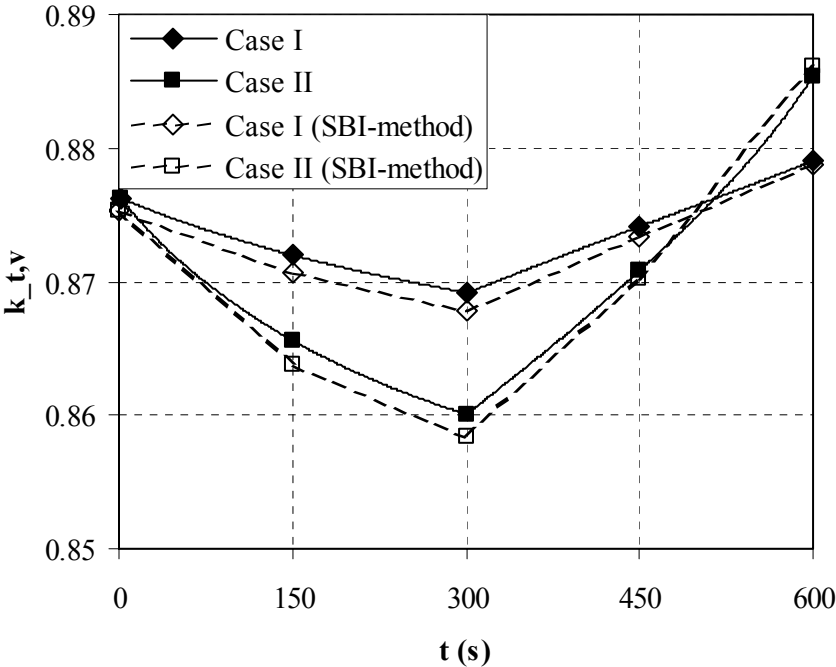


Figure 8. Evolution of  $k_{t,v}$  determined as in [1] for cases I and II.

**f. Numerical accuracy**

In order to draw reliable conclusions from numerical experiments, it must be made sure that the results are independent of the computational mesh, the time step size used and the turbulence model applied. These three influence factors are discussed now. It is important to recognize here that we do not claim to provide an accurate value for  $k_{t,v}$ . Rather, we want to reveal the variation of  $k_{t,v}$ , compared to its initial value, due to heating and cooling of the exhaust gases (and the pipe).

Figure 9 shows the evolution of  $k_{t,v}$  for case I when the time step is made 10 times smaller ( $\delta t = 0.1s$  instead of  $\delta t = 1s$ ). The results are identical, which illustrates that the results are indeed time accurate.

Figure 10 shows the impact of the choice of the computational mesh. The mesh cell sizes are twice as small for the fine grid (i.e. 8 times more cells), but the distance of the first grid point from the inner pipe wall is kept constant, in order not to disturb the effect of the wall functions, applied in the turbulence model. A shift of the  $k_{t,v}$  value is observed, but the variations of  $k_{t,v}$  are identical on both grids. Therefore, it is concluded that the computational grid was sufficiently fine to make reliable observations on the evolution of  $k_{t,v}$ .

Figure 11, finally, shows the impact of the choice of the turbulence model. Again, a shift in the values of  $k_{t,v}$  is observed, but the variations from the initial value are practically identical, independent of the turbulence model choice. This illustrates that the observed behavior is not restricted to a specific turbulence model choice.

In general terms, the numerical experiments have been proven to be reliable.

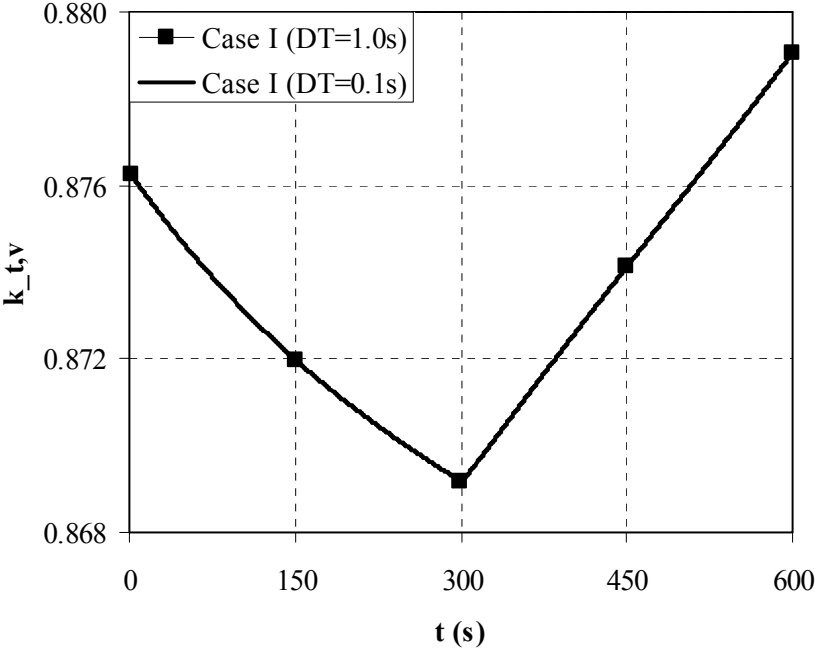


Figure 9. Influence of the time step size on the  $k_{t,v}$  evolution in time for case I.

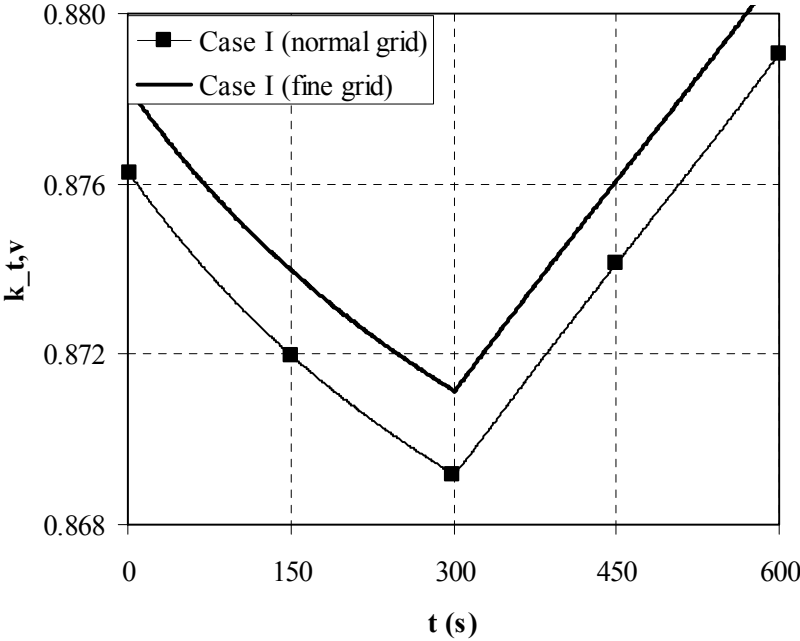


Figure 10. Influence of the computational grid on the  $k_{t,v}$  evolution in time for case I.

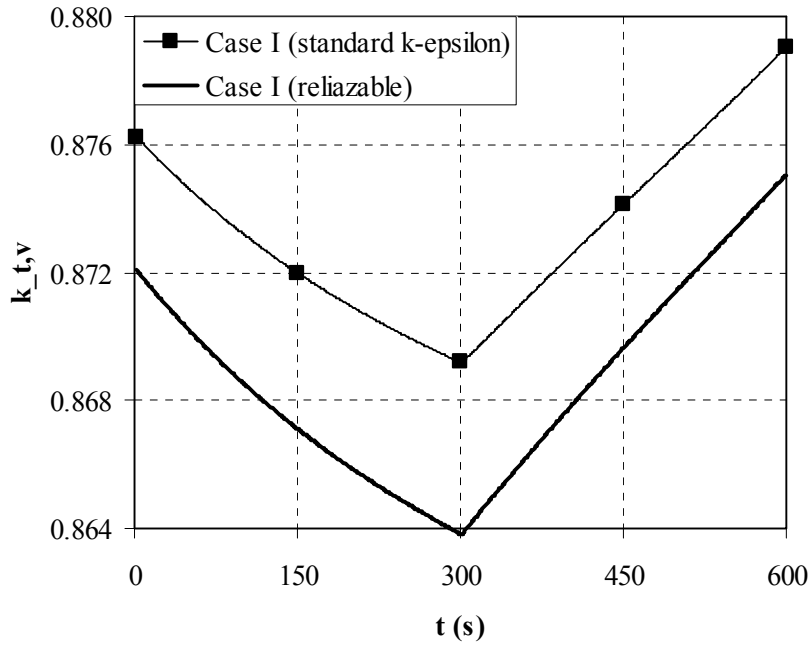


Figure 11. Influence of the turbulence model on the  $k_{t,v}$  evolution in time for case I.

#### 4. Discussion

Obviously, there are many other factors than the one discussed in the present paper that may influence the accuracy of the measurements (and thus classification) in the SBI-testing procedure. Even restricting the discussion to the flow field in the pipe, several important influential features can be identified. Firstly, the unsteadiness in the fire in the SBI test room makes it impossible to keep the exhaust gas extraction rate rigorously constant throughout the test, so that transient phenomena may affect the value of the  $k_{t,v}$ -factor. Secondly, there are bends in the exhaust system ahead of the pipe in which the measurements are performed. Despite the fact that caution is taken to allow the flow to develop, history effects from those curves may affect the turbulence and the mean flow field in a non-negligible manner. Another possible source of influence is the internal roughness of the pipe. Neither of these effects are discussed here.

#### 5. Conclusions

In this paper, numerical experiments have been presented in order to estimate the possible measurement error for the flow rate of the exhaust gases due to heating or cooling, typical for the SBI test. In that test procedure, the flow rate is determined from centerline velocity

measurements, under the assumption of an invariant velocity profile shape, expressed through a factor,  $k_t$ . In order to test the validity of this assumption, the influence of heating and cooling on the velocity profile shape has been investigated numerically.

It has been illustrated that the primary effect of heating or cooling on the velocity profile shape is due to a variation in the Reynolds number. This Reynolds number decreases when the gases are heated, while it increases again when the gases are cooled. The  $k_{t,v}$  value shows a similar behavior: the Reynolds number is not sufficiently high to make  $k_{t,v}$  independent of the Reynolds number.

However, some phenomena cannot be explained from the Reynolds number evolution. A non-negligible secondary effect has been identified: due to heating and cooling of the pipe and the corresponding heat exchange between the pipe solid material and the exhaust gases, there is no longer an unambiguous relationship between the velocity profile shape and the instantaneous molecular Reynolds number. If, on the other hand, an 'effective' Reynolds number is defined, based on the effective viscosity, i.e. the sum of the molecular and the turbulent viscosity, a one-to-one relation is recovered between  $k_{t,v}$  and  $Re_{eff}$ .

All observed phenomena have been explained through variations in fluid density. The turbulence, and consequently the turbulent kinematic viscosity, is hardly affected by the heating and cooling processes, typical for SBI-test situations. It has indeed been illustrated that buoyancy forces do not play a significant role, as could be expected based on the typical Froude number values.

The numerical experiments have been proven to be reliable: neither the time step size, nor the computational cell size or the turbulence model choice, lead to differences in the observations made on the evolution of  $k_{t,v}$ .

## References

- [1] "Reaction to fire tests for building products – Building products excluding floorings exposed to the thermal attack by a single burning item", EN 13823:2002, CEN.
- [2] Sette, B. et al., Temperature effects on the mass flow rate in the SBI and similar Heat Release Rate Test Equipment, Fire and Materials, Under review
- [3] Jones, W.P. and Launder, B.E., "The prediction of laminarization with a two-equation model of turbulence", International Journal of Heat and Mass Transfer, Vol. 15(2), pp. 301-314 (1972).
- [4] Shih, T.H., Liou, W.W., Shabbir, A., Yang, Z. and Zhu, J., "A new k- $\epsilon$  eddy-viscosity model for high Reynolds number turbulent flows", Computers and Fluids, Vol. 23(3), pp. 227-238 (1995).









## **B Annex**

### **B.1. Desiccant**

One of the assumptions in the heat release rate calculations is that the gas coming into the analyser consists of O<sub>2</sub>, CO<sub>2</sub>, (CO) and N<sub>2</sub> only. All water vapour (and water soluble components such as HCl, HCN, etc.) needs to be removed from the sample gas. This is achieved in two steps by means of a cooler unit, which brings down the temperature of the sample gas to approximately 3°C, and a chemical desiccant.

In practice, operators do not always realise the importance of the correct use of the desiccant. If used correctly, it adds to the accuracy of the test method and reduces considerably the uncertainty on the measurement. Throughout the document we will assume a correct use of the desiccant.

This paragraph however, tries to highlight some of the pitfalls that one may encounter.

A first point of attention is that the user must beware of any side effects induced by the desiccant. A good example in this respect is the use of 'Silica Gel'. Silicagel tends to absorb CO<sub>2</sub> and to release it further on in the test when the CO<sub>2</sub> concentration diminishes. As a consequence, response times tend to be sloppy and peaks and dips are flattened.

Therefore laboratories are recommended to use Anhydrous Calcium Sulphate (Drierite) which, apparently, does not have this side effect. Recently however, a few cases have been reported of increased response times using the product without indicator. The indicator is added by the manufacturer and gives a colour indication of the saturation level of the desiccant. Because the indicator is Brome based, several national authorities have prohibited the use of it.

Another point of attention is that the indicator should not be used as a trigger to change the product at the risk of making erroneous measurements. This is demonstrated in the graph below where the oxygen concentration is measured under invariable conditions.

In test 1, the Anhydrous Calcium Sulphate in both the gas sample line and the reference gas line are renewed prior to the test. In test 2, only the reference gas line contains Anhydrous Calcium Sulphate and the product is removed from the gas sampling line. After approximately two hours in test number 2, the product starts to get saturated and some vapour is left in the sample gas. As a result the vapour pressure increases and the oxygen concentration drops. After approximately four hours from the start of the experiment, the desiccant of the reference gas gets saturated with a resulting increase of measured oxygen concentration as can be seen from both tests.

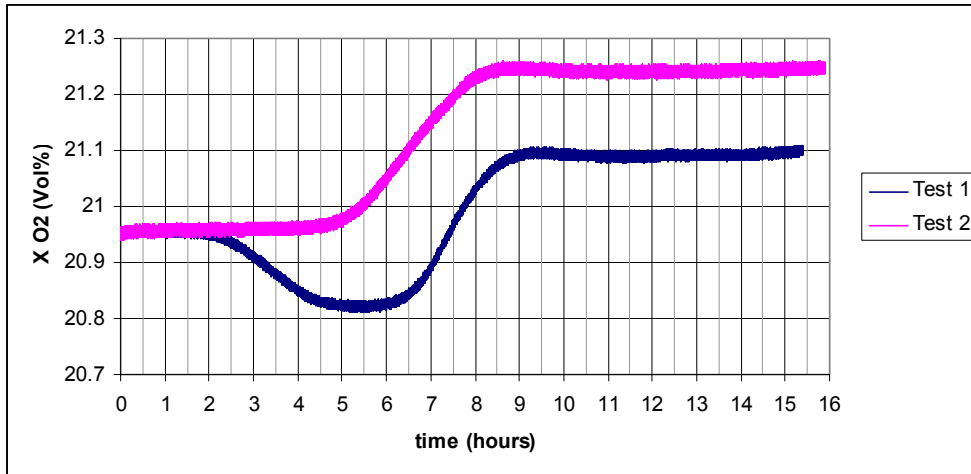


Figure 68. Influence on concentration measurement of desiccant getting saturated

## B.2. Time constant thermocouples

Determination of the response time for an insulated thermocouple of diameter 0,5mm, positioned perpendicular to an air flow of 8m/s.

Physical properties of air (300 K):

density	$\rho$	1.16	[kg/m <sup>3</sup> ]
kinematic viscosity	$\nu$	$15.89 \cdot 10^{-6}$	[m <sup>2</sup> /s]
thermal conductivity	$k$	$26.3 \cdot 10^{-3}$	[W/m.K]

Assumed physical properties thermocouple

density	$\rho$	8000	[kg/m <sup>3</sup> ]
heat capacity	$c$	500	[J/kg.K]
diameter	$D$	$0.5 \cdot 10^{-3}$	[m]

Assumptions on exhaust gases

same physical properties as ambient air			
mean velocity	$v$	8	[m/s]

Other symbols:

$\tau$	time constant	[s]
$A$	contact surface of the thermocouple	[m <sup>2</sup> ]
$V$	volume of the thermocouple	[m <sup>3</sup> ]
$h$	convective heat transfer coefficient	[W/m <sup>2</sup> .K]

A further assumption is that the temperature rise of the actual thermocouple is governed by the equation:

$$h.A.(T_f - T) = \rho.c.V. \frac{\partial T}{\partial t} \quad [ B.1 ]$$

*This is not entirely true since there will also be heat transfer between the thermocouple and the inner duct surface.*

Which leads to the equation

$$T - T_f = e^{-\frac{h.A}{\rho.C.V}t} = e^{-\frac{t}{\tau}} \quad [ \text{B.2} ]$$

with the time constant  $\tau$  defined as

$$\tau = \frac{\rho.C.V}{h.A} \quad [ \text{B.3} ]$$

Apart from the physical properties of the thermocouple and its dimensions, the time constant is determined by the convective heat transfer coefficient  $h$ .

The heat transfer coefficient may be determined using a correlation for the Nusselt number

$$Nu = \frac{h.D}{k} \quad [ \text{B.4} ]$$

An empirical relationship<sup>[25]</sup> for wires normal to the flow is given by:

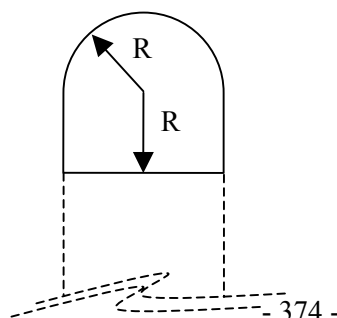
$$Nu = (0.44 \pm 0.06).(Re)^{0.50} \approx 7 \pm 1 \quad [ \text{B.5} ]$$

So the Nusselt number is function of the Reynolds number which is based on the wire diameter  $D$ , the free stream velocity  $v$  and the dynamic viscosity  $\nu$ .

$$Re = \frac{v.D}{\nu} = \frac{8 * 5 * 10^{-4}}{15.89 * 10^{-6}} \cong 250 \quad [ \text{B.6} ]$$

The estimated convective coefficient then becomes  $h \approx 370 \pm 50 \text{ W/m}^2.\text{K}$

What remains to be determined is an estimate for the ratio 'volume' to 'exposed area' of the thermocouple tip.



$$\frac{V}{A} = \frac{\frac{1}{2} \frac{4}{3} \pi R^3 + \pi R^2 R}{\frac{4\pi R^2}{2} + 2\pi R R} = \frac{5}{12} R = 0.1042 * 10^{-3} \text{ [m]} \quad \text{[ B.7 ]}$$

The time constant  $\tau$  then becomes  $\tau \approx 1.15\text{s} \pm 0.15\text{s}$  at temperatures around 300K. In the limit case of T=600K and a velocity of 16m/s the time constant decreases to approximately 0.8 s.

### B.3. Time constant duct system

The order of magnitude of the time constant of the duct system is estimated out of the empirical relationship for turbulent flow in the entrance region of smooth tubes as recommended by Nusselt<sup>[32]</sup>

$$Nu = 0.036 Re^{0.8} Pr^{1/3} \left( \frac{D}{L} \right)^{0.055} \quad \text{for } 10 < L/D < 400 \quad [ \text{B.8} ]$$

where D represents the inner duct diameter and L is the distance from the entrance.

It must be said that errors in the order of  $\pm 25\%$  are not uncommon so that the derived time constant should be read as an order of magnitude rather than as an absolute number.

The duct inner diameter is 0.315m, the distance from the entrance is 6m and the physical properties of the stainless steel, which is 2mm thick, are  $\rho = 7800 \text{ kg/m}^3$  and  $c=440 \text{ J/kg.K}$ .

Furthermore it is assumed that the fluid has the same properties as air and that the velocity in the duct changes with temperature to obtain constant mass flow rate at the height of the measurement section.

The initial mean velocity at room temperature is 7.7m/s which, in the set-up of the SBI, corresponds with a volume flow rate of 0.6 m<sup>3</sup>/s as required by the standard[2].

T(K)	v(m/s)	Re(-)	Pr(-)	Nu(-)	h(W/m <sup>2</sup> .K)	$\tau_{\text{duct}}$ (s)
300	7.7	152 500	0.707	382	31.9	225
350	9.0	135 500	0.700	347	33.0	217
400	10.3	123 000	0.690	319	34.3	209

**Table 4: Estimate of the time constant of the SBI duct system**

The time constant  $\tau_{\text{duct}}$  is derived out of the convection coefficient assuming that the heat transfer between the fluid and the duct wall is governed by convective heat transfer only.

$$\tau_{\text{duct}} = \frac{\rho c V}{h A} \quad [ \text{B.9} ]$$



$V/A$  is the ‘volume to surface area’ ratio of the inner duct. So roughly speaking, the time constant of the duct lies around 220s. It is now legitimate to state that ‘if transient thermal effects play a role on  $k_t$  and  $m$ , they can only be eliminated by maintaining the same burning conditions for at least two times  $\tau_{\text{duct}}$ ’.

If the transient effects are confirmed, they introduce an additional uncertainty on  $k_t$  and  $m$ . Furthermore, calibration procedures like the step calibration should then be revised to increase the settling time – which is now set to one minute – to something like ten minutes.

Note that the hood and collector, which are located just in front of the ductwork, have an even greater time constant.

## B.4. Time constant hood

A second time constant for the heating of the vermiculite insulation boards of the exhaust hood is also derived.

Assumed physical properties vermiculite (Thermax SNO 450)

density	$\rho$	475	[kg/m <sup>3</sup> ]
heat capacity	$c$	1000 (840 to 1080)	[J/kg.K]

Assumed mean convective coefficient  $h=20\text{W/m}^2\cdot\text{K}$  (very rough estimate; difficult to estimate since the Reynolds number changes substantially through the hood; also the mixing of the combustion gases with ambient air is still not finalised)

The volume to surface ratio for the exposed stainless steel up to the thermocouple is

$$\frac{V}{A} = \frac{4.50 \cdot 10^{-3}}{A} \cong 50 \cdot 10^{-3} \quad [\text{m}] \quad \text{[ B.10 ]}$$

The second time constant – which is difficult to determine – related to the thermal inertia of the hood is in the order of  $\tau=1200\text{s}$ .

## B.5. Radiation effect thermocouples

The energy equation for steady state reduces to:

$$F\varepsilon\sigma A_r(T_{duct}^4 - T^4) + h.A_c.(T_f - T) = 0 \quad [ B.11 ]$$

Which leads to the equation

$$T_f - T = \frac{F\varepsilon\sigma A_r(T_{duct}^4 - T^4)}{hA_c} \quad [ B.12 ]$$

Assuming that:

- the view factor  $F=1$ ;
- the emissivity  $\varepsilon = 0.9$ ;
- the radiation heat transfer area  $A_r$  is equal to the area for heat transfer by convection  $A_c$ ;
- $T_{duct} = 310$  K (approximate temperature when changing from auxiliary to main burner);
- case 1:  $T_1 = 370$  K (heptane calibration: max temperature difference of  $60^\circ\text{C}$  between wall and temperature any time in the test);
- case 2:  $T_2 = 490$  K (material M03 in SBI-RR 1: max temperature difference of  $180^\circ\text{C}$  between wall and temperature any time in the test; see Figure 69)
- $h = 370$   $\text{W/m}^2.\text{K}$  (annex B.2)

and knowing that:

- $\sigma = 56,7 * 10^{-9}$ ;

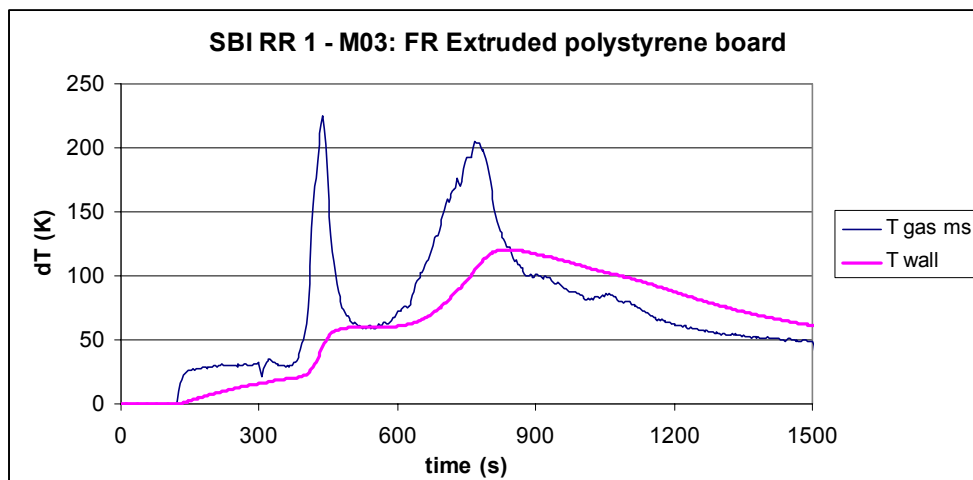


Figure 69. Wall and gas temperature evolution for material M03 in SBI RR1

The choice for material M03 (SBI RR1) is based on the knowledge that this material – in the given set-up – results in a SBI class E, which is considered the worst class to be tested in the SBI.

The error in the first case is estimated at  $-1.3^{\circ}\text{C}$  while for the second case the error is estimated at  $-6.7^{\circ}\text{C}$ . As can be seen the resulting error is non-linear due to the fourth power effect of radiation. So instead of a triangular deviation with width  $-6.7^{\circ}\text{C}$ , a normal distribution with coverage factor 3 (99.7%) will be assumed. This brings down the standard uncertainty to  $-2.2^{\circ}\text{C}$ .

In most tests, the wall temperature remains below the gas temperature in the first 900s (= 600s sample exposure) of the test. This is the time interval used for calculating the values used for classification FIGRA, THR600s, SMOGRA and TSP600s. Therefore the standard uncertainty will be taken as a one sided distribution. For completeness it must be said that both FIGRA and especially SMOGRA are sometimes calculated based on data from the second part of the test (>900s). This will however be disregarded since most often in those cases the wall temperature remains below the gas temperature.

## B.6. Chemical composition of commercial grade propane

Chemical composition of commercial grade propane<sup>[79][83]</sup> (example of analysis):

- ethane + ethene: 2 %
- propane: 94,9 %
- propene: 0,8 %
- n-butane + iso-butane: 2,3 %

Relevant standard: NBN.T 52-706

	composition	E <sup>[26]*</sup> MJ/kg O <sub>2</sub>	H <sup>o[26]*</sup> MJ/kg	(E)	(H <sup>o</sup> )
Propane	94.9%	12.774	46.35	12.123	43.986
Propene	0.8%	13.38	45.79	0.107	0.366
Ethane/ethene	2.0%	12.75/13.78	47.49/47.17	0.255/0.276	0.950/0.943
n-butane/iso-butane	2.3%	12.77/12.62	45.72/45.17	0.294/0.290	1.052/1.039
Σ	100.0%		Σ	12.775/12.799	46.335/46.354
Deviation from 100% pure propane (%)				0.006/0.195	-0.033/0.008
Standard error on reported values (%)				0.032	0.032
Combined standard uncertainty (%)				0.033/0.20	0.046/0.033

\* the values for propane are taken from annex B.7

The standard uncertainty on the chemical composition is assumed to be equal to the deviation between the theoretical and calculated values.

The standard uncertainties on the reported values<sup>[26][49]</sup> for E are estimated to be 0.004MJ/kg for propane (annex B.7) and are chosen somewhat arbitrary – in view of the relatively small influence – to 0.01 MJ/kg O<sub>2</sub> for all other components.

The standard uncertainty related to H<sup>o</sup> values is set to 0.015MJ/kg for propane.

estimated out of Table 17 which summarises a series of values that can be found in the literature<sup>[26][49][30][39]</sup>.

Based on Table 17 and the above considerations, the standard error of mean on the heat of combustion for all substances used in this document will be taken, fairly arbitrarily, as 0.02 MJ/kg

## B.7. Estimation of uncertainty on Heats of combustion

<b>Carbon dioxide</b>														
Hf (kJ/mol)	tolerance			Reference					Hf	Heat of formation			kJ/mol	
-393.522	0.05			Chase	1998				u(x)	Standard uncertainty on component x				
-393.522	0.4			Cox, Wagman, et al	1984				Hc	Heat of combustion			kJ/mol	
									H	Gross calorific value			MJ/kg	
									Hnett	Nett calorific value			MJ/kg	
									r0	Oxygen - Fuel mass ratio			-	
<b>Water (liquid)</b>														
-285.83	0.042			Chase	1998									
-285.83	0.04			Cox, Wagman, et al	1984									
<b>Water (gas)</b>														
-241.826	0.042			Chase	1998									
-241.826	0.04			Cox, Wagman, et al	1984									
<b>Methane</b>														
16.04246	0.00085	(molecular weight)												
C	1	12.0107	0.0008	O2	2		CO2	1						
H	4	1.00794	0.00007				H2O	2						
O	0	15.9994	0.0003				HCl							
N	0	14.0067	0.0002				N2							
Cl	0	35.453	0.002											
Hf (kJ/mol)	u(x)	Hc (water cu(x))		Reference	year	H (MJ/kg)	u(x)	%H by mas	Hnett	u(x)	r0	u(x)	Hnett/r0	u(x)
-74.873	0.34	-890.309	0.35	Chase	1998	55.497	0.022	25.13%	50.011	0.022	3.989263	0.00022	12.536	0.00556
-74.5	0.4	-890.7	0.4	Pittam and Pilcher	1972	55.521	0.025	25.13%	<b>50.035</b>	<b>0.025</b>	3.989263	0.00022	<b>12.542</b>	<b>0.0063</b>
-74.85	0.31	-890.35	0.3	Prosen and Rossini	1945	55.5	0.019	25.13%	<b>50.013</b>	<b>0.019</b>	3.989263	0.00022	<b>12.537</b>	<b>0.00481</b>
73.4	1.1	-891.8	1.1	Roth and Banse	1932	55.59	0.069	25.13%	<b>50.104</b>	<b>0.069</b>	3.989263	0.00022	<b>12.56</b>	<b>0.01731</b>
		-890.16	0.3	Rossini	1931	55.488	0.019	25.13%	<b>50.001</b>	<b>0.019</b>	3.989263	0.00022	<b>12.534</b>	<b>0.00481</b>
Hf (kJ/mol)	u(x)	Hc (water cu(x))		Reference										
-74.873	0.34	-802.301	0.35	Chase	1998				<b>50.011</b>	<b>0.02</b>	3.989263	0.00022	<b>12.536</b>	<b>0.00481</b>
									<b>50.033</b>	0.045	0.025		<b>12.542</b>	0.011
										95% conf.	80% conf.			95% conf.
										0.0400%				0.0384%

<b>Propane</b>														
44.09562	0.00246	(molecular weight)												
C	3	12.0107	0.0008	O2	5		CO2	3						
H	8	1.00794	0.00007				H2O	4						
O	0	15.9994	0.0003				HCl							
N	0	14.0067	0.0002				N2							
Cl	0	35.453	0.002											
Hf (kJ/mol)	u(x)	Hc (water)	u(x)	Reference	year	H (MJ/kg)	u(x)	%H by mas	Hnett	u(x)	r0	u(x)	Hnett/r0	u(x)
-104.7	0.5	-2219.186	0.51	Pittam and Pilcher	1972	50.327	0.012	18.29%	46.335	0.012	3.628342	0.00021	12.77	0.00339
-103.8	0.59	-2220.086	0.6	Prosen and Rossini	1945	50.347	0.014	18.29%	46.355	0.014	3.628342	0.00021	12.776	0.00393
		-2219.9	0.5	Rossini	1934	50.343	0.012	18.29%	<b>46.351</b>	0.012	3.628342	0.00021	<b>12.775</b>	0.00339
		-2207	-	Guinchant	1918	50.05		18.29%	46.058		3.628342	0.00021	12.694	0.00073
Hf (kJ/mol)	u(x)	Hc (water)	u(x)	Reference										
-104.7	0.5	-2043.17	0.51	Pittam and Pilcher	1972				<b>46.335</b>	0.011	3.628342	0.00021	<b>12.77</b>	0.00312
-103.8	0.59	-2044.07	0.6	Prosen and Rossini	1945				<b>46.355</b>	0.013	3.628342	0.00021	<b>12.776</b>	0.00366
									<b>46.347</b>	0.0299	0.013		<b>12.774</b>	0.008
										95% conf.	80% conf			95% conf.
										0.0645%				0.0626%
<b>Heptane</b>														
100.2019	0.00571	(molecular weight)												
C	7	12.0107	0.0008	O2	11		CO2	7						
H	16	1.00794	0.00007				H2O	8						
O	0	15.9994	0.0003				HCl							
N	0	14.0067	0.0002				N2							
Cl	0	35.453	0.002											
Hf (kJ/mol)	u(x)	Hc (water)	u(x)	Reference	year	H (MJ/kg)	u(x)	%H by mas	Hnett	u(x)	r0	u(x)	Hnett/r0	u(x)
-224.4	0.79	-4816.894	0.81	Prosen and Rossini	1945	48.072	0.009	16.09%	44.558	0.009	3.512774	0.00021	12.685	0.00267
-225.9	1.3	-4815.394	1.31	Davies and Gilbert	1941	48.057	0.013	16.09%	44.543	0.013	3.512774	0.00021	12.68	0.00378
		-4817	8	N/A	N/A	48.073	0.08	16.09%	<b>44.559</b>	<b>0.08</b>	3.512774	0.00021	<b>12.685</b>	<b>0.02279</b>
Hf (kJ/mol)	u(x)	Hc (water)	u(x)	Reference										
-224.4	0.79	-4464.862	0.81	Prosen and Rossini	1945				<b>44.559</b>	<b>0.008</b>	3.512774	0.00021	<b>12.685</b>	0.0024
-225.9	1.3	-4463.362	1.31	Davies and Gilbert	1941				<b>44.544</b>	<b>0.012</b>	3.512774	0.00021	<b>12.681</b>	0.0035
									<b>44.554</b>	0.034	0.022		<b>12.684</b>	0.005
										95% conf.	80% conf			95% conf.
										0.0763%				0.0394%



## Local references

Cox, J.D.; Wagman, D.D.; Medvedev, V.A., CODATA Key Values for Thermodynamics, Hemisphere Publishing Corp., New York, 1984, 1.

Chase, M.W., Jr., NIST-JANAF Thermochemical Tables, Fourth Edition, J. Phys. Chem. Ref. Data, Monograph 9, 1998, 1-1951.

Furuyama, S.; Golden, D.M.; Benson, S.W., Thermochemistry of the gas phase equilibria  $i\text{-C}_3\text{H}_7\text{I} = \text{C}_3\text{H}_6 + \text{HI}$ ,  $n\text{-C}_3\text{H}_7\text{I} = i\text{-C}_3\text{H}_7\text{I}$ , and  $\text{C}_3\text{H}_6 + 2\text{HI} = \text{C}_3\text{H}_8 + \text{I}_2$ , J. Chem. Thermodyn., 1969, 1, 363-375

Guinchant, M.J., Etude sur la fonction acide dans les derives metheniques et methiniques, Ann. Chem., 1918, 10, 30-84

Pittam, D.A.; Pilcher, G., Measurements of heats of combustion by flame calorimetry. Part 8.- Methane, ethane, propane, n-butane and 2-methylpropane, J. Chem. Soc. Faraday Trans. 1, 1972, 68, 2224-2229

Prosen, E.J.; Rossini, F.D., Heats of combustion and formation of the paraffin hydrocarbons at 25° C, J. Res. NBS, 1945, 263-267

Rossini, F.D., The heats of combustion of methane and carbon monoxide, J. Res. NBS, 1931, 6, 37-49

Rossini, F.D., Calorimetric determination of the heats of combustion of ethane, propane, normal butane, and normal pentane, J. Res. NBS, 1934, 12, 735-750

Roth, W.A.; Banse, H., Die verbrennungs- und bildungswarme von kohlenoxyd und methan, Arch. Eisenhütten., 1932, 6, 43-46

Rossini, F.d.; Knowlton, J.W., Calorimetric determination of the heats of combustion of ethylene and propylene, J. Res. NBS, 1937, 19, 249-262

Wiberg, K.B.; Fenoglio, R.A., Heats of formation of  $\text{C}_4\text{H}_6$  hydrocarbons, J. Am. Chem. Soc., 1968, 90, 3395-3397

## B.8. Uncertainty analysis on the gas analyser

The gas concentration  $y$  is derived out of calibrations  $C1(x_1, y_1)$  and  $C2(x_2, y_2)$ , and a measurement signal  $x$ .  $y_1$  and  $y_2$  are gas concentrations. In case of the oxygen analyser  $y_1 \cong 17$  Vol% and  $y_2 \cong 20.95$  Vol%. The values  $x_1$  and  $x_2$  are the corresponding signal outputs.

$$y = y_1 + \frac{(y_2 - y_1)}{(x_2 - x_1)}(x - x_1) \quad [ \text{B.13} ]$$

The partial derivatives to the different variables are given by

$$\frac{\partial y}{\partial y_1} = \frac{x_2 - x}{x_2 - x_1} \quad [ \text{B.14} ]$$

$$\frac{\partial y}{\partial y_2} = \frac{x - x_1}{x_2 - x_1} \quad [ \text{B.15} ]$$

$$\frac{\partial y}{\partial x} = \frac{y_2 - y_1}{x_2 - x_1} \quad [ \text{B.16} ]$$

$$\frac{\partial y}{\partial x_1} = \frac{(y_2 - y_1)(x - x_2)}{(x_2 - x_1)^2} \quad [ \text{B.17} ]$$

$$\frac{\partial y}{\partial x_2} = -\frac{(y_2 - y_1)(x - x_1)}{(x_2 - x_1)^2} \quad [ \text{B.18} ]$$

and the combined standard uncertainty by

$$u(y) = \frac{1}{(x_2 - x_1)} \sqrt{[u(y_1)(x_2 - x)]^2 + [u(y_2)(x - x_1)]^2 + [u(x)(y_2 - y_1)]^2 + \left[ u(x_1) \frac{(y_2 - y_1)(x - x_2)}{(x_2 - x_1)} \right]^2 + \left[ u(x_2) \frac{(y_2 - y_1)(x - x_1)}{(x_2 - x_1)} \right]^2} \quad [ \text{B.19} ]$$

Since the signal  $x$  is already converted to Vol% concentrations prior to the calculations,  $x$  and  $y$  values are almost equal. For oxygen for example,  $y_2 = 20.95$  Vol% (concentration of oxygen in dry air, by definition; implies that  $u(y_2 = 0)$ ) and  $x_2$  is the mean concentration of oxygen between  $t = 30$  s and 90 s. A value for  $x_2$  could be for example  $x_2 = 20.95094$

## B.9. Uncertainty analysis on the oxygen analyser

Oxygen analyser; Measuring range 4 Vol%			4	Vol%				
Measuring range (MR)	Specification	Expected variations	Units	Uncertainty (ppm)	Coverage factor	Probability distribution	Standard uncertainty (ppm)	
17-21 Vol%								
<b>Uncertainty contribution measurement</b>								
Ambient air temperature	< 0.5% on MR/10K	2	K	40	3	normal	13	
Pressure measuring gas	< 0.2% on MR/1% pressure variance	100	Pa	8	3	normal	3	
Power supply	< 0.1% on MR for +/-10%			40	3	normal	13	
Linearity	Linear							
Noise	SBI Noise & Drift calibration			27	1	normal	27	
Drift (half an hour)	SBI RR2 - P2 MDF - UGENT Test 1			58	1	rectangular	33	
u(M)								<b>47</b>
<b>Uncertainty contribution calibration point 2 (calibration prior to every test)</b>								
Noise	SBI Noise & Drift calibration	( 20 samples)		27	1	normal	6	
u(C2)								<b>6</b>
<b>Uncertainty contribution calibration point 1 (daily calibration)</b>								
Drift (als max-min over periode van 10 uren; 95% confidence interval)								
Ambient air temperature	< 0.5% on MR/10K	5	K	100	3	normal	33	
Pressure measuring gas	< 0.2% on MR/1% pressure variance	1000	Pa	80	3	normal	27	
Power supply				40	3	normal	13	
Linearity	Linear							
Noise	SBI Noise & Drift calibration			27	1	normal	27	
Drift (one working day)	SBI Noise & Drift calibration			37	1	rectangular	21	
u(C1)								<b>56</b>
<b>Uncertainty contribution calibration gas</b>								
Calibration gas	0.02Vol% ABS (17Vol%)			200	2	normal	100	

## B.10. Uncertainty analysis on the carbon dioxide analyser

Carbon dioxide analyser; Measuring range 4 Vol%			4 Vol%				
Measuring range (MR)	Specification	Expected variations	Units	Uncertainty (ppm)	Coverage factor	Probability distribution	Standard uncertainty (ppm)
<b>O-4 Vol%</b>							
<b>Uncertainty contribution measurement</b>							
Ambient air temperature	<1% on MR/10K	2	K	80	3	normal	27
Pressure measuring gas	< 0.15% on MR/1% pressure variance	100	Pa	6	3	normal	2
Power supply	< 0.1% on MR for +/-10%			40	3	normal	13
Linearity	< 0.5% on MR			200	3	normal	67
Noise	SBI Noise & Drift calibration			39	1	normal	39
Drift (half an hour)	SBI RR2 - P2 MDF - UGENT Test 1			25	1	rectangular	14
u(M)							<b>84</b>
<b>Uncertainty contribution calibration point 2 (calibration prior to every test)</b>							
Noise	SBI Noise & Drift calibration	( 20 samples)		39	1	normal	<b>9</b>
u(C2)							<b>9</b>
<b>Uncertainty contribution calibration point 1 (daily calibration)</b>							
Drift (als max-min over periode van 10 uren; 95% confidence interval)							
Ambient air temperature	<1% on MR/10K	5	K	100	3	normal	33
Pressure measuring gas	< 0.15% on MR/1% pressure variance	1000	Pa	60	3	normal	20
Power supply				40	3	normal	13
Linearity	non applicable (calibration point)						
Noise	SBI Noise & Drift calibration			39	1	normal	39
Drift (one working day)	SBI Noise & Drift calibration			36	1	rectangular	21
u(C1)							<b>60</b>
<b>Uncertainty contribution calibration gas</b>							
Calibration gas	0.5% REL (3.5Vol%)			175	2	normal	88



## B.11. Transient error first order system

In the Laplace domain, a first order system is written as

$$H(s) = \frac{1}{1 + s\tau} \quad [ \text{B.20} ]$$

The relation between an input  $f(t)$  and the output  $y(t)$  in the Laplace domain is given by

$$F(s)H(s) = Y(s) \quad [ \text{B.21} ]$$

or, combining the two above equations,

$$F(s) = Y(s) + \tau s Y(s) \quad [ \text{B.22} ]$$

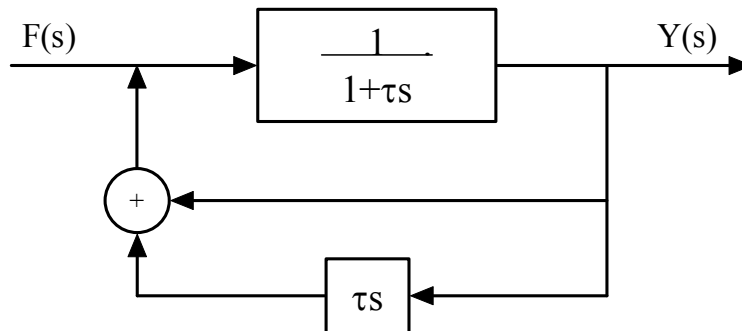


Figure 70. Relationship between input and output in a first order system

or rewriting it in a different notation this becomes

$$\mathcal{L}\{f(t)\} = \mathcal{L}\{y(t)\} + \tau[s\mathcal{L}\{y(t)\} - y(0) + y(0)] \quad [ \text{B.23} ]$$

whereby  $\mathcal{L}$  represents the Laplace transform symbol. Note that in this step, we have taken the inverse  $H^{-1}(s)$  of the systems transfer function. Since  $H(s)$  acts like a low pass filter with cutoff frequency  $1/\tau$ , the inverse will behave as an amplifier for frequencies above  $1/\tau$ . This means that when restoring the 'true' input signal out of the output, high frequency noise on the output signal will be amplified. This

can easily be seen by taking the sine response of the inverse system (replacing  $s$  by  $j\omega$  whereby  $\omega$  is the sine frequency and  $j$  represents imaginary numbers).

$$H^{-1}(j\omega) = 1 + \tau\omega j \quad [ \text{B.24} ]$$

The gain and phase change are then given by

$$|H^{-1}(j\omega)| = \sqrt{[\text{Re } H^{-1}(j\omega)]^2 + [\text{Im } H^{-1}(j\omega)]^2} = \sqrt{1 + (\tau\omega)^2} \quad [ \text{B.25} ]$$

$$\arg H^{-1}(j\omega) = \arctan \frac{\text{Im } H^{-1}(j\omega)}{\text{Re } H^{-1}(j\omega)} = \arctan(\tau\omega) \quad [ \text{B.26} ]$$

If  $y$  is continuous and  $y'$  is piecewise continuous on any interval  $0 \leq t \leq A$ , and if further there exists constants  $K$ ,  $a$  and  $M$  such that  $|y(t)| \leq Ke^{at}$  for  $t \geq M$ , this can be rewritten as<sup>[28]</sup>

$$\mathcal{L}\{f(t)\} = \mathcal{L}\{y(t)\} + \tau\mathcal{L}\{y'(t)\} + \tau y(0) \quad [ \text{B.27} ]$$

Taking the inverse Laplace transform and assuming that  $y(0)=0$ , the transient error can be calculated as

$$e(t) = f(t) - y(t) = \tau y'(t) \quad [ \text{B.28} ]$$

The inverse transform of the constant  $\tau y(0)$ , if different from zero, results in a Dirac impulse.



## B.12. Conversion factor upper to lower heat of combustion

In fires, most often, water will not be present in the combustion products in the liquid phase though in the gas phase. This requires an amount of energy which explains the difference in heat of formation of liquid H<sub>2</sub>O and H<sub>2</sub>O in the gas phase ( $\Delta H_f^0(l) = -285.830 \pm 0.042$  kJ/mol and  $\Delta H_f^0(g) = -241.826 \pm 0.042$  kJ/mol<sup>[20]</sup>). This enthalpy difference together with the atomic mass of the Hydrogen atom  $M_H = 1.00794 \pm 0.00007$  kg/kmol results in the conversion factor

$$C = 1000 \frac{\Delta H_f^0(l) - \Delta H_f^0(g)}{2M_H} \quad \text{MJ/kg} \quad [\text{B.29}]$$

$$\frac{\partial C}{\partial \Delta H_f^0(l)} = \frac{1000}{2M_H} \quad [\text{B.30}]$$

$$\frac{\partial C}{\partial \Delta H_f^0(g)} = -\frac{1000}{2M_H} \quad [\text{B.31}]$$

$$\frac{\partial C}{\partial M_H} = -\frac{C}{M_H} \quad [\text{B.32}]$$

$$u(C) = \sqrt{\left(\frac{1000}{2M_H} u(\Delta H_f^0(l))\right)^2 + \left(\frac{1000}{2M_H} u(\Delta H_f^0(g))\right)^2 + \left(\frac{C}{M_H} u(M_H)\right)^2} \quad [\text{B.33}]$$

## B.13. Composition Heptane

Dear Madam/Sir,

from our responsible product manager I've got the following statement:

For n-heptane extra pure 1.04365 we specify a purity of >99 %. The effective batch values are between 99.3 % and 99.8 %. The water content, which isn't part of our product specification, is below 0,01 % (effective mostly below 0,001 %). So water isn't relevant in this context. We assume that the rest which is not specified consists of divers hydrocarbons, so called related substances. But they are not determined more precisely.

With kind regards

Hans-Ulrich Röhr

Group VWR / CMGs, Life Science & Analytics - Business Services

Location: C11/614

Phone: +49(0)6151 72 6210

Fax: +49(0)6151 72 916210

Email: Hans-Ulrich.Roehr@merck.de

Merck KGaA

Frankfurter Str. 250

D 64293 Darmstadt

Home: [www.merck.de](http://www.merck.de)

----- Weitergeleitet von Petra Werner/EMD/Merck am 13.08.2004 14:11 -----

"Bart Sette"

<Bart.Sette@UGent An: <chemdat@merck.de>

Thema: n-Heptane extra pure 104365

13.08.2004 13:36

Dear Madame/Sir,

In relation to a PhD research project I need to estimate the uncertainty on the heat of combustion of your product 104365.

According to the specifications the product has a purity better than 99%.

Can it be so that the remaining 1% consists entirely of water (or other species not releasing any energy) or is this very unlikely?

If not, what is this rest fraction most likely composed of?

Thank you very much for your kind cooperation.

Bart

Bart Sette

University Gent

Department of Flow, Heat and Combustion Mechanics

Ottergemsesteenweg 711

B-9000 GENT (BELGIUM)

tel.: +32-9-243.77.50

fax: +32-9-243.77.51

bart.sette@ugent.be

## B.14. Electronic damping O<sub>2</sub> and CO<sub>2</sub> analysers

Comments on the time constants for the electronic damping of the O<sub>2</sub> and CO<sub>2</sub>-signals (Siemens)

From: Galonska Gerd <gerd.galonska@siemens.com>  
To: "bart.sette@rug.ac.be" <bart.sette@rug.ac.be>  
Subject: Zeitkonstanten OXYMAT 6  
Date sent: Wed, 16 Oct 2002 13:44:06 +0200

Sehr geehrter Herr Sette,  
zu Ihrer Frage zu den Zeitkonstanten im Oxymat 6 folgende Erklärung:

Bei den angegebenen Zeitkonstanten handelt es sich um 90%- Zeiten, die einstellbar sind und mit dem in der Regelungstechnik bekannten Begriff "Tau" wie folgt zusammenhängen:  $t_{90} = 2,3026 \times \text{Tau}$ . Was es mit  $t_i$  und  $t_a$  auf sich hat ist in der Betriebsanleitung erklärt. Jetzt noch zu den speziellen Fragen: Die Signalverarbeitung erfolgt mit Hilfe einer gleitenden Mittelwertbildung, wobei die Abtastrate des Messwertes ca. 240 ms beträgt. Je nach eingestellter Zeitkonstante wird ein gewichteter gleitender Mittelwert gebildet, wobei mit steigender Zeitkonstante die Gewichtung eingelesener neuer Messwerte abnimmt. Dies entspricht im Endeffekt einem Tiefpassfilter erster Ordnung. Über Grenzfrequenz und Dämpfung können bei dieser realisierten Rauschunterdrückung keine genauen Angaben gemacht werden. Im Endeffekt entsprechen die eingegebenen Werte den 90%- Zeiten, wobei allerdings die pneumatischen Verhältnisse des Messsystems (Totzeit) nicht berücksichtigt wurden.

Gerd Galonska  
Siemens AG  
Abt.: A&D PI2  
Östliche Rheinbrückenstrasse 50  
76181 Karlsruhe  
Tel.: 0721-595-4292  
Fax: 0721-595-6375  
Mail: [gerd.galonska@siemens.com](mailto:gerd.galonska@siemens.com)

## B.15. Cross sensitivity of the Oxymat 6E analyser<sup>[76]</sup>

Residual gas (concentration 100 % v/v)		Zero deviation in % v/v O <sub>2</sub> absolute	Residual gas (concentration 100 % v/v)		Zero deviation in % v/v O <sub>2</sub> absolute
<b>Organic gases</b>			<b>Noble gases</b>		
Acetic acid	CH <sub>3</sub> COOH	-0.64	Argon	Ar	-0.25
Acetylene	C <sub>2</sub> H <sub>2</sub>	-0.29	Helium	He	+0.33
1,2 Butadiene	C <sub>4</sub> H <sub>6</sub>	-0.65	Krypton	Kr	-0.55
1,3 Butadiene	C <sub>4</sub> H <sub>6</sub>	-0.49	Neon	Ne	+0.17
iso-Butane	C <sub>4</sub> H <sub>10</sub>	-1.30	Xenon	Xe	-1.05
n-Butane	C <sub>4</sub> H <sub>10</sub>	-1.26			
1-Butene	C <sub>4</sub> H <sub>8</sub>	-0.96	<b>Inorganic gases</b>		
iso-Butene	C <sub>4</sub> H <sub>8</sub>	-1.06	Ammonia	NH <sub>3</sub>	-0.20
cyclo-Hexane	C <sub>6</sub> H <sub>12</sub>	-1.84	Carbon dioxide	CO <sub>2</sub>	-0.30
Ethene	C <sub>2</sub> H <sub>4</sub>	-0.49	Carbon monoxide	CO	+0.07
Ethylene	C <sub>2</sub> H <sub>4</sub>	-0.22	Chlorine	Cl <sub>2</sub>	-0.94
Dichlorodifluoromethane (R12)	CCl <sub>2</sub> F <sub>2</sub>	-1.32	Dinitrogen monoxide	N <sub>2</sub> O	-0.23
n-Heptane	C <sub>7</sub> H <sub>16</sub>	-2.4	Hydrogen	H <sub>2</sub>	+0.26
n-Hexane	C <sub>6</sub> H <sub>14</sub>	-2.02	Hydrogen bromide	HBr	-0.76
Methane	CH <sub>4</sub>	-0.18	Hydrogen chloride	HCl	-0.35
Methanol	CH <sub>3</sub> OH	-0.31	Hydrogen fluoride	HF	+0.10
n-Octane	C <sub>8</sub> H <sub>18</sub>	-2.78	Hydrogen iodide	HI	-1.19
n-Pentane	C <sub>5</sub> H <sub>12</sub>	-1.68	Hydrogen sulphide	H <sub>2</sub> S	-0.44
iso-Pentane	C <sub>5</sub> H <sub>12</sub>	-1.49	Oxygen	O <sub>2</sub>	+100
Propane	C <sub>3</sub> H <sub>8</sub>	-0.87	Nitrogen	N <sub>2</sub>	0.00
Propylene	C <sub>3</sub> H <sub>6</sub>	-0.64	Nitrogen dioxide	NO <sub>2</sub>	+20.00
Trichlorofluoromethane (R11)	CCl <sub>3</sub> F	-1.63	Nitrogen oxide	NO	+42.94
Vinyl chloride	C <sub>2</sub> H <sub>3</sub> Cl	-0.77	Sulphur dioxide	SO <sub>2</sub>	-0.20
Vinyl fluoride	C <sub>2</sub> H <sub>3</sub> F	-0.55	Sulphur hexafluoride	SF <sub>6</sub>	-1.05
1,1 Vinylidene chloride	C <sub>2</sub> H <sub>2</sub> Cl <sub>2</sub>	-1.22	Water	H <sub>2</sub> O	-0.03

Zero error due to diamagnetism and paramagnetism of residual gases with nitrogen as the reference gas at 60 °C and 1 bar absolute (according to IEC 1207/3).



